SDMS DOCID# 1143129

United Heckathorn Superfund Site: Tier 2 Sediment Transport Study

February 2014

Prepared for:
CH2M HILL under contract to EPA Region 9

Prepared by:
Sea Engineering, Inc.
200 Washington Street, Suite 210
Santa Cruz, CA 95060
Tel: (831) 421-0871
Fax: (831) 421-0875

Contents

List of Figures iii

List of Tables v

List of acronyms used in the report vi

Executive Summary vii

1.0 Introduction 1

2.0 Site Description 4

2.1 Sediment Bed 5

2.2 Tidal Hydrodynamics 10

2.3 Anthropogenic Processes 11

3.0 Tier 2 Field Efforts 11

3.1 Hydrodynamic and Water Quality Data Collection 11

3.1.1 Methods 12

3.1.2 Results 14

3.2 Tracer Study 17

3.2.1 Study Implementation 18

3.2.2 Deployment 19

3.2.3 Sampling 20

3.2.4 Results 21

3.3 Sedflume Analysis 24

3.3.1 Core Collection 24

3.3.2 Core Processing 24

3.3.3 Results 25

4.0 Sediment Transport Analysis 29

4.1 Natural Sediment Transport 30

4.2 Anthropogenically Forced Sediment Transport 33

4.2.1 Field Data– Tug events 33

4.2.2 Prop Scour Analysis 35

4.3 Hydrodynamic Model 54

4.3.1 Model Domain and Grid Creation 54

4.3.2 Boundary Conditions 55

4.3.3 Model Validation 56

4.3.4 Model Results 57
5.0 Refined Sediment Transport CSM and Sediment Budget 66
5.1 Sediment Transport Process Summary 67
5.2 Conceptual Sediment Budget 69
6.0 Summary and Sediment Management Questions 71
6.1 Site Management Questions 72
7.0 Reference 73

List of Figures

Figure 1.Location of Richmond Harbor. 3
Figure 2. Bathymetric map of the Lauritzen Channel and surrounding Santa Fe Channel. 5
Figure 3. Sediment disturbance due to vessel activity. 7
Figure 4. Bathymetric Change from 2007 to 2012. 8
Figure 5. Younger Bay Mud Mass in 2013 9
Figure 6. Example pressure data illustrating semi-diurnal tidal variability. 10
Figure 7. Bottom-mount platform with ADCP and YSI water quality sonde indicated. 12
Figure 8 Location of ADCP Platforms and Transects 13
Figure 9. Current velocity (upper), current direction (middle), and TSS (bottom) as a function of time and height above the sediment bed measured at the mouth of the Lauritzen Channel. Water depth is indicated with solid black lines. 15
Figure 10. Time series of sediment flux derived from mid-water column ADCP measurements at the mouth (upper panel) and head (lower panel) of the Lauritzen Channel. The red lines indicate daily averaged sediment flux. 17
Figure 11. Magnet moorings and grab sampling locations. 20
Figure 12. Mass recovered from magnets and grab samples during the particle tracer study... 23
Figure 13. Map of Sedflume coring locations. 26
Figure 14. Sedflume in the Santa Cruz, CA, SEI laboratory. 27
Figure 15. Time series of water depth (upper), TSS (middle), and band-pass filtered TSS (lower) collected within 1-m above the sediment bed at the mouth of the Lauritzen Channel. Red indicates flood tide periods and ebb tide periods are illustrated in blue. 30
Figure 16. The left three panels show time series of water depth (upper), TSS (middle), and sediment flux (lower). Band-pass and low-pass filtered (30-hr cut-off frequency) TSS and sediment flux are shown in blue and red, respectively. Positive flux is out of the system (i.e. ebb tide) and negative flux is into the system (i.e. flood tide). The right two panels show coherence between TSS and water depth (upper) and sediment flux and water depth (lower). Statistically significant coherence periods are denoted with red stars and their periods are labeled in units of hours. Data outside of the cut-off frequencies for tidal variability are shaded in gray. TSS and flux data are from within 1-m above the sediment bed. 31

Figure 17. Time series of band-pass (blue) and low-pass (red) filtered near-bottom shear stress computed from data collected within 1-m of the sediment bed at the mouth (upper panel) and head (lower panel) of the Lauritzen Channel. The black, dashed lines denote the critical shear stress for sediment resuspension determined from Sedflume experiments (0.43 Pa and 0.2 Pa at the mouth and head of the Lauritzen Channel, respectively). 32
Figure 18. The average size distribution of particles collected within 2-m of the sediment bed at the mouth (left panel) and head (right panel) of the Lauritzen Channel averaged over ebb tide periods (blue lines) and flood tide periods (red lines). 33
Figure 19. Time series of water depth (upper), high-pass filtered TSS (middle), and near-bottom shear stress (bottom) measured within 1-m above the sediment bed. Green dots indicate periods when high-pass filtered TSS exceeded an operationally-defined threshold value of 60 mg/L but near bottom-shear stress did not exceed the critical shear stress for erosion of surface sediment as determined from the Sedflume experiments. Red dots indicate periods when near-bottom shear stress exceeded the critical shear stress for erosion. Data were collected at the mouth of the Lauritzen Channel. 34
Figure 20. Time series of water depth (upper), high-pass filtered TSS (middle), and near-bottom shear stress (bottom) measured at the head of the Lauritzen Channel. Data were collected within 1-m of the sediment bed. Red dots indicate periods when near-bottom shear stress exceeded the critical shear stress for erosion of surface sediment as determined from Sedflume experiments. Green dots indicate periods when high-pass filtered TSS exceeded an operationally-defined threshold value of 40 mg/L. 35
Figure 21. Schematic of propeller wash and ship wake model coordinate system..... 37
Figure 22. Profile lines used to create the beds for the Transiting Case of the propeller wash and ship wake model. 43
Figure 23. Contour plot of the ship wake component of the bottom velocity (m/s) along Transect 5 as a function of time for Vessel 2 running at 100% of its maximum power. The tiop panel is a plot of the starting bathymetry along the transect. 44
Figure 24. Contour plot of the propeller component of the bottom velocity (m/s) along Transect 5 as a function of time for Vessel 2 running at 100% of its maximum power. The top panel is a plot of the starting bathymetry along the transect. 45
Figure 25. Contour plot of the total bottom velocity (m/s) along Transect 5 as a function of time for Vessel 2 running at a 100% of its maximum power. The top panel is a plot of the starting bathymetry along the transect. 46
Figure 26. Contour plot of the bed shear stress (Pa) along Transect 5 as a function of time for Vessel 2 running at a 100% of its maximum power. The Top panel is a plot for the starting bathymetry along the transect. 47
Figure 27. Bed Velocity due around Transect 2 due to 100% power from Vessel 2..... 50
Figure 28. Bed Shear Stress around Transect 2 due to 100% power from Vessel 2. 51
Figure 29. Bed erosion around Transect 2 due to 100% power from Vessel 2. 52
Figure 30. United Heckathorn hydrodynamic and sediment transport model domain and grid. 55
Figure 31. Tidal boundary conditions at the southern forced boundary of the model. 56
Figure 32. Locations of boundary condition data. 56

Figure 33. Water level comparison at mouth of Lauritzen Channel. Upper: Full study period. Lower: Zoomed in plot of boxed area in shown in the upper panel. 57
Figure 34. Distribution of mass at the sediment bed due to Vessel 1 parameters 1 day after release during maximum flood tide. Black Star denotes release point. 59
Figure 35. Distribution of suspended sediment due to Vessel 1 parameters 1 day after release during maximum flood tide. Black Star denotes release point. 60
Figure 36. Distribution of mass at the sediment bed due to Vessel 2 parameters 1 day after release during maximum flood tide. Black Star denotes release point. 61
Figure 37. Distribution of suspended sediment due to Vessel 2 parameters 1 day after release during maximum flood tide. Black Star denotes release point. 62
Figure 38. Distribution of mass at the sediment bed due to Vessel 1 parameters one day after release during a slack low tide event. Black Star denotes release point. 63
Figure 39. Distribution of suspended sediment due to Vessel 1 parameters one day after release during a slack low tide event. Black Star denotes release point. 64
Figure 40. Distribution of mass at the sediment bed due to Vessel 2 parameters one day after release during a slack low tide event. Black Star denotes release point. 65
Figure 41. Distribution of suspended sediment due to Vessel 2 parameters one day after release during a slack low tide event. Black Star denotes release point. 66

List of Tables

Table 1. YBM accumulation volume and mass in the Lauritzen Channel. 7
Table 2. Statistics for depth-averaged hydrodynamics and sediment parameters measured by instrumentation moored at the mouth and the head of the Lauritzen Channel. 15
Table 3. Sediment properties and critical shear stress by core interval measured during the Sedflume analysis. 28
Table 4. Statistics for hydrodynamic and sediment parameters collected within 1-m above the sediment bed at the mouth and the head of the Lauritzen Channel. 29
Table 5. Statistics for band-pass and low-pass filtered near-bottom shear stress. Data were from within 1-m above the sediment bed. 32
Table 6. Site-wide average values of sediment core properties from Sedflume analysis. 38
Table 7. Ship parameters used in the propeller wash and ship wake model. 39
Table 8. Maximum bottom velocity (m/s), maximum bed shear (Pa), maximum bed erosion (cm) and the average TSS concentration in Lauritzen Channel given different vessel and profile combinations for transiting case. 48
Table 9. Total sediment mass resuspended into system from Vessel 1 and Vessel 2 operating at different fractions of their maximum power when transiting from Manson to the mouth of the Lauritzen Channel. 49
Table 10. Stationary vessel scour analysis results. 53
Table 11. TSS values for sediment distribution analysis. 58
Table 12. Percentage of deposited sediment by location. 68

List of Appendices

Appendix A. Hydrodynamic Field Study
Appendix B. PARTRAC Sediment Tracking Study
Appendix C. Sedflume Analysis

List of acronyms used in the report

ABS: Acoustic Backscatter

ADCP: Acoustic Doppler Current Profiler

BPH: Brake Horsepower

CSM: Conceptual Site Model

DDT: Dichlorodiphenyltrichloroethane

DGPS: Differential Global Positioning System

EFDC: Environmental Fluid Dynamics Code

FFS: Focused Feasibility Study

FSP: Field Sampling Plan

LISST: Laser in Situ Scattering and Transmissometry

LRTC: Levin Richmond Terminal Corporation

MLLW: Mean Lower Low Water

NOAA: National Oceanic and Atmospheric Administration

OBM: Older Bay Mud

POTW: Publicly Owned Treatment Works

PSD: Particle Size Distribution

REE: Rare Earth Element

SEI: Sea Engineering Inc.

TPE: Transport Pathway Evaluation

TSS: Total Suspended Solids

USDA: United States Department of Agriculture

USEPA: United States Environmental Protection Agency

YBM: Younger Bay Mud

YSI: Yellow Springs Inc.

Executive Summary

Sea Engineering, Inc. (SEI) performed field and analytic activities to obtain hydrodynamic, water quality, and sediment data and to quantify sediment dynamics in the Lauritzen Channel of the United Heckathorn Superfund Site in Richmond, California. The field investigation involved measurements of system-wide current velocities, water quality, sediment characteristics and erosion rates, and a particle tracer study. Analytic activities included numerical modeling to elucidate the effects of ship wake and propeller scour and hydrodynamics on sediment transport processes.

A Tier 2 sediment transport conceptual site model (CSM) was developed from field and analytic results to address sediment management questions. The sediment management questions and findings are summarized below.

- What is the source(s) of the sediment accumulating in the Lauritzen Channel?

  The channel is low energy and provides an ideal environment for deposition of sediment. Results from the Tier 2 study indicate that the sediment accumulating in the Lauritzen Channel primarily originates from San Francisco Bay and that the local outfalls have minimal yearly averaged input.

- How does sediment transport lead to the redistribution of contamination within the Lauritzen Channel, or movement of contamination out of the channel?

  Vessel activity is the primary source of resuspension and redistribution in the Lauritzen Channel. The tidal velocities are very low throughout the channel, allowing for sediment deposition. The Tier 2 tracer study provided evidence of vessel resuspension and redistribution of sediment from the tracer locations to other areas throughout the channel. Vessel propeller scour analysis and numerical modeling showed that while a vessel can scour up to approximately 10 cm of sediment, greater than 90% of this sediment would settle locally. It can thus be inferred that redistribution of contamination would primarily be confined within the Lauritzen Channel. A portion of the material resuspended during an ebb tide could be transported out to the Santa Fe Channel; however, the study showed the mass to be limited (less than 7%).

- If part of the Lauritzen Channel is actively remediated, could sediment transport lead to the recontamination of the remediated area?

  Natural transport processes alone (e.g., tidal currents) would not lead to recontamination of remediated areas. However, high contaminant concentrations in locations with potential for disturbance by anthropogenic activities (e.g., vessel propeller or keel scour) could be redistributed to actively remediated areas.

This document presents the results of the Tier 2 sediment transport study. The results of the Tier 1 and Tier 2 studies will be evaluated in conjunction with the results of the source identification study, dichlorodiphenyltrichloroethane (DDT) fate and transport evaluation, long-

term monitoring data, and data from previous investigations to further refine the CSM for the site and support the development of remedial alternatives in the focused feasibility study.

1.0 Introduction

The United Heckathorn Superfund Site is located in Richmond Harbor on the east side of San Francisco Bay in Contra Costa County, California (Figure 1). From the mid-1940s to the mid-1960s, the site was used for processing, packaging and shipping pesticides. Although many types of pesticides were processed on the site, DDT[1] and Dieldrin are the primary contaminants of concern. The remedy selected for the marine portion of the site in the 1994 Record of Decision (United States Environmental Protection Agency (USEPA), 1994) consisted of dredging and offsite disposal of sediment from the Lauritzen Channel and Parr Canal, followed by at least five years of post-remediation monitoring. The remedy for the upland part of the site included capping and institutional controls. The remedies for the marine and upland portions of the site were completed in 1997 and 1999, respectively. Post-remediation monitoring data indicate that sediments in the Lauritzen Channel still have unacceptably high levels of DDT and Dieldrin (Anderson, et al., 2000; Antrim & Kohn, 2000). A focused feasibility study (FFS) is being performed to address residual contamination in the channel sediment.

The amounts of sediment and sediment-associated DDT that are being transported into and out of the Lauritzen Channel and redistributed within the Lauritzen Channel are not known. A study of sediment dynamics in the Lauritzen Channel has been performed because (1) sediment has accumulated in the channel since the remedy was completed; (2) surface and subsurface sediment DDT concentrations are above the remediation goal; (3) the source(s) of the sediment and sediment-associated contamination have not been definitively identified; and (4) additional cleanup cannot occur until any active, ongoing source(s) are controlled.

The sediment transport analysis was performed using a phased (tiered) approach as described in the U.S. Navy's *User's Guide for Assessing Sediment Transport at Navy Facilities* (Blake, Chadwick, White, & Jones, 2007). In a Tier 1 study, sediment transport is assessed using basic site characterization data (e.g. bathymetric surveys, tidal ranges, sediment contaminant data) and analyses to address sediment management questions. A Tier 1 Study was completed in April 2013 (Sea Engineering Inc, 2013).

This document presents the results of the Tier 2 sediment transport study developed from the results of the Tier 1 study. The Tier 2 study focused on collection of site-specific data and more refined data analyses, including the use of analytical and numerical methods as outlined in the Field Sampling Plan (FSP) for the Tier 2 sediment transport study (CH2M HILL; Sea Engineering Inc., 2013). The results of the Tier 1 and Tier 2 studies will be evaluated in conjunction with the results of the source identification study, DDT fate and transport evaluation, long-term

[1] Dichlorodiphenyltrichloroethane; for the purposes of this report, "DDT" refers to the sum of all 4,4'- and 2,4'- isomers of DDT, DDD, and DDE. Dieldrin is present at lower concentrations but co-occurs with DDT; therefore, the report focuses on DDT.

monitoring data, and data from previous investigations to refine the conceptual site model (CSM) for the site and support the development of remedial alternatives in the FFS.

The primary goals of the overall sediment transport study are to address the following sediment management questions:

- What is the source(s) of the sediment accumulating in the Lauritzen Channel?
- How does sediment transport lead to the redistribution of contamination within the Lauritzen Channel, or movement of contamination out of the channel?
- If part of the Lauritzen Channel is actively remediated, could sediment transport lead to the recontamination of the remediated area?

Due to the complexity of the processes affecting sediment and contaminant transport in the Lauritzen Channel, multiple lines of evidence were used to fully address the management questions. The Tier 2 sediment transport study characterizes the sediment erosion/resuspension and transport processes in Lauritzen Channel as follows:

- Hydrodynamic data, suspended solids, particle tracking, and sediment bed data were analyzed to determine transport and potential recontamination within the Lauritzen Channel. The analysis provided a key input to the FFS.
- Erosion potential was assessed using a propeller scour model to quantify sediment mixing depths and volumes during typical vessel operations. Model calibration and validation were accomplished using the bathymetric, sediment erosion, and suspended solids data.
- Sediment resuspension, transport, and deposition were modeled for the study site using the hydrodynamics model, Environmental Fluid Dynamics Code (EFDC). EFDC determined spatial and temporal patterns of resuspended sediment and associated contaminant transport in the Lauritzen and Santa Fe Channels. The primary goal of the modeling was to determine transport and deposition patterns of material resuspended during various anthropogenic events.
- The quantitative model was coupled with the analysis of the field data to refine the CSM and help provide answers to sediment management questions. The updated quantitative sediment and contaminant fate and transport CSM can guide the remedial alternative development and analysis in the FFS.

The Tier 2 evaluation uses data from previous investigations at the United Heckathorn site, field measurements from the summer of 2013 led by Sea Engineering, Inc. (SEI), and specific modeling analyses. This report is organized as follows:

- Site Description
- Tier 2 Field Efforts
- Sediment Transport Analysis
- Refined Sediment Transport CSM and Sediment Budget
- Summary and Sediment Management Questions

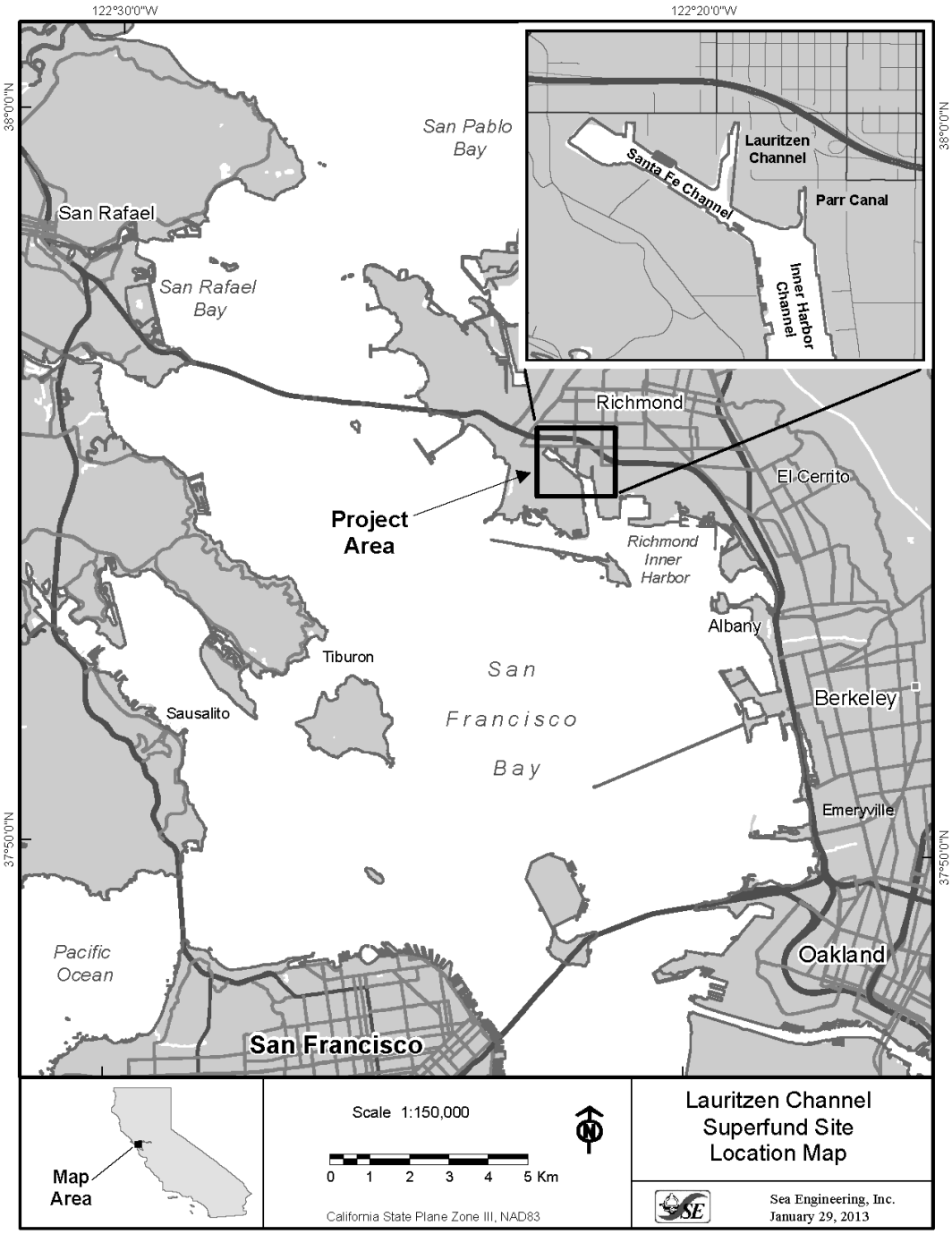

Figure 1.Location of Richmond Harbor.

2.0 Site Description

The Lauritzen Channel is a tidal waterway inside the Richmond Harbor on the eastern shoreline of central San Francisco Bay, California, USA. The Lauritzen Channel is a single spur inside the Richmond Harbor off of the Santa Fe Channel (Figure 1). The harbor was originally intertidal marsh that was dredged and filled in the 1920s to provide a deepwater berthing area for commercial and private vessels (White, Kohn, Gardiner, & Word, 1994). An extensive offshore breakwater provides protection from waves generated in the central San Francisco Bay and beyond. The tidal range in the harbor is approximately -0.6 to 2.1 m Mean Lower Low Water (MLLW). The shorelines of the harbor are generally armored with rip-rap, sandy gravel fill, or pile-supported structures (White, Kohn, Gardiner, & Word, 1994). The upland regions surrounding the harbor are generally level and at heights of 2.1 to 3.3 m MLLW. The Lauritzen Channel is approximately 0.5 km long and 40 m wide at the head widening to over 100 m at the mouth. The depths in the channel range from 3 to 12 m MLLW (Figure 2). Presently, Manson Construction Company occupies the western shoreline and the Levin Richmond Terminal occupies the eastern shoreline.

The most recent maintenance dredging of the Lauritzen Channel occurred in 1985. Between August 1996 and 1997, approximately 107,945 cubic yards of total sediment were removed from the Lauritzen Channel and the Parr Canal during remediation activities. Of the total amount, 105,325 cubic yards were removed from the Lauritzen Channel. The sediment was disposed of offsite at designated disposal facilities. Clean sand was placed to a nominal thickness of 6 inches over dredged portions of the Lauritzen Channel to facilitate colonization by benthic organisms (Chemical Waste Management Inc, 1997). A thicker layer of sand (approximately 18 inches) was reportedly placed in inaccessible areas that were impractical to dredge (i.e., areas with pilings). No sand was placed underneath the Levin pier because the slope was too steep to hold sand. The sand was hydraulically pumped from a barge into the channel. A bathymetric survey was performed after sand placement was completed; however, the distribution and thickness of the sand layer do not appear to have been verified. No other dredging activities have been conducted in the Lauritzen Channel since 1997.

A December 2012 site survey documented a number of small outfall pipes on the banks of the Lauritzen Channel (CH2M HILL, 2013(a)). One 1.5 m diameter concrete culvert at the northern end of the channel is a City of Richmond municipal outfall that provides the primary storm drainage from the surrounding area into the channel. Storm water runoff from the upland remediated area of the United Heckathorn site is monitored and discharged to City of Richmond publicly-owned treatment works (POTW). In October 2012, EPA installed a flap gate on the municipal outfall at the head of the channel to prevent DDT-contaminated sediment from moving into the storm drain system during high tide. The outfalls are described in detail in the *Source Identification Study Report* (CH2M HILL, 2013(b)).

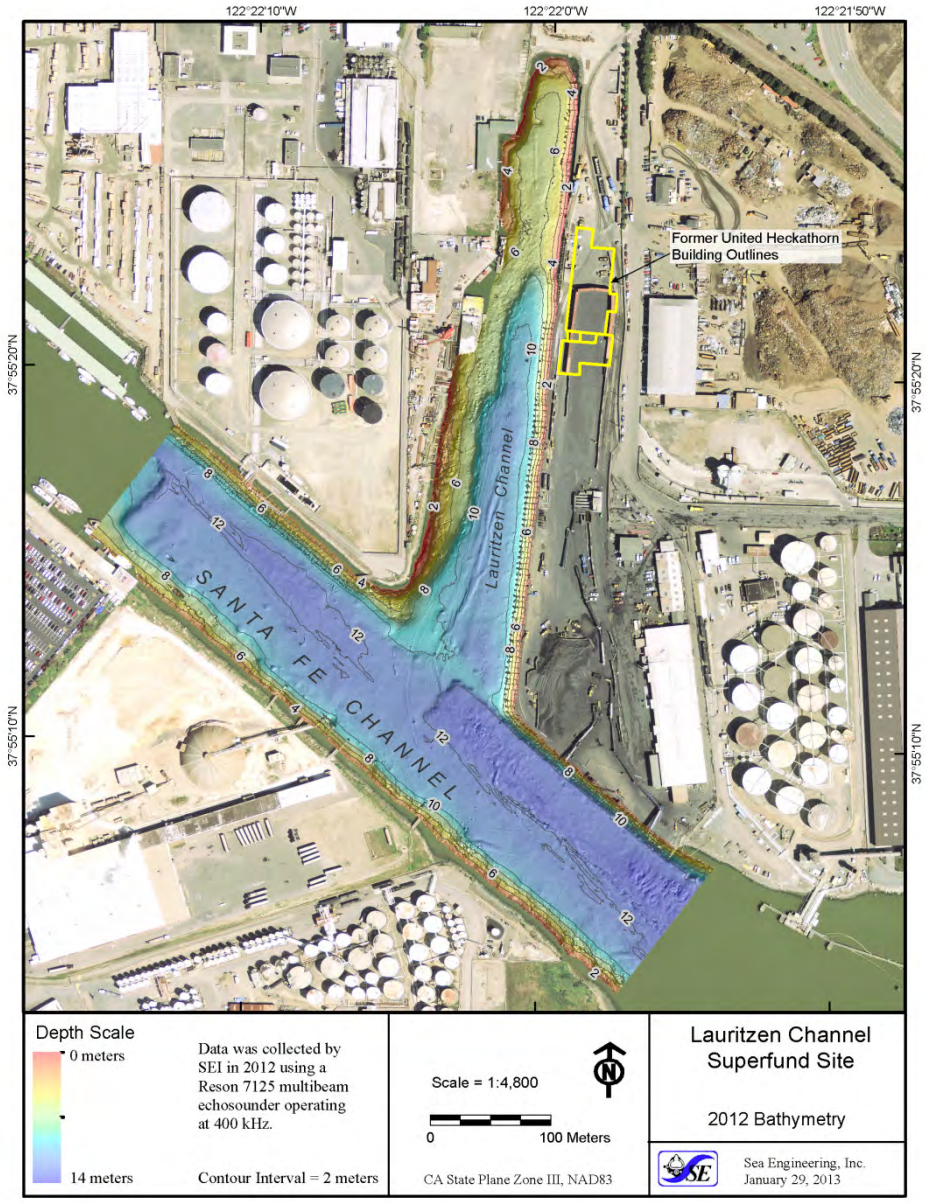

Figure 2. Bathymetric map of the Lauritzen Channel and surrounding Santa Fe Channel.

2.1 Sediment Bed

In 2012, SEI conducted high resolution multibeam bathymetric and sidescan sonar surveys to characterize the present state of the bottom sediment in the Lauritzen Channel. Figure 2 shows the results of the bathymetric survey. The survey clearly shows the extents of the dredged channel adjacent to the Levin terminal (Berths B and C), the shallower regions at the head of the channel, and the deeper dredged channels in the Santa Fe Channel with the deepest area on the south side of the Levin terminal (Berth A) to accommodate the largest ships in this portion of the Santa Fe Channel.

The bathymetric and side scan sonar surveys reveal features that form in response to processes occurring at the channel bottom. Features typical of scour by a vessel propeller or the keel of a vessel dragging along the bottom (i.e. linear furrowing) are evident in the survey. Further south in the channel, these linear furrow features become more evident, particularly in the deeper dredged channel. In the region of higher ship and associated tug activity near the Manson Construction and Levin facilities, there are more scour features. Of additional note are the "crater" features near the Manson facility. When Manson brings large crane barges into this area, the large vertical spuds are dropped into the sediment to anchor the barges in place. The craters are the bottom expression due to these spuds. Figure 3 provides delineation of these features by type developed as part of the Tier 1 analysis. The effects of these processes on sediment fate and transport are discussed later in this report.

Bathymetric survey data were used to characterize sediment accumulation in the Lauritzen Channel after remedial dredging was completed in 1997. Multiple partial bathymetric surveys were conducted between 1998 and 2007. These surveys were conducted using a lower resolution single beam surveying system and supporting detailed information regarding the survey procedures (e.g. survey equipment, benchmarks) is not available. However, comparison of bathymetric change was conducted to ascertain large changes in sediment bed elevation. Figure 4 shows the changes in the channel bed elevation between the 2007 and 2012 surveys. Overall, sediment accumulation is seen in the deep dredged berth near the Levin terminal. The shallower regions adjacent to the Manson facility show apparent sediment erosion. The northern portion of the channel generally exhibits sediment accumulation with some regions of erosion. While useful in visualizing general trends in accumulation, the uncertainty in the absolute elevations of these surveys does not allow for direct calculation of volume of sediment accumulated in the Channel.

Accumulation rates can be determined from the Younger Bay Mud (YBM) thickness identified in individual cores from coring efforts in 1999, 2003, 2007, and 2013[2]. The accumulated YBM volume is assumed to be representative of the new sediment accumulation since dredging for the datasets after the 2001 period. It is unknown what portion of the YBM represents new deposition prior to 2001. Multiplying the YBM thicknesses in the individual cores by the average solids densities of those cores provides a mass per unit area. By generating spatially-interpolated surfaces of thickness and density, sediment mass can be determined for each time period. The calculated sediment volumes and masses are shown in Table 1. On average, between 2001 and 2013, the channel experienced approximately 3,600 cy/year (2,752 m^3/yr) of sediment accumulation. Figure 5 shows the YBM mass interpolated over the channel. The northern end of the Levin berth has experienced the highest accumulation. One region near the shore of the Manson facility shows high YBM accumulation and the northern end of the channel shows moderate YBM accumulation. The northern shoreline of the Manson facility

[2] The 1999/2003 data were combined for analysis because the 2003 cores were intended to fill spatial data gaps in the 1999 core locations. The combined data set is referred to as 2001.

shows the lowest YBM accumulation consistent with the highest regions of disturbance (Figure 3).

Table 1. YBM accumulation volume and mass in the Lauritzen Channel.

Year	YBM Volume (cy)	YBM Volume (m^3)	YBM Mass (kg)
2001	22,862	17,467	15,731,336
2007	38,292	29,255	26,319,230
2013	66,163	50,549	45,478,880

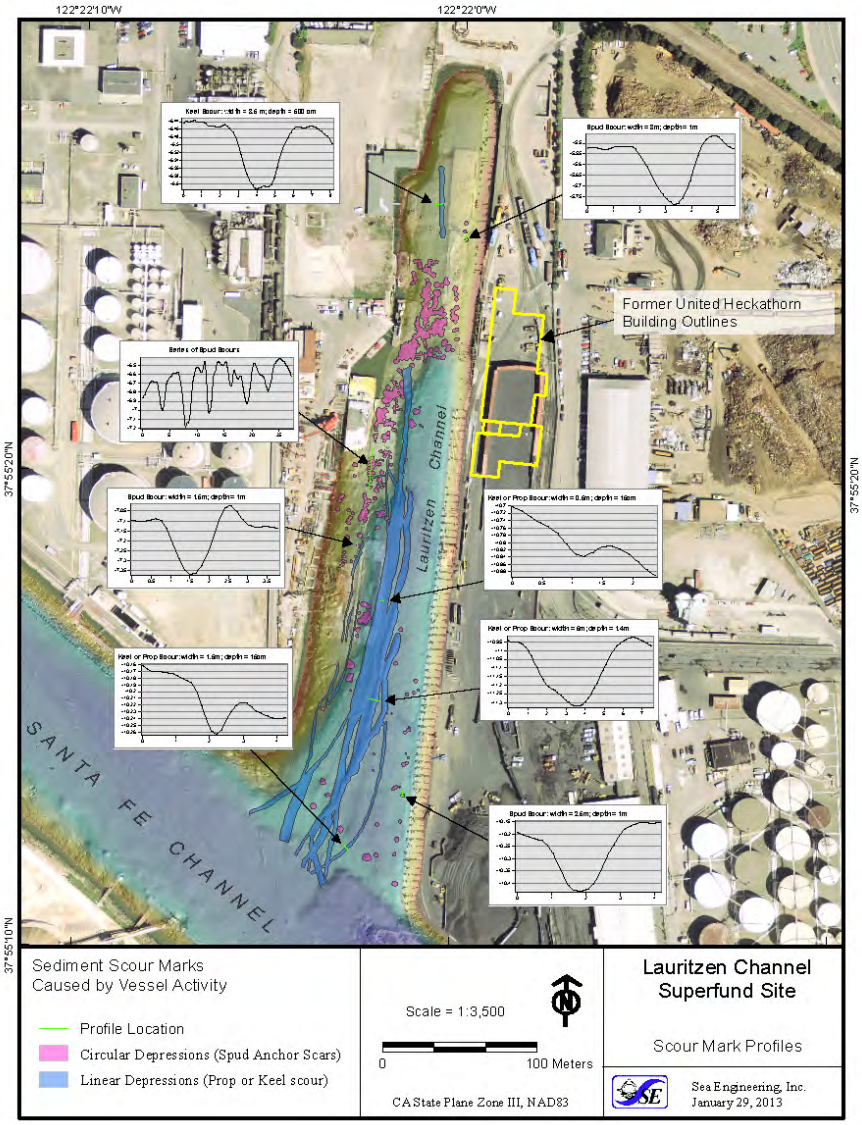

Figure 3. Sediment disturbance due to vessel activity.

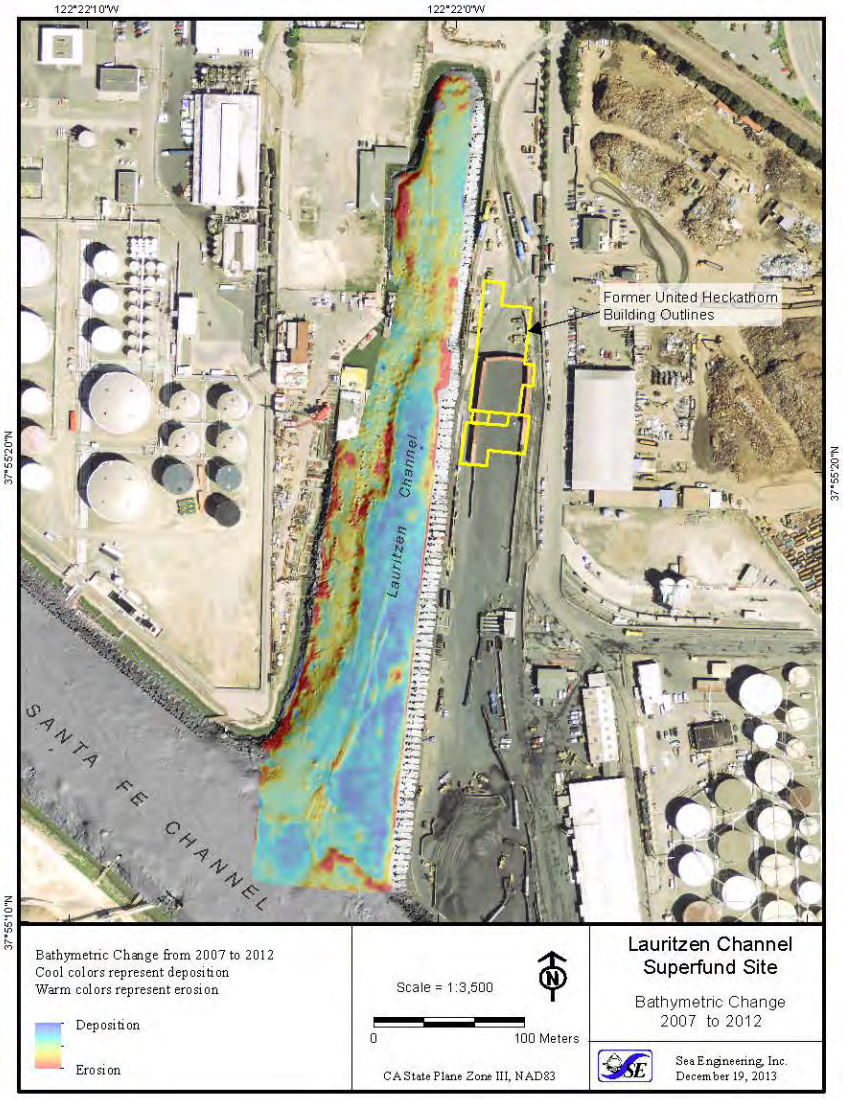

Figure 4. Bathymetric Change from 2007 to 2012.

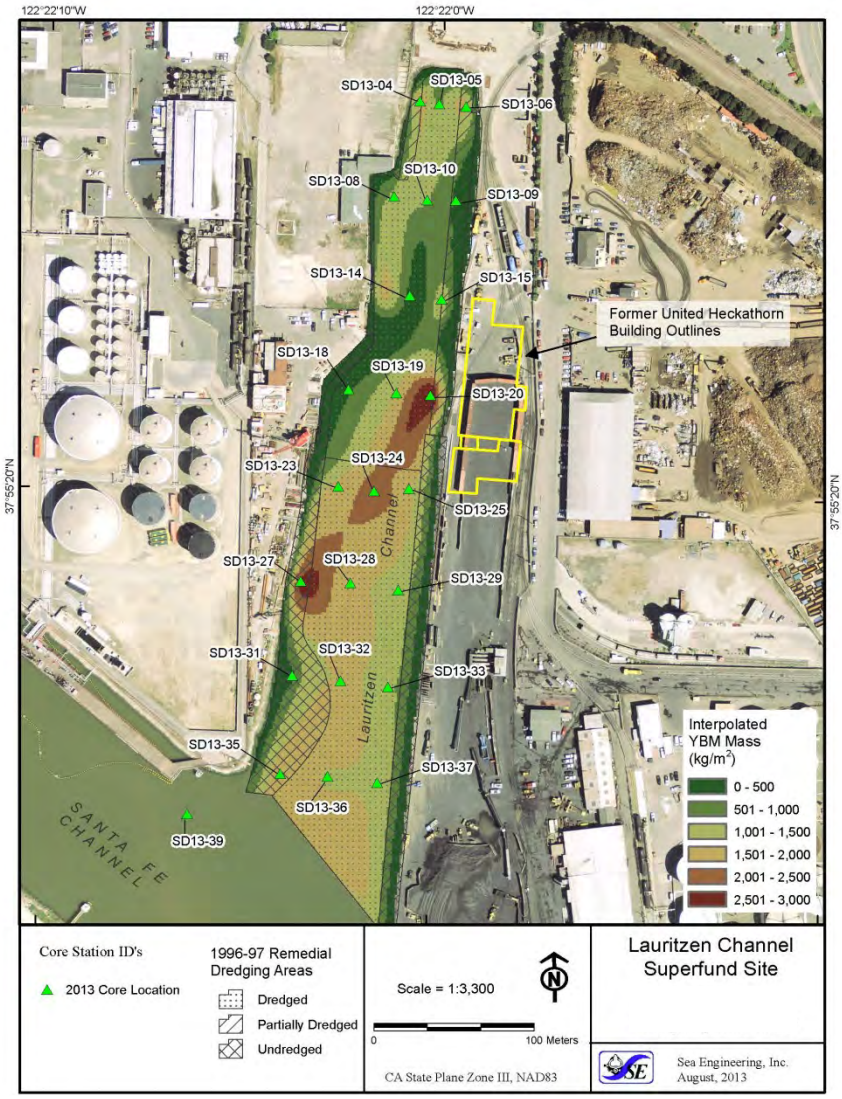

Figure 5. Younger Bay Mud Mass in 2013.

2.2 Tidal Hydrodynamics

The Lauritzen and Santa Fe Channels are manmade features designed to provide low energy environments for vessel berthing. The region is further protected from San Francisco Bay by an extensive offshore breakwater designed to block any waves into the area. In low energy protected harbors such as these channels, regional sediments tend to accumulate in the dredged channels. The deeper dredged channels in Richmond Harbor overall have historically required periodic dredging due to the generally depositional environment.

The Lauritzen Channel is dominated by the tidal hydrodynamics of San Francisco Bay. The region experiences a semi-diurnal tide from the Pacific Ocean. The tide generally results in two high and two low tides per day with a dominant tidal period of 12.42 hours (M2 semi-diurnal tidal constituent). Figure 6 shows an example of the local semi-diurnal tides. The average yearly tidal range in the harbor is approximately -0.6 to 2.1 m MLLW. Wave activity in the channel is negligible due to the offshore protection. Additionally, the narrow nature of the channels and relatively deep water negate the effects of any wave generation within the channels on hydrodynamics or sediment transport. The characteristics of the channels support the tidal dominance on circulation in the Lauritzen Channel.

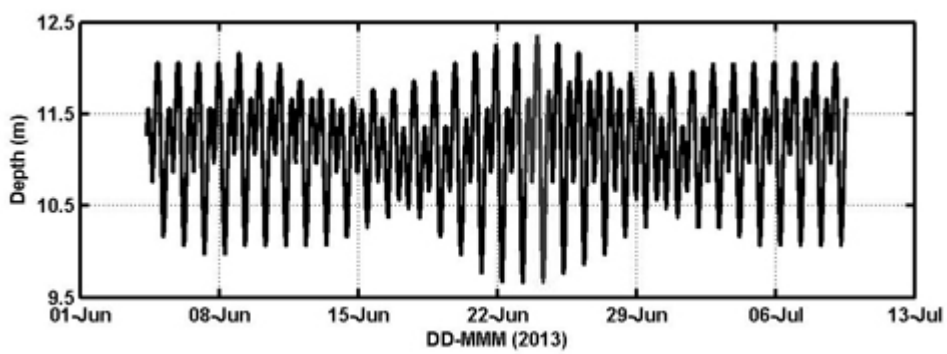

Figure 6. Example pressure data illustrating semi-diurnal tidal variability.

Determining the movement of water particles and their residence times in a tidal system can be calculated using a few characteristic values. The residence time is the most basic calculation. The Tier 1 analysis indicated that a parcel of water could remain in the Channel for approximately 2.5 days before being exchanged. For a small channel such as the Lauritzen, this is a fairly long residence time and the Channel could be considered to have low circulation.

Given the cross sectional area at the mouth of the channel and the tidal prism, the maximum tidal velocity in the Lauritzen Channel can be calculated. In the Tier 1 analysis, an average maximum velocity of approximately 1 cm/s was calculated as the depth-averaged velocity over the cross-section. Locally higher velocities can be driven by currents in the Santa Fe Channel, winds, and/or by abrupt changes in bathymetry; however, the basic analysis suggests that velocities are very low in the Lauritzen Channel.

For fine silt and clay such as the sediment in the Lauritzen Channel, a screening value of 0.1 Pa is commonly used for both the critical shear stress for erosion and deposition (Blake et al., 2007). A velocity of 1 cm/s generates a negligible shear stress; therefore, erosion due to the average tidal current is not expected. Furthermore, the low tidal shear stresses would allow sediment particles transported into the region to settle out. The deposition rates would be particularly high in the deepest, lowest velocity areas. Section 3 provides further details of the Tier 2 field studies developed to address sediment resuspension potential.

2.3 Anthropogenic Processes

The Lauritzen and Santa Fe Channels are active waterways with ship and barge berthing activities that have the potential to affect sediment transport patterns. In general, both transiting vessels and stationary vessels pushing against an object (pier or barge) can mobilize sediment. The potential for sediment transport in the Lauritzen Channel due to propeller scour is evaluated in Section 4.2.2.

3.0 Tier 2 Field Efforts

The purpose of the Tier 2 Sediment Transport Study field efforts was to further quantify the key processes involved in sediment transport in the Lauritzen Channel as informed by the Tier 1 analysis and with particular emphasis on the management questions. Specific project objectives and studies to address these objectives are listed below.

- Erosion potential of sediment due to natural and anthropogenic processes.
    - Tracer Study
    - Sedflume Analysis
- Magnitude and frequency of sediment resuspension and the magnitude and direction of net sediment flux.
    - Hydrodynamic and Water Quality Data Collection
    - Tracer Study
- Quantity of sediment transport in areas of high vessel activity.
    - Hydrodynamic and Water Quality Data Collection
    - Tracer Study

These studies are outlined in the following sections.

3.1 Hydrodynamic and Water Quality Data Collection

The primary objective of the hydrodynamic data collection was to determine the magnitude of tidal velocities in the system, identify sediment resuspension events, and determine the magnitude and direction of sediment flux. The following section outlines the field measurements.

3.1.1 Methods

SEI deployed two bottom-mounted mooring platforms, each equipped with a Teledyne RDI 1200 kHz Workhorse Sentinel Acoustic Doppler Current Profiler (ADCP) and a Yellow Springs, Inc. (YSI) water quality sonde with temperature, pressure, and optical turbidity probes (Figure 7). The ADCPs were mounted "uplooking" on bottom-mount platforms and programmed to collect data every 10 minutes at a vertical cell spacing of 0.25 m. The water quality sondes were fixed to the bottom-mount platforms. Water quality data were collected every 15 minutes at a height of 0.5 m above the seabed. The two instrumented platforms were deployed at the mouth and near the head of the Lauritzen Channel in approximately 11 m and 7 m mean water depth between 4 June and 9 July 2013 (Figure 8).

Figure 7. Bottom-mount platform with ADCP and YSI water quality sonde indicated.

Figure 8 Location of ADCP Platforms and Transects

Water samples for analysis of total suspended solids (TSS) were collected for the purpose of relating moored backscatter time series data to analytical TSS data over a range of tidal conditions. Water column profiles of particle size distribution (PSD) from surface to about 0.5 m above the bed were also collected near the two bottom-mounted platforms using a LISST-100X, type C. PSDs were measured between approximately 3 μm and 280 μm. The median particle diameter (D_{50}), 10th percentile (D_{10}), 90th percentile (D_{90}), and cumulative volume particle size distributions were computed from Laser in situ Scattering and Transmissometry (LISST) data.

A “downlooking” ADCP was mounted on the port side of the vessel and measured the spatial distribution of the vertical current profile in the system concurrently with a differential global positioning system (DGPS) for sub-meter scale location accuracy. The vessel-mounted ADCP was programmed to collect data at 0.25 m vertical bins. ADCP surveys were conducted on 4 and 5 June and 8 and 9 July 2013 following the three transect lines indicated in Figure 8. The ADCP transects were conducted in both directions (i.e. back and forth) across each transect line to reduce directional bias in the data.

Current meter and acoustic backscatter (ABS) data from the moored and mobile (i.e. vessel-mounted) ADCPs were used to calculate sediment flux at the mouth and head of the Lauritzen Channel. Sediment flux is generally defined as the product of flow rate, Q (units of volume per time), and TSS (units of mass per volume):

$$F = Q * TSS \qquad \text{Eq. 1}$$

where flux is represented by F and is in units of mass per time. TSS as a function of time and depth was derived from ADCP measured ABS (Downing, Thorne, & Vincent, 1995; Shulkin & Marsh, 1962; Thorne, Vincent, Hardcastle, Rehman, & Pearson, 1991; Gartner, 2004)). Briefly, ABS was computed from the ADCP-measured echo intensity (EI) following:

$$ABS = 10 \log_{10}(EI) + BS + WA \qquad \text{Eq.2}$$

where BS is the two-way transmission loss due to beam spreading and WA is the correction for the acoustic absorption of water. ABS was related to TSS determined in the laboratory from collected water samples, collocated with the ADCP.

Flow rate as a function of time and depth was obtained by correlating cross-channel flow rate measured by the vessel-mounted ADCP with current velocity measured by the moored, bottom-mounted ADCP at specific times of data collection. Least-squares linear regression analysis was employed to quantify the depth-dependent relationship between cross-channel flow rate, Q(z), and moored current velocity, U(z) for each of the 18 transects:

$$Q(z) = m(z) * U(z) + b(z) \qquad \text{Eq.3}$$

where m(z) and b(z) are the depth-dependent slope and y-intercept of the best-fit lines between Q(z) and U(z) at each bin, z. The slopes and intercepts, m(z) and b(z), were then applied to moored current velocity signals to derive time series of flow rate as a function of depth, Q(z). Sediment flux was computed as the product of Q and TSS.

More details regarding hydrodynamic and water quality data collection and results can be found in Appendix A.

3.1.2 Results

Measured current velocities were generally very low and varied with tidal oscillations (Figure 9). Current velocities were typically higher near the surface. Infrequent increases in current velocity were observed near the sediment bed. These maximal peaks in velocity extended from the bottom throughout the water column. Similar patterns were observed at both moored platform locations. The time-averaged depth-averaged velocity magnitude over the period of deployment was near 0.01 m/s at both the mouth and the head of the Lauritzen Channel (Table 2).

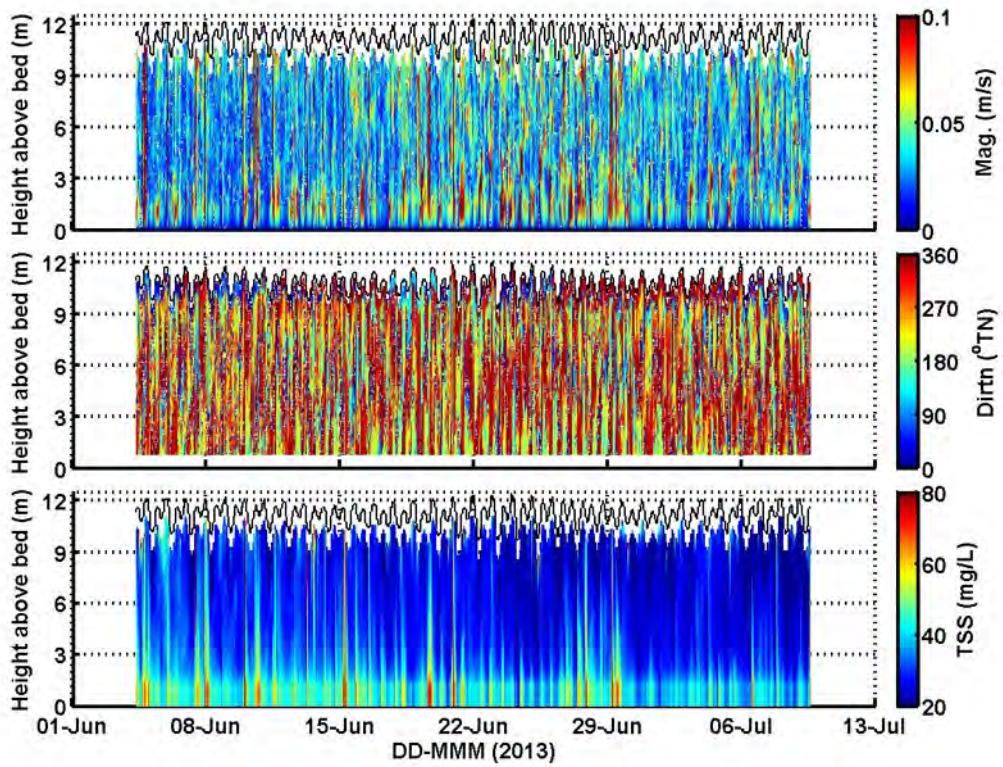

Figure 9. Current velocity (upper), current direction (middle), and TSS (bottom) as a function of time and height above the sediment bed measured at the mouth of the Lauritzen Channel. Water depth is indicated with solid black lines.

Table 2. Statistics for depth-averaged hydrodynamics and sediment parameters measured by instrumentation moored at the mouth and the head of the Lauritzen Channel.

	Mean	Minimum	Maximum	Standard deviation
Mouth				
Current velocity (m/s)	0.01	0	0.24	0.01
TSS (mg/L)	29.7	20.1	92.8	5.0
D_{10} (μm)	8.1	5.3	61.6	2.84
D_{50}(μm)	41.7	9.4	196.8	20.0
D_{90}(μm)	153.3	25.8	277.2	53.0
Head				
Current velocity (m/s)	0.006	0	0.10	0.004
TSS (mg/L)	22.7	15.4	70.2	3.1
D_{10} (μm)	7.15	5.3	118.0	5.5
D_{50}(μm)	36.0	10.3	179.8	20.2
D_{90}(μm)	141.9	26.8	282.7	50.5

Similar to most systems, TSS increased from minimal values at the surface to greater concentrations at the sediment bed. TSS appeared to vary with tidal oscillations and exhibited intermittent, high frequency spikes in concentration that decreased from high values at the bed to lower values near the surface (Figure 9). Time-averaged, depth-averaged TSS was greater at the mouth (29.7 mg/L) than at the head (22.7 mg/L) of the Lauritzen Channel (Table 2). Particle diameters were greater at the mouth as well; time-averaged, depth-averaged D_{50} was 41.7 μm at the mouth and 36.0μm at the head of the channel (Table 2). The LISST measures the size of the in-situ particles in the water column including flocculated and unflocculated particles.

Sediment flux was minimal, as expected given the extremely low current velocities recorded in the Lauritzen Channel. Sediment flux variability, like current velocity, oscillated with the tides such that daily averaged sediment flux was negligible at both the mouth and head of the Channel (Figure 10). The total daily averaged sediment flux over the 34 day mooring deployment period was near zero kg/s at both locations. The near zero sediment flux was observed during a one-month dry period. Overall net accumulation in San Francisco Bay typically occurs during the wet fall and winter periods.

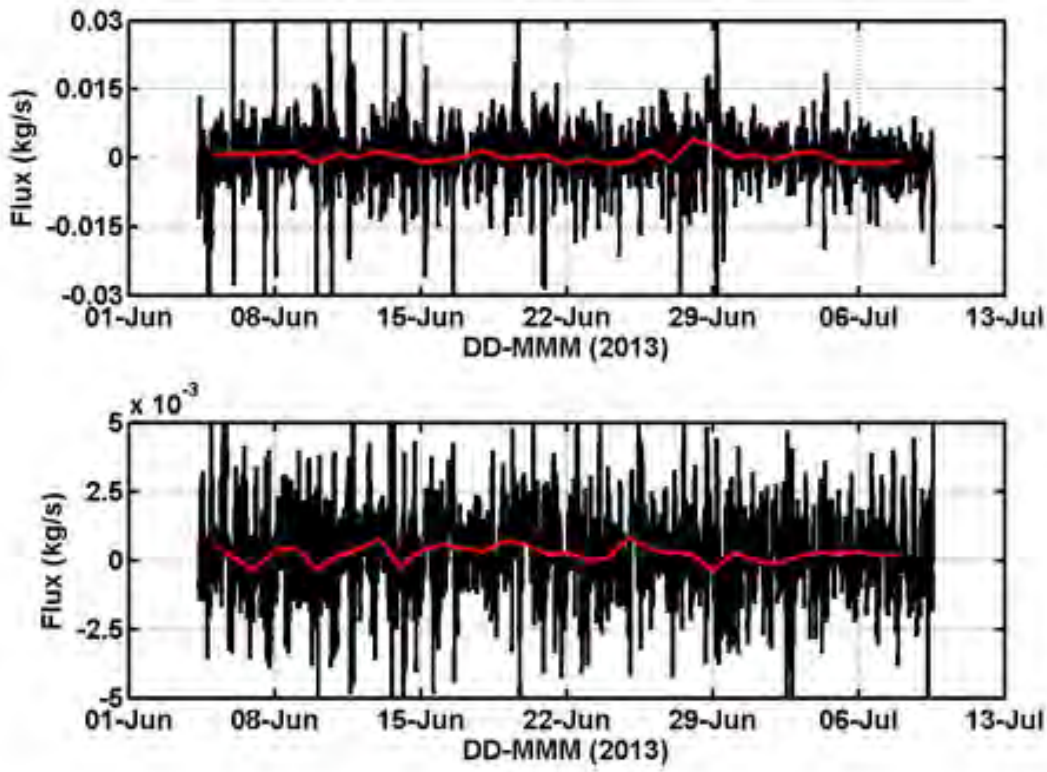

Figure 10. Time series of sediment flux derived from mid-water column ADCP measurements at the mouth (upper panel) and head (lower panel) of the Lauritzen Channel. The red lines indicate daily averaged sediment flux.

3.2 Tracer Study

Partrac Ltd. was contracted by SEI to provide sediment particle tracking services for the United Heckathorn Superfund Site to assess the fate of bottom sediment impacted by tidal currents and velocities associated with local propeller wash. Partrac developed a dual signature silt tracer of two colors (green and red). Tracer masses of 175 kg for each color were released in the form of low profile, frozen blocks onto the seabed at two locations in the central region of the Lauritzen Channel. Assessment of the mobilization and transport of the silt particles was achieved through the use of powerful, in situ moorings of permanent magnets and collection of sediment grabs. This methodology is otherwise known as Transport Pathway Evaluation (TPE).

TPE is a method in which a sediment transport pathway is visualized using a mass of uniquely labeled fluoro-magnetic (tracer) particles (White T. , 1998) . Tracer particles are released into the environment and subsequent capture of these particles in space and/or time provides information on the localized transport direction and rate (Black, Wilson, & Evans, 2007). TPE experiments require the manufacture of sediment analogues called 'tracers', which behave in a

similar way as native sediment. Partrac manufactures tracers with two unique signatures associated with every tracer grain – fluorescent color and magnetic character. These characteristics enable identification and extraction of tracers from environmental samples with the use of powerful (11,000 Gauss) bar-type magnets. Rarely are environmental particles found which are both fluorescent in color and magnetic; this thereby provides a firm foundation for the use of 'dual signature' tracers in tracking the movement of sediment.

A tracer specification for use in the studies was developed from particle size distributions reported in the Tier 1 study. The tracer specifications were:

- Size range: coarse-medium silt tracer (ca. 20 – 70 μm)
- Density: mineral density (~2300 – 2900 kg m^{-3})
- Color; 2 fluorescent colors (red: green)
- Para-magnetic[3] attribute
- Quantity (kg): 175 kg x 2 (red: green)

Partrac manufactured two 175 kg tracer batches of differing color (red and green) according to this specification. The tracers met a series of underlying assumptions (see (Foster, 2000)):

- The tracer's hydraulic and bio-organic properties mimic those of the sediment of interest and therefore the tracer is transported in the same fashion as the native sediment.
- The tracer does not change properties through time (at least over the timescales of interest) and can be monitored.
- The tracer does not manifestly change the transporting system in any way.

Appendix B summarizes the characterization tests performed on the tracer.

3.2.1 Study Implementation

The tracer was delivered to SEI's office in 25 kg batches in moist form. During manufacture about 10-15% by mass seawater was added to each batch principally to reduce in advance surface active effects associated with the tracer, which substantially simplifies tracer deployment. It also saves time in the field as it means that the tracer batches, as delivered, can be frozen directly without intervention or addition of additional seawater. All delivered tracer was frozen for 2.5 days at 9°F. During this time small sub-samples of tracer were taken as archive samples.

A background site survey was undertaken as part of the TPE/sediment particle tracking methodology. The purpose of the background survey was to establish several conditions:

[3]Paramagnetism is a form of magnetism whereby the paramagnetic material is only attracted when in the presence of an externally applied magnetic field.

- The nature, and typical mass, of naturally magnetic (but non-fluorescent) particulates in the water column; this information is of generic use in regard to the use of suspended magnets to collect magnetic tracer material.
- The nature, and typical mass, of naturally magnetic (but non-fluorescent) particulates in the bedded sediment; this information is of generic use in regard to the analytical methodology used to determine tracer dry mass in sediment samples.
- The abundance, if any, of naturally occurring magnetic *and* fluorescent particulates at the site.
- The need to collect sediment material for use in preparation of standard curves within the analytical methodology.

The site survey utilized a suspended magnet and bottom sediment grab samples (1 upstream of the tracer drop zone, 1 downstream) prior to deployment of tracers on 13 June 2013.

3.2.2 Deployment

On 13 June 2013, each batch of the tracer was deployed. Frozen tracer blocks were rolled onto a tarpaulin sheet and wrapped up by rolling the sheet over the block several times (this minimized contact of the block with seawater on the way to the seabed); two operators then attached ropes to eyelets at the corners of the tarpaulin and gently and slowly lowered the block to the seabed. Once it was on the seabed the tarpaulin was then unrolled slowly leaving the block to slide onto the surface of the seabed. The tarpaulin sheet was then slowly recovered. The locations for each of the patches of the tracer deployed are presented in Figure 11.

Powerful cylindrical rare earth element (REE) magnets, either short (0.3 m; 1 foot) or long (0.6 m; 2 feet) in length, were utilized in this experiment. These were encapsulated in plastic sheaths with end caps and integrated on a mooring line suspended ~1 m and ~2 m above the bed. For 8 of the 12 the magnet moorings, a long magnet (0.6 m) was positioned near the bed (~1 m above the bed), and a short magnet positioned ~1 m above this. The remaining 4 of the 12 utilized two short magnets connected at ~1 m above the bed. In total, 12 magnet moorings were deployed largely around the periphery of the Lauritzen Channel (locations shown in Figure 11). The peripheral locations of the magnet moorings, while not optimal from a sampling standpoint, were necessary so as to not interfere with potential vessel traffic during the study.

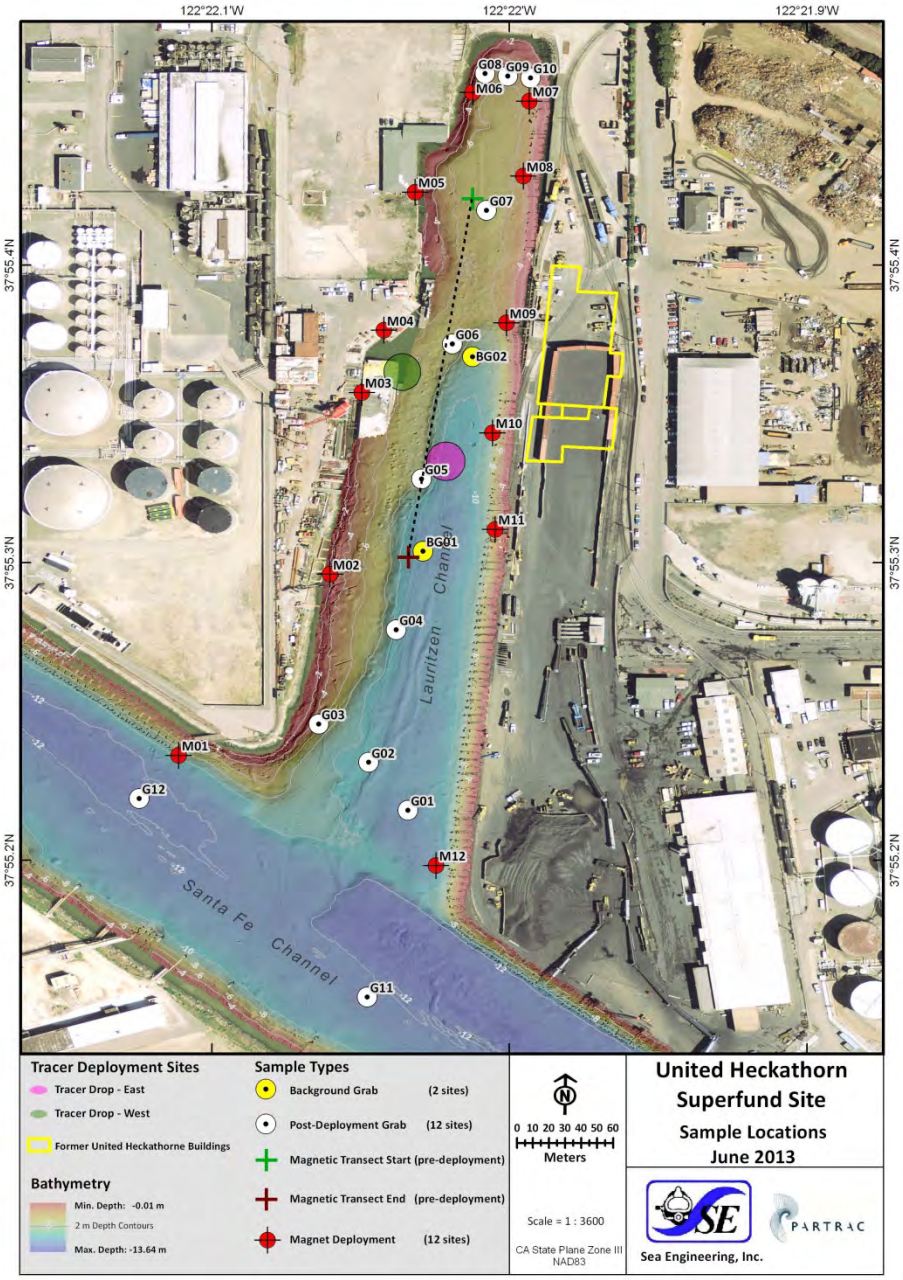

Figure 11. Magnet moorings and grab sampling locations.

3.2.3 Sampling

Sampling was conducted according to the following schedule:

- Day 0 (*t* = 0; 13 June 2013)
- Day 1 (*t*= ~24 hours; 14 June 2013)
- Day 2 (*t* = ~48 hours; 15 June 2013)
- Day 4 (*t*= ~76 hours; 17 June 2013)

- Day 6 (*t* = ~120 hours; 19 June 2013)
- Day 14 (*t* = ~336 hours; 25 June 2013).

All the magnets were serviced and grabs of bed sediment at a series of pre-determined locations (Figure 11) were collected following the scheduled outlined above. Servicing of the magnets involved recovery of the mooring line, careful removal of the sheath of each magnet, and transfer of the sheath to a sample bag, followed by installation of a new clean sheath. The magnet moorings were recovered from the water on Day 14.

Grab samples of bed sediment were collected with a small petit-ponar-style grab. Upon recovery, each sample was inspected to assess that the suitable sample had been retrieved and the surface material of the grab sampler to a depth of 2-3 cm was scooped off with a stainless steel spoon and transferred to a labeled sample bag.

3.2.4 Results

Samples were analyzed according to Partrac procedures outlined in Appendix B. Standard (dose response) curves were developed to relate fluorimetric measurements taken on each sample to tracer dye concentration over the range of dry masses (0 – 1 g) as follows: (0.0 g; 0.1 g; 0.2 g; 0.3 g; 0.4 g; 0.5 g; 0.6 g; 0.7 g; 0.8 g; 0.9 g and 1 g)(Figure 12). Results and qualitative visual descriptions (inspection under black light) are given for every sample in Appendix B.

Figure 12 shows the results of the recovered mass from the periodic sampling during the tracer study. Generally, tracer detected on the magnets (samples along the channel sides) showed material that had been resuspended and transported to a particular magnet between each deployment. The magnet sheaths were replaced between each sampling event. The grab samples (samples designated with a G) showed material that had accumulated at the sampled location since tracer deployment on day 1. It is important to note that the grab sample locations can vary by up to 5 m on sampling events possibly resulting in detection of tracer in one event followed by a non-detect in the next.

- Day 2 showed minimal detection of red tracer on the magnets and 5 detects of green tracer on the east side of the channel while over 60% of the grab samples showed both red and green tracer.
- Day 3 showed 8 samples of red in the upper channel and 90% of the magnets with green samples while over 60% of the grab samples showed both red and green.
- Day 4 showed 5 detects of red and 9 detects of green in the upper and west side channel magnets. Over 66% of the grab samples showed red and green.
- Day 6 showed 1 detect of red and 1 detect of green on the west side channel magnets near the deployment site. Approximately 40% of the grab samples showed red and over 50% show green.
- Day 14 showed 5 detects of red and 12 detects of green in the upper and west side channel magnets. Over 75% of the grab samples showed red and 100% showed green.

Overall the particle tracking study provided important insight into the extents of local sediment transport. It was evident that during every sampling period, tracer was redistributed from both sources in the channel. The magnets generally showed that material resuspended in the water column can be transported into the upper and west side of the channel and occasionally (2 events) along the east side. The grab samples generally all showed tracer presence from both sources throughout the sampling period. By the end of the sampling period, 75% of the samples contained tracer from the deeper red deployment site, while 100% of the samples contained tracer from the shallow green deployment site.

Since tidal currents have been demonstrated as an unlikely source of resuspension, vessel traffic (primarily tug and barge movement on the west side of the channel) was the likely source of tracer movement and responsible for tracer distribution in the channel sediment. In particular, day 3 sampling showed 90% of the magnets with green tracer, which is likely indicative of tug movement over the green deployment location that resulted in tracer dispersal throughout the water column. During this same time period, approximately 60% of the grab samples showed green tracer. The magnet outside the channel showed 2 green detections and grabs showed detection of both red and green material at generally low levels, indicating that there was some level of suspended solids transport out of the channel that was further evaluated in the modeling analysis.

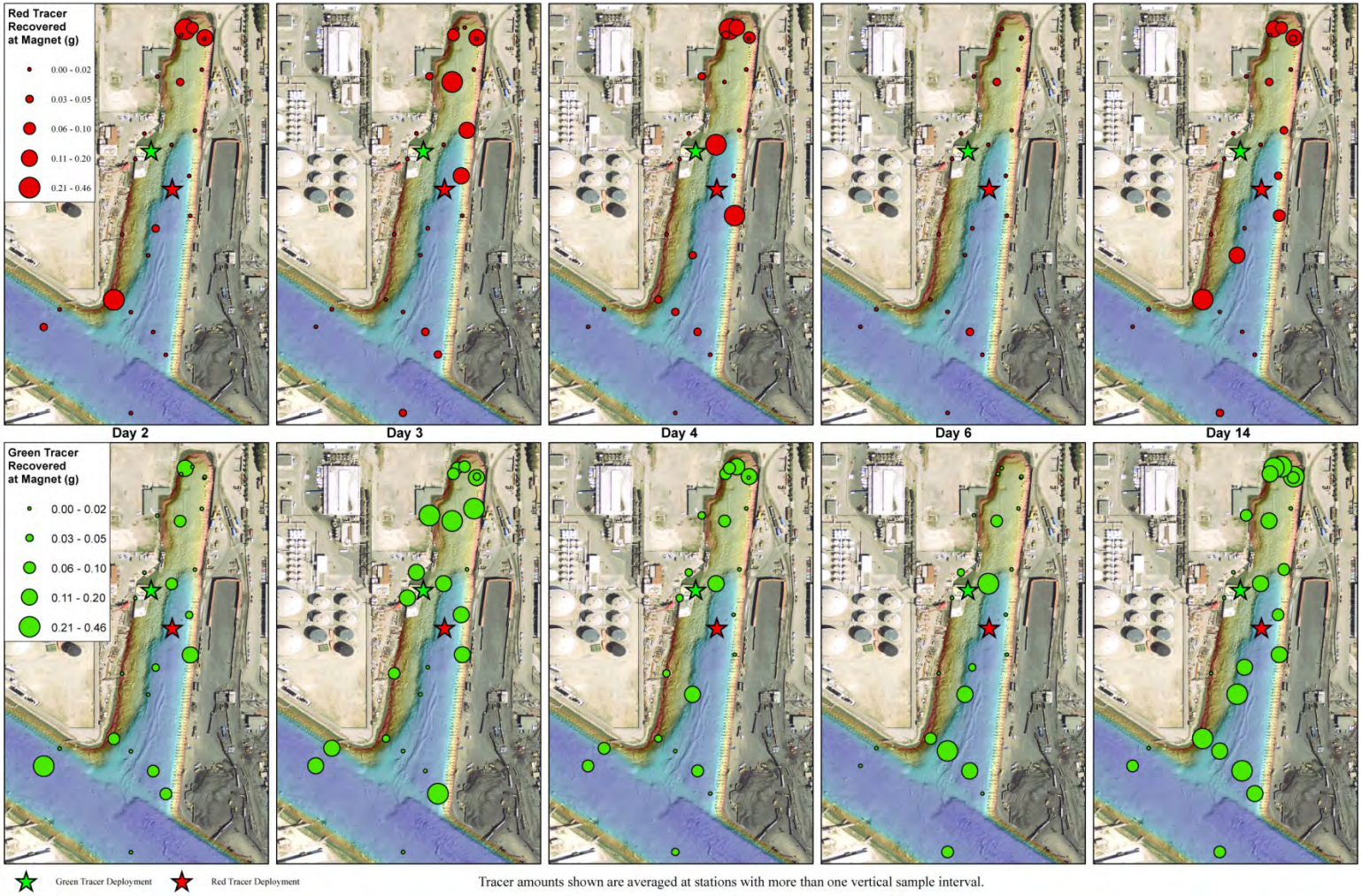

Figure 12. Mass recovered from magnets and grab samples during the particle tracer study.

3.3 Sedflume Analysis

Morphological bed changes in any aquatic system are dictated by complex and dynamically linked relationships between biological activity, hydrodynamic forcing, and sediment characteristics. When analyzing the sediment transport occurring within a system, numerous variables must be considered; one key aspect is the erosion properties and stability of a site's sediment. SEI conducted a Sediment Erosion at Depth Flume (Sedflume) analysis on 10 sediment cores (named SF01 through SF10) obtained from the Lauritzen Channel. The cores were collected in water depths ranging between 5.8 m to 7.9 m. The primary goal of the work was to characterize the erosion rates and physical properties of the sediment within the study area. The cores were eroded during the Sedflume analysis to determine erosion rates as a function of shear stress and depth. In addition, each core was sub-sampled to determine sediment bulk density and particle size distribution at specific depths within the core. Critical shear stresses were also deduced over five vertical intervals in each core.

3.3.1 Core Collection

The ten sediment cores were collected by SEI personnel on 10 and 11 July 2013. At each coring location, a DGPS was used to position a vessel at pre-determined, fixed sampling stations in the Lauritzen Channel. The 10 coring locations are shown in Figure 13; the white squares represent the coring locations. A pole was attached with clamps to a 10 cm by 15 cm rectangular core tube. The core tube was lowered into the water and positioned perpendicular to the sediment bed. Pressure was applied by hand until at least 30 cm and no more than 60 cm of the core tube penetrated into the sediment bed. A valve affixed to the top of the core tube was temporally closed to provide suction when the core was pulled out of the sediment bed. The sediment bed near the mouth of the channel (SF08, SF04, SF05, SF03 and SF09) was stiff and required additional force from a fence-post hammer to achieve core penetration; smaller than 30 cm cores were kept if several core attempts were made at a location and each resulted in recoveries less than 30 cm.

After cores reached the water surface, they were visually inspected for length and quality. Undisturbed cores were capped and secured to minimize sediment disturbance from sloshing water and vessel/vehicle motion. Cores were then transferred from the vessel to land and packed in secure Sedflume core shipping boxes. The cores were then driven by SEI personnel to SEI's EPA certified Sedflume laboratory in Santa Cruz, California. Upon arrival, the cores were again visually inspected to ensure that the sediment structure and surface had been preserved. The cores were then placed in an ambient water bath for preservation until processing.

3.3.2 Core Processing

All Sedflume processing and bulk sediment sampling and measuring (bulk density, Loss on Ignition, and particle sizing) was conducted in SEI's Santa Cruz laboratory. For a complete description of Sedflume and the processing techniques used in the analysis, see Appendix C.

Briefly, each core was processed by first inserting the core barrel and the sediment it contained into the bottom of the Sedflume (

Figure 14). The sediment surface was aligned with the bottom of the Sedflume channel. When fully enclosed, water was forced through the flume and over the sediment surface. The shear stress produced by the flow, and imparted on the particles, causes the sediment to erode. As the sediment on the surface of the core eroded, the remaining sediment in the core barrel was slowly moved upward so that the sediment-water interface remained level with the bottom of the flume. The sediment was moved upward by a piston that was inside the core barrel and was in contact with a hydraulic jack. The jack was driven by the release of pressure that was regulated with a switch and valve system controlled by an operator.

At the start of each core analysis an initial reference measurement was made of the starting core length. The flume was then operated at a specific flow rate corresponding to a particular shear stress, and sediment was eroded. As erosion proceeded, the core was raised if needed to keep the core's surface level with the bottom of the flume. This continued until 10 minutes had passed, or the core had been raised roughly 2 cm. The erosion rate for the applied shear stress was then calculated as:

$$E = \Delta z/T \qquad \text{Eq.4}$$

where E is the Erosion rate, Δz is the amount that the sediment was raised during a particular measurement period, and T is the measurement time interval. Critical shear stresses were then computed for each interval by first fitting the erosion rates to a power law following methods outlined by Roberts (1998)

$$E=A\,\tau^{n} \qquad \text{Eq.5}$$

where τ is the bed shear stress, A, n are constants that depend on the sediment characteristics. Once A and n values were calculated, a critical shear stress was determined by setting the erosion rate equal to 10^{-4} cm/s (operational definition for critical shear stress). The calculated critical shear stress was then checked against the measured erosion rates and a threshold was applied if necessary. Bulk sediment properties and critical shear stress values for each core interval are presented in Table 3. For both qualitative and quantitative details on each core, including cores pictures, core descriptions, and erosion rate and bulk sediment property data, see Appendix C.

3.3.3 Results

The erosion rates of Sedflume cores were highly variable due to inconsistent particle characteristics throughout the cores. The presence of detritus, pebbles, and shells often acted to armor the sediment bed until the applied shear stress was large enough to mobilize these larger particles. When high concentrations of organic material were present in a core, erosion

was often dominated by the mobilization of large chunks of material as organic pieces lifted from the bed surface, while mobilizing the sediment below.

Although erosion rates fluctuated between core intervals, core sediment generally stiffened with depth. This trend is common for sites with cohesive sediment. Calculated critical shear stresses ranged from 0.1 Pa to 1.28 Pa. Cohesive sediment will often self-compact due to the weight of the overlying material. Compaction reduces the potential for sediment mobility. However, Sedflume results must be analyzed in conjunction with other system characteristics, such as hydrodynamic forcing and bed coarsening to assess overall site stability and sediment transport trends.

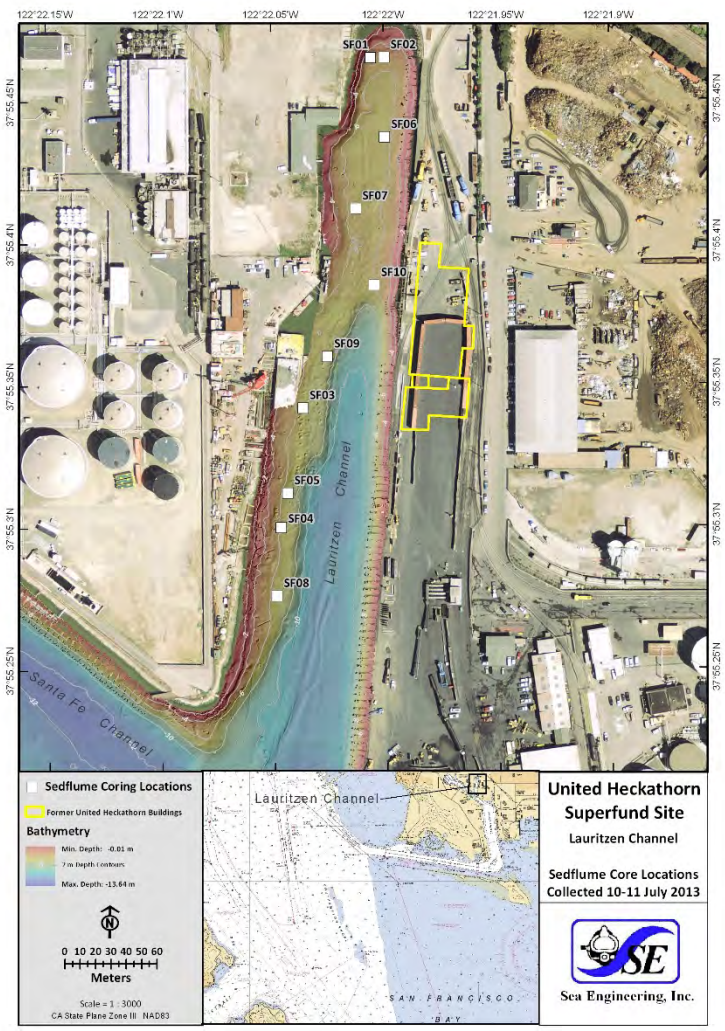

Figure 13. Map of Sedflume coring locations.

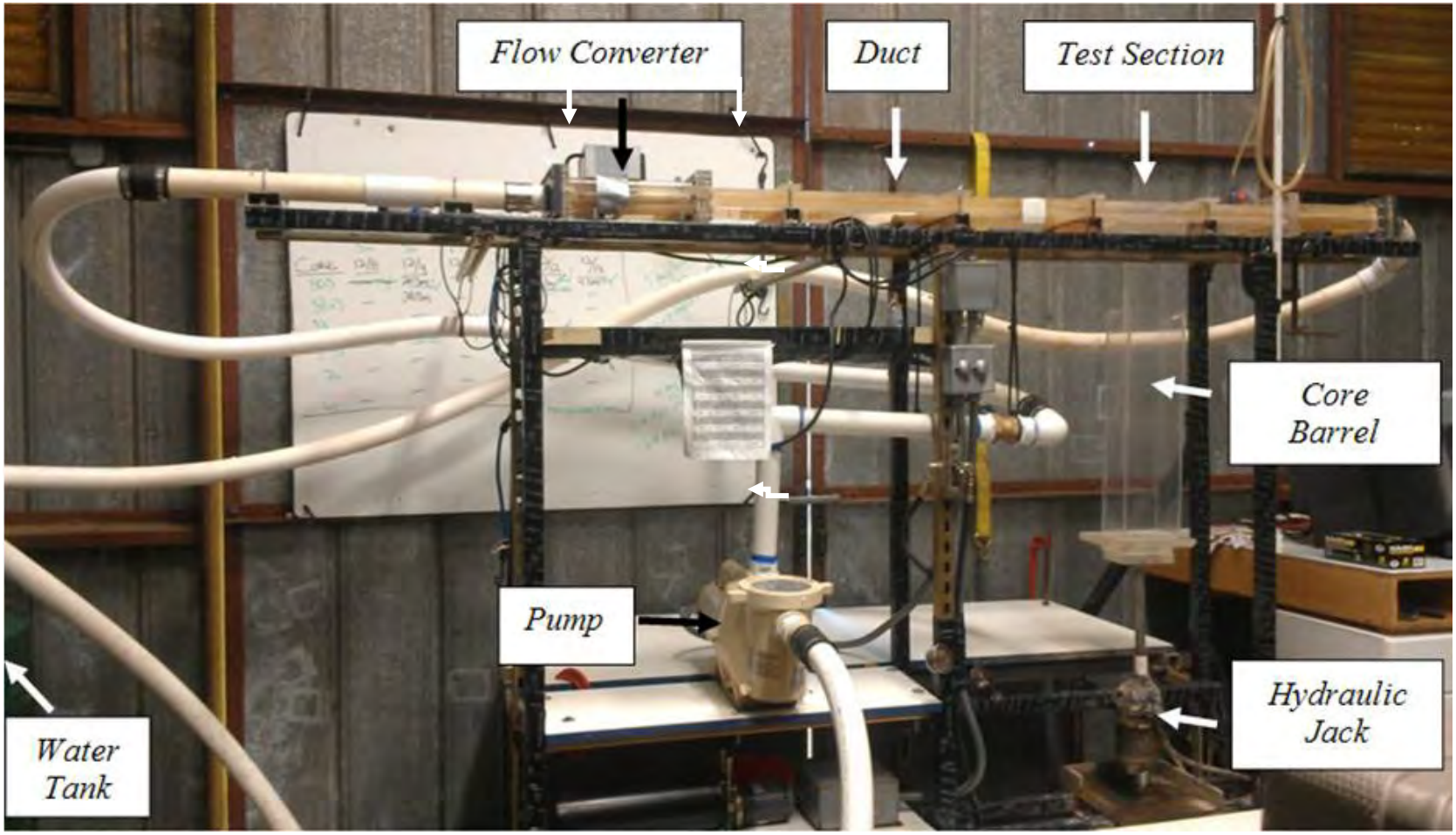

Figure 14. Sedflume in the Santa Cruz, CA, SEI laboratory.

Table 3. Sediment properties and critical shear stress by core interval measured during the Sedflume analysis.

		Core ID									
		SF1	SF2	SF3	SF4	SF5	SF6	SF7	SF8	SF9	SF10
	Lat (N)	37.9244	37.9244	37.9224	37.9217	37.9219	37.9240	37.9235	37.9213	37.9227	37.9231
	Long (W)	-122.3668	-122.3667	-122.3673	-122.3675	-122.3674	-122.3667	-122.3669	-122.3675	-122.3671	-122.3668
Starting Depth (cm)	Interval 1	0.00	0.00	0.00	0.00	0.00	0.00	0.00	0.00	0.00	0.00
	Interval 2	5.60	6.90	8.90	5.30	8.60	6.80	8.20	4.00	3.10	5.30
	Interval 3	10.80	14.60	14.00	10.80	15.60	13.80	15.00	12.90	n/a	13.10
	Interval 4	13.30	24.40	19.00	14.30	22.30	19.00	22.90	n/a	n/a	21.30
	Interval 5	19.50	26.40	28.50	18.00	27.20	21.20	N/A	n/a	n/a	30.60
D10 (um)	Interval 1	2.406	2.109	1.497	1.585	1.616	1.512	1.570	1.576	1.674	1.953
	Interval 2	1.683	2.970	1.655	1.554	1.646	1.461	1.431	1.651	1.685	1.864
	Interval 3	1.580	2.130	1.610	1.629	1.870	1.742	1.753	1.555	n/a	1.605
	Interval 4	2.046	2.126	1.658	1.853	1.426	1.573	1.976	n/a	n/a	1.708
	Interval 5	2.019	2.121	1.658	1.889	1.650	1.625	1.541	n/a	n/a	1.985
D50 (um)	Interval 1	14.90	18.10	5.73	6.43	6.70	5.56	6.04	6.21	7.99	9.48
	Interval 2	6.77	53.89	6.97	6.23	6.88	6.52	5.40	7.63	9.16	7.98
	Interval 3	6.80	11.70	6.80	7.09	11.49	6.51	7.39	6.92	n/a	7.14
	Interval 4	9.80	10.07	6.58	8.78	14.42	5.79	9.31	n/a	n/a	6.89
	Interval 5	8.79	11.26	6.74	9.13	8.40	6.31	6.01	n/a	n/a	10.09
D90 (um)	Interval 1	163.40	369.30	26.97	38.48	57.84	22.94	27.02	34.20	56.91	110.90
	Interval 2	38.41	530.60	43.93	34.35	56.71	25.92	24.18	128.90	55.85	67.87
	Interval 3	41.79	239.30	44.12	59.70	124.40	36.30	72.69	86.70	n/a	62.41
	Interval 4	90.57	130.70	30.08	65.90	38.31	34.27	90.46	n/a	n/a	38.34
	Interval 5	86.35	130.20	53.07	59.50	197.20	38.44	33.82	n/a	n/a	112.70
Dry Bulk Density (g/cm^3)	Interval 1	0.20	0.16	0.13	0.28	0.36	n/a	0.17	0.35	0.40	0.32
	Interval 2	0.34	0.09	0.49	0.52	0.64	0.29	0.29	0.67	0.61	0.28
	Interval 3	0.34	0.32	0.73	0.79	1.22	0.29	0.32	0.76	n/a	0.38
	Interval 4	0.29	0.26	0.52	0.50	1.01	0.34	0.42	n/a	n/a	0.38
	Interval 5	0.35	0.36	0.41	0.43	1.27	0.36	0.43	n/a	n/a	0.51
Critical Shear Stress (Pa)	Interval 1	0.10	0.10	0.20	0.10	0.20	0.22	0.10	0.43	0.10	0.20
	Interval 2	0.80	0.20	0.80	1.04	0.55	0.20	0.21	0.51	0.22	0.40
	Interval 3	0.80	0.80	0.40	0.86	0.20	0.82	0.20	0.61	n/a	0.53
	Interval 4	0.47	0.40	0.40	1.28	0.51	0.80	0.40	n/a	n/a	0.40
	Interval 5	0.52	0.40	1.03	0.40	n/a	n/a	n/a	n/a	n/a	0.80
A	Interval 1	0.00358	0.02688	0.00127	0.00301	0.00201	0.00161	0.00321	0.00060	0.01660	0.00054
	Interval 2	0.00081	NA	0.00026	0.00008	0.00058	0.00649	0.00411	0.00037	0.00652	0.00049
	Interval 3	n/a	0.00238	0.00189	0.00021	0.00772	0.00028	0.00235	0.00029	n/a	0.00054
	Interval 4	0.00072	NA	0.00096	0.00002	0.00191	n/a	0.00112	n/a	n/a	0.00036
	Interval 5	0.00075	0.03342	0.00008	n/a	n/a	n/a	n/a	n/a	n/a	0.00028
n	Interval 1	1.9	2.6	1.7	2.0	2.0	1.8	1.7	2.1	2.2	1.4
	Interval 2	2.5	NA	3.0	4.9	2.9	1.7	2.3	2.0	2.8	1.0
	Interval 3	n/a	4.9	2.9	5.0	2.5	5.3	1.7	2.1	n/a	2.7
	Interval 4	2.6	NA	2.0	7.1	4.4	n/a	2.5	n/a	n/a	1.3
	Interval 5	3.1	3.4	6.4	n/a	n/a	n/a	n/a	n/a	n/a	3.0

4.0 Sediment Transport Analysis

The sediment transport analysis performed to determine processes contributing to sediment resuspension and transport in the Laurtizen Channel included the following elements:

- Erosion potential of sediment due to natural and anthropogenic processes.
    - Natural Sediment Transport
    - Anthropogenically Forced Sediment Transport
- Magnitude and frequency of sediment resuspension and the magnitude and direction of net sediment flux.
    - Natural Sediment Transport
- Quantity of sediment transport in areas of high vessel activity.
    - Anthropogenically Forced Sediment Transport
    - Hydrodynamic Model

The hydrodynamic and sediment transport discussions primarily utilize data collected at 1-m above the sediment bed (Table 4) as these are representative of the near-bed processes important to sediment transport. As expected, due to natural settling of particles in the water column, TSS concentrations were greater and particle size was larger near the bed than for depth-averaged values. The low mean current velocities (3 cm/s and lower) are consistent with the theoretical calculations performed in the Tier 1 sediment transport study.

Table 4. Statistics for hydrodynamic and sediment parameters collected within 1-m above the sediment bed at the mouth and the head of the Lauritzen Channel.

	Mean	Minimum	Maximum	Standard deviation
Mouth				
Current velocity (m/s)	0.03	0	0.17	0.02
TSS (mg/L)	42.5	25.2	129.0	7.9
D_{10} (μm)*	10.5	6.6	15.7	1.7
D_{50}(μm)*	60.7	25.2	128.2	21.8
D_{90}(μm)*	190.4	77.5	274.4	50.2
Head				
Current velocity (m/s)	0.02	0	0.11	0.01
TSS (mg/L)	28.2	18.1	84.5	4.2
D_{10} (μm)*	7.9	5.5	12.4	1.5
D_{50}(μm)*	41.7	18.9	106.1	15.5
D_{90}(μm)*	150.9	48.8	254.6	48.4

*Particle size data within 2-m of the sediment bed were averaged prior to computing statistical parameters.

4.1 Natural Sediment Transport

The principal tidal constituents in San Francisco Bay are the M2 semi-diurnal and K1 diurnal tides (Cheng & Gartner, 1984). The tidal periods of the M2 and K1 tide are approximately 12.42 hours and 23.9 hours, respectively. Therefore, in order to investigate tidal oscillations in hydrodynamic and sediment time series, data were band-pass filtered[4] between 8-hr and 30-hr cutoff frequencies. Results indicated that band-pass filtered TSS generally increased during flood tide and decreased during ebb tide (Figure 15). The magnitude of variability of TSS was dependent on tidal phase. Spring tide produced greater TSS variability, with differences of nearly 30 mg/L between low and high tide (Figure 15). The average standard deviation of TSS at 1-m above the sediment bed was 7.88 mg/L (Table 4).

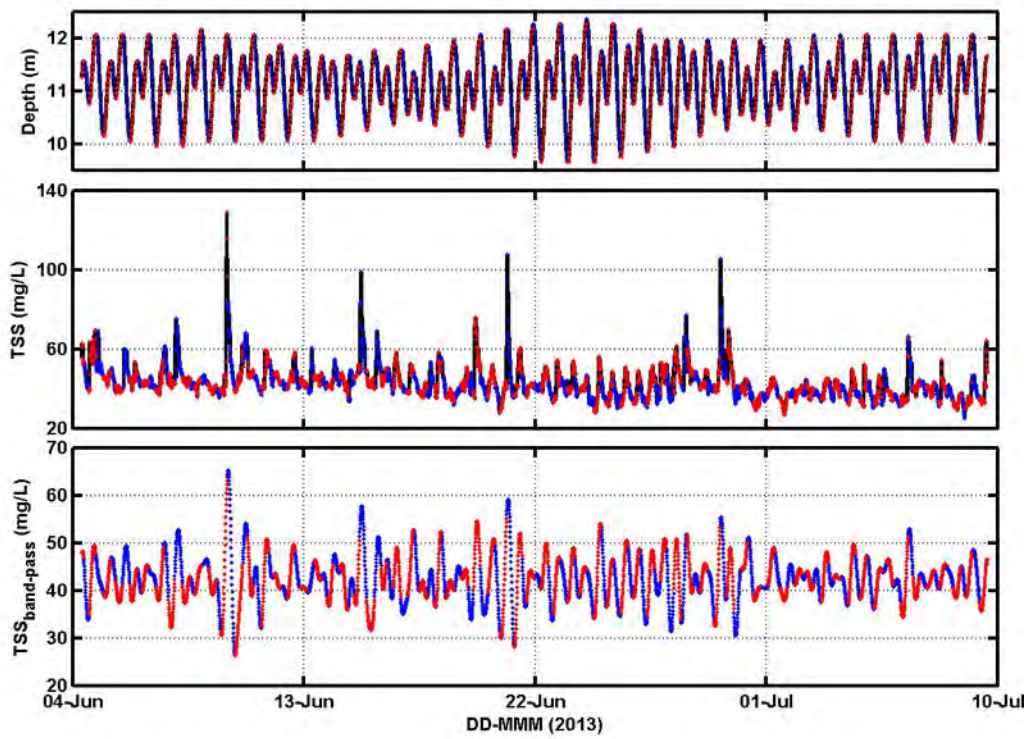

Figure 15. Time series of water depth (upper), TSS (middle), and band-pass filtered TSS (lower) collected within 1-m above the sediment bed at the mouth of the Lauritzen Channel. Red indicates flood tide periods and ebb tide periods are illustrated in blue.

[4] A band-pass filter passes frequencies within a certain range (within the cutoff frequencies) and rejects frequencies outside that range.

Quantitative evidence of the relationship between hydrodynamic processes and sediment movement was provided by statistical coherence[5] between TSS and tidal variability (water depth) and between computed sediment flux (the product of ADCP-derived flow rate and sediment concentration, or TSS) and tidal variability. Statistically significant coherence (95% confidence interval) was found at periods of ~12.5 hrs for TSS and at ~12.5 hrs and ~23.5 hrs for sediment flux (Figure 16). These periods coincided with the periods of the principal tidal constituents (M2 and K1) found in San Francisco Bay.

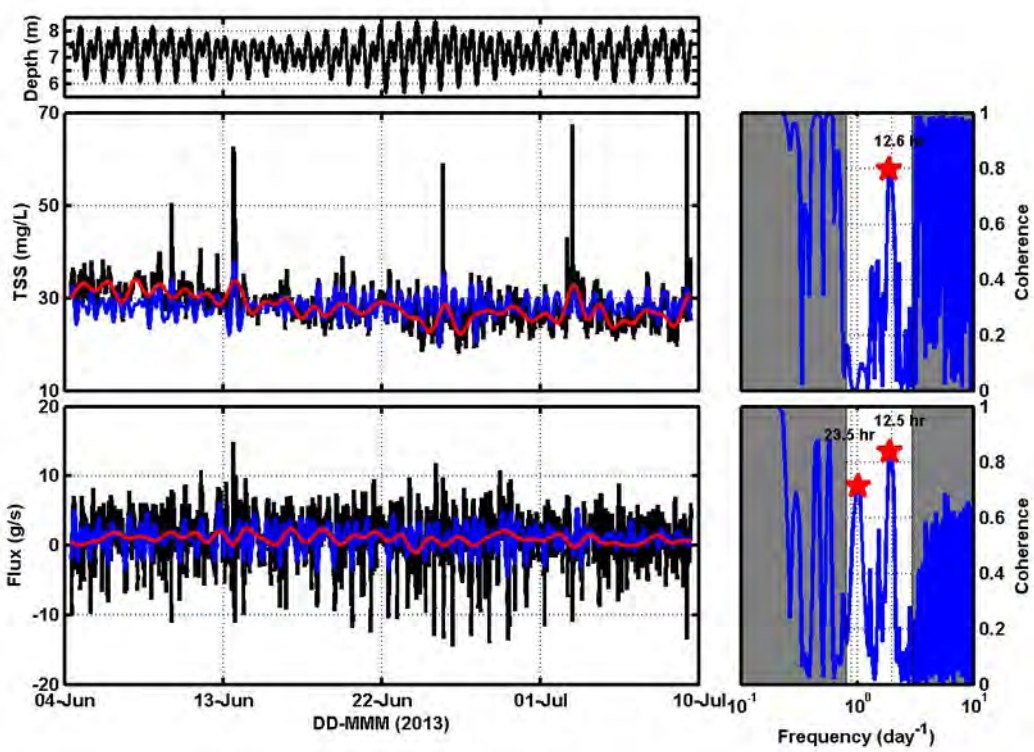

Figure 16. The left three panels show time series of water depth (upper), TSS (middle), and sediment flux (lower). Band-pass and low-pass filtered (30-hr cut-off frequency) TSS and sediment flux are shown in blue and red, respectively. Positive flux is out of the system (i.e. ebb tide) and negative flux is into the system (i.e. flood tide). The right two panels show coherence between TSS and water depth (upper) and sediment flux and water depth (lower). Statistically significant coherence periods are denoted with red stars and their periods are labeled in units of hours. Data outside of the cut-off frequencies for tidal variability are shaded in gray. TSS and flux data are from within 1-m above the sediment bed.

The critical shear stress for resuspension of surface sediment (τ_c) was determined using Sedflume. Sedflume results indicated that τ_c was 0.43 Pa and 0.2 Pa for the mooring platform locations at the mouth and head of the Lauritzen Channel, respectively (see Table 3 and Section 3.3 for more Sedflume details). Band-pass and low-pass (30-hr cutoff frequency) filtered near-bottom shear stress did not exceed the values for critical shear stress at either location

[5] Spectral coherence is a statistic that can be used to examine the relation between two signals or data sets.

(Figure 17). Time-averaged values of band-pass filtered near-bottom shear stress were 0.04 Pa and 0.02 Pa and their maximum values were 0.15 Pa and 0.05 Pa at the mouth and head of the Channel, respectively (Table 5). Therefore, it can be concluded that turbulence was not strong enough to resuspend sediment at frequencies representative of tidal hydrodynamics.

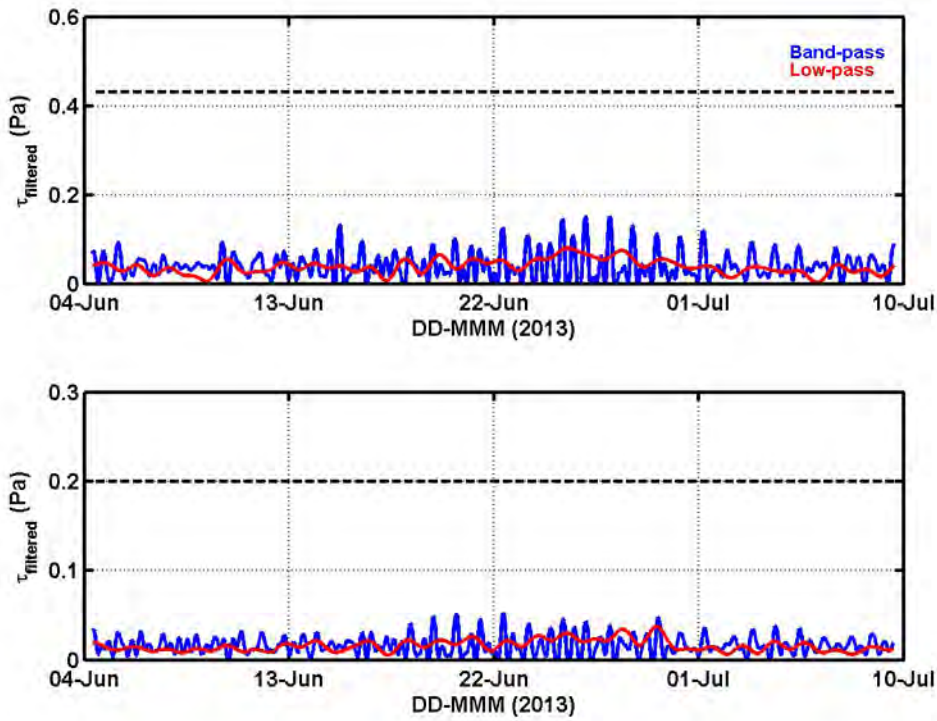

Figure 17. Time series of band-pass (blue) and low-pass (red) filtered near-bottom shear stress computed from data collected within 1-m of the sediment bed at the mouth (upper panel) and head (lower panel) of the Lauritzen Channel. The black, dashed lines denote the critical shear stress for sediment resuspension determined from Sedflume experiments (0.43 Pa and 0.2 Pa at the mouth and head of the Lauritzen Channel, respectively).

Table 5. Statistics for band-pass and low-pass filtered near-bottom shear stress. Data were from within 1-m above the sediment bed.

	Mean	Minimum	Maximum	Standard deviation
		Mouth		
τ (Pa) band-pass	0.04	0	0.15	0.03
τ (Pa) low-pass	0.04	0.002	0.08	0.02
		Head		
τ (Pa) band-pass	0.02	0	0.05	0.01
τ (Pa) low-pass	0.02	0.006	0.04	0.006

While TSS varied with tidal oscillations, particle size distributions in the water column did not vary with the tides at the mouth and were only weakly related to the tides at the head of the

Channel (Figure 18). A general increase in particle concentrations of larger sizes (>100 μm) was observed during flood tide at the head of the Lauritzen Channel. Additionally, a peak in PSD between 6 and 7 μm was observed only during ebb tide conditions at this location. Therefore, no general change in water column suspended solids composition is expected to occur over tidal variations as is common in some estuaries.

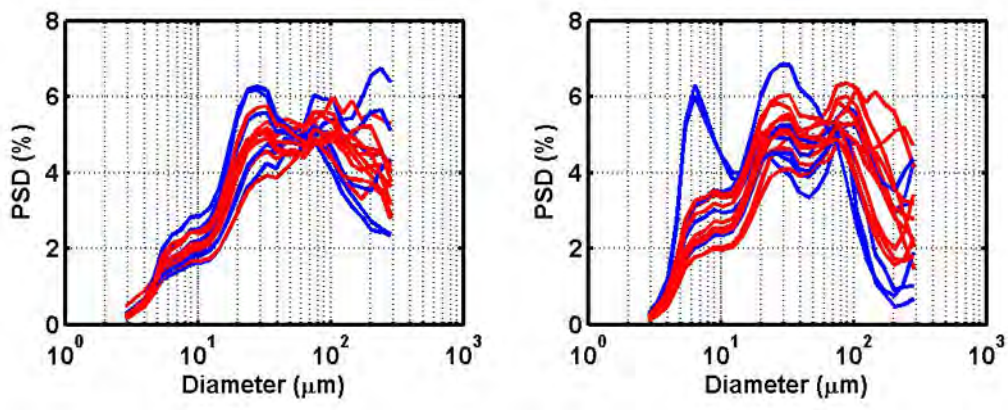

Figure 18. The average size distribution of particles collected within 2-m of the sediment bed at the mouth (left panel) and head (right panel) of the Lauritzen Channel averaged over ebb tide periods (blue lines) and flood tide periods (red lines).

4.2 Anthropogenically Forced Sediment Transport

The Lauritzen and Santa Fe Channels are active waterways with ship and barge berthing activities that have the potential to affect sediment transport patterns. It was therefore necessary to investigate high temporal frequency hydrodynamic and sediment data in order to identify tug and barge events and to relate anthropogenic forcing to sediment resuspension and transport.

4.2.1 Field Data– Tug events

High-pass filtered TSS and time series of near-bottom shear stress were examined in an effort to characterize the effects of anthropogenic activities at the United Heckathorn study site. A high-pass filter allows for the removal of the tidal signal so that other TSS spikes (e.g. non-tidal vessel resuspension) can be clearly identified. The cutoff frequency for high-pass filtered data was 8 hours. Intermittent peaks in TSS were observed six times in high-pass filtered TSS time series (Figure 19 and Figure 20). For the purposes of this evaluation, threshold concentrations were operationally defined as 60 mg/L at the mouth of the Channel and 40 mg/L at the head of the channel. High-pass filtered TSS was found to be elevated above threshold concentrations for 60 to 130 minutes (between 6 and 13 measurements; sampling frequency every 10 minutes).

Near-bottom shear stress exceeded the critical shear stress for erosion of surface sediment for periods of between 20 min and 40 min. The relationship between peaks in TSS and shear stress differed between the two measurement sites. At the mouth of the Lauritzen Channel, peaks in shear stress were more frequent (nine times) than peaks in TSS (six times) over the measurement period. High frequency increases in both TSS and shear stress coincided twice at the mouth of the channel, on 10 June and 15 June 2013 (Figure 19). Peaks in shear stress that were not correlated with peaks in TSS always occurred during flood tide at the mouth, perhaps coincidentally or possibly related to the location of vessel movement relative to the location of the moored bottom instrument platform. TSS increases above 60 mg/L always occurred during slack tide or ebb tide conditions at the mouth of the channel.

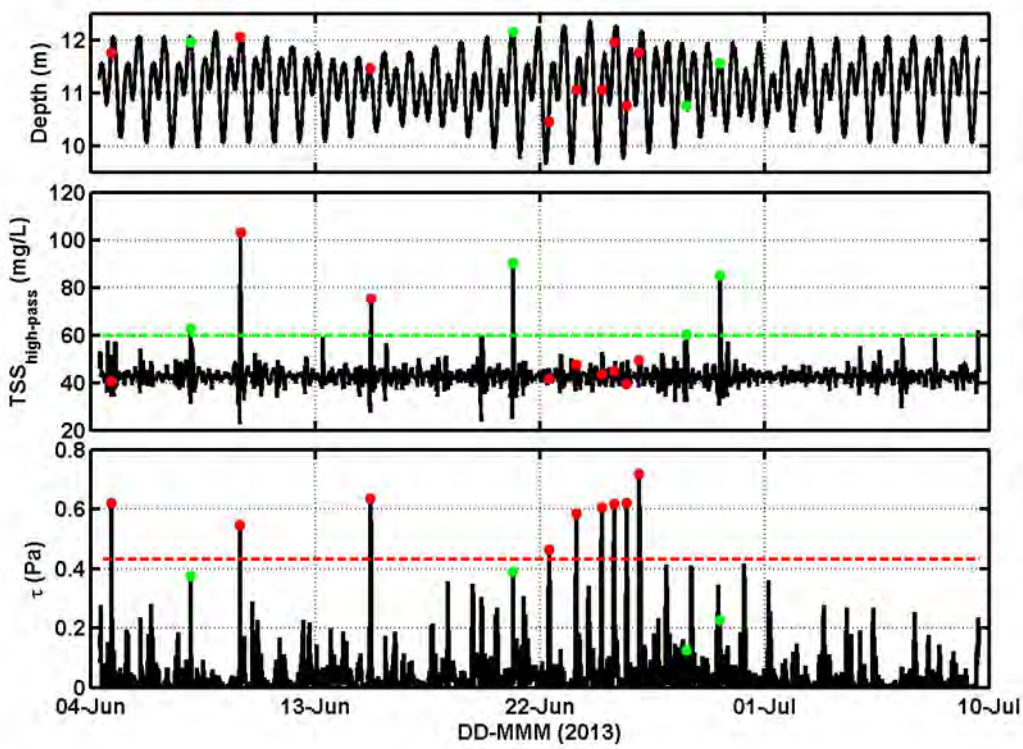

Figure 19. Time series of water depth (upper), high-pass filtered TSS (middle), and near-bottom shear stress (bottom) measured within 1-m above the sediment bed. Green dots indicate periods when high-pass filtered TSS exceeded an operationally-defined threshold value of 60 mg/L but near bottom-shear stress did not exceed the critical shear stress for erosion of surface sediment as determined from the Sedflume experiments. Red dots indicate periods when near-bottom shear stress exceeded the critical shear stress for erosion. Data were collected at the mouth of the Lauritzen Channel.

At the head of the Lauritzen Channel, high frequency increases in TSS and shear stress did not coincide and were not tidally dependent (Figure 20). While TSS increases above 40 mg/L occurred six times, peaks in shear stress were observed five times between 4 June and 10 July 2013. Elevation above critical shear stress spanned no more than two measurements, or 20 minutes in duration. The uncorrelated nature of the intermittent, high frequency peaks in

TSS and shear stress was potentially due to the distance between vessel movement and the location of the moored platform. While there is no detailed record of vessel movement during the deployment period, field observations of tug boat movement during sampling days near the west side of the Channel correlates with spikes in the deployment. Additionally, no other observed process in the channel could be responsible for the elevations in shear stress and sediment resuspension. Therefore, elevated TSS observances were likely sediment plumes generated by vessel movement that were advected toward the moored instrumentation.

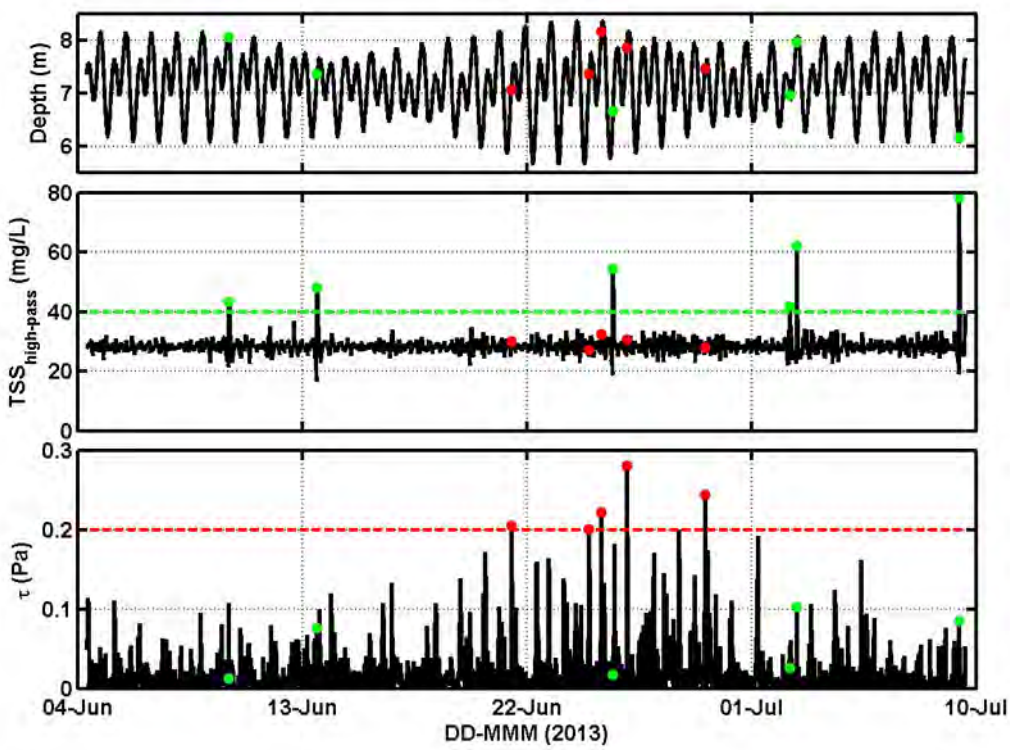

Figure 20. Time series of water depth (upper), high-pass filtered TSS (middle), and near-bottom shear stress (bottom) measured at the head of the Lauritzen Channel. Data were collected within 1-m of the sediment bed. Red dots indicate periods when near-bottom shear stress exceeded the critical shear stress for erosion of surface sediment as determined from Sedflume experiments. Green dots indicate periods when high-pass filtered TSS exceeded an operationally-defined threshold value of 40 mg/L.

4.2.2 Prop Scour Analysis

Vessel-induced bed scour was evaluated using a propeller wash and ship wake model and site-specific Sedflume and bathymetry data. The propeller wash and ship wake model used was based on an approach developed by the U.S. Army Corps of Engineers and is presented in detail in the Interim Report for the Upper Mississippi River – Illinois Waterway System Navigation (Maynord, 2000). Near bed velocity changes caused by vessel traffic result from two main components:

1) The wake created by the displacement of water from the vessel and
2) The increase in fluid momentum due to the vessel's rotating propeller.

Both components vary spatially and temporally as a vessel undergoes movement. The net bottom velocity, V_b, can be calculated as the sum of the two components:

$$V_b = V_{wake} + V_{prop} \qquad \text{Eq.6}$$

where V_{wake} is the bottom velocity due to the vessel wake, and V_{prop} is the bottom velocity due to the propeller wash. Wake velocities vary in the longitudinal direction, beginning at the vessel's bow, peaking at the vessel's stern, and then decreasing in the aft direction. Water accelerates at the vessel's propeller and decays in the lateral and longitudinal directions.

Before detailing the equations used in the propeller wash and ship wake analysis, it is important to understand the assumptions and potential shortcomings of the analysis. The propeller wash and ship wake model is based on empirical formulations that were derived from experiments conducted in a navigational flume with little or no field verification. In the current analysis it is assumed the empirical relationships hold in the Lauritzen Channel. The empirical models also greatly simplify the highly turbulent processes that result from propeller rotation. Turbulent fluctuations that may affect velocities and fluid-solid interactions at the bed are not fully represented in the model. Observations during field activities noted tug movement on a daily basis near the Manson facility; however, little information was available on the exact types of vessels frequently operating in Lauritzen Channel or their traffic patterns. Field observations noted during the ADCP deployments and tracer study were used to guide the assumptions related to vessel size and operations. Although the bed scour analysis is based on several assumptions that need to be considered when assessing the model results and accuracy, the analysis gives order-of-magnitude predictions of scour depths and suspended sediment load resulting from tug boat activity in the Lauritzen Channel. Model results were compared to TSS concentrations measured during identified tug boat vessel activities during the ADCP deployments, and calculated scour depths were checked against trends in the bathymetry data to ensure the model results were reasonable.

Bottom velocity components were calculated in a coordinate system fixed to a moving vessel with the x direction aligned with the direction of vessel movement (positive in aft direction) and the y direction aligned perpendicular with the vessel's centerline (Figure 21). The origin [x,y = (0,0)] was centered on the vessel's propeller.

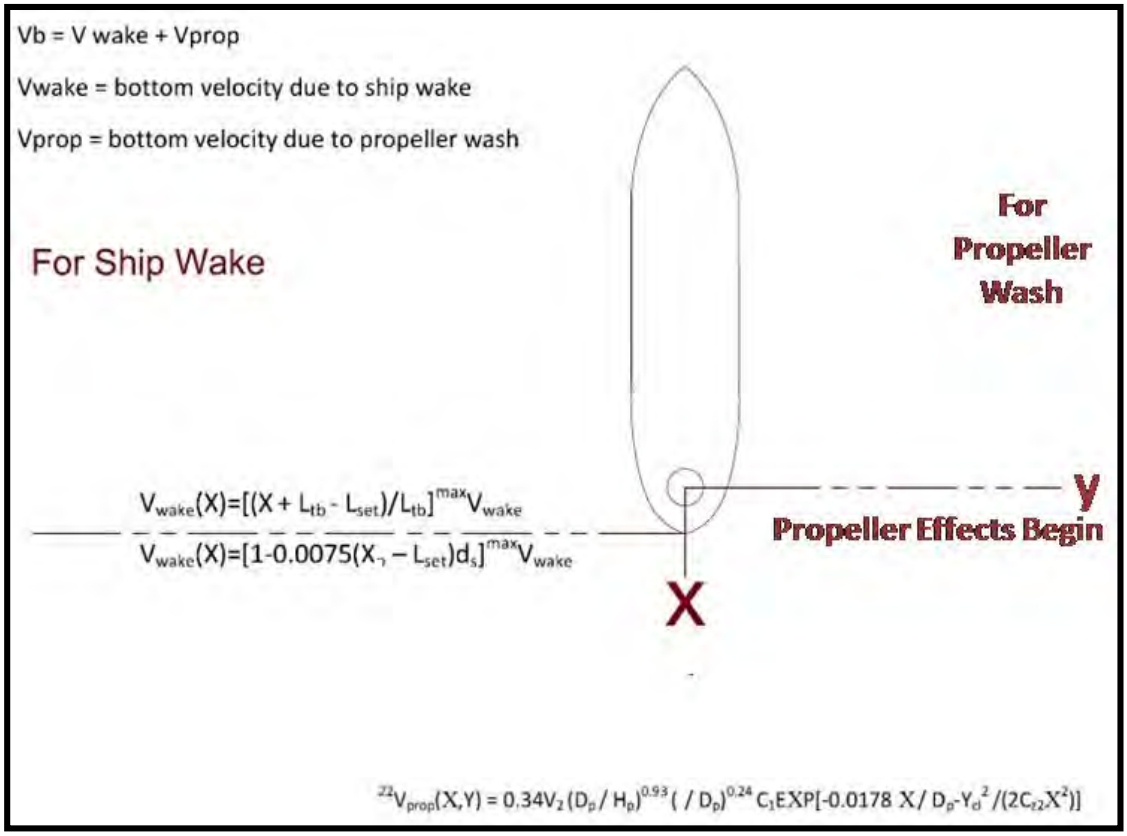

Figure 21. Schematic of propeller wash and ship wake model coordinate system.

With the coordinate system illustrated in Figure 21, the wake bottom velocity component (V_{wake}) can be computed from the following piecewise function:

For any point forward of the vessels stern ($x < L_{set}$),

$$V_{wake}(x) = [(x + L_{tb} - L_{set}) / L_{tb}]\ {}^{max}V_{wake}. \qquad \text{Eq. 7}$$

For any point behind the vessel stern ($x > L_{set}$),

$$V_{wake}(x) = [1 - 0.0075(x - L_{set})/d_s]\ {}^{max}V_{wake} \qquad \text{Eq.8}$$

Where L_{tb} is the length of the vessel, L_{set} is the distance from the vessel's stern to the propeller, d_s is the vessel draft, and ${}^{max}V_{wake}$ is the maximum wake velocity given by:

$${}^{max}V_{wake} = -0.78\ (d_s / h)^{1.81}\ (V_a - V_g) \qquad \text{Eq. 9}$$

where V_a is the ambient average channel velocity, h is the water depth, and V_g is the vessel speed relative to the sediment bed. With the same coordinate system, the bottom velocity due to the vessel propeller is defined by the following piecewise function:

For any point forward of the vessels prop ($x < 0$),

$$V_{prop}(x,y) = 0. \qquad \text{Eq.10}$$

for any point behind the vessel stern ($x>L_{set}$),

$$V_{prop}(x,y) = 0.34\ V_2\ (D_p/H_p)^{0.93}\ (x/D_p)^{0.24}\ C_1\ EXP[-0.0178\ x/D_p - y^2/(2\ C_{z2}x^2)] \qquad \text{Eq.11}$$

Where D_p is the propeller diameter, H_p is the distance from the propeller axis to the sediment bed, C_1 is a propeller coefficient (0.85 for Kort propeller), C_{z2} is a distance coefficient ($C_{z2} = 0.84\ (x/D_p)^{-0.62}$), and V_2 is the velocity increase caused by a second propeller and is given by:

$$V_2 = (1.13 / D_p)\ (31.82\ P_{hp}^{0.974} - 5.4\ (V_a - V_g)^2\ P_{hp}^{0.5})/\ \rho)^{1/2} \qquad \text{Eq. 12}$$

where P_{hp} is the ship's horsepower. Once bottom velocities were known, the quadratic stress law was used to calculate bed shear stresses:

$$\tau = \rho C_f V_b^2 \qquad \text{Eq.13}$$

where C_f is the bottom friction coefficient, estimated using (Parker, 2004):

$$C_f = k^2 Ln^{-2}(11\ h/k_s) \qquad \text{Eq. 14}$$

where k is von Karman's constant (0.4), and k_s is the effective bed height roughness (taken as two times the average D_{90} of the sediment in the Sedflume cores, or 0.00017 m).

Results from the propeller wash and ship wake analysis were coupled with the Sedflume data to calculate erosion rates as a function of bed shear stress. A site-wide average for the A and n coefficients were logarithmically (for A) and arithmetically (for n) averaged over five 6-cm intervals (Table 6). A specific core's interval contributed to the site-wide average interval if the end depth fell within the cumulative averaged interval thickness; a 6-cm depth interval was chosen because it was close to the average interval size in the Sedflume analysis. The site-averaged A and n values were then utilized to determine a critical shear stress (τ_{crit}) for each interval. Interval-averaged dry bulk density values were also computed to allow for suspended sediment mass to be computed. By integrating the erosion rates over time, bed scour and sediment loadings due to vessel activity in the Lauritzen Channel were calculated.

Table 6. Site-wide average values of sediment core properties from Sedflume analysis.

Interval	Depth Range (cm)	A	n	τ_{crit}	Dry Bulk Density (g/cm^3)
1	0-6	0.00230	1.9	0.20	0.28
2	6-12	0.0019	2.5	0.31	0.33
3	12-18	0.00085	2.6	0.43	0.43
4	18-24	0.00059	3.4	0.60	0.48
5	24+	0.00087	3.4	0.53	0.58

Due to the infrequent use of the Levin Richmond Terminal Corporation (LRTC) berth in the channel in comparison with the near daily use of the Manson Construction facilities, two main vessel operational patterns were identified in the Lauritzen Channel that had potential to

significantly affect sediment transport. Tug boats berthing at Manson Construction were observed motoring in and out of the channel on several occasions (vessel names were Peter M. and Fat Cat). Manson Construction tug boats were also observed maneuvering a barge into the channel by pushing up against the barge's side. While this was occurring, the tugboat was nearly stationary, but the vessel was in gear and the propeller was spinning (force from the propeller was balanced by the weight of the barge). No logs of Manson tug activity are available. A barge was observed tied to LRTC's dock, but Levin had no shipping activity in the Lauritzen. The barge was moved on June 3rd during the instrument deployment, but the specifics of the operations are not available.

In order to best estimate ship scour and associated sediment transport processes, the two vessel operation types were investigated separately. The approaches for analyzing each are presented in the paragraphs that follow, where the separate cases are referred to as the Transiting Case and the Stationary Case. For both cases, two sets of ship parameters were investigated to give a range of effects (Table 7). Because data were not available for the two tug boats observed in the Lauritzen Channel (Peter M. and Fat Cat), parameters for comparable tugboats berthed in San Francisco Bay were used. Based on observations, Silia, which is operated by Greger Pacific Marine, is thought to be similar in size to Peter M and was used for parameter specification (Vessel 1 in Table 7) (Greger Pacific Marine, 2013). The Foss Maritime harbor tug, Edith Foss, was used as a representative vessel for the Fat Cat (supplied values for Vessel 2 in Table 7) (Foss Maritime Company, 2013). Although the Silia and Edith Foss may not identically match the vessels operating within Lauritzen Channel, it is believed these tug boats are realistic representations of the types of vessels that operate within the channel. As mentioned above, the parameters used in the analysis are ship length (L_{tb}), ship draft (d_s), distance from stern to propeller (L_{set}), propeller diameter (D_p), maximum power in terms of brake horsepower (P_{hp}), and the propeller type. L_{set} and depth of propeller (deltap) were not defined for the Silia or Edith Foss, so they were estimated based on ratios derived from similar sized vessels. L_{set} was computed as 1/10 the length of the vessel, and deltap was defined as ¾ the ship draft.

Table 7. Ship parameters used in the propeller wash and ship wake model.

	L_{tb} (m)	D_s (m)	L_{set} (m)	D_p (m)	deltap (m)	Proptype
Vessel 1	16.76	2.13	1.67*	1.25	1.58*	Kort Nozzle
Vessel 2	23.46	3.47	2.35*	2.13*	2.13*	Kort Nozzle

* Indicates values that were estimated

Bottom velocities increased as vessels moved in and out of the Lauritzen Channel due to the vessel's wake and propeller wash. To estimate the potential for erosion given a transiting vessel, bottom velocities, shear stresses, and erosion rates were calculated at five different transects within Lauritzen Channel. The transects are shown in Figure 22. Cross-sectional depths along each transect were extracted from the digital elevation map. The following steps

were then applied to each transect line to calculate bottom shear stresses and erosion rates given the formulations for V_{prop} and V_{wake} as a function of vessel transit time. It was assumed that the vessel's bow crossed the transect at t = 0 and was moving at a constant rate V_g for time T in a straight line perpendicular to the transect.

1) Because bottom velocities along the transect are dependent on the location of the propeller relative to the transect, the distance between the propeller and the transect was calculated every second from t = 0 to t = T.
2) Knowing the distance from the propeller to the transect, which is the x coordinate in the bottom velocity equations for the given setup, bottom velocities along the transect were calculated.
3) Bottom shear stresses and erosion rates were then computed using the site-wide averaged A, n, and critical shear stress values.
4) The bed profile along the transect was adjusted by calculating the bed height change, which was the product of the erosion rate and the time step between iterations (1 second). The bed was only eroded if the shear stress at the bed was greater than the critical shear stress.
5) The process was repeated from t = 0 to t = T. After running this process for both vessel types on all five transects, it was found that after 2 minutes of vessel transit time the effects of the vessel on bottom velocities along the transect were minimal. T was accordingly chosen as 2 minutes.

The six steps were applied to each transect for both vessels given four different percentages of their maximum power (25%, 50%, 75% and 100%). Various maximum powers were investigated to give a range of the effects that could occur depending on how fast vessels move in and out of the Lauritzen Channel; however, it is likely that vessel movement occurs in the channel using 25% or lower of the maximum power. The six steps were designed to be an iterative process that accounts for bed erosion as the vessel passes.

As a ship moved past a point, the influence of each velocity component (V_{prop} and V_{wake}) varied in magnitude. When the vessel's bow first passed a particular transect, the bed velocities increased due to the bow wake. A typical contour plot of V_{wake} as a function of time is shown inFigure 23. This particular plot was created at Transect 5 for vessel 2 operating at 100% of its maximum power; however, the spatial velocity trends were similar for both vessel types and all power percentages. The magnitude of the velocities changed, but spatial distribution varied only slightly. The vertical gray line in Figure 23 denotes the centerline position of vessel 2 as it transited past the transect. The two horizontal black lines mark the time when the propeller (top line) and stern (bottom line) crossed the transect. The bed profile of Transect 5 is given in the top panel. V_{wake} increased as the vessel began motoring over the transect and peaked as the stern passed. After this time, V_{wake} decreased as the boat traveled further away from the transect and was nearly zero after roughly a minute and a half. V_{wake} was also dependent on the water depth. On the edges of the transect, where waters are shallower, V_{wake} was relatively

large. This suggests that near shoreline areas may be the most influenced by vessel wakes. However, the equations used in the propeller wash and ship wake model become less reliable in steep slope regions because they were derived from flat bottom experiments and analysis. To avoid steep side slope regions where the model is not applicable, the transects were cut at a depth of roughly 6 m (20 m contour line).

A typical contour plot of V_{prop} is shown in Figure 24, with the boat centerline and propeller and stern passing times. Again, this particular plot was created at Transect 5 for vessel 2 operating at 100% of its maximum power but the trends were consistent for all boat and transect combinations. Before the propeller passed the transect, V_{prop} was zero along the profile but sharply increased immediately after it passed. For this particular boat-transect combination, V_{prop} reached a maximum of 0.93 m/s roughly 25 seconds after transiting began. As the vessel motored further from the transect, the magnitude of V_{prop} dissipated. Total bottom velocities, V_b, are shown in Figure 25. Being a combination of V_{wake} and V_{prop}, V_b was highest in shallow regions and directly behind the vessel once it passed the transect.

A contour plot of bed shear stress derived from V_b as a function of time is presented in Figure 26. Times and locations along the transect that experienced large shear stress corresponded to larger erosion depths. Maximum bed velocities, shear stresses, erosion depths, and predicted TSS concentration for all boat, transect and power combinations are presented in Table 8. The maximum bed erosion of all cases, 0.50 cm, occurred for vessel 2 transiting over profile 5 at full power. The analyses presented did not take into account bed armoring or deposition, so the erosion depth values are likely an upper limit to what actually occurs. The TSS concentrations presented in Table 8 were calculated assuming that all sediment that mobilized remained in the water column and dispersed uniformly in the vicinity of the transect. This assumption is not completely accurate; however, given the turbulent mixing that occurred due to propeller rotation, it is likely valid.

To estimate the total mass of sediment that would enter the water column in the Lauritzen Channel if the vessels transited from Manson (Transect 1) to the mouth of the Lauritzen Channel (Transect 5), the average TSS concentrations from each individual transiting event were examined in conjunction with water volumes in the channel. Water volumes for the segments between transects were computed from the distance between neighboring transects and bathymetry profiles as follows:

1) *Water volume between Transect 1 and Transect 2* – the water volume between Transect 1 and Transect 2 was calculated by multiplying the distance between Transect 1 and Transect 2 by the cross sectional area of the water column at Transect 1 (assuming a 0 m tide relative to MLLW). The cross sectional area of Transect 1 was chosen for the volume calculation because it best represents the channel from Transect 1 to Transect 2.
2) *Water volume between Transect 2 and Transect 3* – the water volume between Transect 2 and Transect 3 was calculated by multiplying the distance between Transect 2 and Transect 3 by the cross sectional area of the water column at Transect 2

(assuming a 0 m tide relative to MLLW). The cross sectional area of Transect 2 was chosen for the volume calculation because it best represents the channel from Transect 2 to Transect 3.

3) *Water volume between Transect 3 and Transect 5* – the water volume between Transect 3 and Transect 5 was calculated by multiplying the distance between Transect 3 and Transect 5 by the average cross sectional area of the water column of Transect 3, Transect 4, and Transect 5 (assuming a 0 m tide relative to MLLW). The average cross sectional area was used because the berth is uniformly expanding between *Transect 3 and Transect 5.*

Once the water volumes were known, the sediment mass in each segment was calculated by multiplying the calculated volume by the TSS concentration for the segment. The total mass into the system was then computed as the sum of the mass in each segment. Total mass input predictions for both vessel types under all power percentages investigated are presented in Table 9. Because Vessel 1 did not cause erosion for any profile-power fraction considered, it never mobilized sediment. Under full power, Vessel 2 caused 699 kg of sediment to be suspended into the water column. When considering these mass predictions, it is important to remember that any coarse grain sediments that are mobilized will quickly settle from the water column, reducing the chance of large-scale transport. Under 20% power, Vessel 2 mobilized 20 kg of sediment when moving from Manson to the mouth of the Lauritzen Channel.

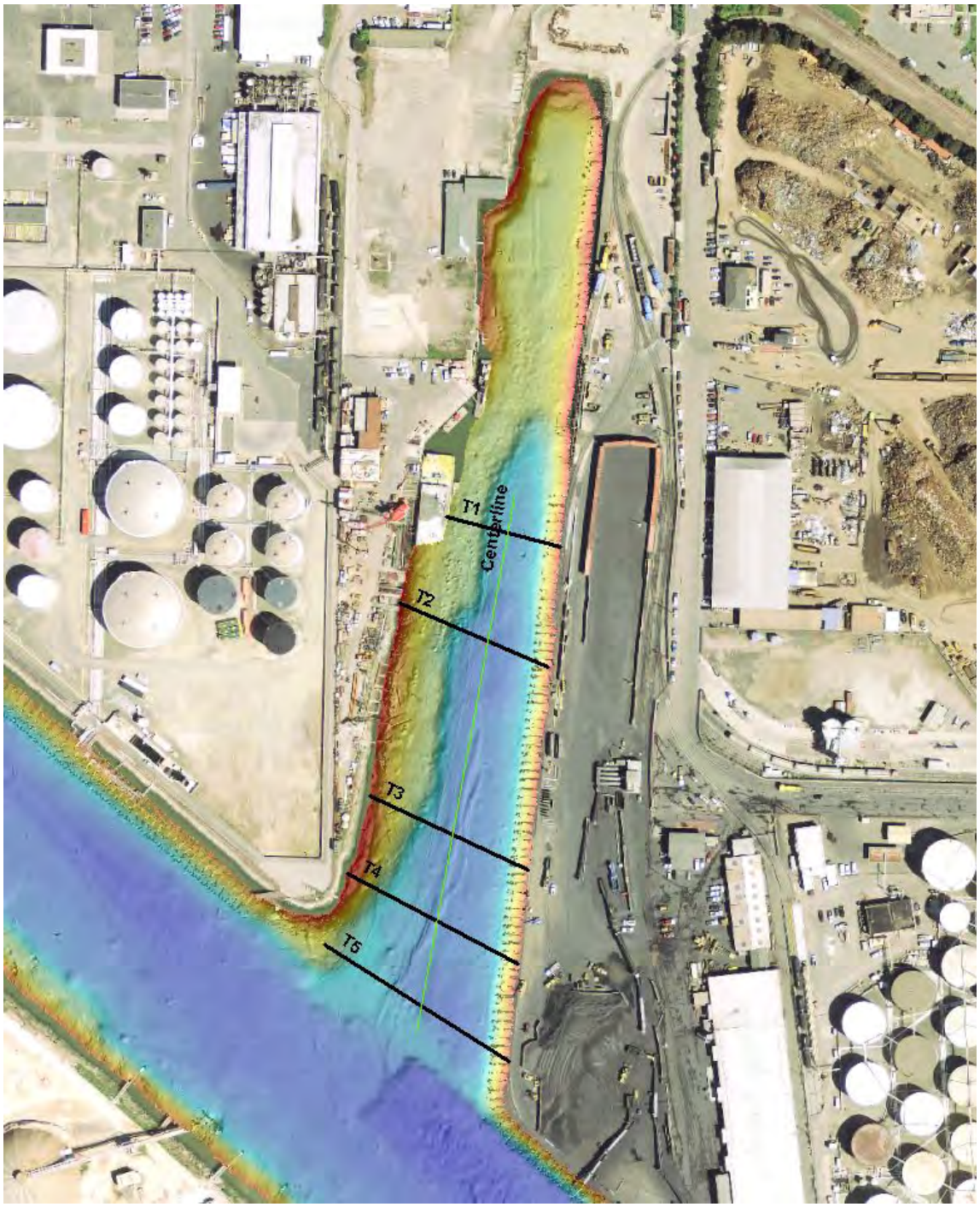

Figure 22. Profile lines used to create the beds for the Transiting Case of the propeller wash and ship wake model.

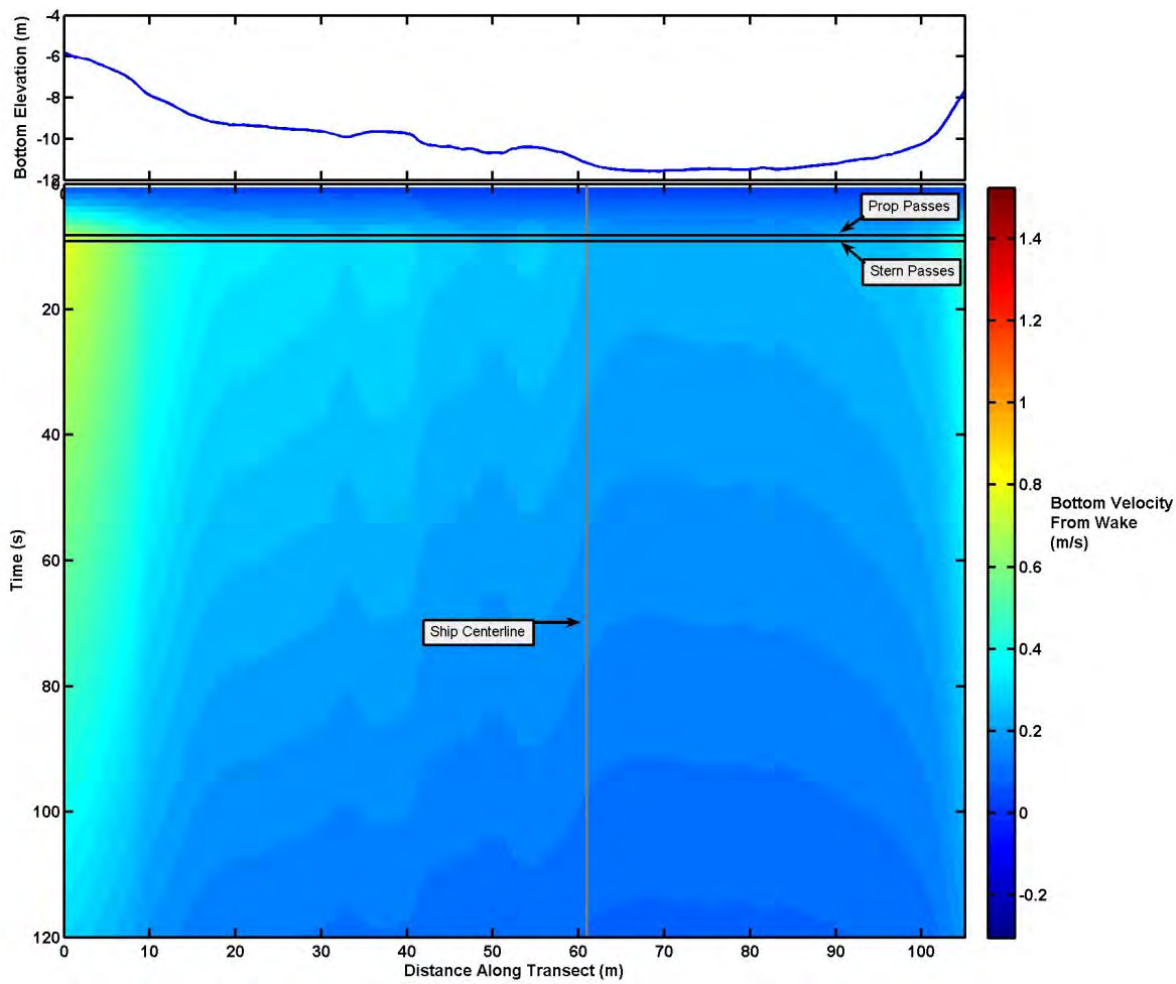

Figure 23. Contour plot of the ship wake component of the bottom velocity (m/s) along Transect 5 as a function of time for Vessel 2 running at 100% of its maximum power. The tiop panel is a plot of the starting bathymetry along the transect.

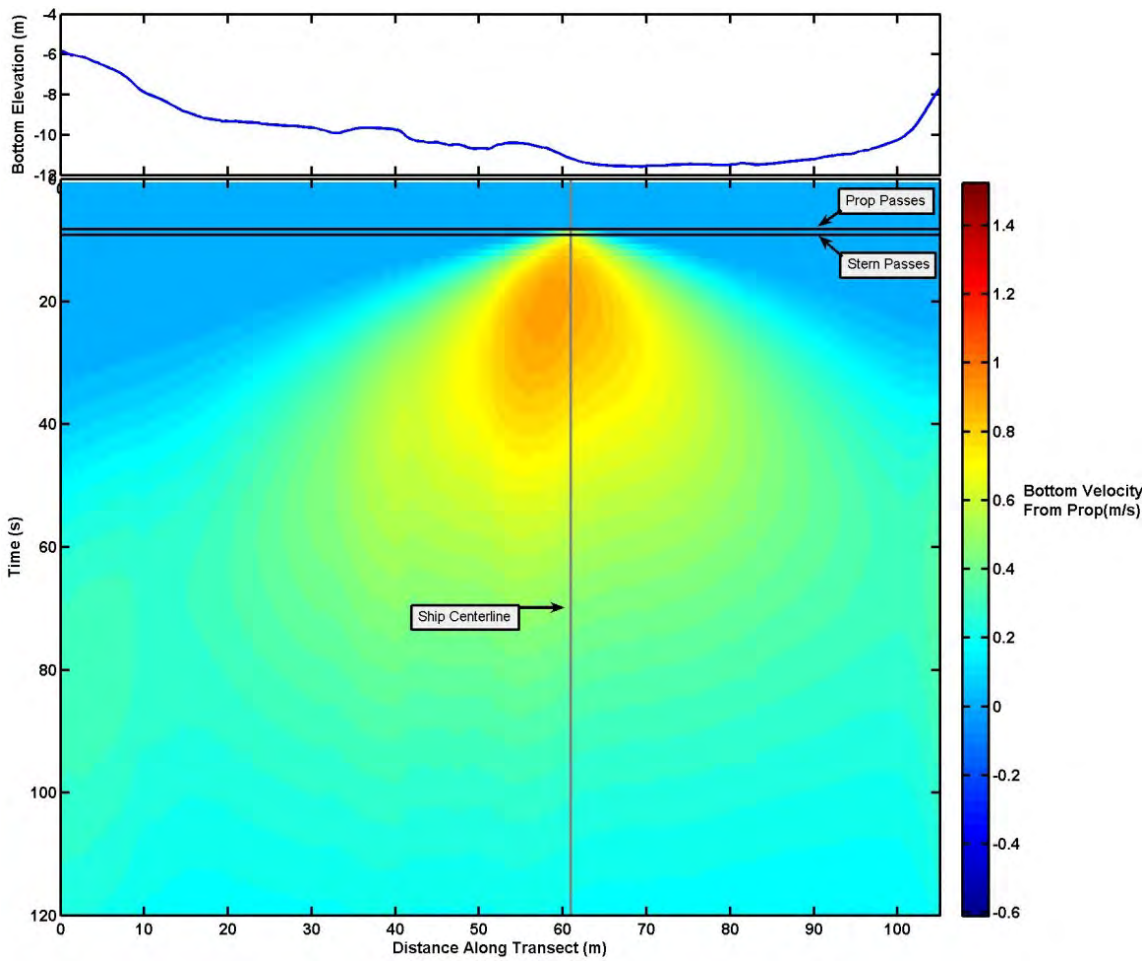

Figure 24. Contour plot of the propeller component of the bottom velocity (m/s) along Transect 5 as a function of time for Vessel 2 running at 100% of its maximum power. The top panel is a plot of the starting bathymetry along the transect.

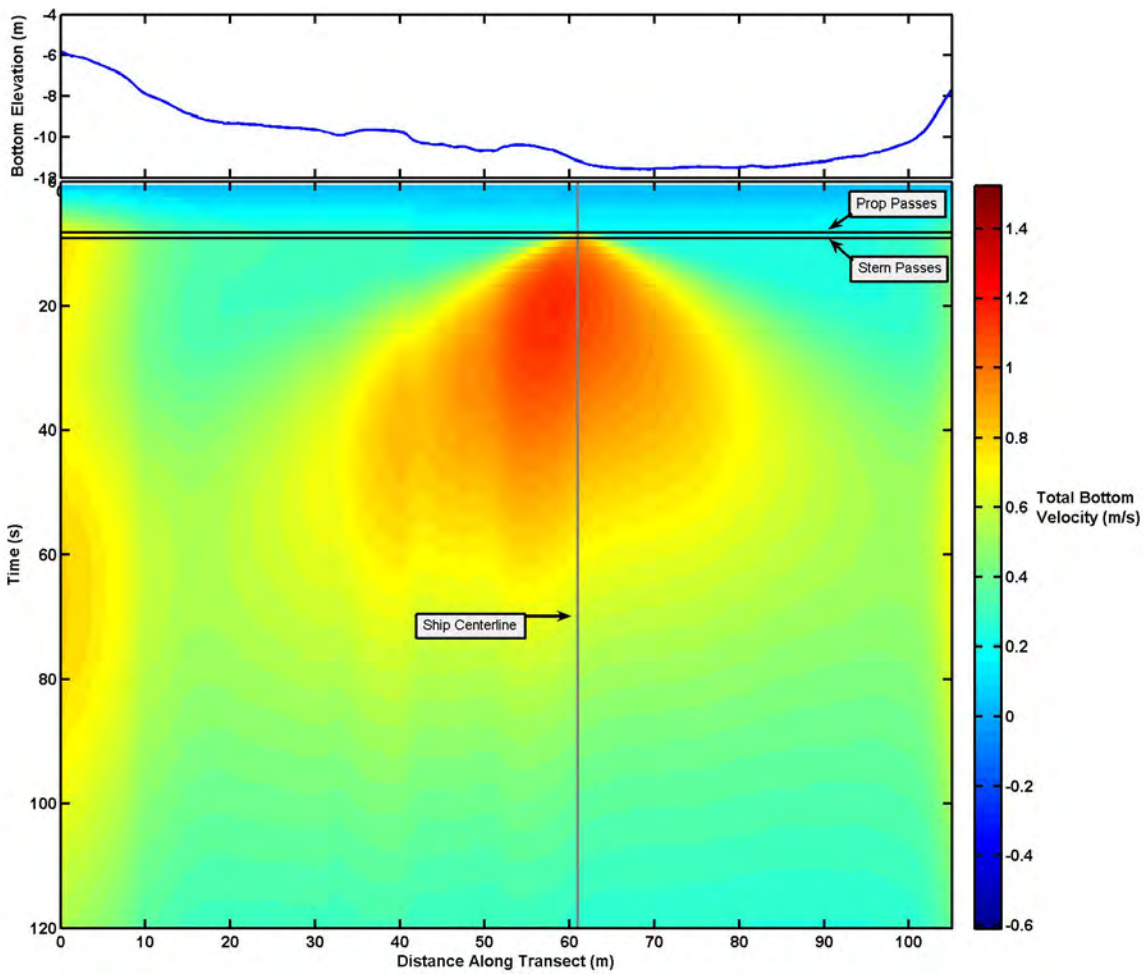

Figure 25. Contour plot of the total bottom velocity (m/s) along Transect 5 as a function of time for Vessel 2 running at a 100% of its maximum power. The top panel is a plot of the starting bathymetry along the transect.

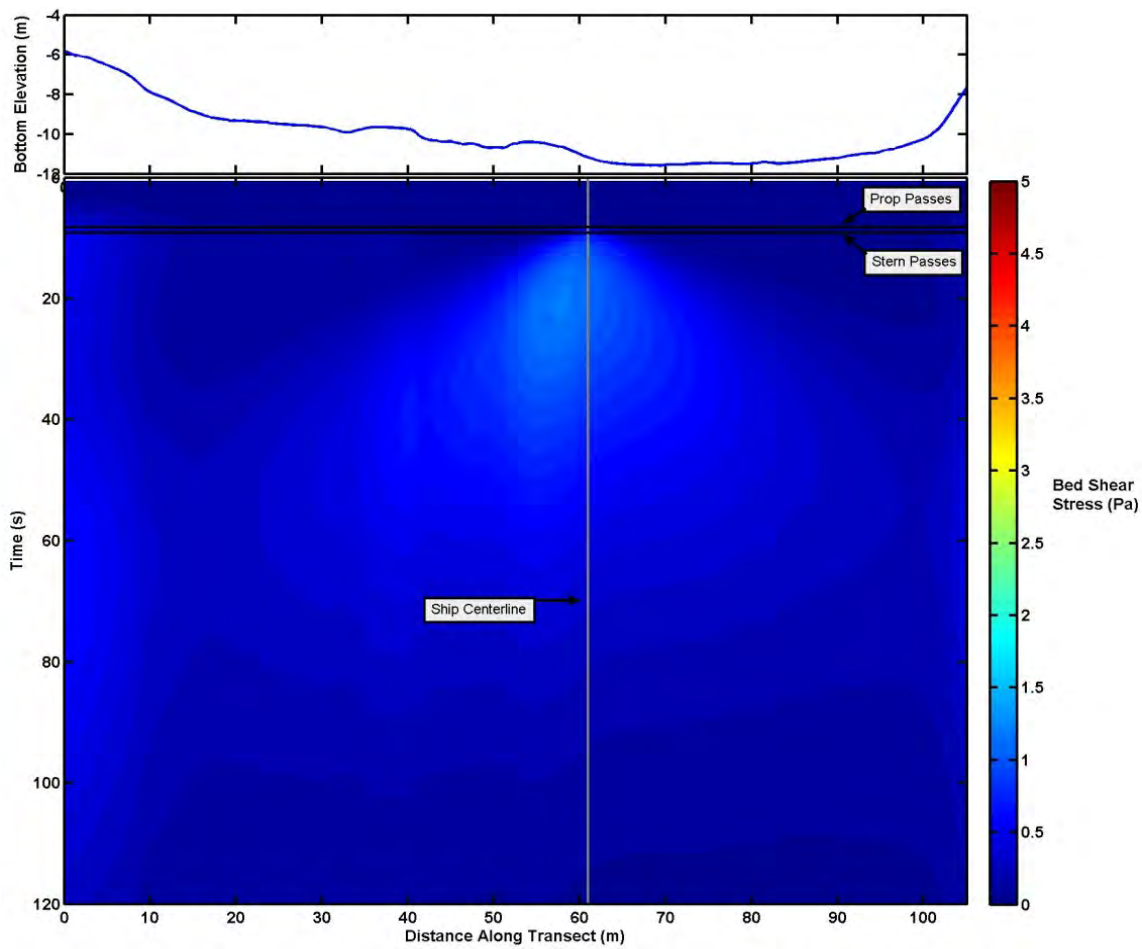

Figure 26. Contour plot of the bed shear stress (Pa) along Transect 5 as a function of time for Vessel 2 running at a 100% of its maximum power. The Top panel is a plot for the starting bathymetry along the transect.

Table 8. Maximum bottom velocity (m/s), maximum bed shear (Pa), maximum bed erosion (cm) and the average TSS concentration in Lauritzen Channel given different vessel and profile combinations for transiting case.

			Max Bottom Velocity (m/s)	Max Bed Shear (Pa)	Max Bed Erosion (cm)	Average TSS Concentration of Domain (mg/L)
100 % Throttle	Profile 1	Vessel 1	0.69	0.43	0.00	0.0
		Vessel 2	1.55	2.13	0.03	4.5
	Profile 2	Vessel 1	0.63	0.35	0.00	0.0
		Vessel 2	1.40	1.94	0.06	2.8
	Profile 3	Vessel 1	0.64	0.36	0.00	0.0
		Vessel 2	1.69	2.89	0.49	10.5
	Profile 4	Vessel 1	0.65	0.38	0.00	0.0
		Vessel 2	1.66	2.76	0.39	2.3
	Profile 5	Vessel 1	0.63	0.36	0.00	0.0
		Vessel 2	1.16	1.19	0.00	0.1
75 % Throttle	Profile 1	Vessel 1	0.61	0.33	0.00	0.0
		Vessel 2	1.25	1.46	0.01	1.1
	Profile 2	Vessel 1	0.55	0.27	0.00	0.0
		Vessel 2	1.30	1.67	0.03	1.1
	Profile 3	Vessel 1	0.56	0.28	0.00	0.0
		Vessel 2	1.58	2.52	0.26	5.1
	Profile 4	Vessel 1	0.57	0.29	0.00	0.0
		Vessel 2	1.55	2.40	0.20	1.1
	Profile 5	Vessel 1	0.56	0.27	0.00	0.0
		Vessel 2	1.03	0.94	0.00	0.0
50 % Throttle	Profile 1	Vessel 1	0.50	0.23	0.00	0.0
		Vessel 2	1.09	1.14	0.00	0.1
	Profile 2	Vessel 1	0.46	0.18	0.00	0.0
		Vessel 2	1.18	1.38	0.01	0.3
	Profile 3	Vessel 1	0.49	0.25	0.00	0.0
		Vessel 2	1.45	2.11	0.11	2.1
	Profile 4	Vessel 1	0.48	0.23	0.00	0.0
		Vessel 2	1.42	2.01	0.09	0.5
	Profile 5	Vessel 1	0.46	0.19	0.00	0.0
		Vessel 2	0.88	0.68	0.00	0.0
25 % Throttle	Profile 1	Vessel 1	0.37	0.12	0.00	0.0
		Vessel 2	0.93	0.85	0.00	0.0
	Profile 2	Vessel 1	0.38	0.14	0.00	0.0
		Vessel 2	1.03	1.04	0.00	0.0
	Profile 3	Vessel 1	0.49	0.25	0.00	0.0
		Vessel 2	1.28	1.64	0.04	0.6
	Profile 4	Vessel 1	0.48	0.23	0.00	0.0
		Vessel 2	1.25	1.56	0.03	0.1
	Profile 5	Vessel 1	0.33	0.10	0.00	0.0
		Vessel 2	0.78	0.60	0.00	0.0

Table 9. Total sediment mass resuspended into system from Vessel 1 and Vessel 2 operating at different fractions of their maximum power when transiting from Manson to the mouth of the Lauritzen Channel.

		Total Mass Resuspended Into Lauritzen Canal With Ship Moving from Profile 1 to Profile 5 (kg)
100% Throttle	Vessel 1	0
	Vessel 2	699
75% Throttle	Vessel 1	0
	Vessel 2	290
50% Throttle	Vessel 1	0
	Vessel 2	96
25% Throttle	Vessel 1	0
	Vessel 2	20

The procedures for determining suspended sediment loads caused by transiting vessels were modified to analyze the bed effects of a stationary vessel with a spinning propeller. For the stationary analysis, vessels were assumed fixed in position, but operating at a constant power for 10 minutes. This situation mimics a tug boat pushing against the side of a barge. Sediment beds were constructed for the stationary analysis by taking the five bed profiles examined in the Transiting Case, and extending the profiles roughly 30 m in both the north and south direction (i.e. assumed constant channel geometry in near proximity to the profile locations). Vessels were placed in the created domain 15.25 m from the western shoreline oriented with the propeller facing toward the center of the channel. Bottom velocities, bed shear stresses, and bed erosion were calculated in a similar fashion as the Transiting case with two main exceptions: 1) the bed velocity had no wake component because the vessels were stationary, and 2) the bed was analyzed over a domain instead of a transect. The stationary analysis was carried out for both Vessel 1 and Vessel 2 at the same four power percentages as the Transiting Case (25%, 50%, 75% and 100%). Again, the computations were iterative; near-bottom velocities, bed shear stresses, and erosion rates were calculated every second from t = 0 to t = 10 minutes, and the bed elevation was adjusted accordingly between time steps. The site-wide averaged sediment properties given in Table 6 were used in the analysis.

A contour plot of bottom velocities over the entire domain created using Transect 2 are presented in Figure 22. Profile lines used to create the beds for the Transiting Case of the propeller wash and ship wake model. The results are for Vessel 2 operating at 100% power at the end of the 10 minute period; however, the spatial velocity distributions were similar for all other combinations and times. The conical velocity distribution was consistent over all constructed domains but varied in magnitude with bathymetry changes between domains. The location of Vessel 2 in Figure 27 is marked by a white circle. Note that Figure 27 differs from the bottom velocity plot for the Transiting Case (Figure 24) in that it gives bottom velocities as a function of positioning (x and y) not distance along transect and time.

Similarly, bed shear stresses are presented in Figure 28. A maximum shear stress of 2.38 Pa occurred directly behind the propeller roughly five propeller diameters away. Erosion occurred when shear stress in a cell was greater than the critical shear stress of erosion of sediment. A spatial map of total erosion after a 10 minute time period is shown in Figure 29. Peak values for all three variables (bottom velocity, bed shear stress, and erosion) occurred approximately 10 m behind the propeller. High velocities occur at the far end of the model domain which is a shallow steep sloped region of bathymetry at the head of the Lauritzen Channel.

Maximum bottom velocities, maximum bed shear stresses, maximum bed erosion, and average TSS concentration over the domain are presented in Table 10 for all vessels, power and bed configurations analyzed. Average concentrations were calculated by assuming that all mobilized sediment remained suspended in the water column and uniformly mixed throughout the domain. The presented concentration values do not account for particle settling. The greatest erosion (approximately 10 cm) occurred for Vessel 2 operating at full power at Transect 3. Erosion depths created by Vessel 1 were less than 1 cm for all combinations except for Profile 2 with 100% power which had a maximum scour depth of approximately 10 cm. Maximum bed shear stresses ranged from 0.11 Pa to 2.52 Pa.

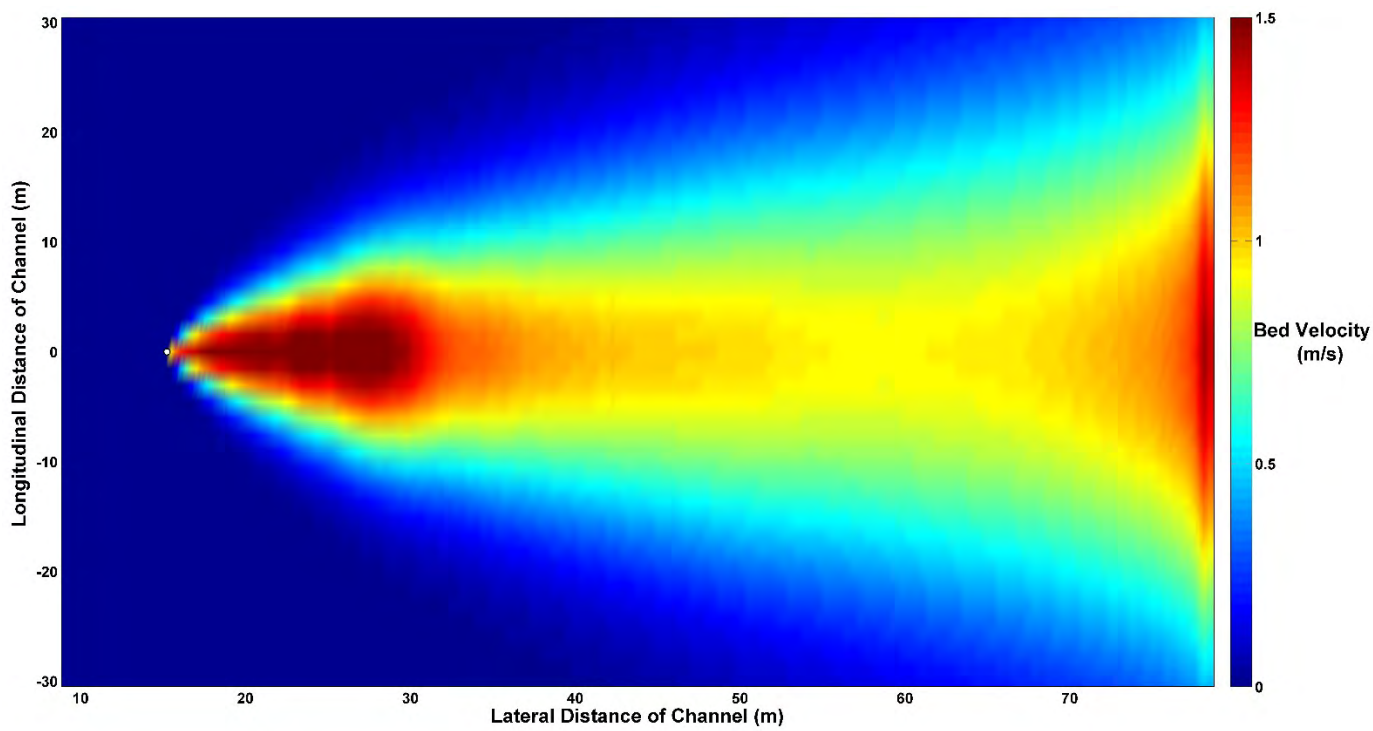

Figure 27. Bed Velocity due around Transect 2 due to 100% power from Vessel 2.

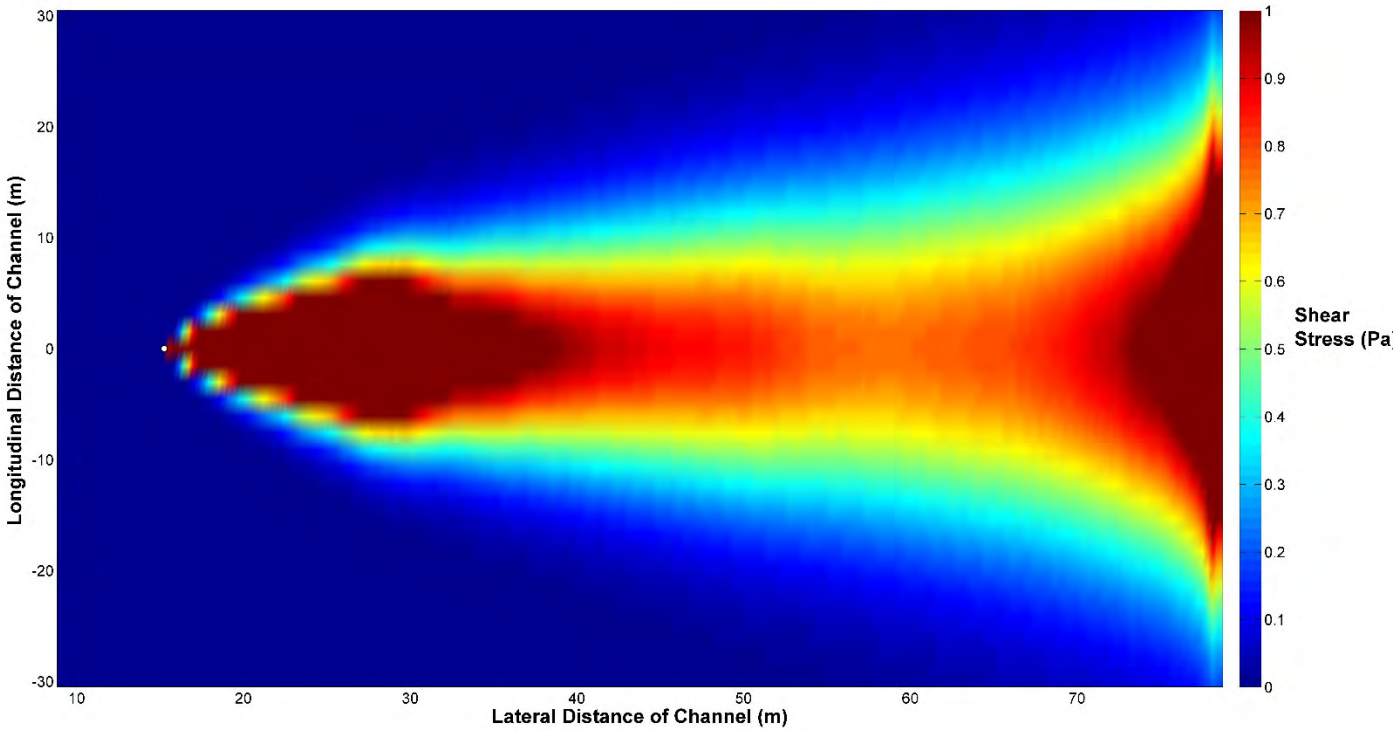

Figure 28. Bed Shear Stress around Transect 2 due to 100% power from Vessel 2.

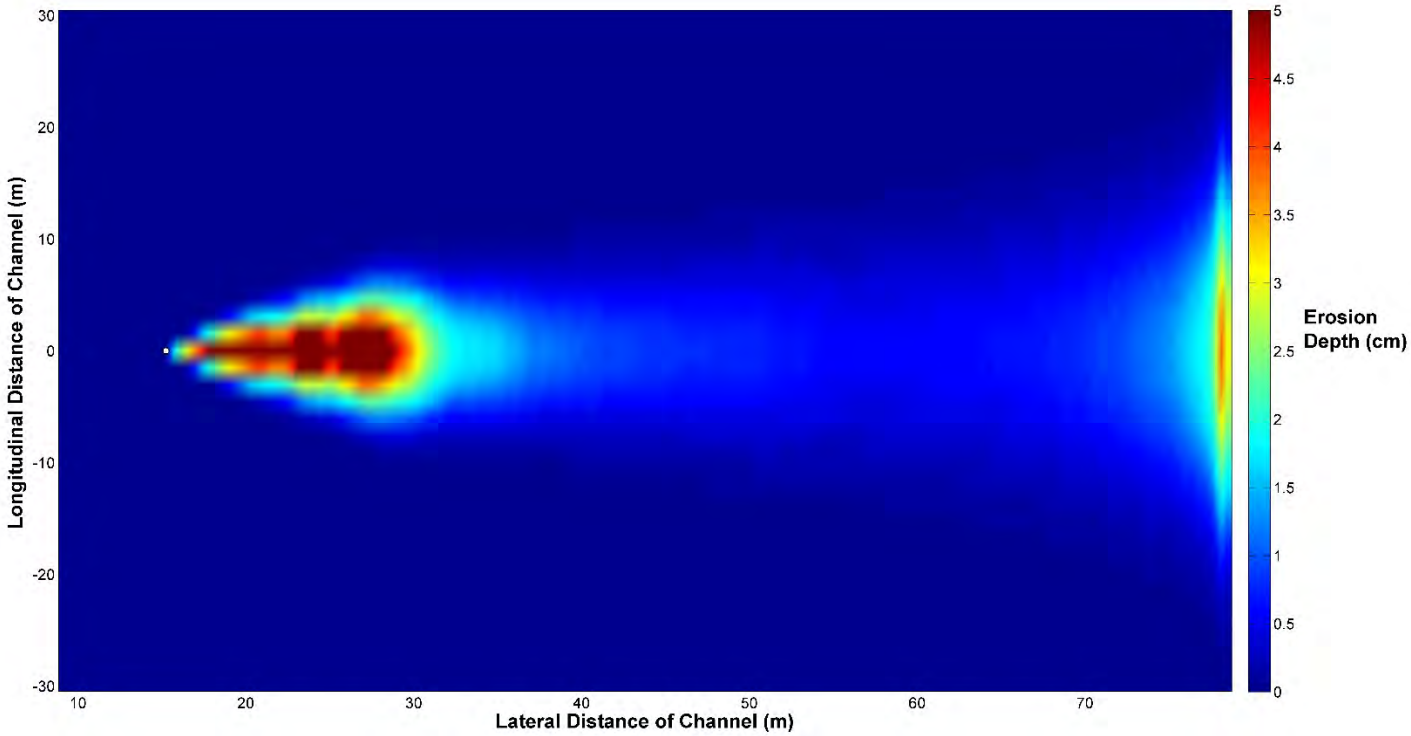

Figure 29. Bed erosion around Transect 2 due to 100% power from Vessel 2.

Table 10. Stationary vessel scour analysis results.

			Max Bottom Velocity (m/s)	Max Bed Shear (Pa)	Max Bed Erosion (cm)	Average TSS Concentration of Domain (mg/L)	Total Sediment Mass (kg)
100 % Throttle	Profile 1	Vessel 1	0.83	0.65	0.38	4.3	19.9
		Vessel 2	1.49	2.08	4.70	75.3	349.5
	Profile 2	Vessel 1	1.03	1.02	1.10	10.8	51.1
		Vessel 2	1.58	2.38	8.22	169.7	918.9
	Profile 3	Vessel 1	1.07	1.11	1.50	8.0	40.9
		Vessel 2	1.62	2.52	10.68	146.9	894.2
	Profile 4	Vessel 1	0.76	0.55	0.25	2.0	14.6
		Vessel 2	1.31	1.61	2.62	88.9	681.2
	Profile 5	Vessel 1	0.71	0.46	0.16	1.5	14.3
		Vessel 2	1.20	1.34	1.97	63.4	636.0
75 % Throttle	Profile 1	Vessel 1	0.73	0.49	0.19	0.8	3.2
		Vessel 2	1.31	1.59	2.56	38.5	177.5
	Profile 2	Vessel 1	0.90	0.08	0.59	4.8	22.3
		Vessel 2	1.39	1.84	3.36	83.0	450.2
	Profile 3	Vessel 1	0.94	0.84	0.74	3.5	17.4
		Vessel 2	1.43	1.97	3.99	69.8	429.2
	Profile 4	Vessel 1	0.66	0.41	0.12	0.5	3.4
		Vessel 2	1.14	1.22	1.73	43.6	332.5
	Profile 5	Vessel 1	0.62	0.34	0.08	0.3	3.2
		Vessel 2	1.04	1.02	1.19	30.3	302.8
50 % Throttle	Profile 1	Vessel 1	0.60	0.33	0.07	0.0	0.1
		Vessel 2	1.07	1.07	1.36	13.9	63.9
	Profile 2	Vessel 1	0.73	0.52	0.22	1.5	6.8
		Vessel 2	1.15	1.24	1.70	32.4	171.1
	Profile 3	Vessel 1	0.77	0.56	0.27	1.0	4.9
		Vessel 2	1.18	1.34	1.90	26.4	157.3
	Profile 4	Vessel 1	0.55	0.27	0.00	0.0	0.0
		Vessel 2	0.97	0.82	0.70	16.3	107.9
	Profile 5	Vessel 1	0.51	0.23	0.00	0.0	0.0
		Vessel 2	0.86	0.69	0.44	8.5	83.1
25 % Throttle	Profile 1	Vessel 1	0.42	0.17	0.00	0.0	0.0
		Vessel 2	0.76	0.54	0.25	0.9	3.8
	Profile 2	Vessel 1	0.53	0.26	0.00	0.0	0.0
		Vessel 2	0.82	0.64	0.37	3.9	18.3
	Profile 3	Vessel 1	0.55	0.29	0.00	0.0	0.0
		Vessel 2	0.85	0.69	0.44	2.7	13.3
	Profile 4	Vessel 1	0.39	0.14	0.00	0.0	0.0
		Vessel 2	0.67	0.42	0.10	0.3	1.9
	Profile 5	Vessel 1	0.36	0.11	0.00	0.0	0.0
		Vessel 2	0.61	0.35	0.08	0.1	0.5

4.3 Hydrodynamic Model

To better understand flow patterns and sediment transport at the United Heckathorn Superfund Site, a hydrodynamic and sediment transport model was developed using the Environmental Fluid Dynamics Code (EFDC). EFDC is a public domain modeling system that is currently maintained by Tetra Tech, Inc. and supported by the United States Environmental Protection Agency (USEPA). The modeling framework has been widely used to model hydrodynamic patterns and water quality in rivers, lakes, and coastal areas, with peer reviewed applications at over 50 sites (Hayter, 2006). EFDC solves depth-averaged Navier-Stokes equations and can be run in 2D or 3D (in 3D, vertical velocity components are solved using sigma layering and mass conservation) on both rectangular and curvilinear grids. Since tidal resuspension is not a concern in the system, the primary use of the model is to evaluate the dispersion of material resuspended during vessel activities. Model setup, model calibration and validation, and model results are presented below.

4.3.1 Model Domain and Grid Creation

A domain was chosen for the hydrodynamic model such that the circulation patterns in the Lauritzen Channel were accurately simulated. The domain extended from the turning basin in the northwest edge of the Santa Fe Channel to Richmond Inner Harbor. It included Richmond Yacht Harbor, Lauritzen Channel, and Parr Canal. In order to increase modeling resolution in the Lauritzen Channel, a curvilinear grid was created with varying resolution. In total, the domain contained 1,453 cells with 7 vertical sigma layers. The Santa Fe Channel was gridded with 637 relatively coarse cells (average area of 716 m^2) that increased in resolution near the mouth of the Lauritzen Channel (Figure 30). The Lauritzen Channel was meshed with high resolution using 816 cells with an average area of 49 m^2. Bathymetry data from the multibeam survey conducted by SEI during Tier 1 investigation was interpolated onto the grid by averaging all depth values within a cell. Cells that did not contain any bathymetry data were interpolated using a nearest neighbor approximation.

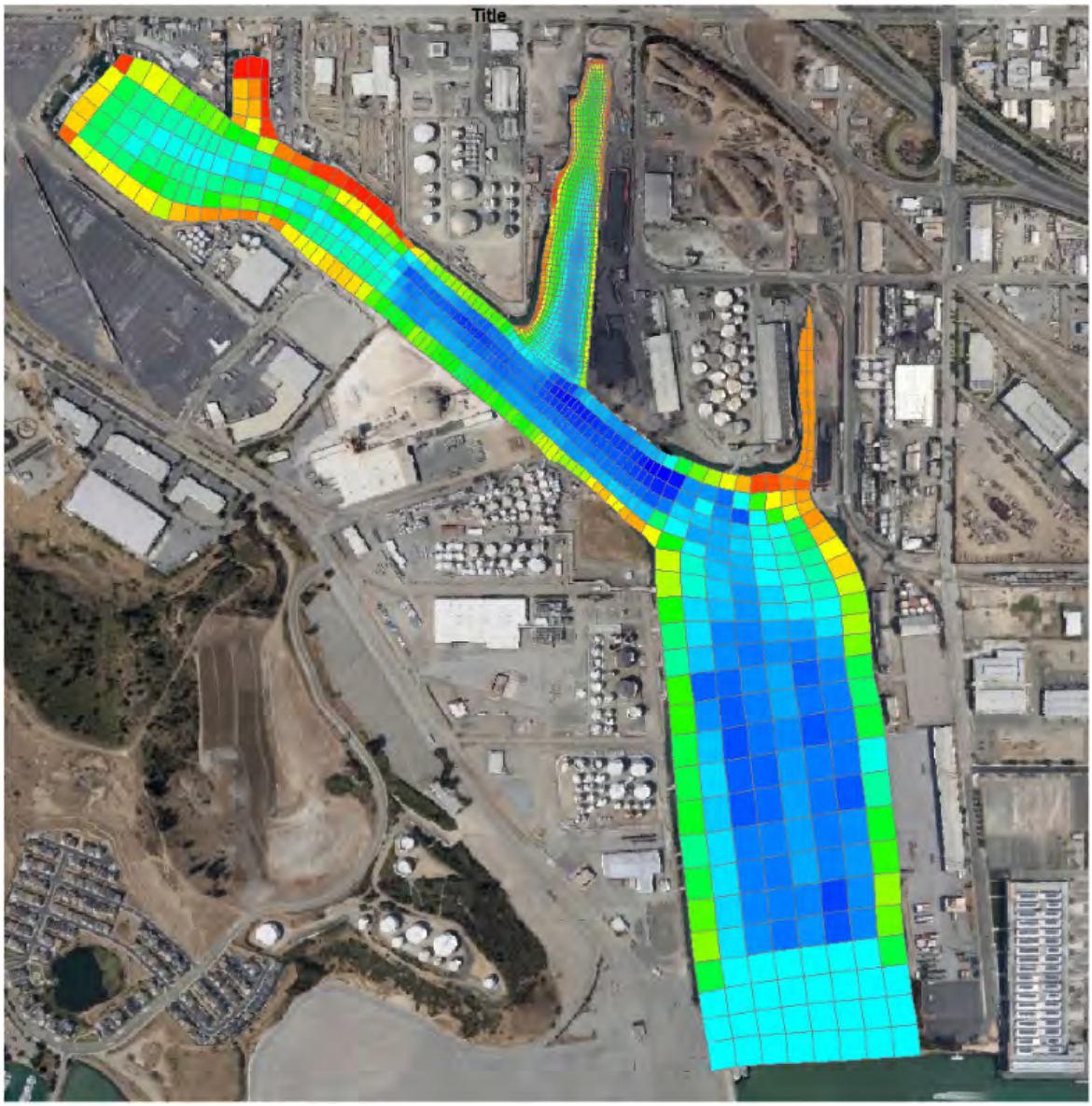

Figure 30. United Heckathorn hydrodynamic and sediment transport model domain and grid.

4.3.2 Boundary Conditions

The hydrodynamic model was forced by two conditions: 1) a water level was specified at the southern end of the Santa Fe Channel (southernmost boundary), and 2) a wind shear was applied uniformly over the domain. The specified water levels are displayed in Figure 31, which were obtained from the tidal predictor at the Richmond Inner Harbor station shown in Figure 32. Wind data came from the National Oceanic and Atmospheric Administration (NOAA) station at Richmond, CA. The Richmond station was chosen because data at the Point Potrero Station, nearest the study site, was incomplete for the study period.

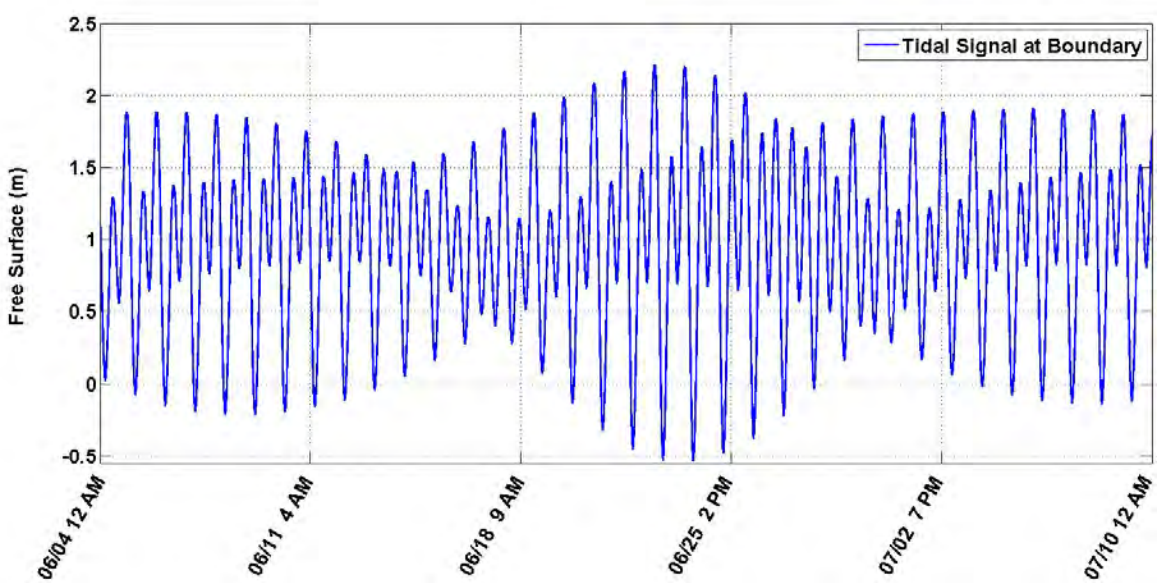

Figure 31. Tidal boundary conditions at the southern forced boundary of the model.

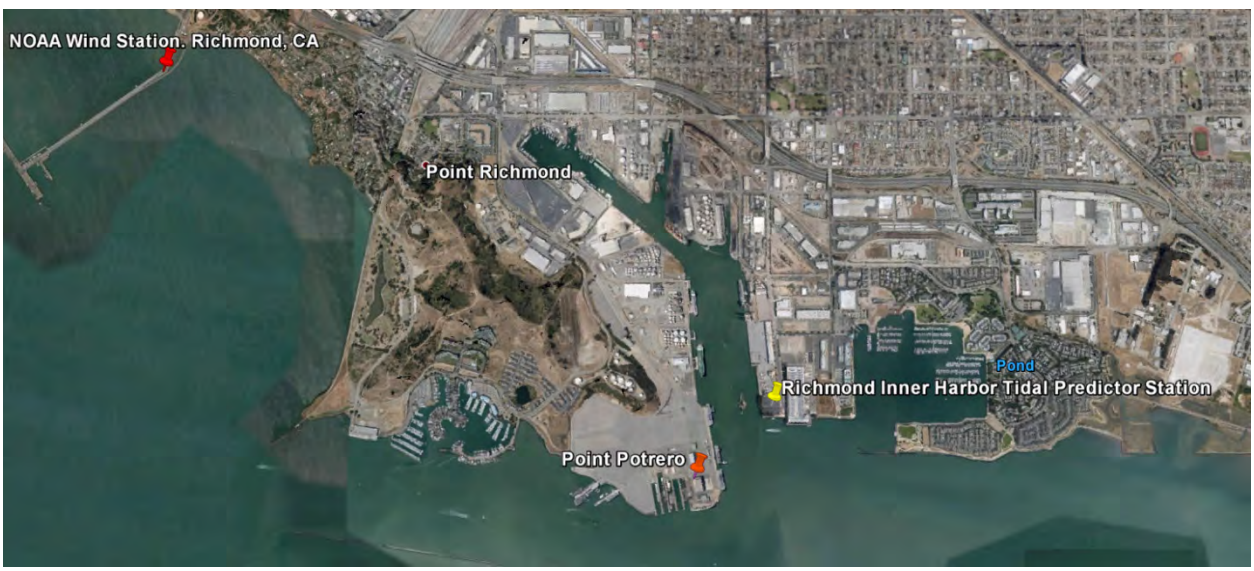

Figure 32. Locations of boundary condition data.

4.3.3 Model Validation

Modeled water level fluctuations were consistent with ADCP recorded water levels at both locations in the Lauritzen Channel. Figure 33 shows the entire study period for the station at the mouth of the Channel. The bottom panel highlights the consistency between modeled and measured water surface elevations in finer detail. The comparison of modeled to measured water level is very good with no drift over the 34 day measurement period. Some stair-stepping in the model data can be seen due to model output intervals (15 min.)

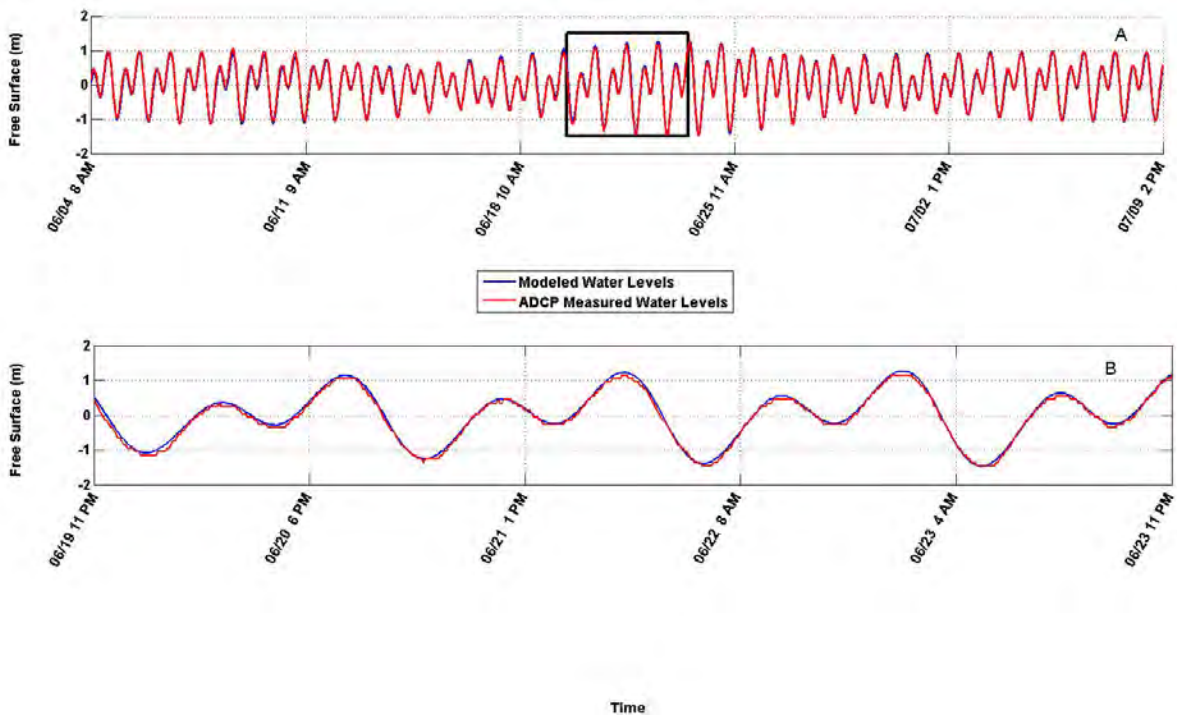

Figure 33. Water level comparison at mouth of Lauritzen Channel. Upper: Full study period. Lower: Zoomed in plot of boxed area in shown in the upper panel.

Velocities within the water column obtained at Station 1 from the ADCP were compared and used as a measure for the model velocities. Velocities were compared throughout the water column due to the multidirectional, low velocities (< 5 cm/s) recorded by the ADCP. Velocities from the ADCP were averaged based on the sigma layer thickness at each timestep from the model. Velocities were filtered to isolate variability due to tides. The modeled tidal velocities were within 2 to 3 cm/s (~ 30%) of the peak measured velocities but the low signal-to-noise velocities in the system did not facilitate direct model comparison. Analytical solutions of tidal velocities based on the tidal prism of the channel produced velocities consistent with the model (average velocities of 1 cm/s). The water levels described above were used as the primary calibration and validation metrics. Overall, the model was insensitive to adjustments in background eddy viscosities and bottom roughness, typical of similar systems, giving confidence in the model for the applications below.

4.3.4 Model Results

A study of the distribution of suspended sediment due to propeller wash from a stationary vessel was conducted to evaluate the patterns of sedimentation in Lauritzen Channel. Transects 1 and 4, corresponding to the location of the Manson Construction Company and LRTC sites were chosen to assess distribution characteristics. A total of 16 simulations assessing each vessel type at each location over peak flood, peak ebb, slack high water, and slack low water conditions were performed. TSS values in Table 11 were input at the propeller locations coincident with the stationary scour analysis.

Table 11. TSS values for sediment distribution analysis.

Transect	Vessel	TSS (mg/L)
1	1	32.5
	2	109.7
4	1	25.9
	2	242.9

TSS values were calculated as the ratio of mass flux and flowrate.

$$\boldsymbol{TSS} = \frac{\boldsymbol{Mass\ Flux}}{\boldsymbol{Flow}} \qquad \text{Eq. 16}$$

where Mass Flux was defined as the total mass suspended in the stationary propeller scour analysis over the duration of the suspension event. Flow was based on the maximum velocity experienced at the bed applied to the propeller area. Two sediment size classes were applied to the model representing two distinct grain sizes. Class 1 had a particle diameter of 10 µm and was based on the average D_{50} over all sediment cores collected for Sedflume analysis as representative of resuspended sediment. Class 2 was defined as the average D_{50} obtained during the LISST deployment as representative of what is in the water column and had a diameter of 51 µm. Settling velocities were calculated from (Cheng N. , 1997).

Sediment distributions in Figure 34 through Figure 41 are displayed as concentration suspended in the water column in mg/L or as deposited sediment mass in kg one day after release at a location along Transect 1. These figures represent conditions during the flood and slack low water events corresponding to maximum and minimum velocities present in the system. Transect 1 was chosen due to the significant tugboat traffic at the Manson Construction Company's facility and estimates of TSS input by both vessels was applied using the most conservative values related to the 100% horsepower approximations.

Sediments deposited to the bed during a flood tide event based on vessel 1 parameters are shown in Figure 34. Suspended sediments that have not yet settled after one day are shown in Figure 35. Both figures show confinement to the Lauritzen Channel. Larger initial TSS concentrations for Vessel 2 resulted in a greater distribution of sediment and an overall larger mass deposited to the bed (Figure 36) and still suspended within the water column one day after release (Figure 37). In this case, the deposited sediment was still confined to the channel, but the suspended sediment extended into the Santa Fe Channel. This suggests that the coarser sediments were settling out but the finer material remained in suspension and was transported throughout the system. Distribution of sediment during and after a slack tide event predominantly resulted in the confinement of both deposited and suspended sediment to the Lauritzen Channel as seen in Figure 38 through Figure 41. Most sediment quickly deposited near the mobilization point along the western edge of the Lauritzen channel, and did not reach the eastern bank. Similarly, sediments that remained suspended in the water column predominantly remained along

the western bank. Sediment suspended by Vessel 2 during slack tide, was transported to the main section the channel but was confined to the immediate vicinity of the channel mouth. In all cases where sediment was found outside of the Lauritzen Channel, higher masses were found near the shallower banks rather than in the deeper, larger flow regions near the center. These results are consistent with the particle tracking study's findings that solids released in Lauritzen Channel are being transported throughout the Lauritzen Channel over time.

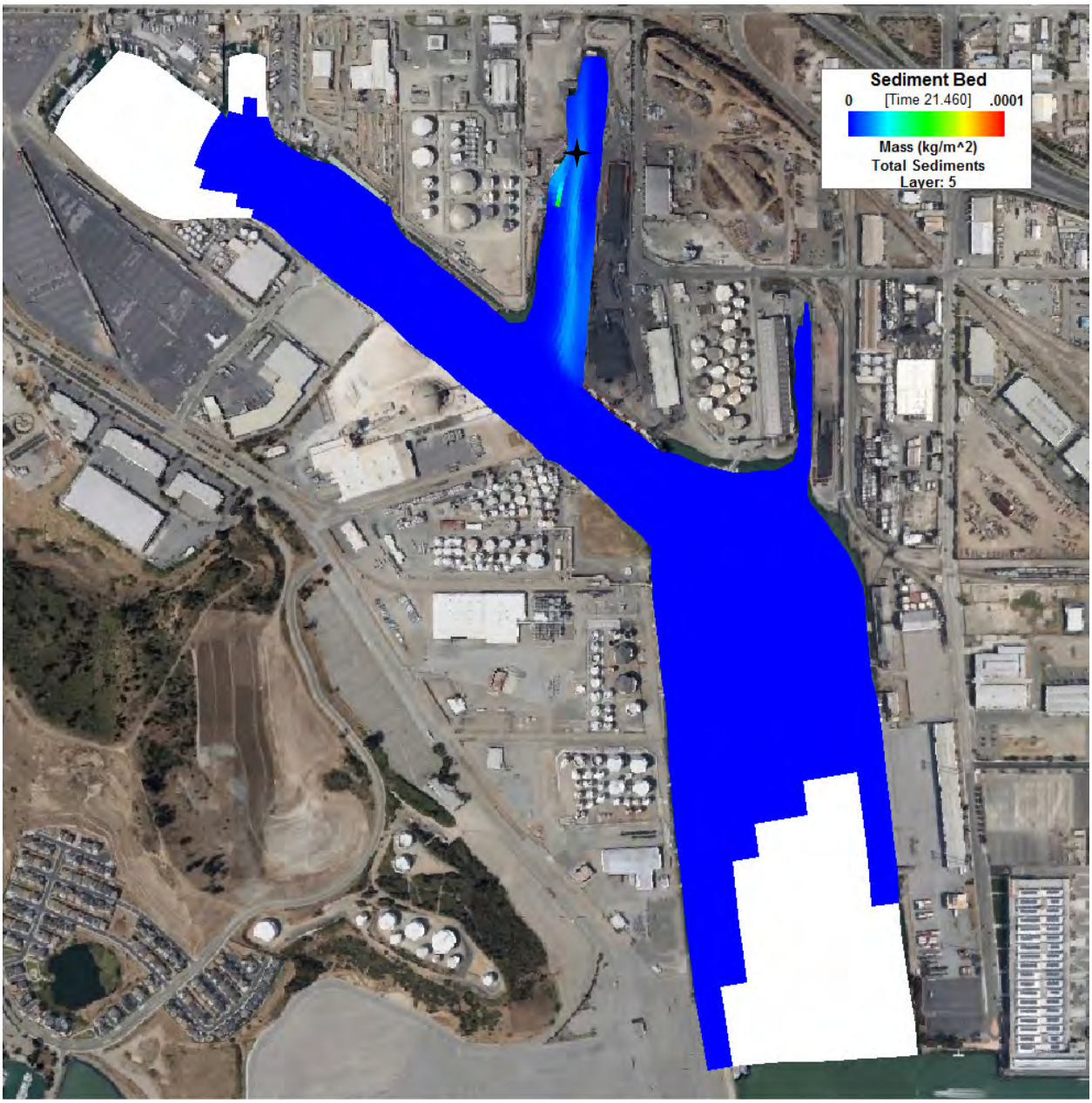

Figure 34. Distribution of mass at the sediment bed due to Vessel 1 parameters 1 day after release during maximum flood tide. Black Star denotes release point.

Figure 35. Distribution of suspended sediment due to Vessel 1 parameters 1 day after release during maximum flood tide. Black Star denotes release point.

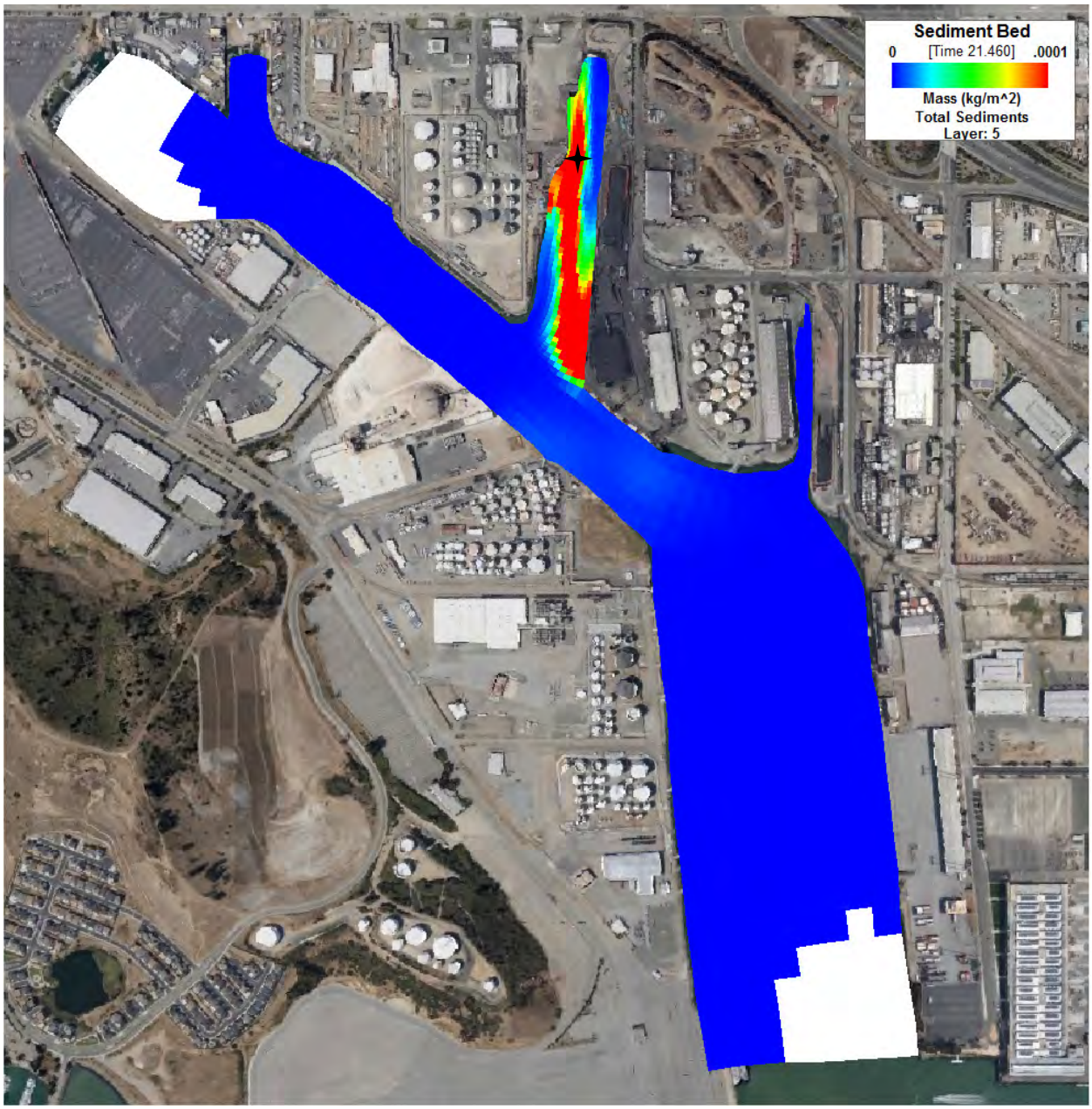

Figure 36. Distribution of mass at the sediment bed due to Vessel 2 parameters 1 day after release during maximum flood tide. Black Star denotes release point.

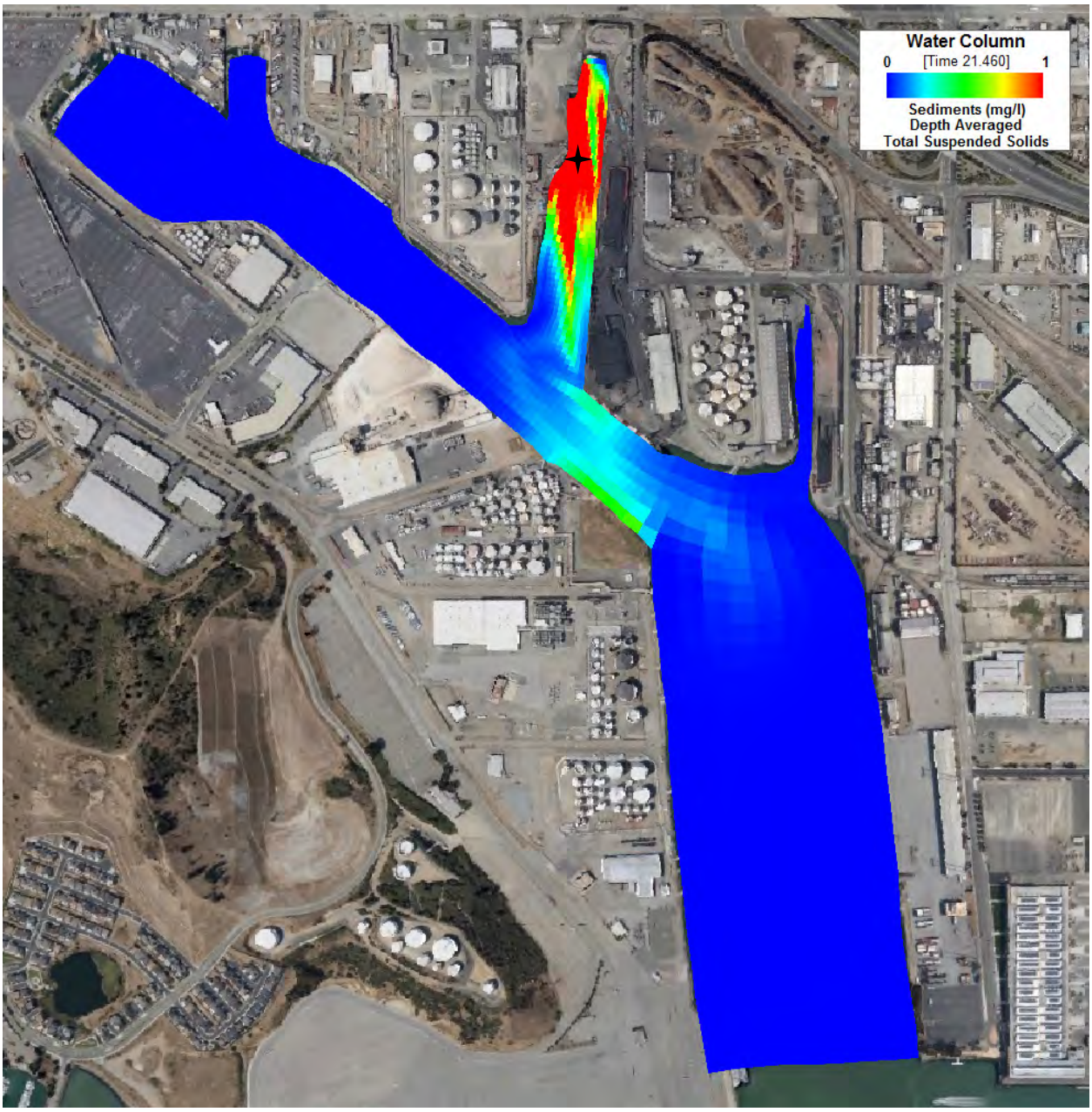

Figure 37. Distribution of suspended sediment due to Vessel 2 parameters 1 day after release during maximum flood tide. Black Star denotes release point.

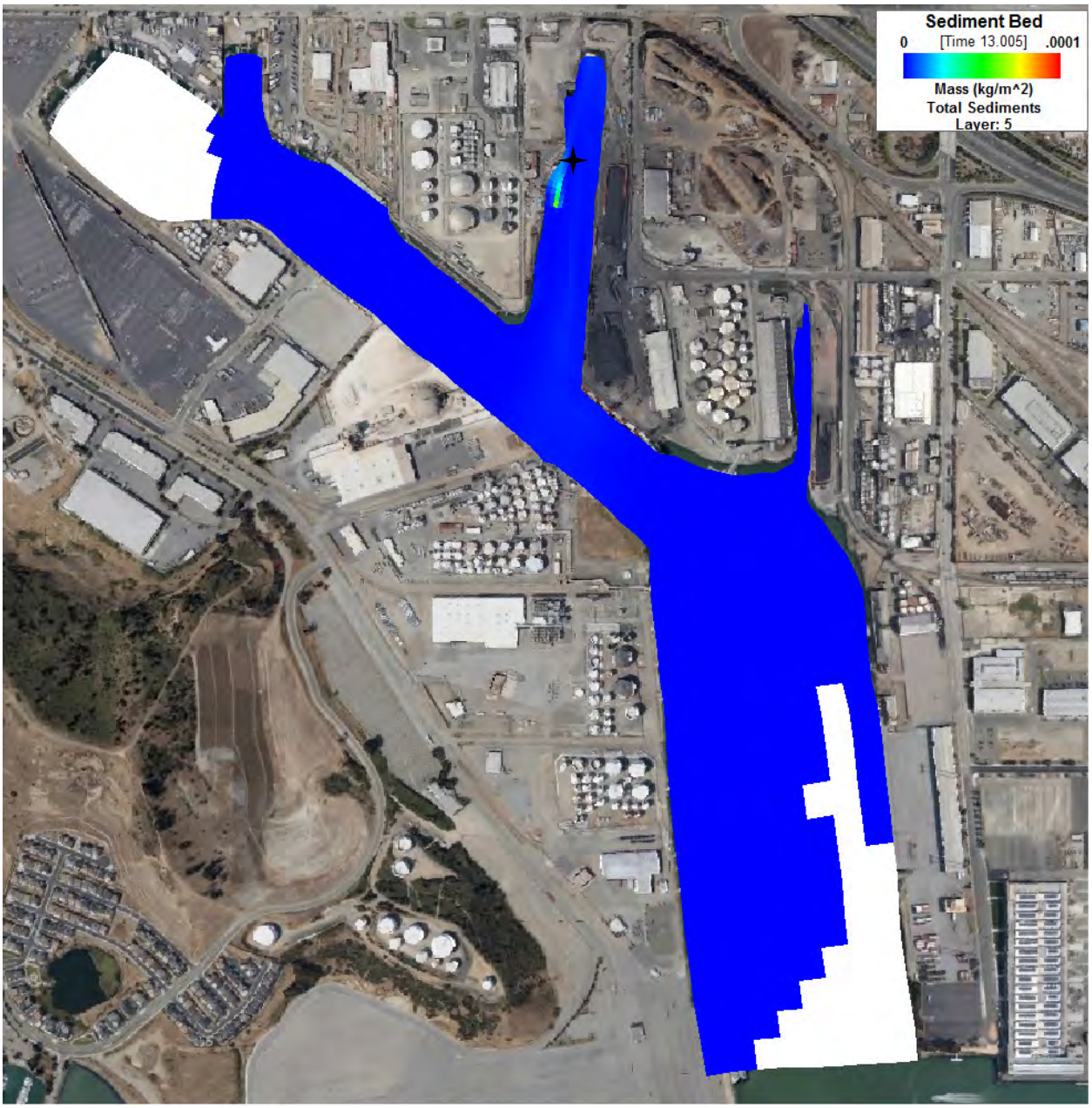

Figure 38. Distribution of mass at the sediment bed due to Vessel 1 parameters one day after release during a slack low tide event. Black Star denotes release point.

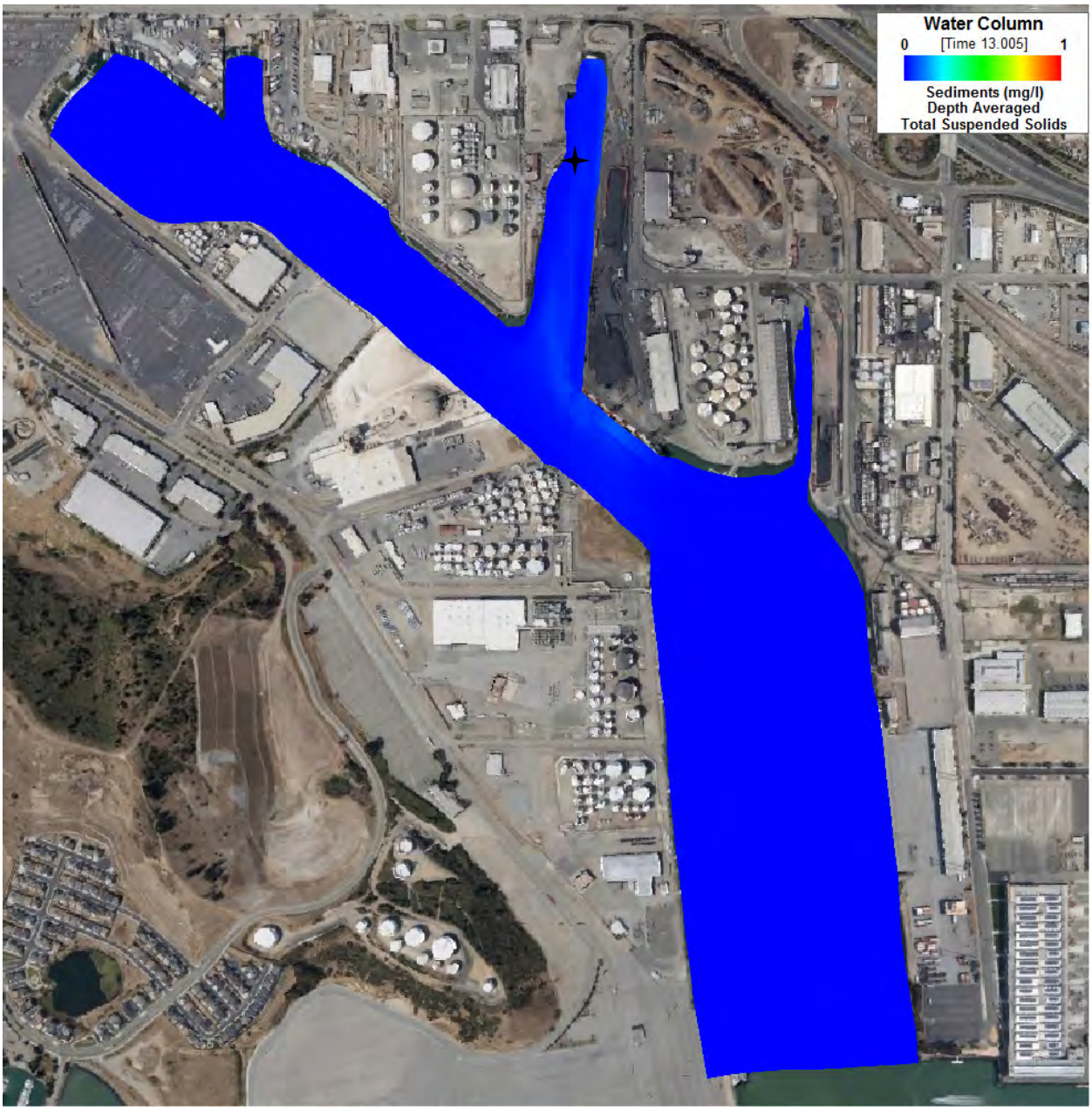

Figure 39. Distribution of suspended sediment due to Vessel 1 parameters one day after release during a slack low tide event. Black Star denotes release point.

Figure 40. Distribution of mass at the sediment bed due to Vessel 2 parameters one day after release during a slack low tide event. Black Star denotes release point.

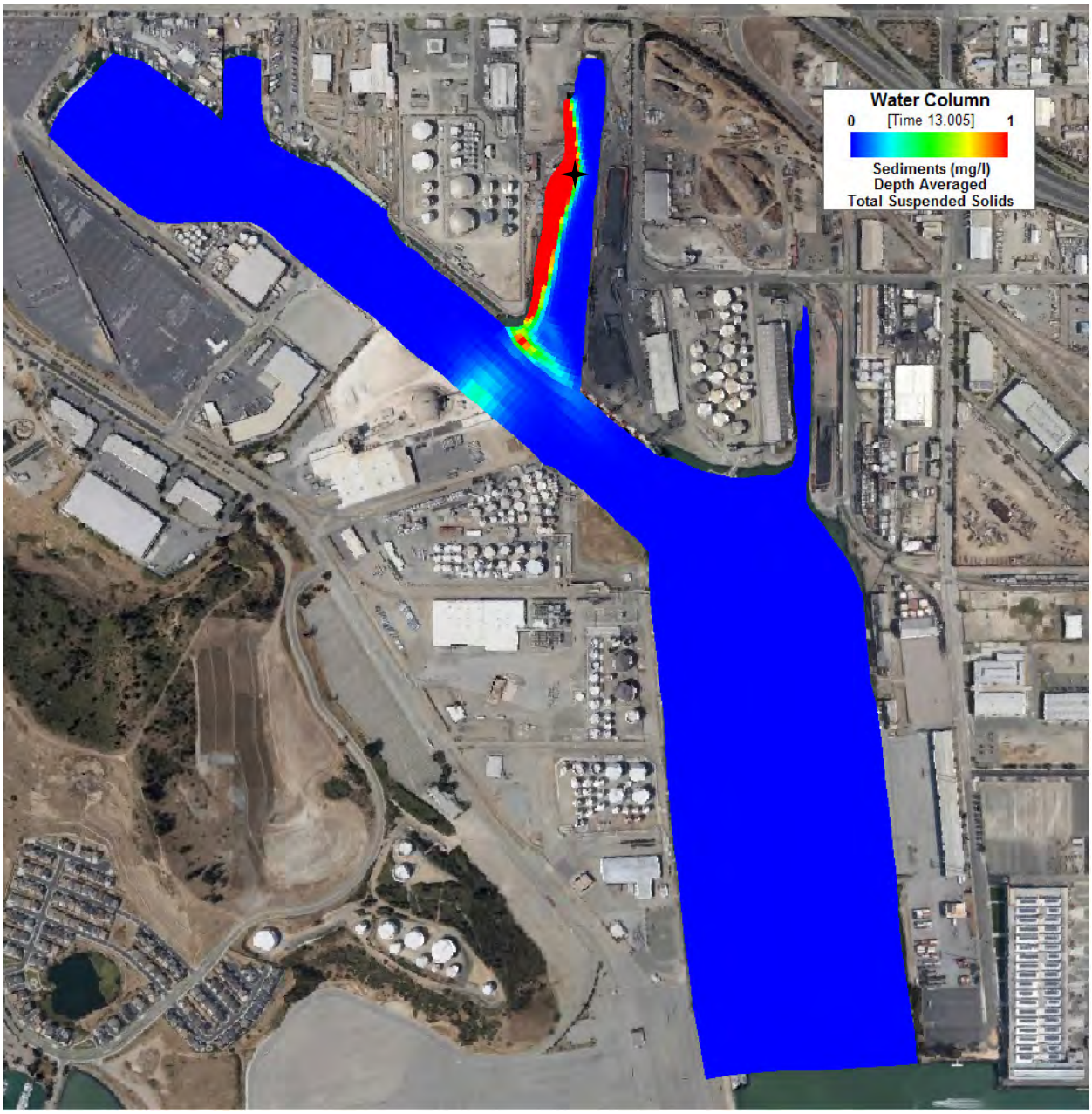

Figure 41. Distribution of suspended sediment due to Vessel 2 parameters one day after release during a slack low tide event. Black Star denotes release point.

5.0 Refined Sediment Transport CSM and Sediment Budget

At the Lauritzen Channel, where sediment-bound contaminants are the key risk factor, a sediment transport CSM is critical to addressing sediment management questions. The sediment transport CSM synthesizes all available data, describes a mass balance (i.e., a simple representation of all inputs and outputs to a system), and describes inferred sediment transport patterns (areas of deposition and erosion) based on grain size distribution, contaminant distribution, and hydrodynamic data. Potential

sediment transport trends were originally identified and described for the Lauritzen Channel in the Tier 1 CSM. The description was based the available data during Tier 1 investigations. In the paragraphs that follow, the Tier 1 CSM is refined to incorporate the data and results from Tier 2.

5.1 Sediment Transport Process Summary

In the absence of anthropogenic activity, the Lauritzen Channel is a low energy, constructed channel that is dominated by tidal circulation. Time-averaged, depth-averaged current velocity measured by both the ADCPs near the mouth and head of the Lauritzen Channel was near 0.01 m/s. Velocities calculated from the hydrodynamic model were similar in magnitude to the measured ADCP values, further validating the low energy of system. The small tidal velocities in the channel limit any potential for sediment resuspension due to tidal currents. Critical shear stresses measured during the Sedflume analysis ranged from 0.1 Pa to 1.28 Pa, while time-averaged tidally induced near-bottom shear stresses derived from the ADCP data were 0.04 Pa and 0.02 Pa for the mouth and head of the Lauritzen Channel, respectively (Table 5). Even the maximum tidally induced near-bottom shear stresses measured by the ADCPs (0.15 Pa) was only slightly above the measured critical shear stresses from the Sedflume analysis. It is concluded that turbulence fluctuations originating from tidal currents do not play a significant role in mobilizing sediment in the Lauritzen Channel. Generally, with the continuation of the San Francisco Bay as a primary sediment source, the channel on the whole is a sediment sink as seen in the continuous accumulation of YBM. In the absence of anthropogenic activity (e.g. dredging, vessel operations), the channel would continue to fill until a dynamic equilibrium between the tides and sediment sources is achieved (Bearman, Friedrichs, Jaffe, & Foxgrover, 2010).

The geophysical surveys show that vessel scour and spud anchoring activities have a widespread effect on mixing sediment up to 0.5 m in depth over wide swaths. The propeller wash and ship wake model used to assess the effects of vessel activity showed that the larger sized vessels operating in the Lauritzen Channel have the potential to mobilize sediment. Resuspension caused by a stationary vessel pushing against a barge or dock area was shown to be greater than resuspension from a transiting vessel, though both vessel operation types can lead to sediment suspension by increasing near-bottom velocity and the corresponding bed shear stress. The stationary vessel scour averages 1.4 cm of sediment resuspension with a maximum depth of approximately 10 cm. The wake caused by a transiting vessel, however, has a chance of mobilizing sediment near or under piers and in shoreline areas throughout the channel as a whole. However, the mass of sediment suspended during this type of operation would be low in comparison to the sediment suspended behind an operating stationary vessel. Overall, the vessel scour analysis shows that the deeper 0.5 m scour marks may be due to vessel keels dragging in the sediment instead of propeller scour. A keel drag would constitute a sediment mixing with very little net resuspension compared to the propeller scour even though the mixing at the bed is greater.

The particle tracking study also provided important insight into the importance of vessel activity on sediment transport. It was evident that during every sampling period, tracer was redistributed from both source areas in the channel. The magnets generally showed that material resuspended in the water column can be transported to the upper and west side of the channel and occasionally (2 events) along

the east side. The grab samples generally showed tracer presence from both sources throughout the sampling period. Since tidal currents have been demonstrated to be a negligible source of resuspension, vessel traffic (primarily tug and barge movement on the west side of the channel) was the likely source of tracer movement and responsible for tracer distribution in the channel sediment. The magnet outside the channel indicated that there was detectable transport out of the channel; however, the mass of material was at the detection limit of the method (i.e. very low mass). The modeling analysis also showed this to be a very low magnitude pathway.

The modeling simulations indicated that sediment deposition was minor to nonexistent outside of the Lauritzen Channel 1 day after releasing a hypothetical sediment plume comparable in size to the largest event that is expected from vessel activity. The results presented in Table 12 indicate over 93% of the sediment was deposited within Lauritzen Channel. In the model, some of the finer grained sediment remained suspended in the water column and advected into the Santa Fe Channel, but TSS concentrations were below 0.5 mg/L for even the most conservative case with the largest vessel (Vessel 2) operating at 100% power. Elevated TSS concentrations measured by the ADCPs likely resulted from sediment plumes generated by vessel activity, but it is difficult to correlate increased bottom velocity to the TSS spikes because of the potential for advective transport; an ADCP platform can be unaffected by a propeller jet but close enough to measure the advected sediment plume. All evidence suggests the net effect of vessel activities is a vertical mixing of the sediment, high local dispersion, and low far-field dispersion of sediment resuspended during vessel activities. The contaminant distribution pattern seen in the RI, which was characterized by over an order of magnitude decline in sediment DDT concentration with increasing distance from the Lauritzen Channel, further confirms low net transport out of the channel (White, Kohn, Gardiner, & Word, 1994). The low tidal circulation indicates that most of the sediment suspended during vessel operations would disperse locally and settle within the channel. Transport out of the Lauritzen Channel to the Santa Fe Channel does occur, but the sediment transport measurement and analysis conducted suggests that it is limited (approximately 7% of the resuspended material).

Table 12. Percentage of deposited sediment by location.

	Vessel 1		Vessel 2	
	Flood	Ebb	Flood	ebb
Percent Deposited - Lauritzen Channel	98.45	97.48	93.28	96.61
Percent Deposited - Santa Fe Channel	1.55	2.52	6.72	3.39

The net effect of the vessel activity in the low energy depositional channel can also be examined by looking at trends in YBM mass (Figure 5) and bathymetric change (Figure 4). Both show general accumulation behavior of sediment in the Lauritzen Channel. The largest amount of sediment accumulation is in the berth on the east side of the channel. The accumulation is occurring in the region where currents are likely the lowest, causing the dredged berth to behave locally as a sediment trap. Conversely, the west side of the channel, which experiences high vessel activity in shallow regions, exhibits low to no sediment accumulation of YBM and potential erosion in the bathymetric change (Figure 4). Finally, the head of the channel with low energy shallow water and moderate barge activity

shows a moderate YBM accumulation and a mix of potential erosion and deposition. Although each line of evidence has uncertainty associated with it, they are completely independent of each other and all express similar trends, thereby increasing the confidence in the overall pattern.

Since the remedial dredging and sand placement in 1996 and 1997, no dredging activities have been conducted in the Lauritzen Channel. Follow-on sampling in the channel revealed that the sand layer was not present in the majority of cores, including those where the YBM and Older Bay Mud (OBM) interface was present. The sampling additionally revealed that the sand distribution was heterogeneous throughout the channel. The fact that the sand, where present, is often buried to a depth of 0.5 m or more shows that there has been either deposition or downward mixing of the sand at locations throughout the channel (or both).The patchy distribution of the sand could be due to some combination of inconsistent sand placement and sediment disturbance.

Contaminants, particularly DDT, can also act as an indicator of sediment movement. Contaminant patterns in the Lauritzen Channel show heterogeneity similar to the sand distribution. The highest DDT concentrations are in regions of sediment accumulation in the head of the channel and the deep area on the east side of the channel. Lower concentrations are present along the west side of the channel, consistent with the thin YBM layer and potential sediment erosion in this region. It is important to note that bioturbation can mix sediment over an interval of a few mm to about 10 cm depending upon the resident species. However, given the large-scale mixing and heterogeneity in both the vertical and lateral distribution of sediment and DDT in the channel, it can generally be considered a secondary process with respect to sediment transport.

In summary, the Lauritzen Channel is a low-energy protected region with tidal velocities that are not likely to result in resuspension. The low energy coupled with sediment input from San Francisco Bay result in a net sediment accumulation in the channel. Ongoing vessel operations in the channel are responsible for localized mixing of the sediment bed, resuspension, and redistribution of sediment within the channel. A portion of the resuspended material may also be tidally dispersed into the Santa Fe Channel. The net effect of sediment transport processes in Lauritzen Channel is likely a heterogeneous distribution of contaminants with generally higher concentrations in areas of low sediment accumulation.

5.2 Conceptual Sediment Budget

A sediment budget is developed to account for the external inputs, outputs, and storage of sediment in a region due to the net effects of all of the sediment transport processes. The budget provides a useful tool for accounting for sediment and evaluating the effects of any changes to the system. Essentially the sediment budget is described by:

$$Sediment\ Input - Sediment\ Output = \Delta Sediment\ Storage$$

At a contaminated site in particular, the sediment budget provides the basis for accounting for contaminated sediment movement into and out of the system and storage within the system. The goal of the conceptual sediment budget is to identify the external inputs and outputs of sediment to the

system and identify potential methods for quantifying these processes. It is important to note that processes such as propeller scour can significantly alter deposition and erosion patterns within the system while the external exchange of sediment between the channel and the estuary remains unchanged if the mobilized sediment settles before transporting out of the channel. The propeller wash and ship wake model showed that up to 900 kg of sediment can be mobilized if the larger sized vessel operating in the Lauritzen Channel is stationary and running at 100% of its power for 10 minutes. This scenario is unlikely, but it gives a conservative upper limit to the amount of sediment that can be mobilized from vessel activity. The sediment transport modeling showed that the largest fraction of the suspended sediment settled within a 100 m of the vessel activity and did not contribute to the overall sediment budget of the Lauritzen Channel.

The key external sediment inputs to the Lauritzen Channel are the tidal delivery of sediment from San Francisco Bay and upland runoff during wet weather. The bay provides a constant delivery of silt and clay to the margins, including harbors. Tidal delivery of sediment was investigated by examining sediment fluxes calculated from the ADCP data. Sediment flux oscillated with tidal variability; daily averaged flux values were negligible. When summed over the entire 34 day deployment period, the net sediment transport due to tidal delivery was nearly zero. However, the ADCPs were deployed during summer months when sediment delivery from the bay is generally low (Schoellhamer, 1996). Had the ADCPs been deployed during winter months, increased flux from the bay may have been more apparent. In order to quantify the overall mass exchange of the Lauritzen Channel with the Santa Fe Channel over a long time period, additional ADCP data are required, particularly during winter months.

The delivery of sediment from upland sources is primarily due to the municipal stormwater outfall at the head of the channel. Data are not readily available on the yearly flow and associated sediment load associated with the outfall. Because little rainfall occurred during the ADCP deployment period, no effects of the outfall were seen in the water column with the exception of anecdotal observations of a TSS plume near the outfall that was not detected at either of the platforms. The “Simple” method of load estimation from the U.S. Department of Agriculture (1986) can be used for the total load from local upland sources. Assuming the drainage area of the catchment draining into the channel is approximately 100 acres (anecdotal evidence from drainage areas) and the local industrial land use TSS associated with outfall discharges is 120 mg/L (United States Department of Agriculture (USDA); Natural Resources Conservation Service (NRCS), 1986), the local average annual rainfall of 23 in (58 cm) can be used to determine an average yearly sediment load of ~ 20,000 kg.

A balance of sediment sources verifies that the tidal delivery of sediment is the largest order of magnitude external sediment source to the region. The net result of the YBM thickness analysis is that from 2001 to 2013 the sediment accumulation rate is 2.5 million kg/yr. Comparison of the sediment accumulation rate to the loading from the adjacent upland area shows that the upland loading could be responsible for a maximum of 1% of the accumulation in the channel. These calculations, even with associated uncertainty, show that the tidal delivery of sediment from the Bay is the largest contributor of sediment to the channel. Note that while the measured flux of sediment was negligible, the

measurements are only representative of a dry month and not wet periods when the primary delivery of sediment from all sources occurs.

The head of the Lauritzen Channel and the LRTC berth appear to be the regions of most consistent sediment deposition. While the San Francisco Bay does represent the largest external source of sediment, the persistence of high contamination in the channel is most likely due to an incomplete removal during remedial activities as discussed in the Source Identification Study Report (CH2MHILL, 2013b). The propeller wash and ship wake model indicated that the larger vessels operating in the Lauritzen Channel can mobilize sediment and redistribute them within the channel. Given enough time, deposition of sediment from the Bay will bury the contaminants, but the process will be slow because of the remixing from vessel activity.

The sediment outputs are the net result of suspended sediment in the channel that can be transported out by the tide. The key resuspension processes that have been identified are the vessel operations. As discussed, the props, keels, and anchor spuds of vessels may cause localized resuspension. Another source of suspended sediment in the system is suspended solids from outfalls during storm events. Although much of this material is likely to accumulate locally in the Lauritzen Channel, DDT contamination in the Santa Fe Channel suggests that low-level tidal dispersion and transport of sediment resuspended in the channel occurs.

6.0 Summary and Sediment Management Questions

The magnitude and frequency of sediment resuspension and transport due to anthropogenic processes were quantified to accurately determine the potential for sediment accumulation, contaminant redistribution, and potential for recontamination; and to support the development of effective remedial alternatives in the FFS.

The following field activities were performed to provide the necessary data for the transport quantification:

- Acoustic and optical sensors were deployed to measure profiles of velocity and proxies for TSS at two locations.
- Sediment flux throughout the channel was determined from measurements of channel velocity and TSS.
- Erosion rate measurements were made using Sedflume to develop a spatial picture of sediment erosion properties in order to better understand the potential for future sediment mixing, erosion, and transport.
- Sediment tracers were deployed and monitored in an area of high vessel activity to assist in quantifying sediment transport due to vessel activity.

In addition to the field activities, further analytic activities were performed as part of the Tier 2 analysis to support the quantification of the sediment and contaminant transport processes. The following analytic activities were performed:

- A sediment flux analysis was conducted to determine offsite transport and potential recontamination within the Lauritzen Channel based on the field data. The flux analysis provided quantitative information on the movement of sediment in the Channel.
- Erosion potential was determined using models of propeller scour to quantify sediment mixing depths and volumes during typical vessel operations using the bathymetric, sediment erosion, and suspended solids data.
- Modeling of the area using EFDC was performed to determine spatial and temporal patterns of suspended sediment transport in the Lauritzen and Santa Fe Channels. The primary goal of the modeling was to determine transport and deposition patterns of material resuspended during various anthropogenic events.
- The quantitative model was coupled with the field data analysis to refine the CSM. The refined CSM can be used to help answer sediment management questions and help assess the remedial alternatives development.

6.1 Site Management Questions

This document developed a Tier 2 sediment transport CSM for the United Heckathorn Superfund Site. The Tier 2 CSM has been used address the following sediment management questions:

- What is the source(s) of the sediment accumulating in the Lauritzen Channel?

The low energy Lauritzen Channel provides an ideal environment for deposition of sediment. The supply comes primarily from the San Francisco Bay with minimal input (~ 1%) from the outfalls into the Lauritzen Channel. Although the low nature of the flux during the dry period of measurement does not allow for direct quantification, the tidal delivery of sediment on a daily basis, even during the dry summer months, generally indicates that the bay is the primary source of accumulating sediment.

- How does sediment transport lead to the redistribution of contamination within the Lauritzen Channel, or movement of contamination out of the channel?

The velocities measured during the Tier 2 field study verify that the tidal velocities are very low, allowing for sediment deposition. The observations during the Tier 2 study verified the Tier 1 conclusion that vessel activity is the primary source of resuspension and redistribution in the Lauritzen Channel. The tracer study provided evidence of vessel resuspension and redistribution of sediment at the tracer locations throughout the channel. Vessel scour analysis showed that while the vessels can scour up to approximately 10 cm of sediment, the modeling studies showed that the greatest portion of this sediment settles locally leading to local redistribution of contamination within the channel. A portion of the material resuspended, particularly near the mouth during an ebb tide, could be transported out to the Santa Fe Channel; however, the tracer and modeling study showed the mass to be negligible. Evidence indicates that the primary region of resuspension is along the Manson facility and not at the mouth of the channel.

- If part of the Lauritzen Channel is actively remediated, could sediment transport lead to the recontamination of the remediated area?

The natural transport processes alone would not lead to recontamination of the remediated areas. If high contaminant concentrations remain in locations that could be disturbed by anthropogenic activities, they could be redistributed to actively remediated areas.

7.0 Reference

Anderson, B., Hunt, J., Phillips, B., Stoelting, M., Becker, J., Fairey, R., Puckett, H., Stephenson, M., Tjeerdema, R., and Martin, M. (2000). Ecotoxicologic change at a remediated Superfund site in San Francisco, Calilfornia, USA. *Environ. Toxicol. And Chem.*, 19(4) doi:10.1002/etc. 5620190414, 879-887.

Antrim, L., & Kohn, N. (2000). *Post-remediation Biomonitoring of Pesticides and Other Contaminants in Marine Waters and Sediment near the United Heckathorn Superfund Site, Richmond California.* Sequim, WA: Tech. Rep. PNNL-11911 Rev 1, Pacific Northwest National Laboratory.

Bearman, J., Friedrichs, C., Jaffe, B., & Foxgrover, A. (2010). Spatial Trends in Tidal Flat Shape and Associated Environmental Parameters in South San Francisco Bay. *Journal of Coastal Research*, 26 (342-349).

Black, K., Wilson, P., & Evans, D. (2007). The use of particle tracking in sediment transport studies: a review. *Coastal and Shelf Sediment Transport, Geological Society of London Special Pub.*, (274) 73-91.

Blake, A., Chadwick, D., White, P., & Jones, C. (2007). *User's Guide for Assessing Sediment Transport at Navy Facilities. Tech Report. 1960, U.S. Navy.* San Diego, CA: SPAWAR Systems Center.

CH2M HILL. (2013(a)). *Summary of Field Activities to Support Phase 4 Source Identification Study United Heckathorn Superfund Site, Richmond, California January 3.*

CH2M HILL. (2013(b)). *Draft Source Identification Study Report, United Heckathorn Superfund Site.* USEPA Region 9.

CH2M HILL; Sea Engineering Inc. (2013). *United Heckathorn Superfund Site: Tier 1 Sediment Transport Study.* April.

Chemical Waste Management Inc. (1997). *Draft Completion Report: Completion Report for Marine Remedial Action on the United Heckathorn Site, Richmond California.*

Cheng, N. (1997). Simplified settling velocity formula for sediment paritcles. *Journal of Hydraulic Engineering, 123(2)*, 149-152.

Cheng, R., & Gartner, J. (1984). *Tides, tidal and residual currents in San Francisco Bay, California-Results of measurements.* Part 1. Description of Data, U.S. Geological Survey Water Resource investigation Report, Menlo Park, Ca.

Downing, A., Thorne, P., & Vincent, C. (1995). Backscattering from a suspension in the near-field of a piston transducer. *J. Acoustic Society of America, 97*, 1614.

Foss Maritime Company. (2013, 8 21). Retrieved from http://www.fossmaritime.com/fleet/#filter=.harbor-tugs & http://www.workboat.com/newsdetail.aspx?id=17981

Foster, I. (2000). *Tracers in Geomorphology,.* Chichister: Wiley.

Gartner, J. (2004). Estimating suspended solids concentrations from backscatter intenisty measured by acoustic Doppler current profiler in San Francisco Bay, Califorina. *Marine Geology, 211*, 169-187.

Greger Pacific Marine. (2013, 8 21). Retrieved from pacifictowboatservice.com: http://pacifictowboatservice.com/tugs.htm

Hayter, E. (2006). *Evaluation of the State-of-the-art Contaminated Sediment Transport and Fate Modeling System.* EPA/600/R-06/108, U.S. Environmental Protection Agency, Washington D.C.

Maynord, S. (2000). *Physical Forces near Commercial Tows, Upper Mississippi River-Illinois Waterway System Navigation Study.* U.S Army Engineer Research and Development Center, Vicksburg, MS.

Parker, G. (2004). *1D Sediment Transport Morphodynamics, with Applications to Rivers and Turbidity Currents.* E-Book located at: http://cee.uiuc.edu/people/parkerg/morphodynamics_e-books.htm. Retrieved from http://cee.uiuc.edu/people/parkerg/morphodynamics_e-book.htm

Roberts, J., Jepsen, R., Gotthard, D., & Lick, W. (1998). Effects of paritcle size and bulk density on erosion of quartz particles. *Journal of Hydaulic Engineering, 124(12)*, 1261-1267.

Schoellhamer, D. (1996). Factos affecting suspended solids concentrations in South San Francisco Bay, California. *Journal of Geophysical Research*, 12087-12095.

Sea Engineering Inc. (2013). *United Heckathorn Superfund Site: Tier 1 Sediment Transport Study.* Santa Cruz, CA.

Shulkin, M., & Marsh, H. (1962). Sound absorption in sea water. *J. Acoustic. Soc. Amer.*, 34,864-865.

Thorne, P., Vincent, C., Hardcastle, P., Rehman, S., & Pearson, N. (1991). Measuring suspended sediment concentrations using acoustic backscatter devices. *Marine Geology, 96*, 7-16.

United States Department of Agriculture (USDA); Natural Resources Conservation Service (NRCS). (1986). *Technical Release 55: Urban Hydrology for Small Watersheds, 2nd Edition.* Washington D.C.

United States Environmental Protection Agency (USEPA). (1994). *EPA Superfund Record of Decision: United Heckathorn Site, Richmond, CA.* EPA/ROD/R09-95/121.

Wall, G., Nystrom, E., & Litten, S. (2006). *Use of an ADCP to Compute Suspended Sediment Discharge in The Tidal Hudson River, New York.* Reston, Virginia; U.S.: U.S. Geological Survey.

White, P., Kohn, N., Gardiner, W., & Word, J. (1994). *The Remedial investigation of Marine Sediment at the United Heckathorn Superfun Site, Tech. Report PNL-9383.* Sequim, WA: Pacific Northwest Laboratory.

White, T. (1998). Status of measurment techniques for coastal sediment transport. *Coastal Engineering*, 17-45.

Appendix A. Hydrodynamic Field Study

Introduction

Sea Engineering, Inc. (SEI) conducted hydrodynamic field studies in the Lauritzen Channel as part of the CH2MHill Tier 2 Sediment Transport Study, United Heckathorn Superfund Site. SEI deployed two bottom-mounted mooring platforms, each equipped with a Teledyne RDI 1200 kHz Workhorse Sentinel Acoustic Doppler Current Profiler (ADCP) and a Yellow Springs, Inc. (YSI) water quality sonde with temperature, pressure, and optical turbidity probes. The two instrumented platforms were deployed at the mouth and near the head of the channel in ~11 m and ~7 m mean water depth between 4 June and 9 July 2013.

SEI also conducted vessel-mounted ADCP surveys during the initial deployment and the final recovery. Water samples for laboratory analysis of total suspended solids concentration (TSS) and vertical profiles of particle size distribution (PSD) using a Sequoia Scientific, Inc. LISST-100X were collected at the moored platform locations during ADCP survey activities.

The primary objective of the hydrodynamic data collection was to determine the magnitude and frequency of sediment resuspension and the magnitude and direction of sediment flux. This document describes hydrodynamic data collection procedures and presents the hydrodynamic data collected during the Tier 2 Sediment Transport Study, Task 2 Hydrodynamic Data Collection. The study area and field sampling assets are shown in Figure 1.

Figure 1. Site map. The locations of the two bottom-mounted platforms are represented by red circles and ADCP survey lines are indicated in green.

Methods

Bottom-Mount Platforms

The ADCPs were mounted "uplooking" on bottom-mount platforms (Figure 2) and programmed to collect data every 10 minutes at a vertical cell spacing of 0.25 m. Factory recommended calibrations and maintenance were performed prior to the initial deployment of the ADCPs. The internal compass checks were performed, the functionality of the electronic circuitry and memory was verified, the battery was tested, and beam continuity was checked to verify transducer functionality.

The water quality sondes were fixed to the bottom-mount platforms as shown in Figure 2. Water quality data were collected every 15 minutes at a height of 0.5 m above the seabed. Optical turbidity measurements were calibrated to USEPA standards using a two-point calibration and calibration standards, 0 NTU and 126 NTU.

Figure 2. Bottom-mount platform with ADCP and water quality sonde (YSI) indicated.

Vessel Surveys

A "downlooking" ADCP was mounted on the port side of the SEI vessel and measured the spatial distribution of the vertical current profile in the system concurrently with a differential GPS for sub-meter scale location accuracy. The vessel-mounted ADCP was calibrated as described in the *Bottom-Mount Platform* section and programmed to collect data at 0.25 m vertical bins. Surveys were conducted on 4 and 5 June and 8 and 9 July 2013 following the three transect lines indicated in Figure 1. The ADCP transects were conducted in both directions (i.e. back and forth) across each transect line to decrease any directional bias in the data. Vessel speed was regulated to a maximum of 1 m/s to reduce velocity prediction errors.

Water samples for analysis of TSS were collected for the purpose of relating moored backscatter time series data to analytical TSS data over a range of tidal conditions. Eighteen samples were collected as nearest as possible to each of the two bottom-mounted platforms at approximately 0.5 m above the bed. Half of the samples were collected during the June surveys and the other half were collected during the July vessel surveying activities.

Water column profiles of PSD from surface to about 0.5 m above the bed were also collected near the two bottom-mounted platforms using a LISST-100X, type C. PSDs were measured between approximately 3 μm and 280 μm. The median particle diameter (d_{50}), 10th percentile (d_{10}), 90th percentile (d_{90}), and cumulative volume particle size distributions were computed from LISST data.

Results

Bottom-Mount Platforms

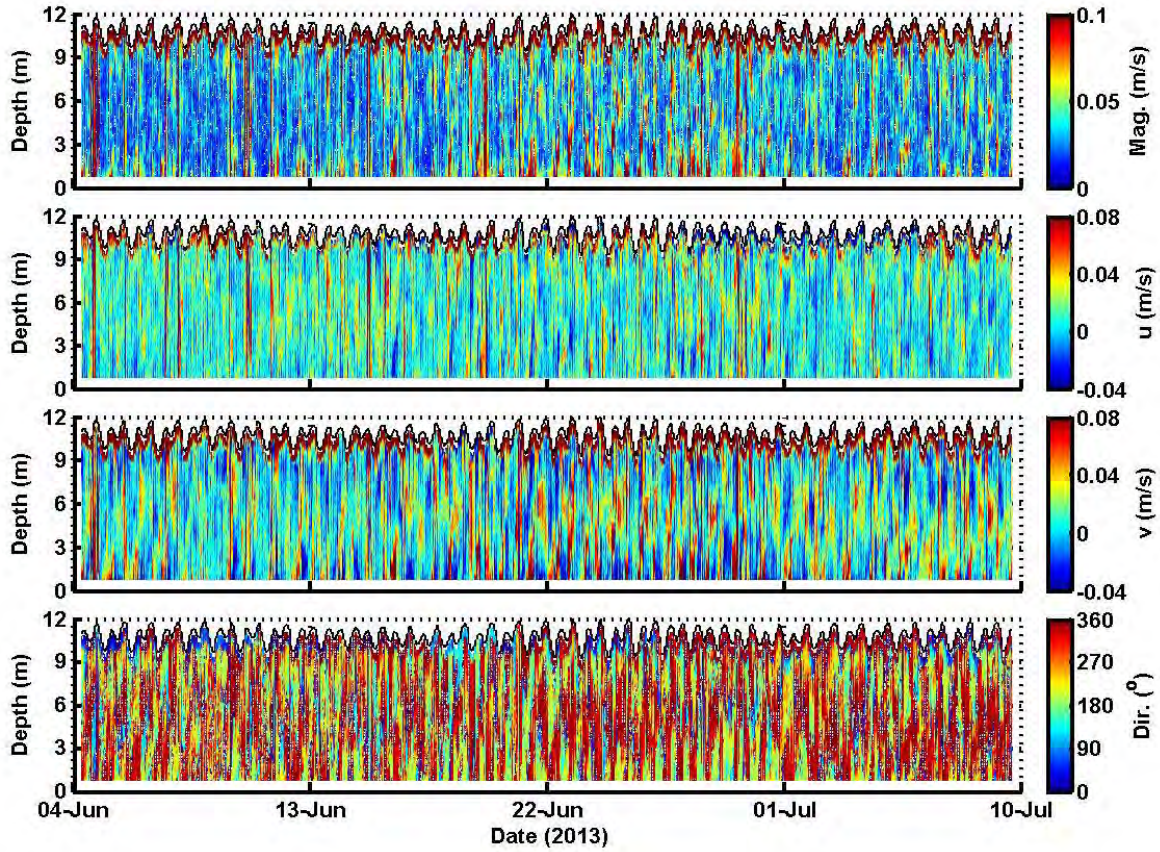

Figure 3. Time and depth resolved current velocity magnitude (top), u and v current components (second and third panels), and current direction recorded at ADCP Platform #1 (mouth of Lauritzen Channel) from 4 June to 9 July 2013.

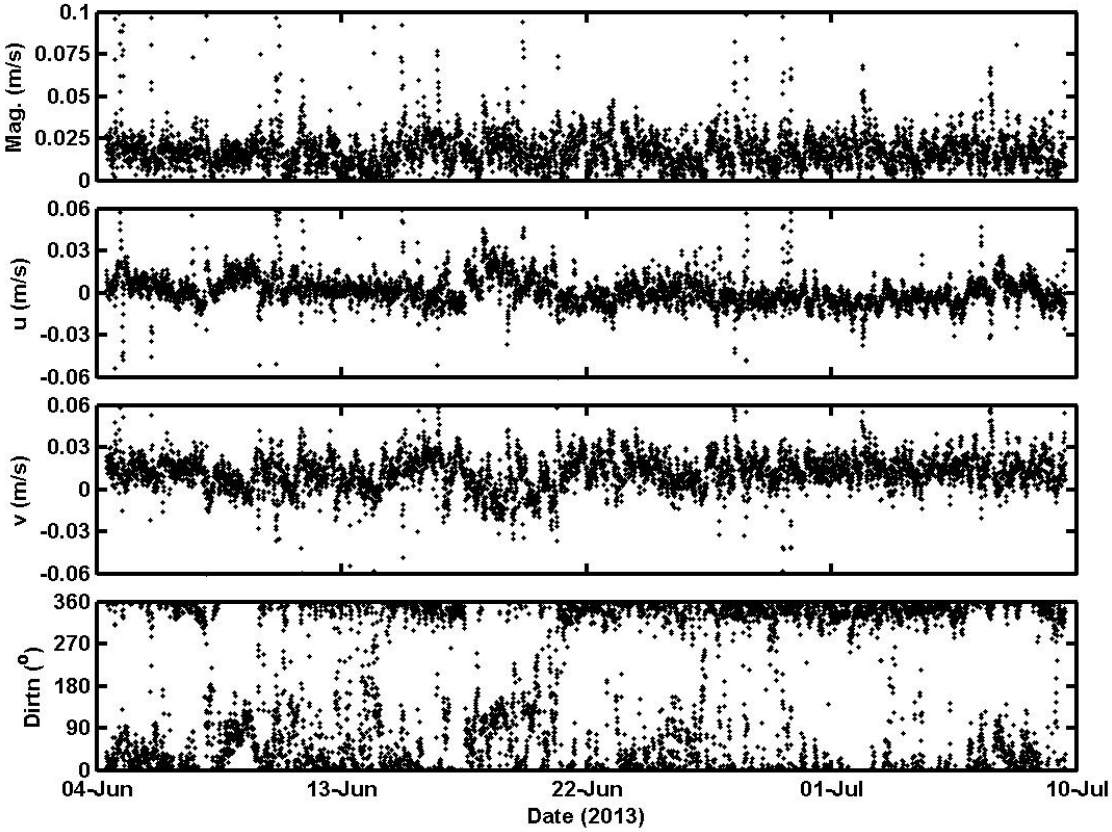

Figure 4. Depth averaged time series of current magnitude (top), u and v current components (second and third panels), and current direction recorded at ADCP Platform #1 (mouth of Lauritzen Channel) from 4 June to 9 July 2013.

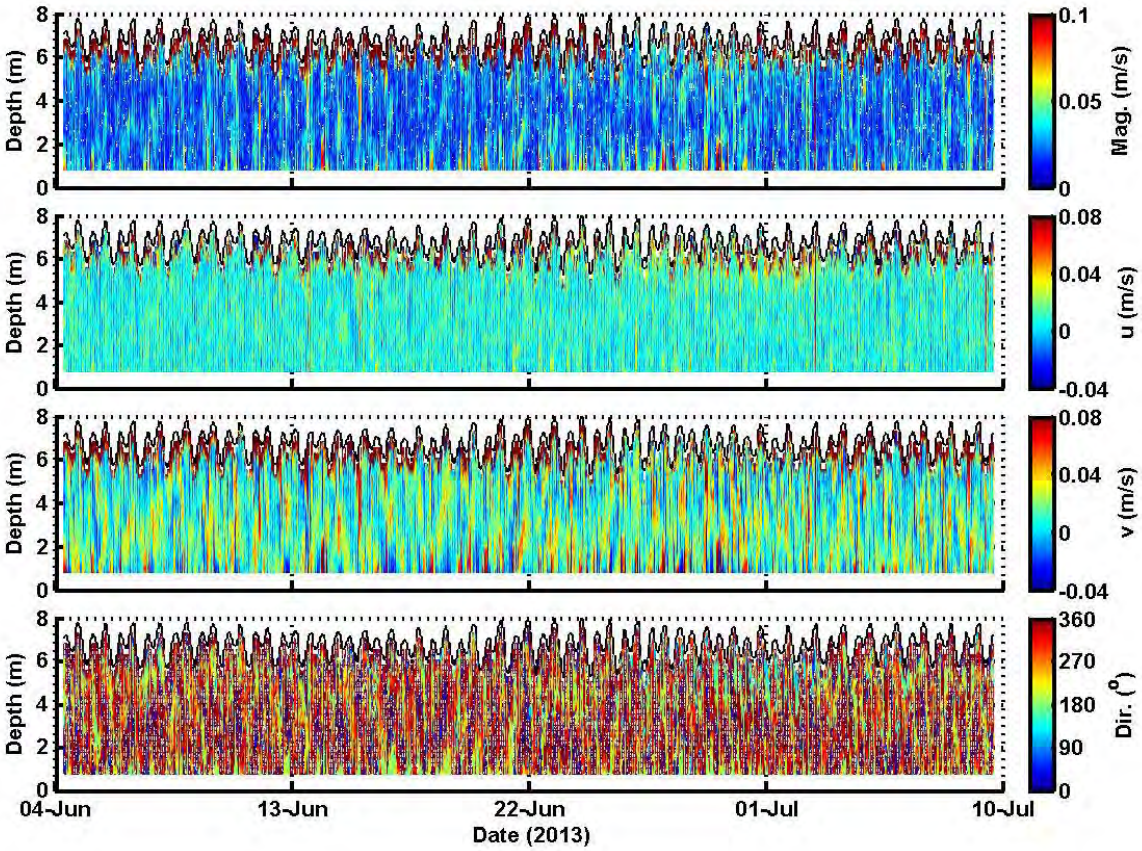

Figure 5. Time and depth resolved current velocity magnitude (top), u and v current components (second and third panels), and current direction recorded by ADCP Platform #2 (near head of Lauritzen Channel) from 4 June to 9 July 2013.

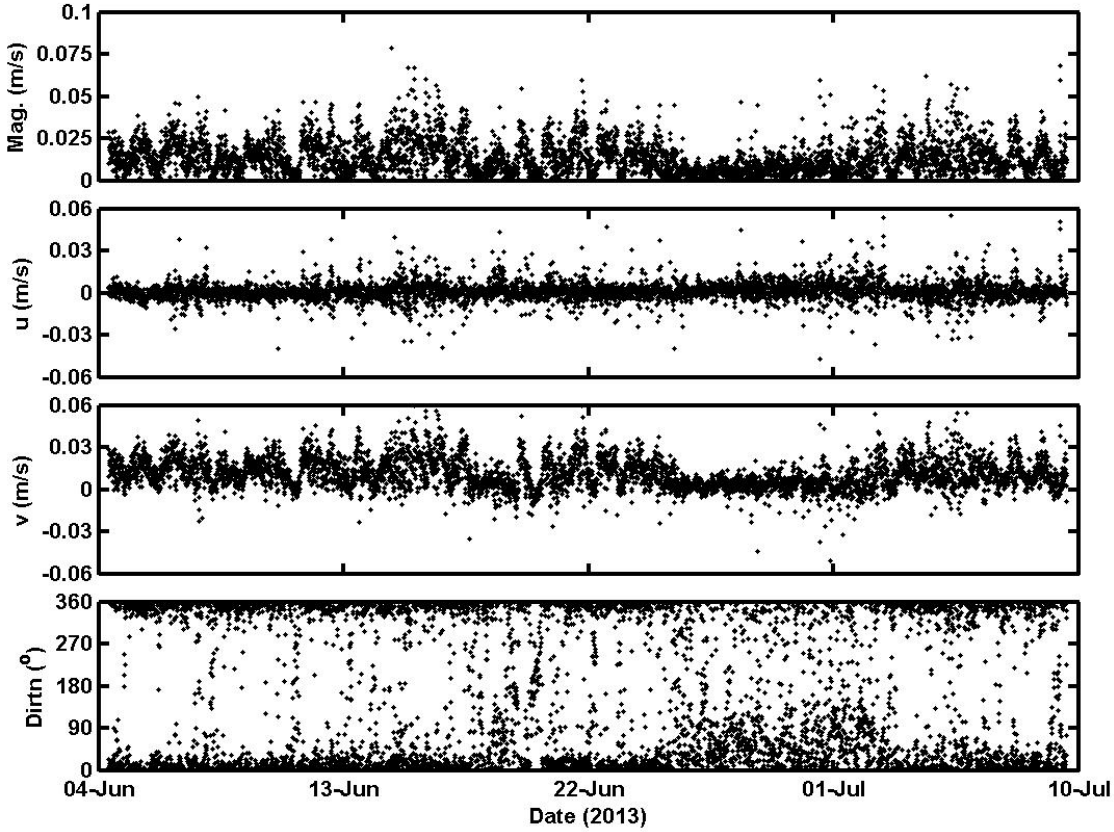

Figure 6. Depth averaged time series of current magnitude (top), u and v current components (second and third panels), and current direction recorded at ADCP Platform #2 (near head of Lauritzen Channel) from 4 June to 9 July 2013.

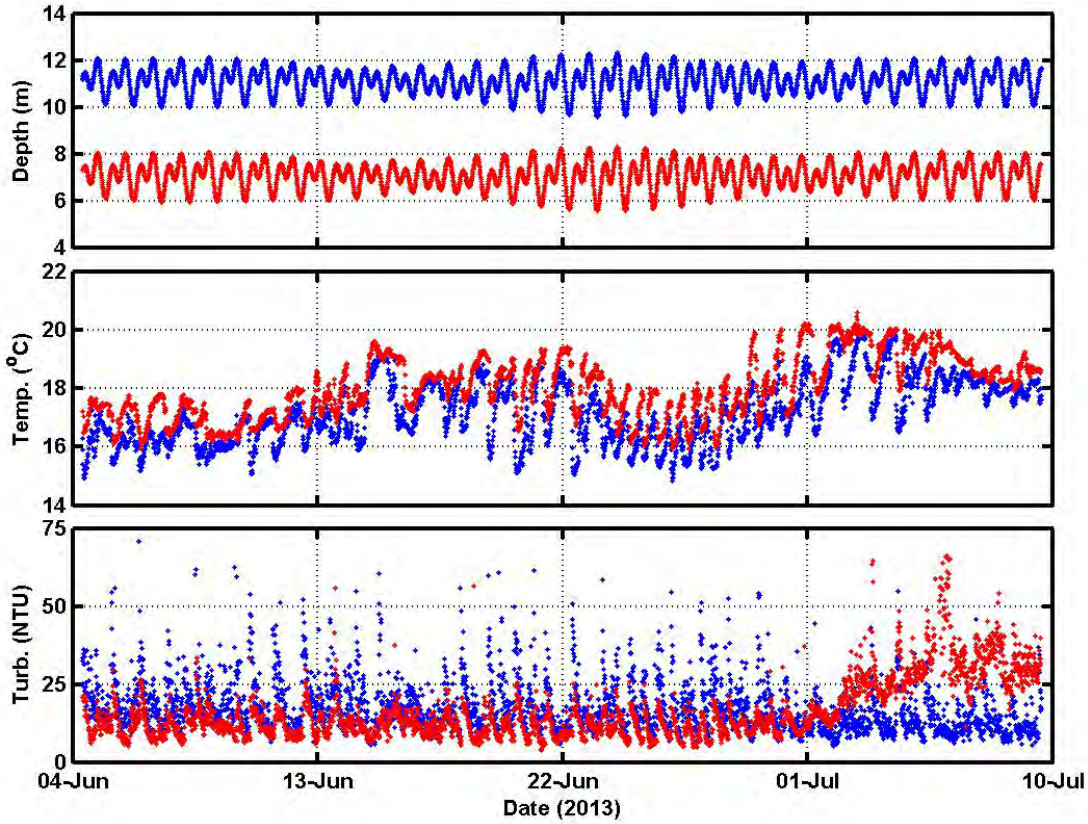

Figure 7. Time series of water depth, temperature, and optical turbidity data collected by the water quality sonde at ADCP Platform #1 (blue) and ADCP Platform #2 (red). ADCP Platform #2 optical turbidity data appear to be affected by biofouling near the end of the deployment period.

Vessel Surveys

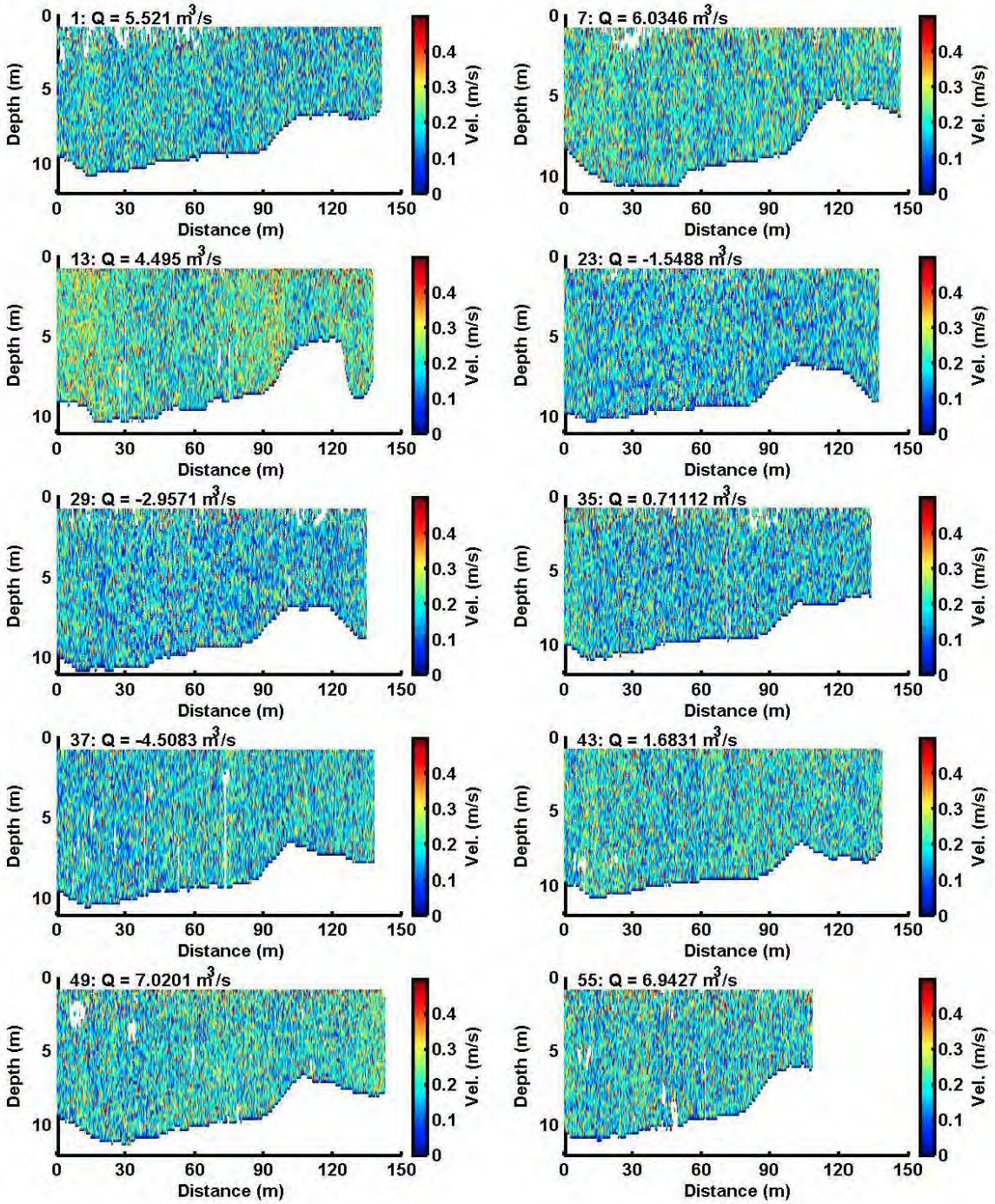

Figure 8. Cross sectional velocity magnitude (m/s) profiles recorded along survey line #1 (see Figure 1) on 4 and 5 June 2013. The flow rate, Q, calculated from each transect is given at the top of each panel alongside each transect number.

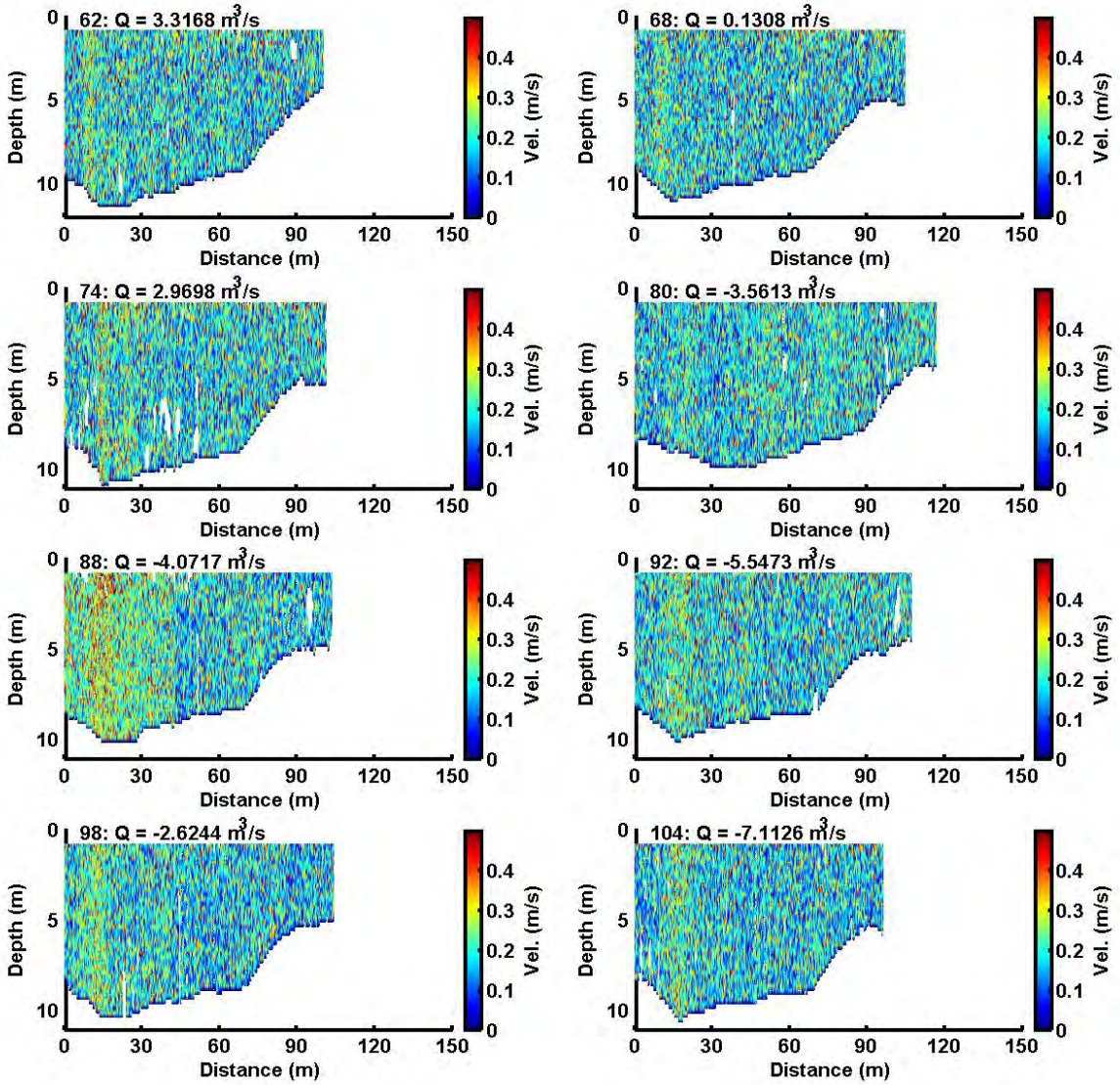

Figure 9. Cross sectional velocity magnitude (m/s) profiles recorded along survey line #1 (see Figure 1) on 8 and 9 July 2013. The flow rate, Q, calculated from each transect is given at the top of each panel alongside each transect number.

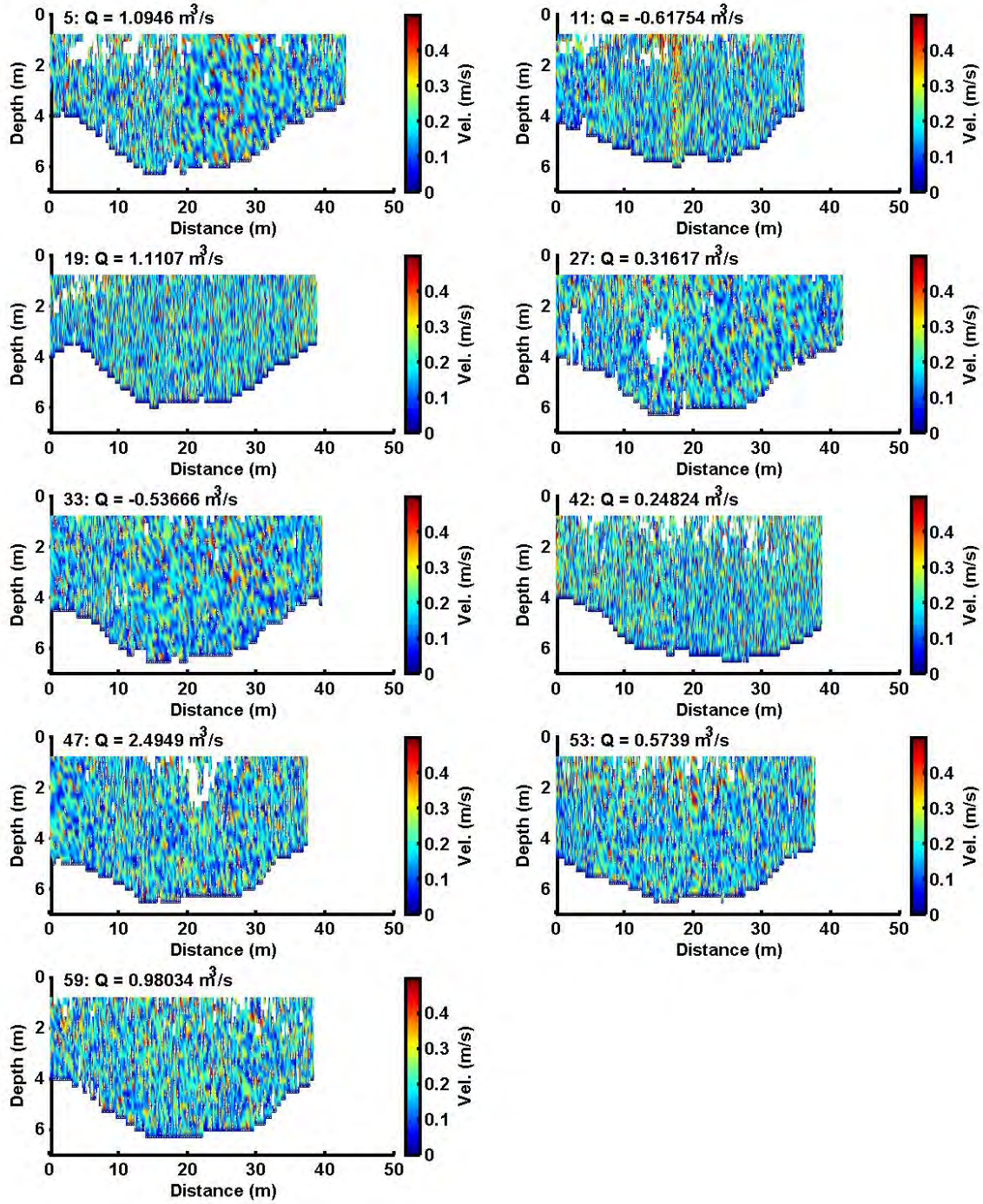

Figure 10. Cross sectional velocity magnitude (m/s) profiles recorded along survey line #2 (see Figure 1) on 4 and 5 June 2013. The flow rate, Q, calculated from each transect is given at the top of each panel alongside each transect number.

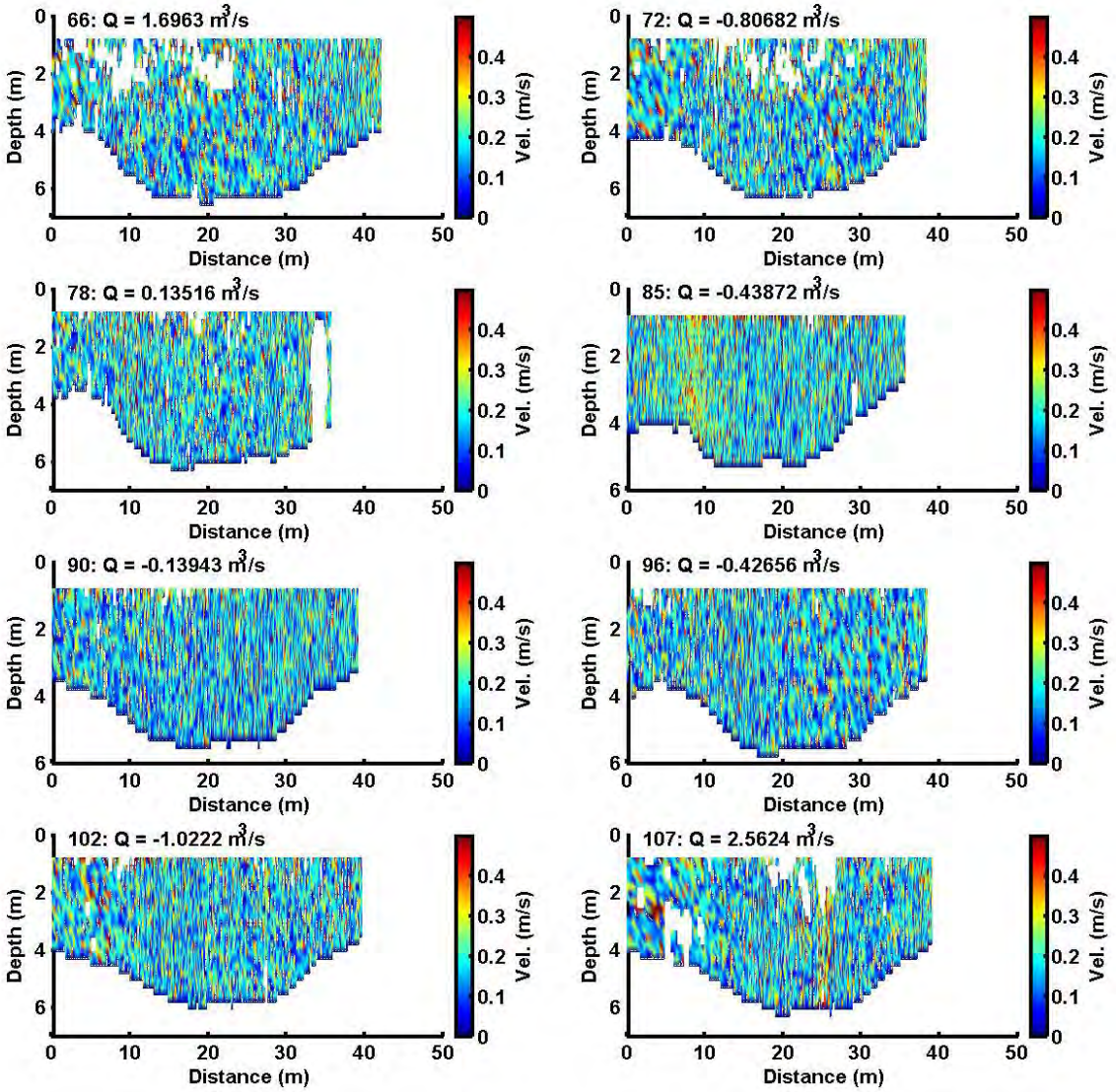

Figure 11. Cross sectional velocity magnitude (m/s) profiles recorded along survey line #2 (see Figure 1) on 8 and 9 July 2013. The flow rate, Q, calculated from each transect is given at the top of each panel alongside each transect number.

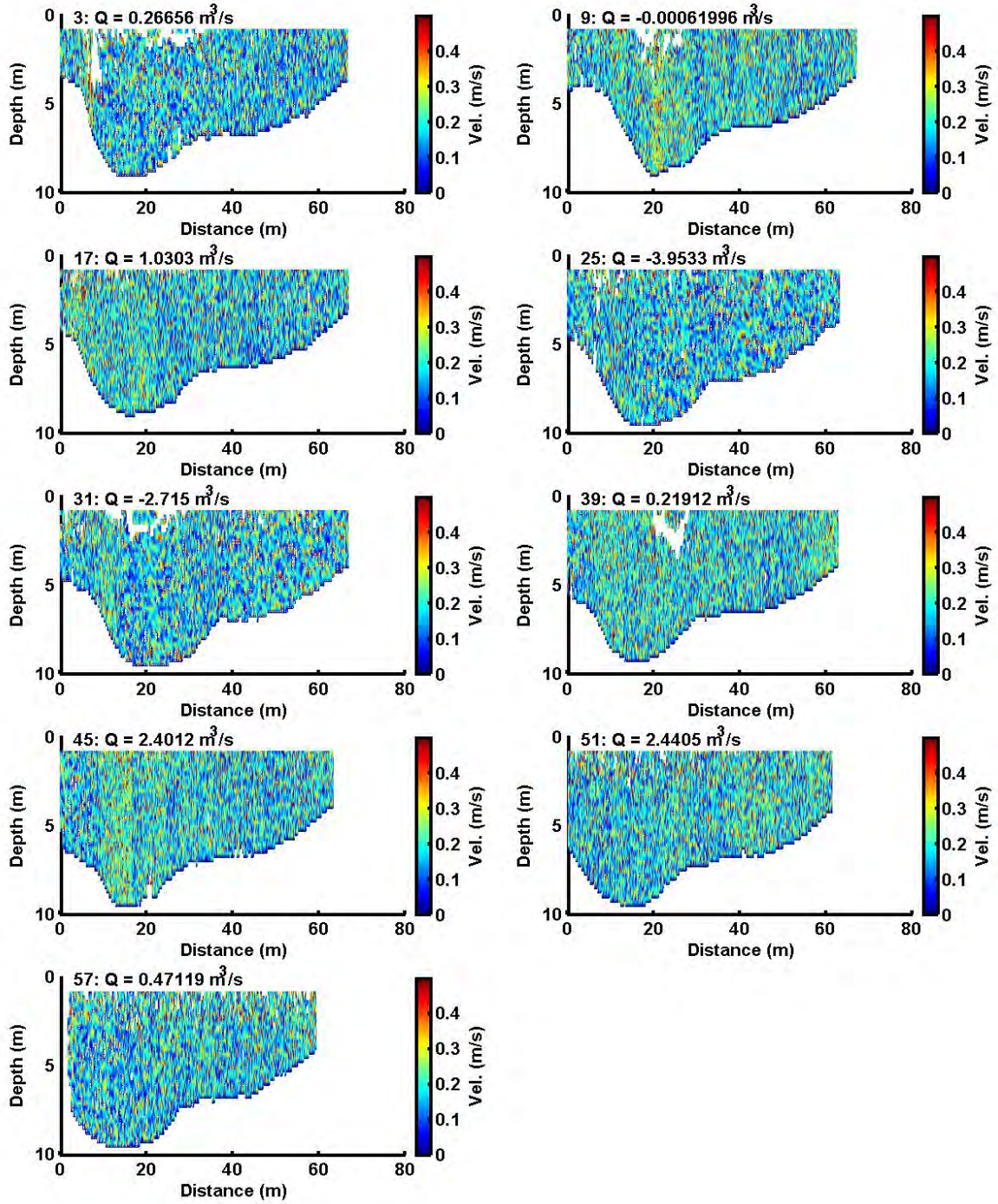

Figure 12. Cross sectional velocity magnitude (m/s) profiles recorded along survey line #3 (see Figure 1) on 4 and 5 June 2013. The flow rate, Q, calculated from each transect is given at the top of each panel alongside each transect number.

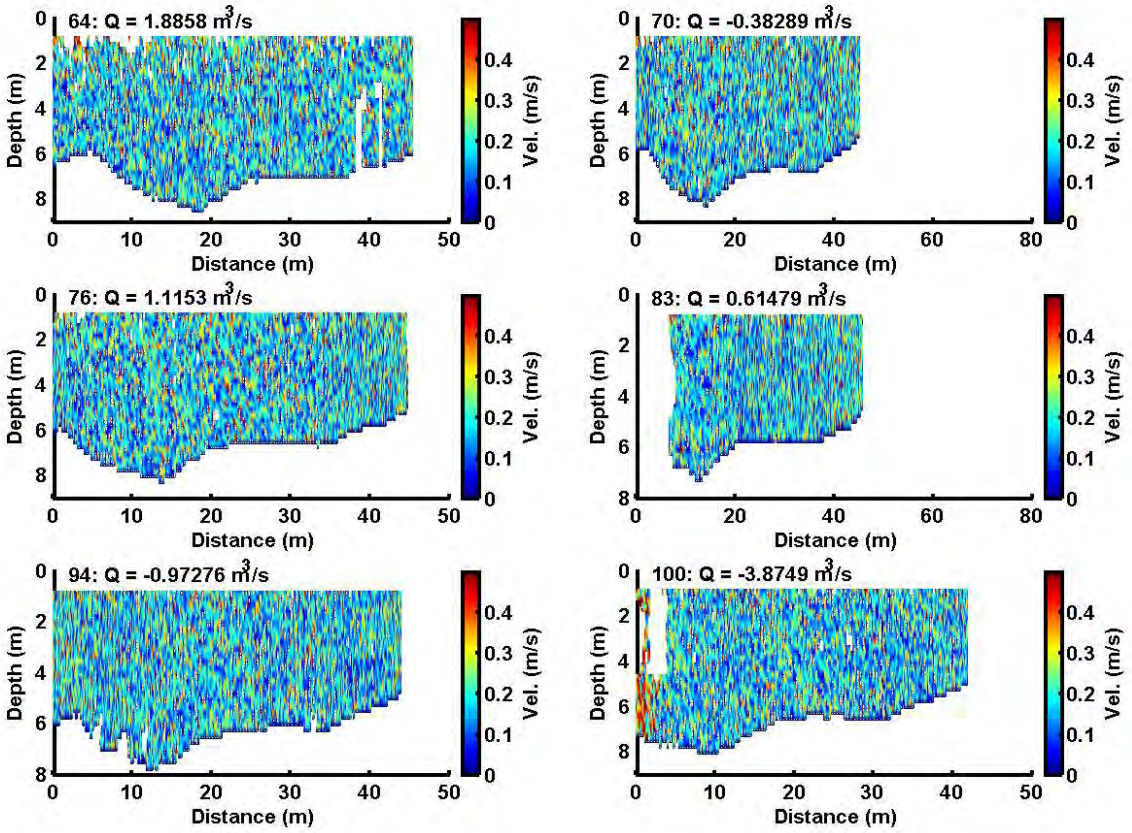

Figure 13. Cross sectional velocity magnitude (m/s) profiles recorded along survey line #3 (see Figure 1) on 8 and 9 July 2013. The flow rate, Q, calculated from each transect is given at the top of each panel alongside each transect number.

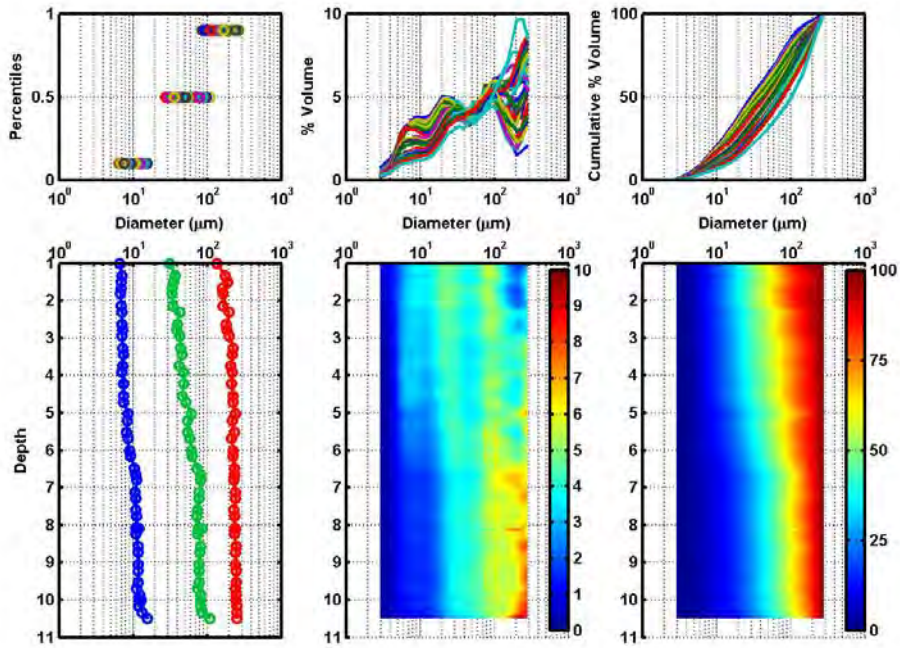

Figure 14. LISST data collected on 4 June 2013 at 12:27 at ADCP Platform #1. Left: d_{10} (blue), d_{50} (green), and d_{90} (red); Middle: Particle size distribution; and Right: Cumulative particle size distribution. The upper row panels are stackplots of all data collected during the downcast and the lower row panels show the downcast vertical profile.

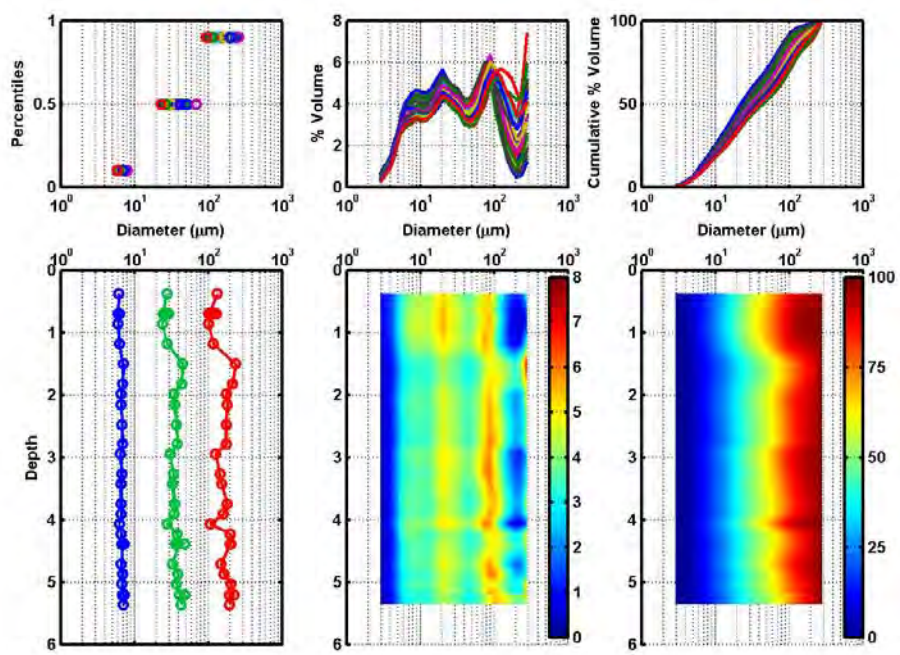

Figure 15. Same as Figure 14 caption but for LISST data collected on 4 June 2013 at 13:26 at ADCP Platform #2. The increase in PSD at larger sizes may be due to optical interference.

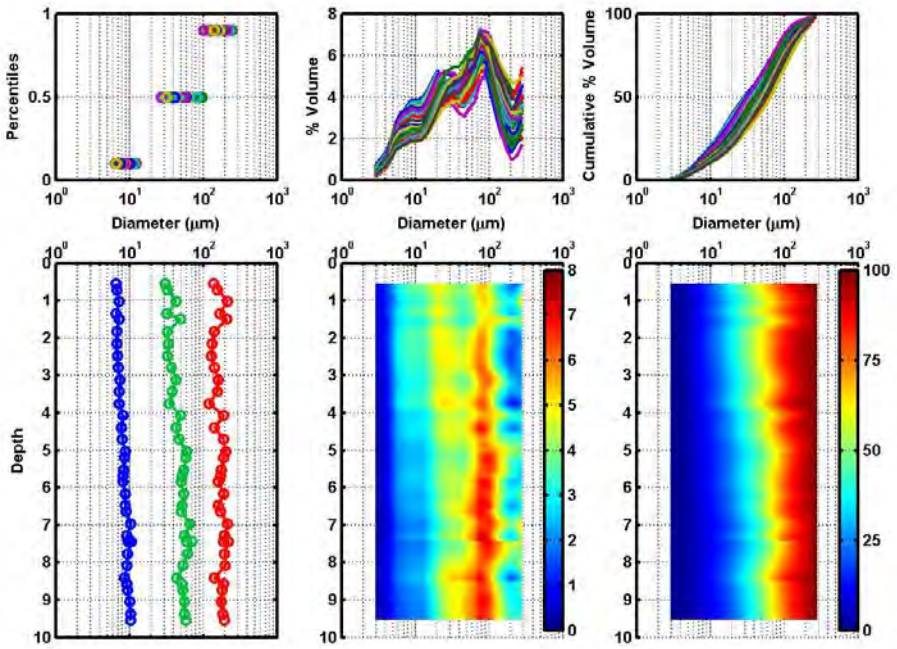

Figure 16. Same as Figure 14 caption but for LISST data collected on 4 June 2013 at 14:24 at ADCP Platform #1.

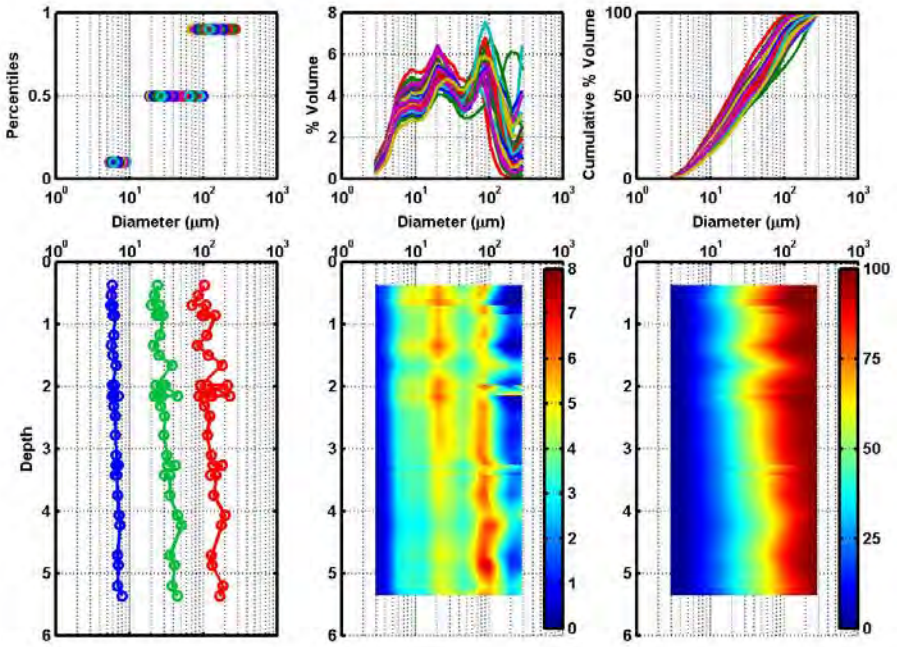

Figure 17. Same as Figure 14 caption but for LISST data collected on 4 June 2013 at 15:05 at ADCP Platform #2.

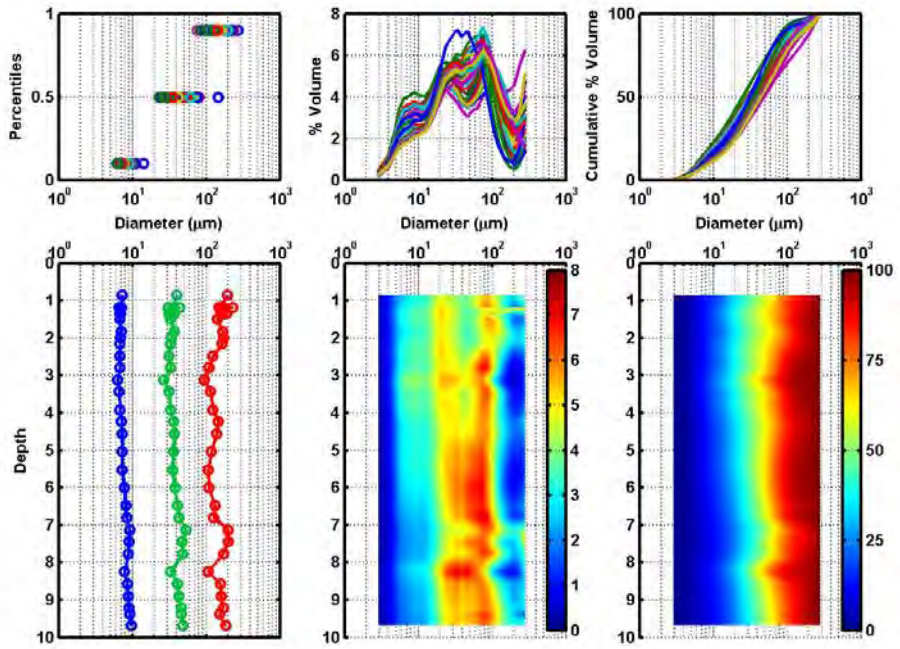

Figure 18. Same as Figure 14 caption but for LISST data collected on 4 June 2013 at 15:46 at ADCP Platform #1.

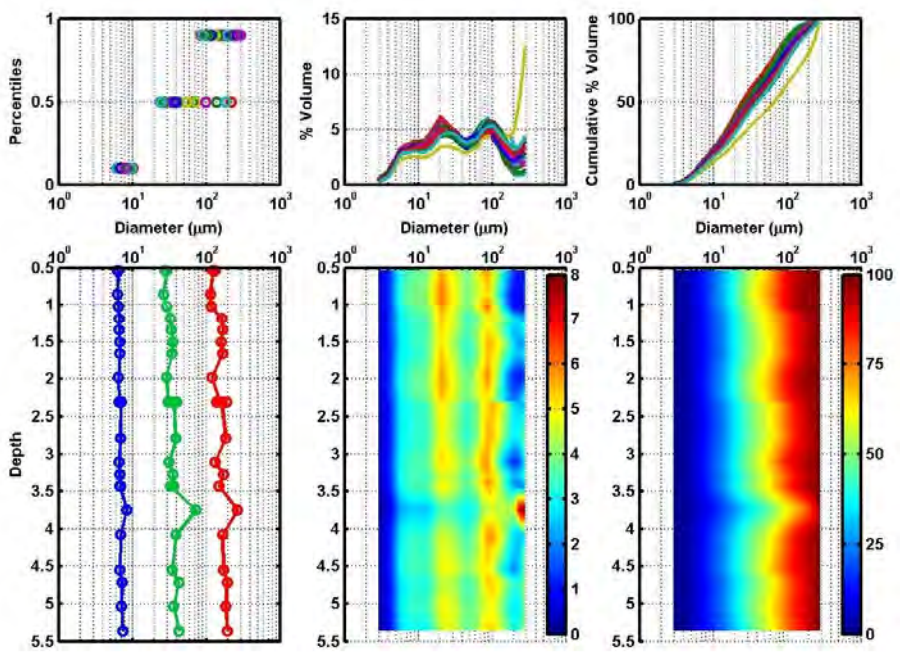

Figure 19. Same as Figure 14 caption but for LISST data collected on 4 June 2013 at 16:42 at ADCP Platform #2. The increase in PSD at larger sizes may be due to optical interference.

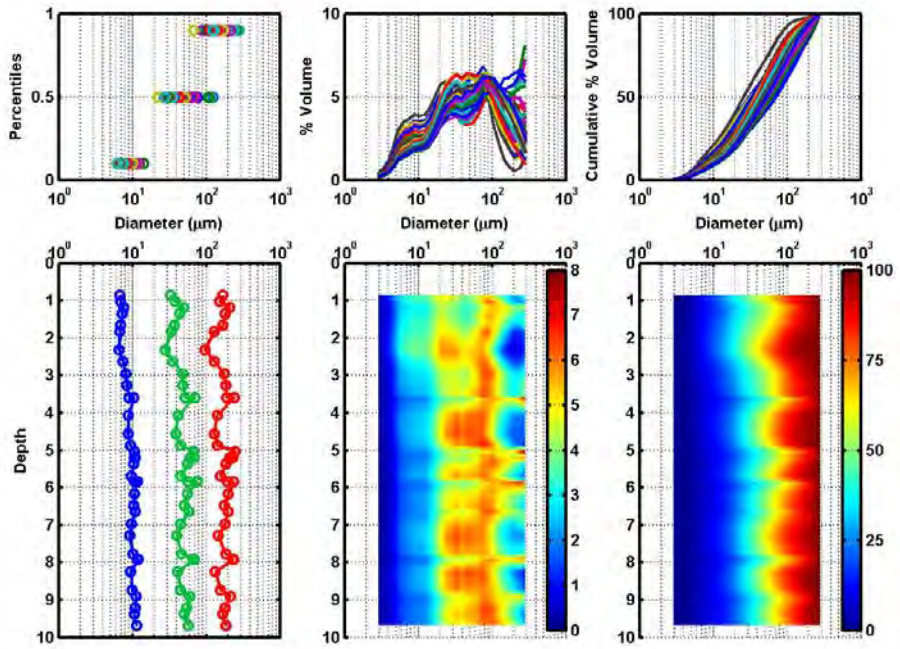

Figure 20. Same as Figure 14 caption but for LISST data collected on 4 June 2013 at 17:57 at ADCP Platform #1.

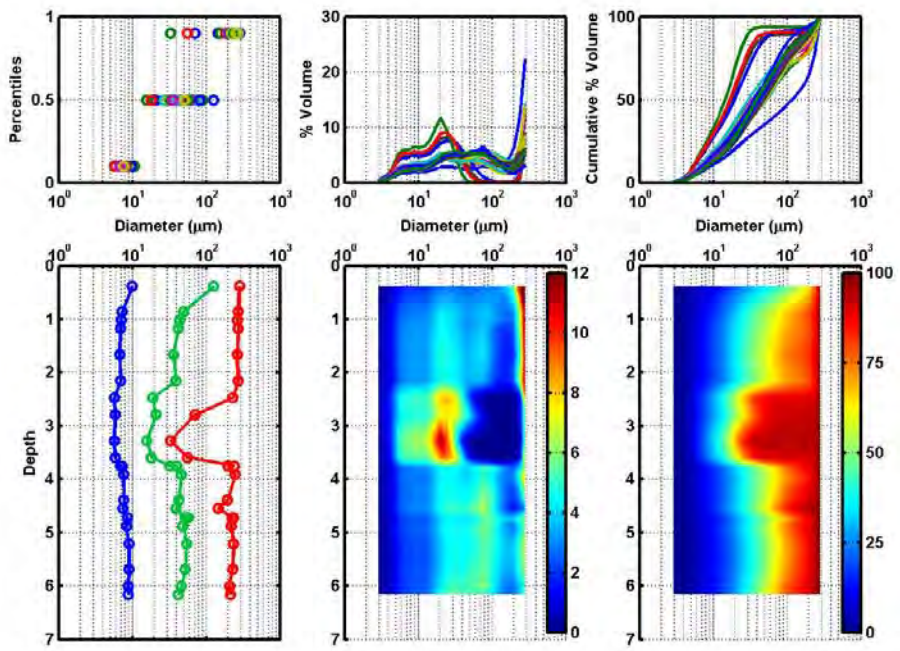

Figure 21. Same as Figure 14 caption but for LISST data collected on 4 June 2013 at 18:24 at ADCP Platform #2. The increase in PSD at larger sizes may be due to optical interference.

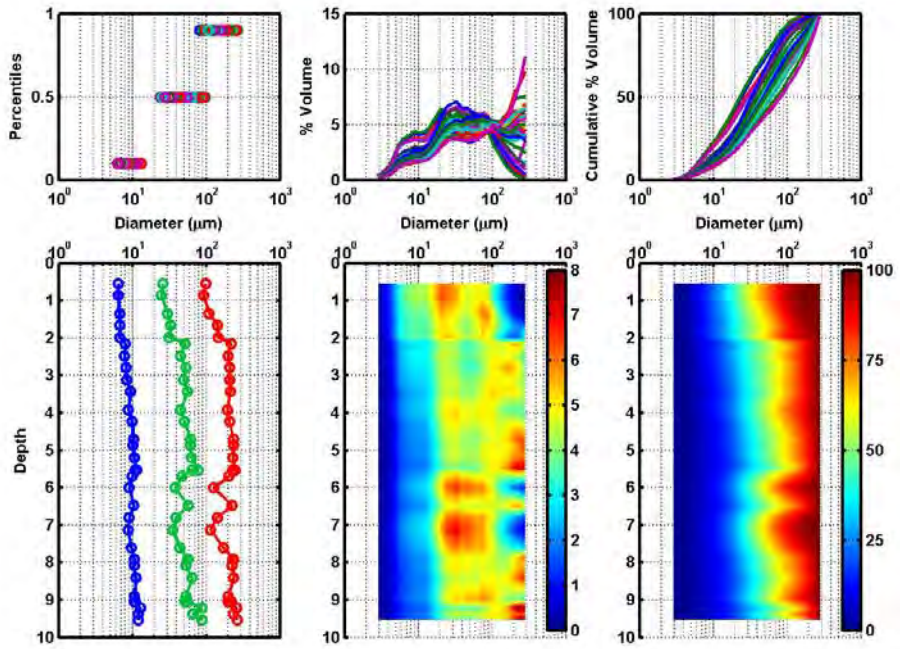

Figure 22. Same as Figure 14 caption but for LISST data collected on 4 June 2013 at 18:44 at ADCP Platform #1. The increase in PSD at larger sizes may be due to optical interference.

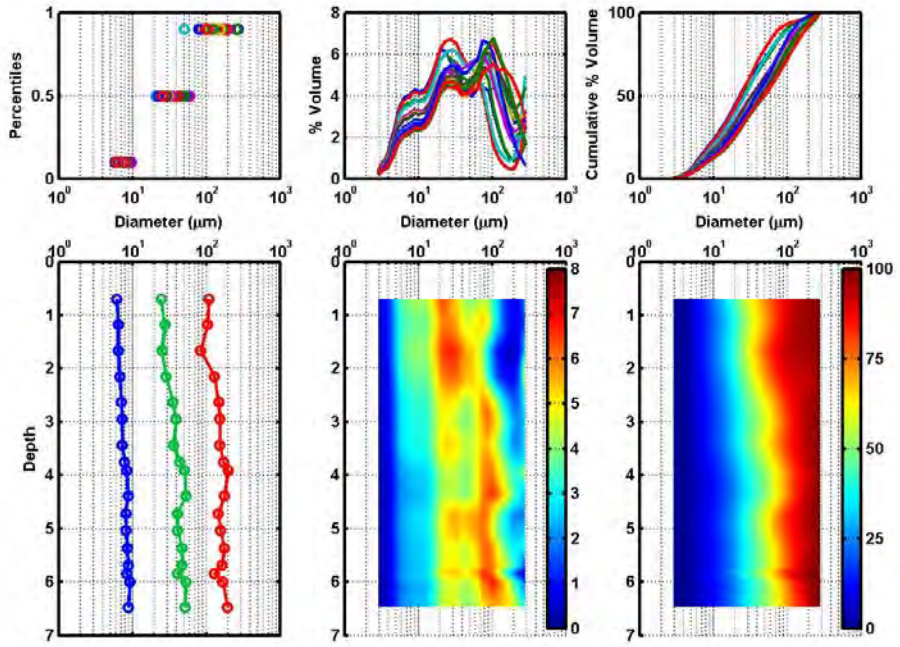

Figure 23. Same as Figure 14 caption but for LISST data collected on 4 June 2013 at 19:13 at ADCP Platform #2.

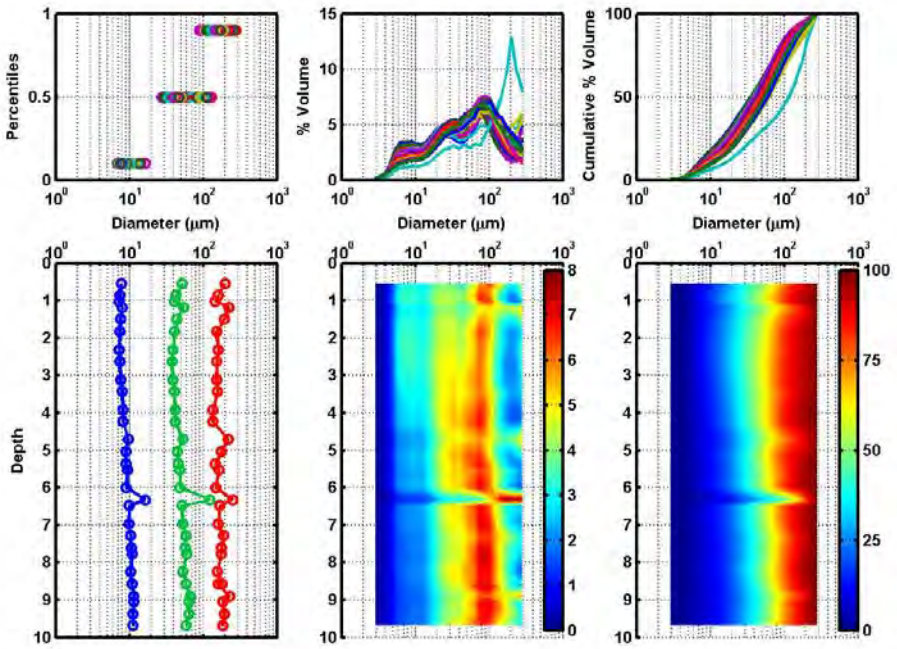

Figure 24. Same as Figure 14 caption but for LISST data collected on 5 June 2013 at 08:48 at ADCP Platform #1.

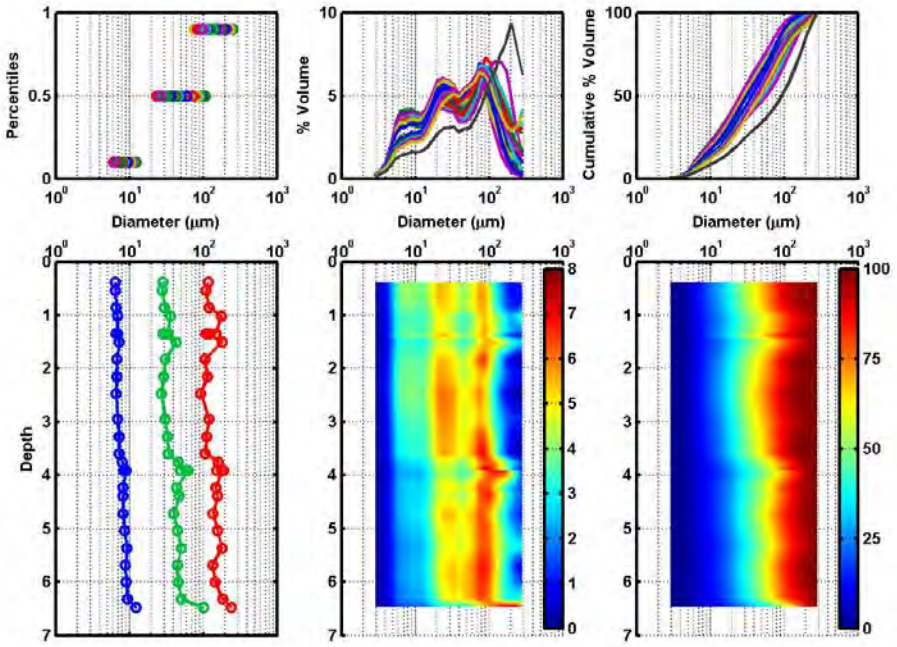

Figure 25. Same as Figure 14 caption but for LISST data collected on 5 June 2013 at 09:37 at ADCP Platform #2.

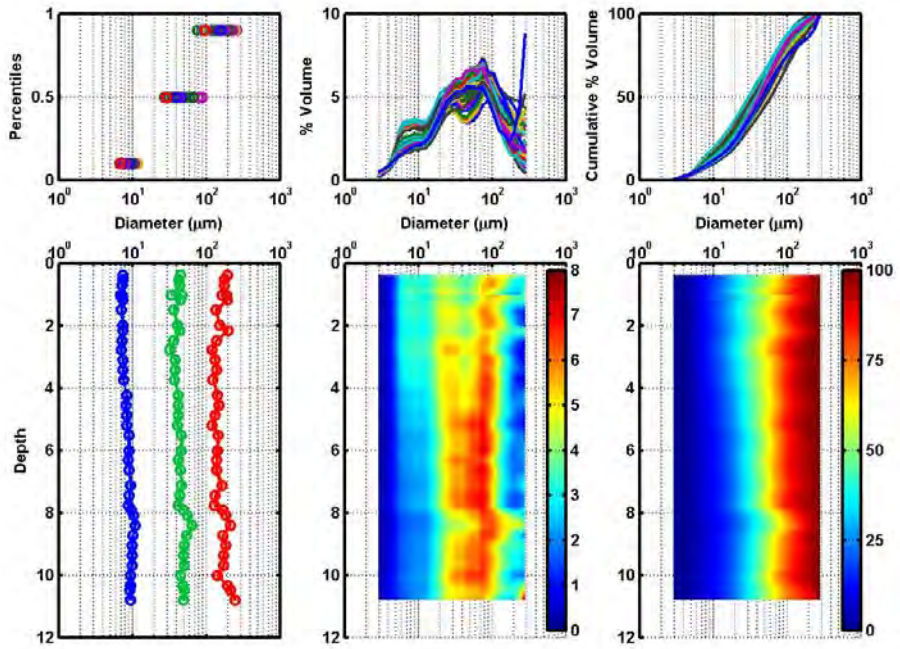

Figure 26. Same as Figure 14 caption but for LISST data collected on 5 June 2013 at 10:13 at ADCP Platform #1. The increase in PSD at larger sizes may be due to optical interference.

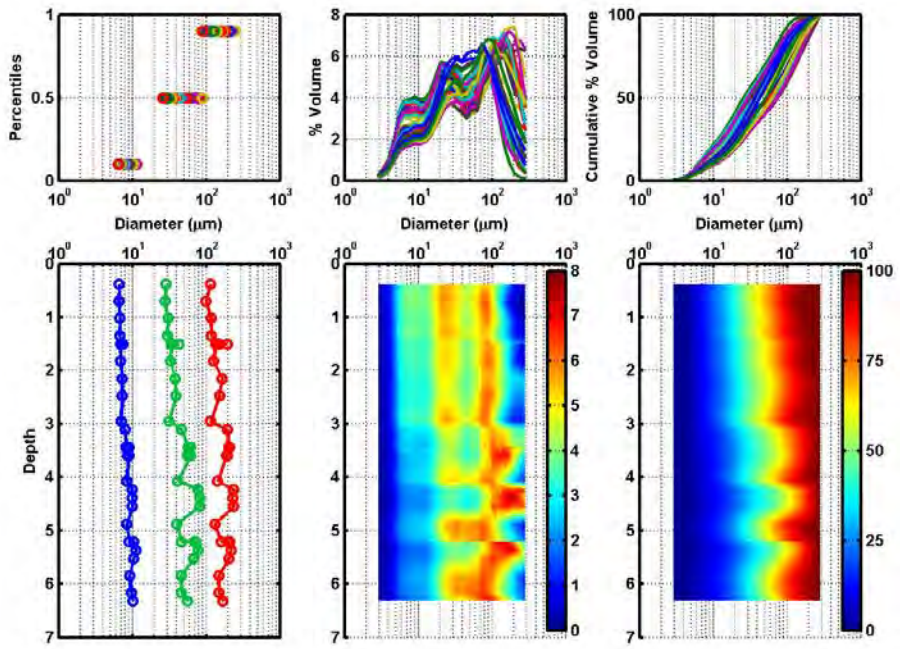

Figure 27. Same as Figure 14 caption but for LISST data collected on 5 June 2013 at 10:48 at ADCP Platform #2.

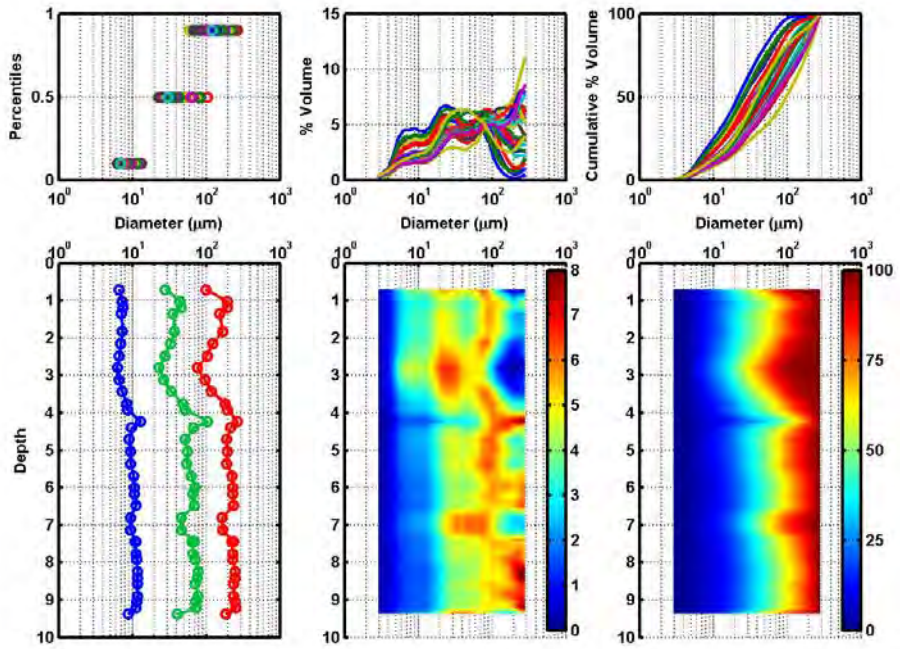

Figure 28. Same as Figure 14 caption but for LISST data collected on 5 June 2013 at 12:48 at ADCP Platform #1.

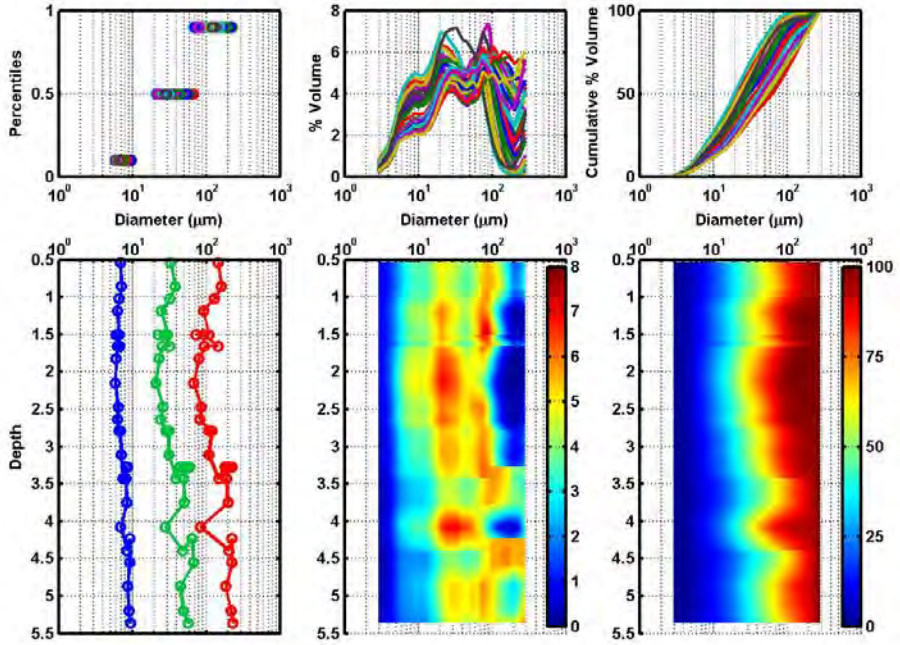

Figure 29. Same as Figure 14 caption but for LISST data collected on 5 June 2013 at 13:42 at ADCP Platform #2.

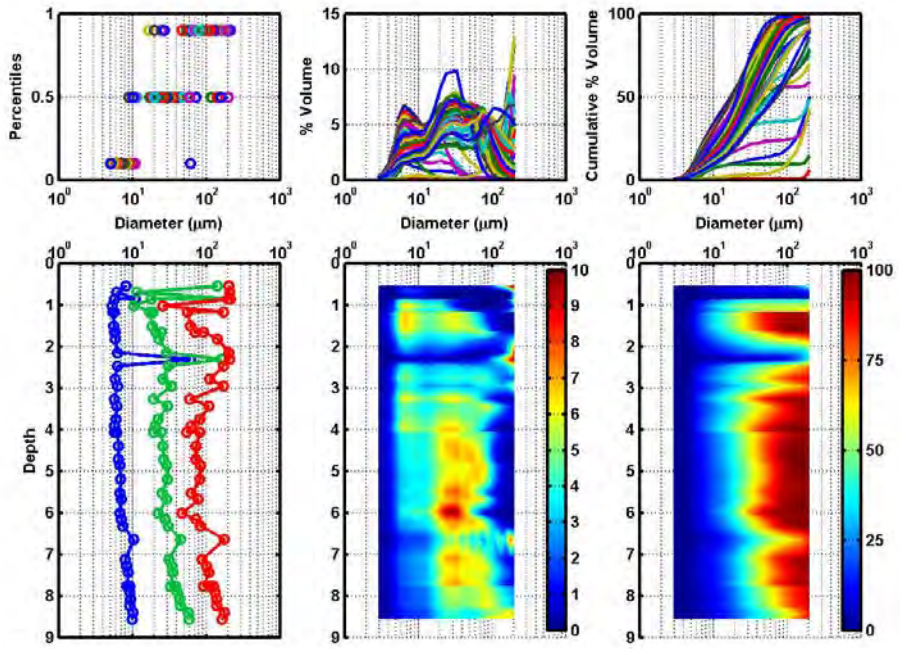

Figure 30. Same as Figure 14 caption but for LISST data collected on 8 July 2013 at 14:55 at ADCP Platform #1. The increase in PSD at larger sizes may be due to optical interference.

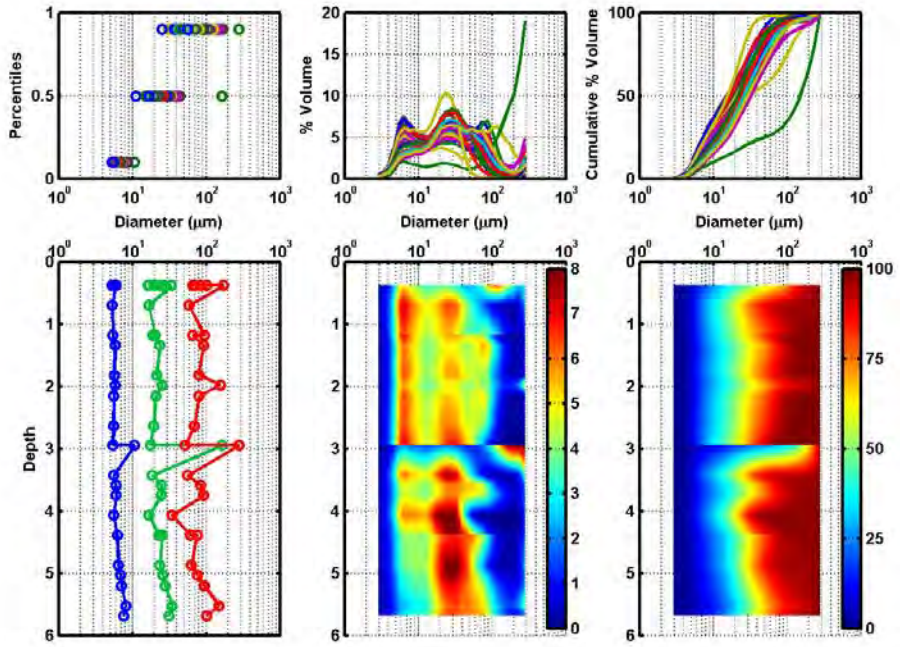

Figure 31. Same as Figure 14 caption but for LISST data collected on 8 July 2013 at 15:31 at ADCP Platform #2. The increase in PSD at larger sizes may be due to optical interference.

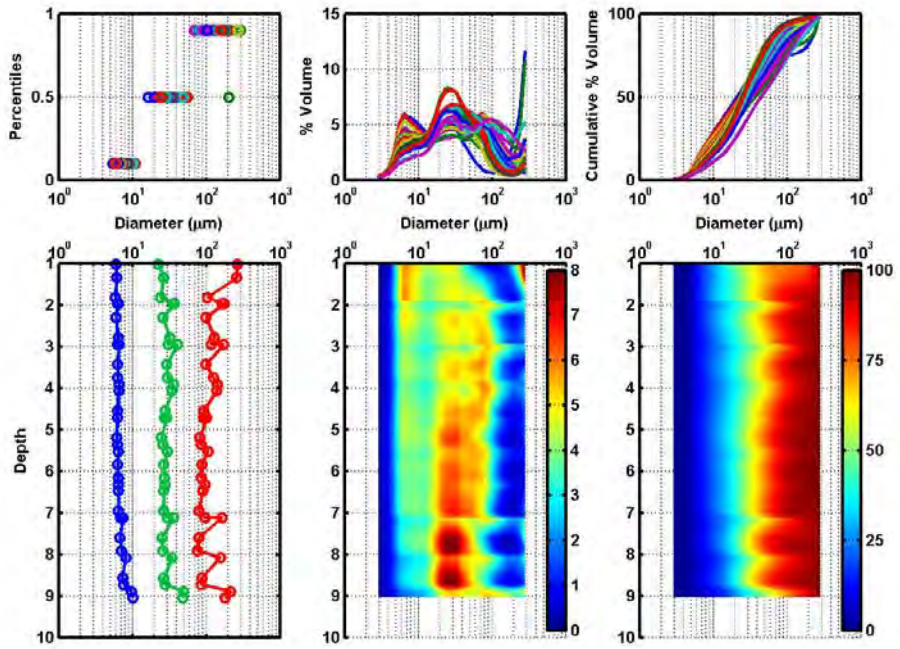

Figure 32. Same as Figure 14 caption but for LISST data collected on 8 July 2013 at 15:56 at ADCP Platform #1. The increase in PSD at larger sizes may be due to optical interference.

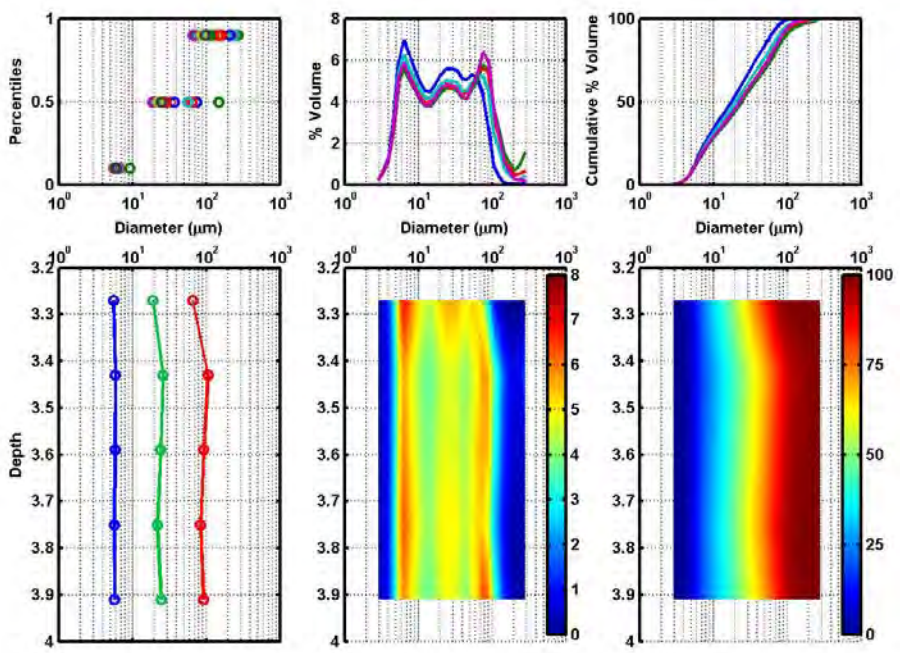

Figure 33. Same as Figure 14 caption but for LISST data collected on 8 July 2013 at 16:28 at ADCP Platform #2.

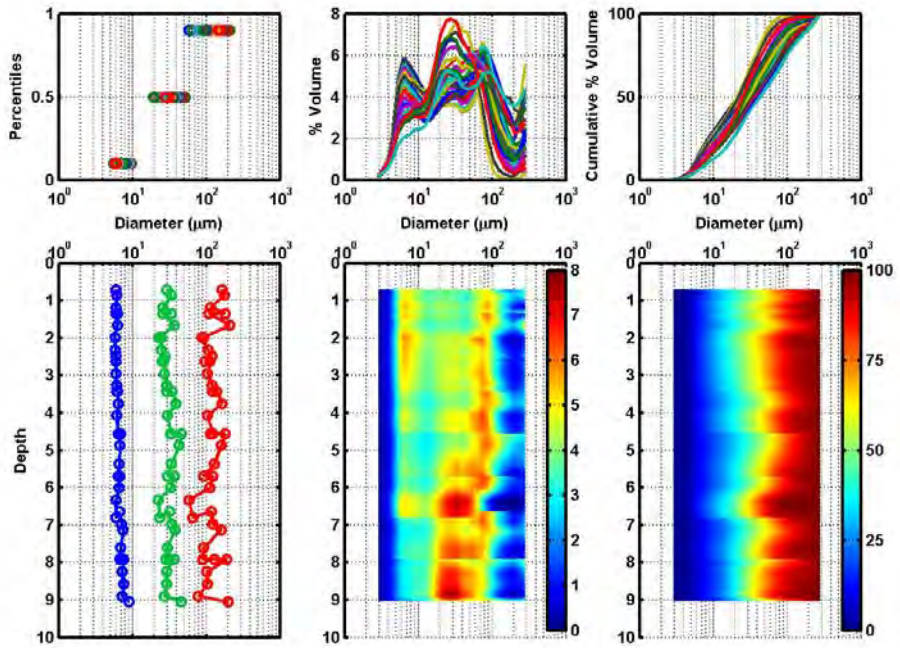

Figure 34. Same as Figure 14 caption but for LISST data collected on 8 July 2013 at 16:54 at ADCP Platform #1.

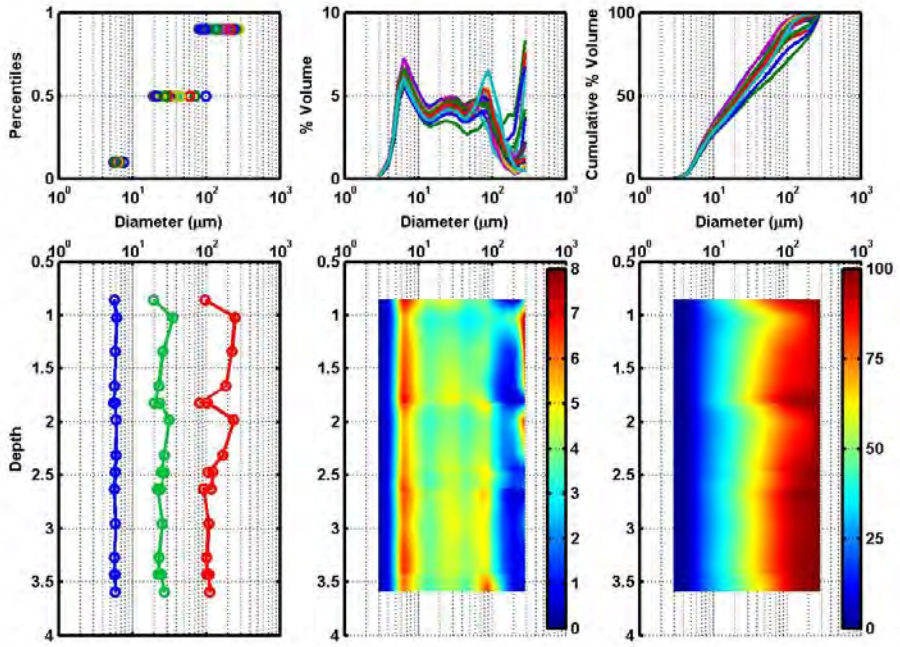

Figure 35. Same as Figure 14 caption but for LISST data collected on 8 July 2013 at 17:35 at ADCP Platform #2.

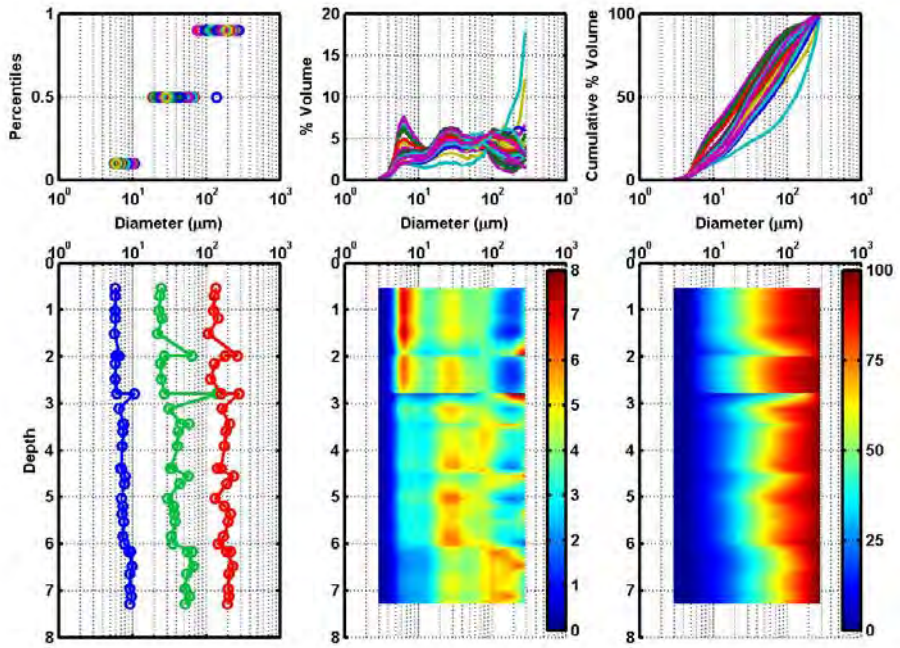

Figure 36. Same as Figure 14 caption but for LISST data collected on 9 July 2013 at 08:21 at ADCP Platform #1.

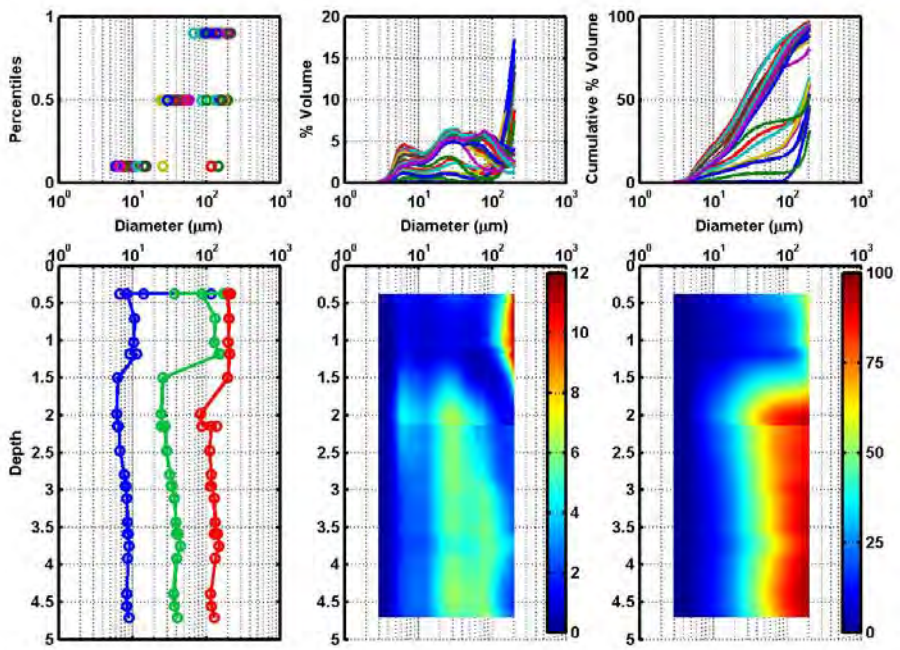

Figure 37. Same as Figure 14 caption but for LISST data collected on 9 July 2013 at 08:53 at ADCP Platform #2.

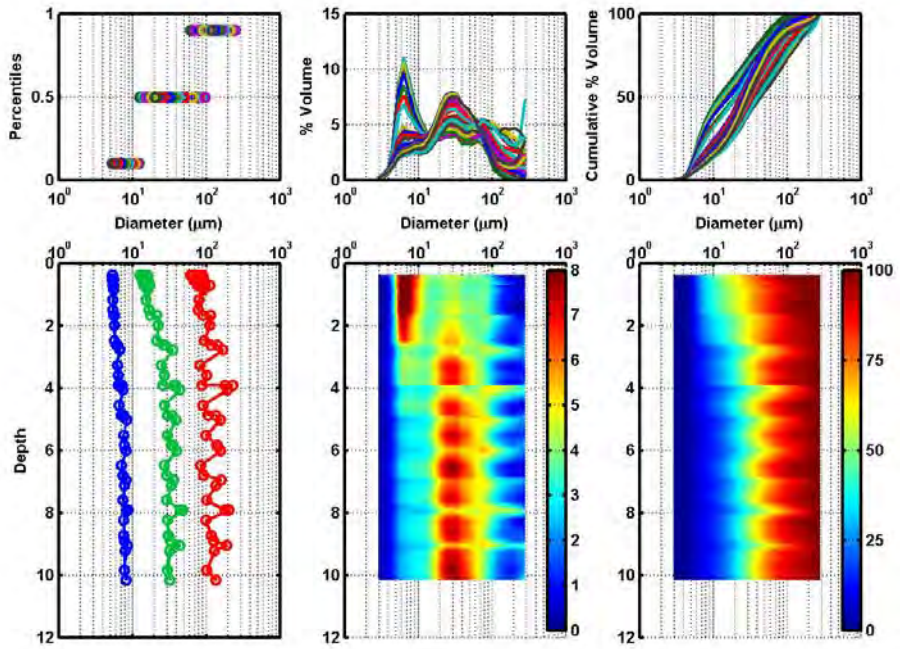

Figure 38. Same as Figure 14 caption but for LISST data collected on 9 July 2013 at 09:23 at ADCP Platform #1.

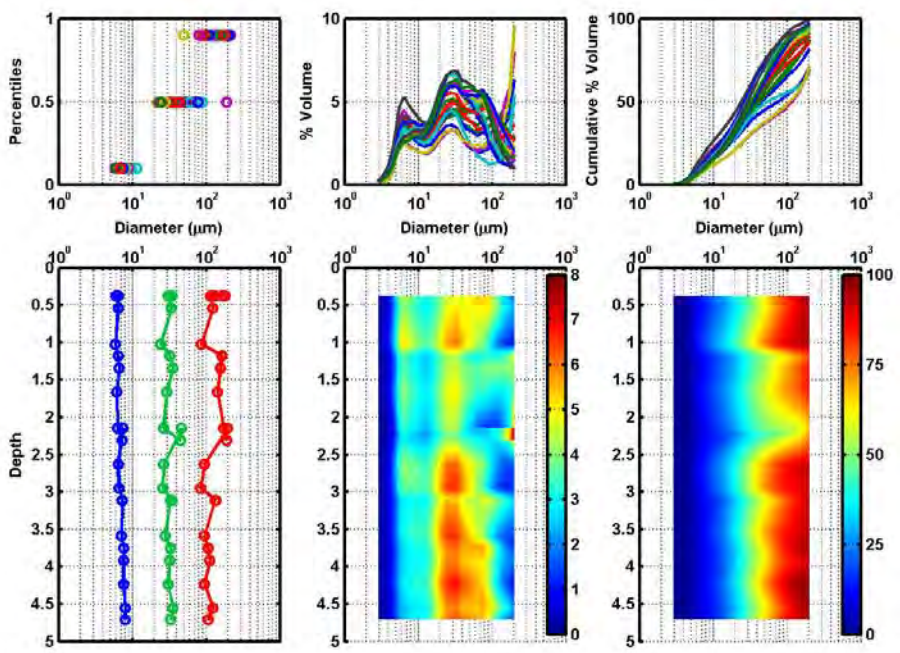

Figure 39. Same as Figure 14 caption but for LISST data collected on 9 July 2013 at 09:40 at ADCP Platform #2.

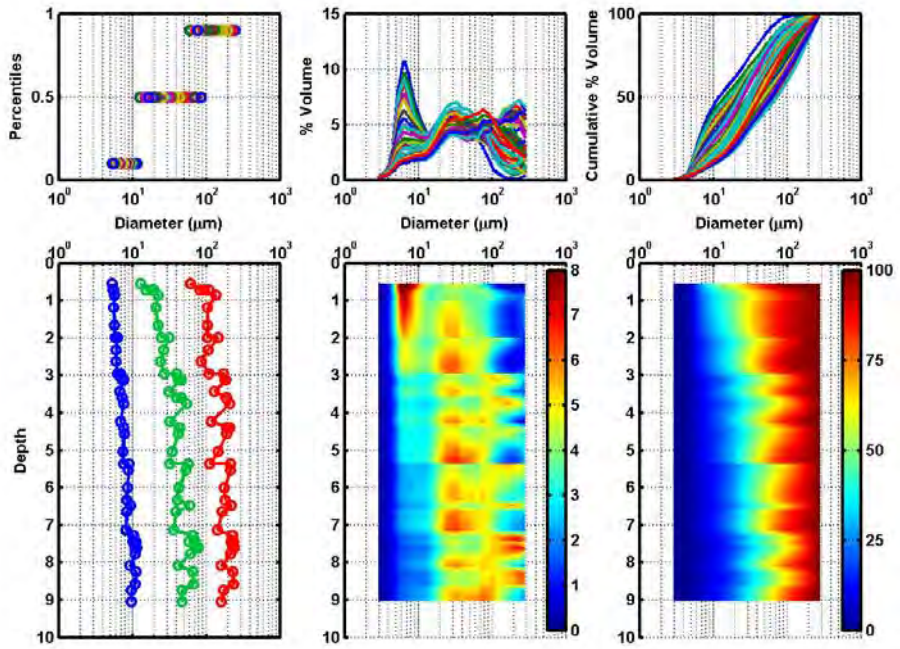

Figure 40. Same as Figure 14 caption but for LISST data collected on 9 July 2013 at 09:58 at ADCP Platform #1.

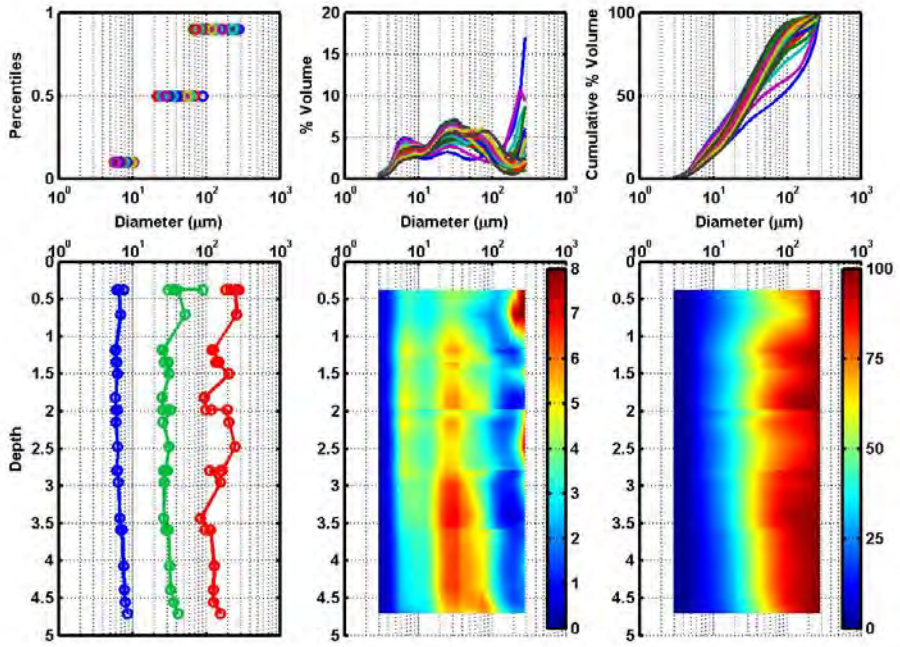

Figure 41. Same as Figure 14 caption but for LISST data collected on 9 July 2013 at 10:25 at ADCP Platform #2.

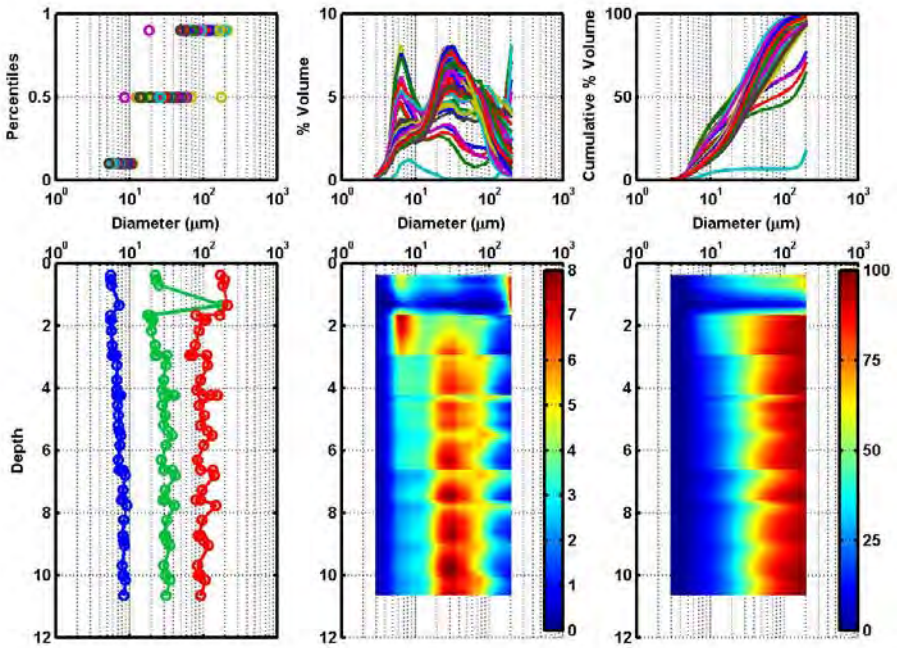

Figure 42. Same as Figure 14 caption but for LISST data collected on 9 July 2013 at 10:41 at ADCP Platform #1.

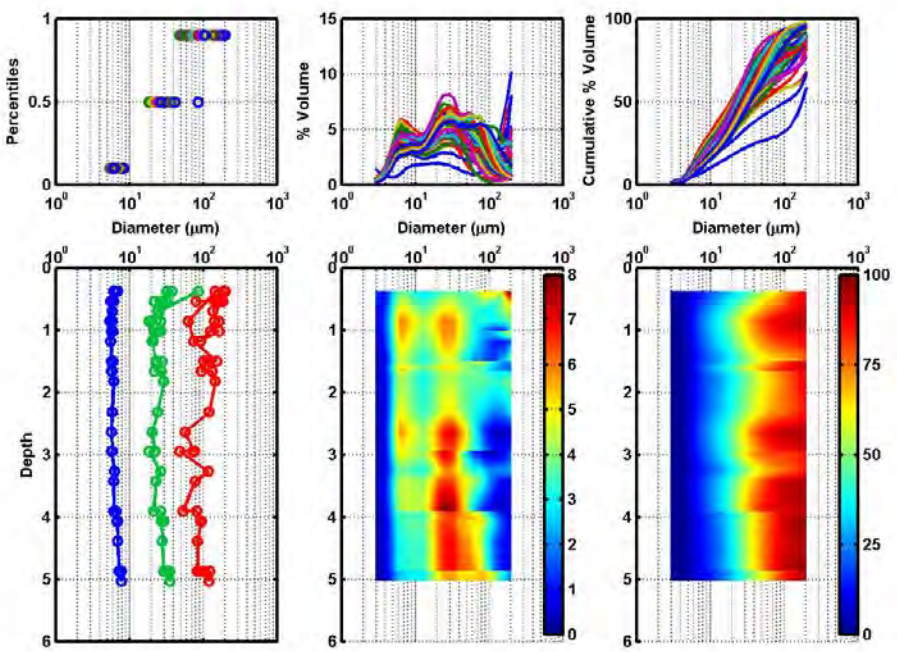

Figure 43. Same as Figure 14 caption but for LISST data collected on 9 July 2013 at 11:04 at ADCP Platform #2.

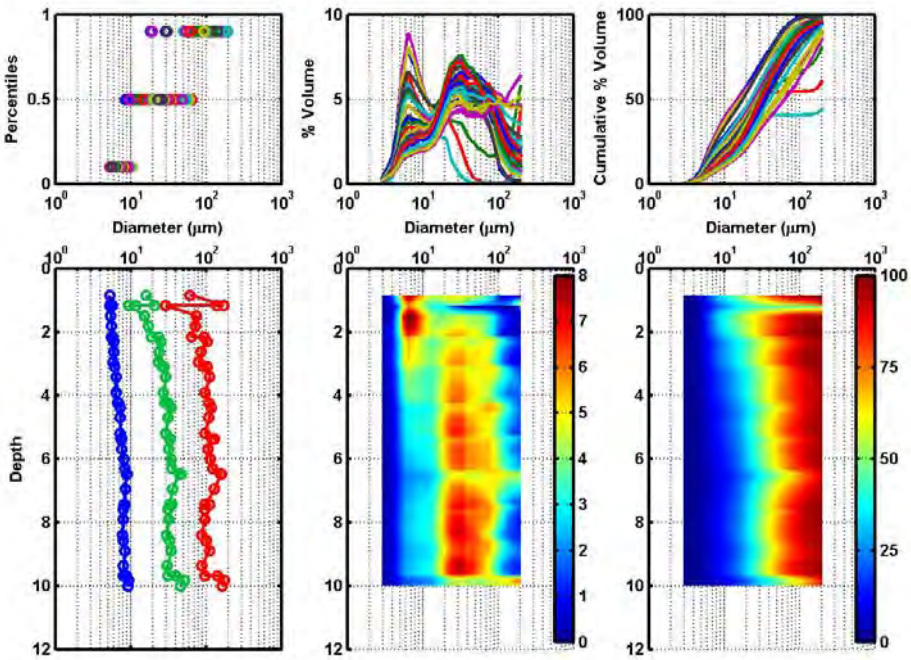

Figure 44. Same as Figure 14 caption but for LISST data collected on 9 July 2013 at 11:20 at ADCP Platform #1.

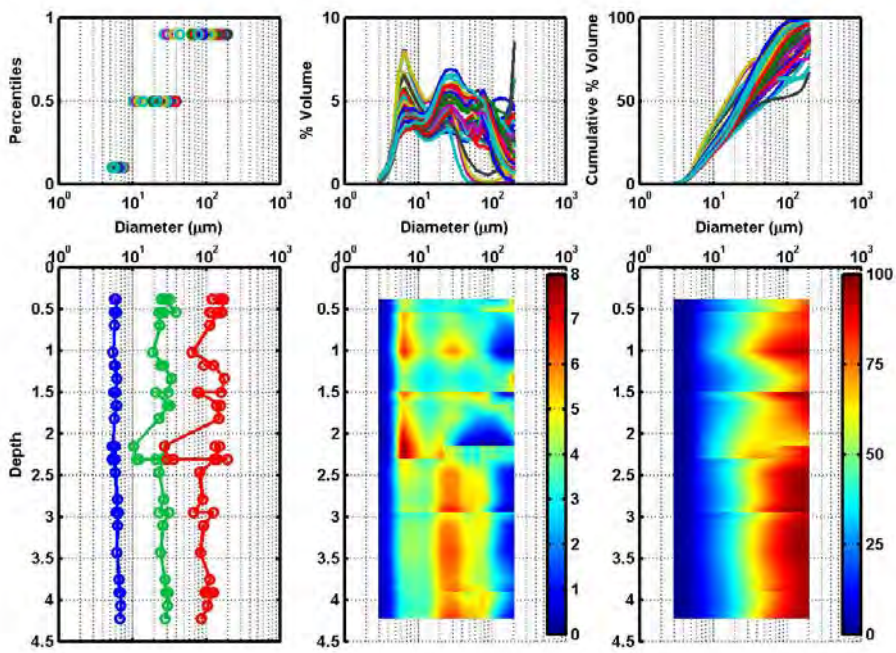

Figure 45. Same as Figure 14 caption but for LISST data collected on 9 July 2013 at 11:36 at ADCP Platform #2.

Total Suspended Solids Concentration (TSS)

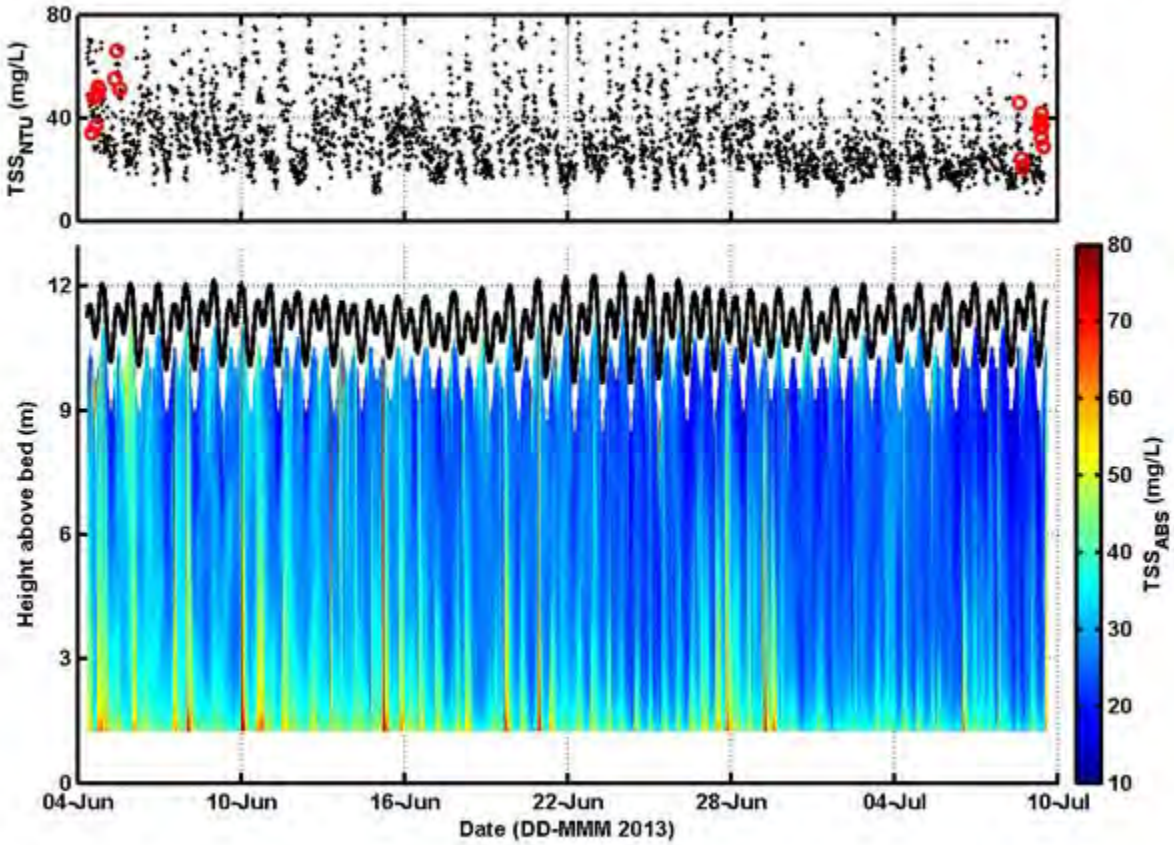

Figure 46. Top: Time series of TSS derived from optical turbidity. The red circles represent TSS derived from water sample data. Bottom: Time and depth resolved TSS derived from ADCP acoustic backscatter. Data are from ADCP Platform #1.

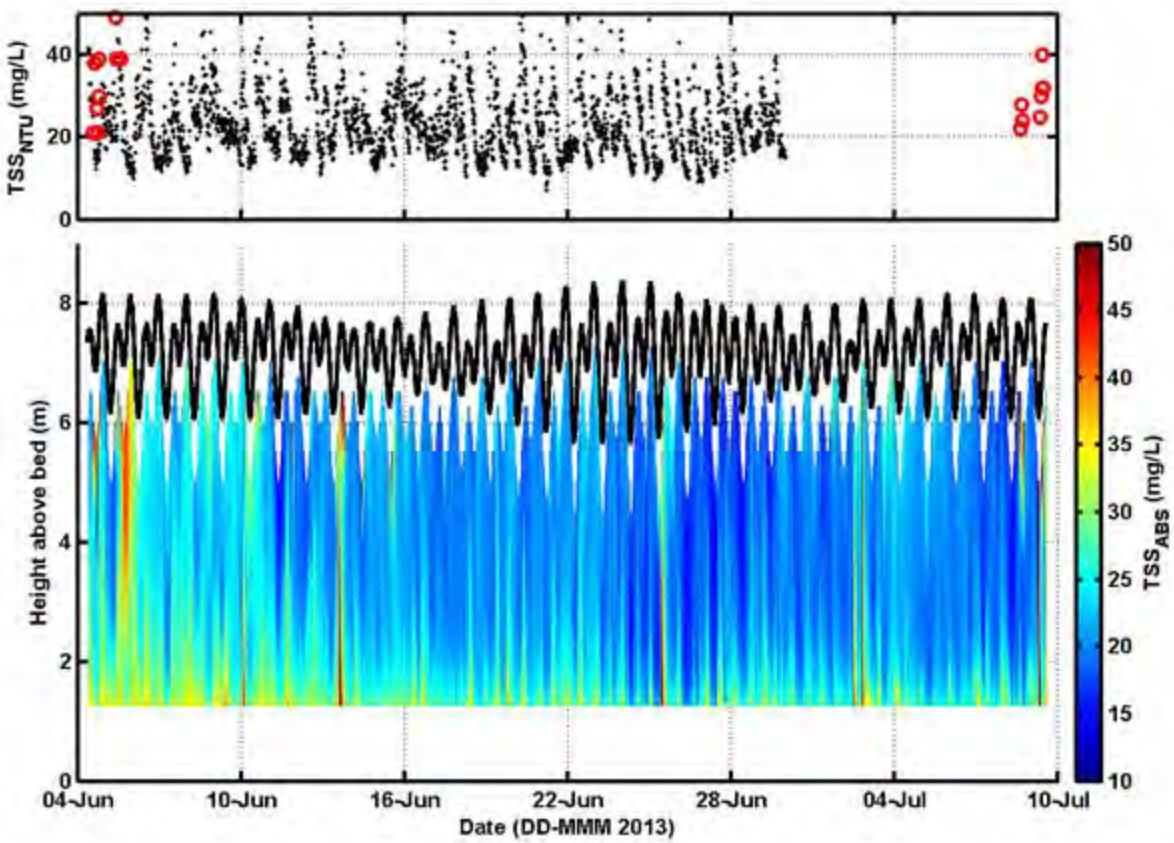

Figure 47. Top: Time series of TSS derived from optical turbidity. Data are biofouled after 30 June 2013. The red circles represent TSS derived from water sample data. Bottom: Time and depth resolved TSS derived from ADCP acoustic backscatter. Data are from ADCP Platform #2.

Appendix B. PARTRAC Sediment Tracking Study

Sea Engineering, Inc.

Heckathorn Superfund Site:

Lauritzen Channel Sediment Tracking Study

Final Draft

September 2013

Partrac Ltd
48 St Andrews Square
Glasgow
G1 5PP

+44 (0) 141 552 3903
info@partrac.com
www.partrac.com

DOCUMENT CONTROL

Version History				
Version	Date	Prepared by	Reviewed by	Approved by
v01	10th September 2013	J Poleykett/K Black	M Wright	K Black

Changes from the Previous Version	
n/a	Original

Recipient	Distribution Method		
	Paper (copies)	PDF	Online
Craig Jones – Sea Engineering Inc.		X	
Holders of controlled copies will automatically be provided with subsequent approved versions of this document when they become available.			

EXECUTIVE SUMMARY

Transport Pathway Evaluation (TPE) is a method in which a sediment transport pathway is visualised using a mass of uniquely labelled fluoro-magnetic (tracer) particles. Tracer particles are released into the environment and subsequent capture of these particles in space and/or time provides information on the localised transport direction and rate.

Partrac Ltd were contracted by SEA Engineering Inc. (Santa Cruz) to undertake a TPE study and provide sediment tracking services at the Heckathorn Superfund Site in the Lauritzen Channel, Port of Richmond ,California, to assess the fate of silt bottom sediments impacted by high mean flows and turbulence associated with local propeller wash.

This report presents information on the tracer specification and testing, method of tracer introduction and sampling design, and tracer analysis and enumeration methods. Results (tracer material dry mass in grammes) from testing of all samples are reported. No interpretation is provided in this report.

CONTENTS

1. INTRODUCTION 7

1.1 Background 7

1.2 Transport Pathway Evaluation (TPE) Using Sediment Tracers 7

2. TRACER DESIGN, MANUFACTURE AND TESTING 8

2.1 Introduction 8

2.2 Size Spectra 8

2.3 Particle Density 9

2.4 Para-Magnetic Attribute 10

2.5 Fluorescent Colour 10

2.6 Summary 12

3. PREPARATORY WORK 13

3.1 Tracer Freezing 13

3.2 Background Data Collection 13

4. ON SITE SURVEY WORK 14

4.1 GPS Position Recording 14

4.2 Deployment of Tracer 14

4.3 Deployment of Magnets 15

4.4 Sampling 16

5. TRACER ENUMERATION 21

5.1 Introduction 21

5.2 Unilux™ Fluorimeters 21

5.3 Methodology 22

6. RESULTS 25

6.1 Dose Response (Calibration) Functions 25

6.2 QC Data – Periodic Testing of Blanks 28

6.3 QC Data – Periodic Testing of Blind Samples (Methodological Accuracy) 28

6.4 QC Data – Unilux Sensor Precision 29

6.5 Tracer Dry Mass 29

7. REFERENCES 40

8. APPENDIX I GENERAL TECHNICAL SPECIFICATION OF THE UNILUX 41

9. APPENDIX II SPECTROFLUORIMETRIC ANALYSIS OF SEDIMENT SAMPLES (STANDARD OPERATING PROCEDURE) 42

10. APPENDIX III: NAVIGATION FIX DATA FOR TRACER MATERIAL SAMPLING DEPLOYMENT AND LOCATIONS 44

1. INTRODUCTION

1.1 Background

Contaminated sediments are found in numerous ports and harbour environments world-wide, where they comprise legacy deposits from historical industrial activities as well as more recent deposits from on-going contamination. Management approaches directed towards decontamination of contaminated seabed sediments require information on the range of processes governing the transport and fate of the contamination.

Partrac Ltd were contracted by Sea Engineering, Inc (Santa Cruz) to provide sediment tracking services for the Heckathorn Superfund Site in the Lauritzen Channel, Port of Richmond , California, to assess the fate of silt bottom sediments impacted by high mean flows and turbulence associated with local propeller wash. Partrac developed a dual signature silt tracer of two colours (green and red). 175 kg quantities of each were released in the form of low profile, frozen blocks onto the seabed at two locations in the central region of the Lauritzen Channel. Assessment of the mobilisation and transport was achieved through the use of powerful, *in situ* moorings of permanent magnets and through collection of sediment grabs. This methodology is otherwise known as 'Transport Pathway Evaluation' (TPE).

1.2 Transport Pathway Evaluation (TPE) Using Sediment Tracers

Transport Pathway Evaluation (TPE) is a method in which a sediment transport pathway is visualised using a mass of uniquely labelled fluoro-magnetic (tracer) particles (White, 1998). Tracer particles are released into the environment and subsequent capture of these particles in space and/or time provides information on the localised transport direction and rate (Black *et al*., 2007). TPE experiments require the manufacture of sediment analogues called 'tracers'; these are particles highly similar to those wishing to be tracked and which therefore behave in a highly similar way as native sediment. Partrac manufacture tracer with two unique signatures associated with every tracer grain – fluorescent colour and magnetic character – in order that they may be both extracted from environmental samples, with the use of powerful (11,000 Gauss) bar type magnets, and identified unequivocally using their fluorescent colour. Rarely are environmental particles found which are both fluorescent in colour *and* magnetic, and this thereby provides a firm foundation for the use of 'dual signature' tracers in tracking the movement of sediments.

The benefits of using powerful *[in situ]* magnets to capture the tracers include:

- Magnets can be left in the field to accumulate tracer (passive sampling);
- Magnets can be used to extract tracer from within a (bottom) sediment sample, thus concentrating tracer for ensuing analysis;
- They are simple to use and require minimal operator time;
- They can encompass a large area very easily thereby allowing a large area to be monitored;
- They immediately indicate the presence/absence of tracer, and can therefore be used to inform adaptive sampling; and
- They generally enable subsequent analysis of tracer particles by mass.

2. TRACER DESIGN, MANUFACTURE AND TESTING

2.1 Introduction

Discussions with Craig Jones (at Sea Engineering, Inc) distilled a tracer specification for use in the studies. This was:

- size range: coarse-medium silt tracer (ca. 20 – 70 µm).
- density: mineral density (~2300 – 2900 kg m^{-3})
- colour; 2 fluorescent colours (red; green).
- para-magnetic[1] attribute; yes.
- quantity (kg): 175 kg x 2 (red; green).

Partrac manufactured two tracer batches of differing colour (red; green) according to this specification. 175 kg of each colour was made.

In order that the use of sediment analogues to track sediment movement in aquatic systems is valid the tracer used should meet a series of underlying assumptions (see Foster, 2000). These are:

1. The tracer's hydraulic and bio-organic properties mimic those of the sediment of interest, and therefore the tracer is transported in the same fashion as the native sediment.
2. The tracer does not change properties through time (at least over the timescales of interest) and can be monitored.
3. The tracer does not manifestly change the transporting system in any way.

The following sections summarise characterisation tests performed on the tracer and are written in relation to [1] and [2].

2.2 Size Spectra

Since the size range was pre-specified, there was no contractual requirement to determine the size spectra of native sediments by measurement and none were made. However, size spectra measurements were made on two small sub-samples of each tracer colour using Malvern Laser Diffraction instrument at Sea Engineering Inc. Figure presents data from these analyses which demonstrate that the two tracer colours have very similar grain size distributions. The Green tracer material has a d_{50} of 41.89 µm, and the Red has a d_{50} of 45.82 µm. The d_{10} and d_{90} of each colour of tracer material are also very similar.

[1] Paramagnetism is a form of magnetism whereby the paramagnetic material is only attracted when in the presence of an externally applied magnetic field.

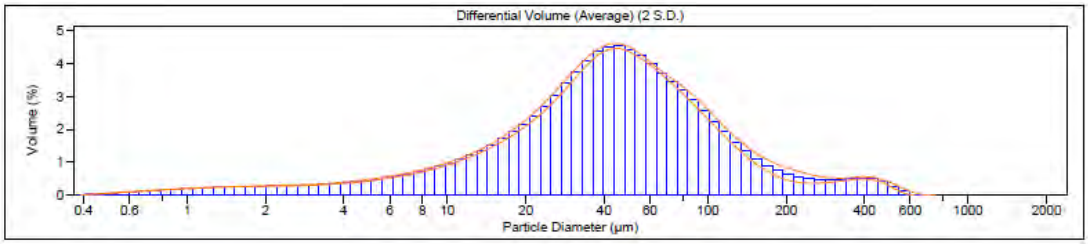

Green Tracer Material Run 1

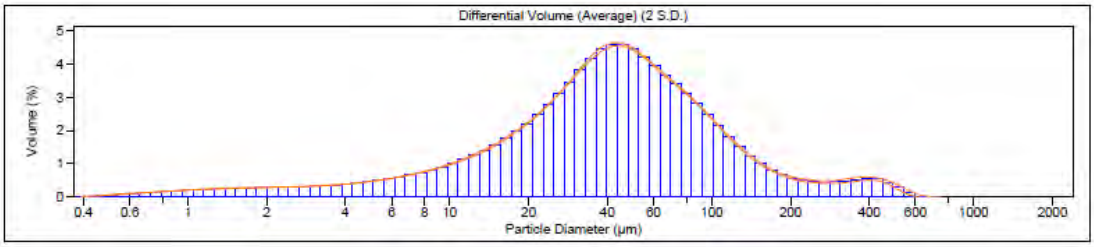

Green Tracer Material Run 2

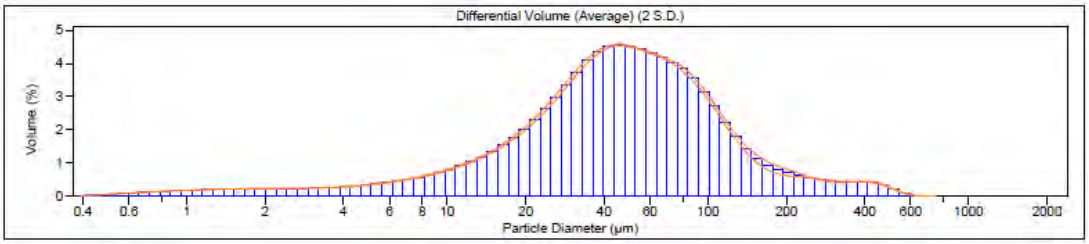

Red Tracer Material Run 1

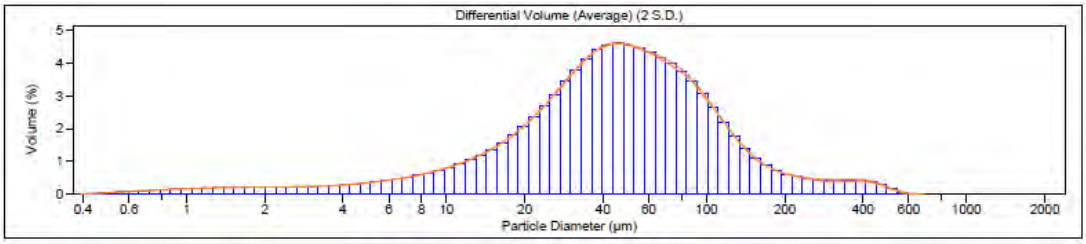

Red Tracer Material Run 2

Figure 2 Particle size spectra of the red and green tracer materials (2 runs of each colour on a Beckman Coulter LS Particle Size Analyser).

2.3 Particle Density

On a similar basis there was no contractual necessity to measure density of the native sediments as the tracer particles are coated, quartzitic mineral particles and understood to be of a sufficiently similar density. However, direct measures of the density were made using a standard volumetric methodology (BS 1377: 1990 Part 2: 8.2). This gave a density of 2,332 kg m^{-3} for the red tracer (1 sample tested) and a density of 2,354 ± 115 kg m^{-3} (3 samples tested) for the green tracer.

2.4 Para-Magnetic Attribute

Particles with para-magnetic attributes were required, in order that magnets could be used both within field sampling and to achieve magnetic separation (i.e. separation of magnetic particles [including tracer]) from non-magnetic sediments). Para-magnetism can be quantitatively confirmed using a specific laboratory test which measures directly the geological mass/volume-specific magnetic susceptibility (λ) of a tracer. This provides an index of the relative ease of which a soil or sediment sample can acquire magnetic attributes in the presence of an applied, low frequency (100 μT) alternating magnetic field. Ferruginous (i.e. iron rich) materials possess a greater propensity to acquire a magnetic attribute, and therefore display relatively high values for λ, whereas largely non-ferrous materials do not. These tests were not undertaken, but a general assessment using the permanent magnets was made to confirm para-magnetic properties for each tracer batch.

2.5 Fluorescent Colour

A sub-sample of each tracer colour was inspected under a fluorescence microscope to determine the integrity of the fluorescent-magnetic coating and the % of coated particles (Figure 3). These tests indicated 100% of particles are coated.

Figure 3: Photograph of both the red and green tracer under black light (UV-A~400nm).

2.5.1 Spectral Characteristics

Each tracer colour possesses spectral characteristics which are a function of the dye incorporated onto particle surfaces during the coating process. The analysis of dye concentration during the tracer enumeration procedure relies upon transmission of light of a specific wavelength - which optimally stimulates the dye to fluoresce (this is known as the 'excitation' wavelength, λ_{ex}) – and measurement of the intensity of light emitted specifically at the wavelength at which the dye is known to fluoresce (this is known as the 'emission' wavelength, λ_{em}). If these values are known then the measurement of dye concentration (and hence in this context tracer dry mass, M) is also optimised.

Figure 4 shows the excitation and emission spectra of the **green** tracer (code: BSR-CH227). The fluorescence excitation spectrum (dark blue line) is obtained by fixing the fluorescence detector wavelength at 523 nm and then scanning the excitation wavelengths. This provides a fluorescence induction spectrum, which is, in effect, an absorption spectrum of the particles. Inversely, the

fluorescence emission spectrum was obtained by fixing the excitation wavelength at 485nm and then scanning the emission wavelengths.

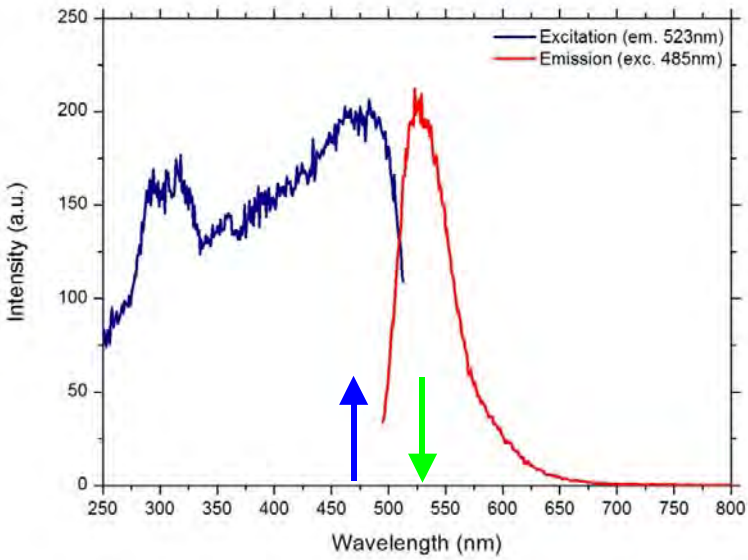

Figure 4 Emission – excitation spectra for the green tracer pigment. The blue and green lines indicate the specific wavelengths at which the analytical fluorimeter stimulates the tracer to fluoresce, and records the resulting fluorescence intensity, respectively.

The spectral characteristics of the red tracer (code: BSR-RD213) are presented in Figure 5. These particles show a similar broad excitation spectrum to the green tracer, but extending from the UV to around 600nm. Fluorescence emission is centred at 610nm. The Unilux instrument commissioned for the red tracer work uses a (LED) light source with output centred at 530nm and detects fluorescence emission centred at 625nm.

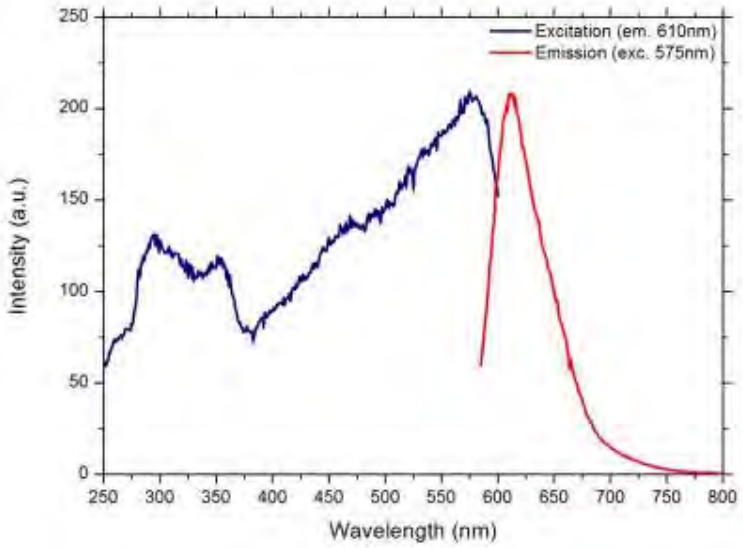

Figure 5 Excitation and emission spectra of red tracer.

The excitation and emission wavelengths for each tracer colour are given in Table 1.

Table 1: Excitation and emission wavelengths for each tracer colour.

Tracer Colour	Excitation Wavelength λ_{ex} (µm)	Emission Wavelength λ_{ex} (µm)
Red	530	625
Green	470	530

2.6 Summary

Table 2 provides a summary of the characteristics of each tracer colour.

Table 2: Summary of the characteristics of each tracer colour.

Colour	Quantity (kg)	d_{10} (µm)	d_{50} (µm)	d_{90} (µm)	Particle Density kg m^{-3}	Particles Fluorescent %
Green	175	8.47	41.89	129.55	2354	100
Red	175	11.2	45.82	128	2332	100

Notes: d_{10} = 10% of particles by weight are smaller than this figure; d_{50} = 50% of particles by weight are smaller than this figure; d_{90} = 90% of particles by weight are smaller than this figure.

3. PREPARATORY WORK

3.1 Tracer Freezing

The tracer was delivered to SEI's office in 25 kg batches in moist form. During manufacture ~10-15% by mass seawater was added to each batch; this is principally to reduce in advance surface active effects associated with the tracer, and this substantially simplifies tracer deployment. It also saves time in the field as it means that the tracer batches, as delivered, can be frozen directly without intervention or addition of additional seawater. All delivered tracer was frozen for 2.5 days at 9 °F in a nearby fisheries storage facility.

During this time small sub-samples of tracer were taken as archive samples.

3.2 Background Data Collection

A 'background' site survey is undertaken as part of the TPE/sediment tracking methodology. The purpose of the background survey is to establish several issues:

- The nature, and typical mass, of naturally magnetic (but non-fluorescent) particulates in the water column; this information is of generic use in regard to the use of suspended magnets to collect magnetic tracer material naturally magnetic (but non-fluorescent) particulates in the
- The nature, and typical mass, of naturally magnetic (but non-fluorescent) particulates in the bedded sediments; this information is of generic use in regard to the analytical methodology used to determine tracer dry mass in sediment samples
- The abundance, if any, of naturally occurring magnetic *and* fluorescent particulates at the site.
- The need to collect sediment material for use in preparation of standard curves within the analytical methodology.

In order to support this a suspended magnet was deployed close to Site M09 on the afternoon of Tuesday 11th June, and 2 bottom sediment grab samples G05 and G06 (1 upstream of the tracer drop zone, 1 downstream) were obtained prior to deployment of tracer on 13th June.

Table 3: Background sample collection 13th June 2013 (*t*=0; M = Magnet; G = Sediment Grab).

Sample Location	Date &Time Sampled
M09	13th June 2013: 10:30
G05	13th June 2013: 10:45
G06	13th June 2013: 11:00

4. ON SITE SURVEY WORK

4.1 GPS Position Recording

All positional detail was recorded and provided by Frank Spada (SEI). This included fixes for:

- each magnet mooring, including the background magnet mooring;
- the location of 'drift magnet' samples;
- the location where the two tracer colours were deployed, and
- all the sediment grabs collected, i.e. background samples, post-deployment QA samples, and sampling interval samples.

A table of the navigational fix data for the above is provided in the Appendix.

4.2 Deployment of Tracer

On 13th June 2013, each batch of the tracer was deployed using a workboat provided by SEI. Frozen tracer blocks were rolled onto a tarpaulin sheet and wrapped up by rolling the sheet over the block several times (this minimised contact of the block with seawater on the way to the seabed); two operators then attached ropes to eyelets at the corners of the tarpaulin and gently and slowly lowered the block to the seabed. Once it was on the seabed the tarpaulin was then unrolled slowly leaving the block to slide onto the surface of the seabed. The tarpaulin sheet was then slowly recovered.

The locations for each of the patches of the tracer deployed are presented in Figure 6.

Figure 6: Location for the Red and Green tracer material drop zones in the Lauritzen Channel.

4.3 Deployment of Magnets

Powerful cylindrical rare earth element (REE) magnets, either short 0.3 m (1 foot) or long 0.6 m (2 feet) in length, were utilised in this experiment (Figure 7). These were encapsulated in plastic sheaths with end caps and integrated in a mooring line which could be suspended in the estuary water e.g. from a piece of infrastructure. Following plumbing of the depth of the bed, at each of the magnet mooring locations, the moorings were positioned so that they would sample ~1 m and ~ 2 m above the bed; for 8 (of the 12) of the magnet moorings a long magnet (0.6 m) was positioned lowermost, and a short magnet positioned ~ 1 m above this; for the remaining 4 (of the 12) two short magnets were connected for the lowermost position. Altogether 12 magnet moorings were deployed attached to items of infrastructure largely around the periphery of the Lauritzen Channel (locations shown in Figure 8). The peripheral locations of the magnet moorings, while not preferred from a sampling standpoint, were necessitated so as to not interfere with potential vessel traffic during the study.

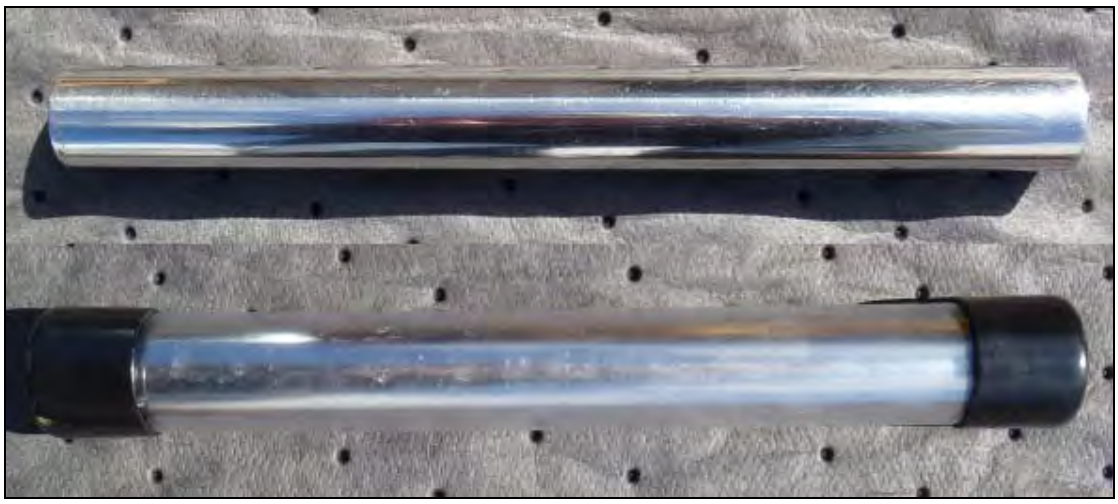

Figure 7 One of the powerful, permanent REE magnets used in this study (top) and housed in the sheath with endcaps (bottom).

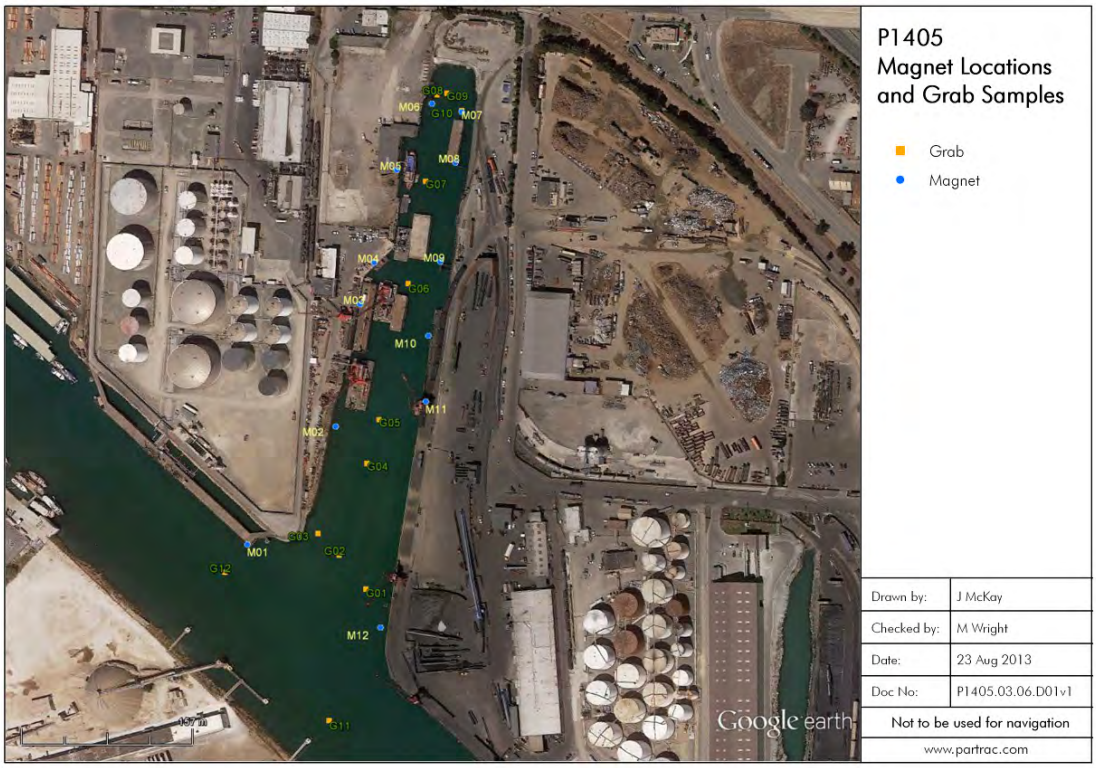

Figure 8: Magnet moorings and grab sampling locations

4.4 Sampling

Sampling was divided into that associated with Day 0 (*t*=0; 13th June, 2013) the tracer deployment day, and then successive, post-introduction sampling. For the latter sampling was undertaken on:

- Day 1 (*t*=~24 hours; 14th June, 2013);
- Day 2 (*t*=~48 hours; 15th June, 2013);
- Day 4 (*t*=~76 hours; 17th June, 2013);
- Day 6 (*t*=~120 hours; 19th June, 2013); and
- Day 14 (*t*=~336 hours; 19th June, 2013).

On each of the above occasions all the magnets were serviced and grabs of bed sediment at a series of pre-ordained locations (as designated by SEI see Figure 8) were collected. Servicing of the magnets involved recovery of the mooring line, careful removal of the sheath of each magnet and transfer of the sheath to a sample bag, followed by installation of a new clean sheath. The magnet moorings were recovered from the water on Day 14.

Grabs samples of bed sediment were collected with a small petit-ponar-style grab; upon recovery each sample was inspected to assess that the suitable sample had been retrieved and the surface material [of the grab sampler] to a depth of 2-3 cm was scooped off with a stainless steel spoon or spatula, and transferred to a labelled sample bag.

4.4.1 Post-Deployment (*t*=0 hours; Day 0) QA Sampling (13th June, 2013)

Two bottom grabs were collected, one ~50 m upstream of the tracer drop zone and approximately on the channel axis, and a second ~50 m downstream of the tracer drop zone and similarly on the tidal axis. The aim of these samples is to provide a simple check on the spread and deposition – if any – of tracer into the surrounding seabed area in the hours immediately following introduction.

This was supported by the collection of 3 magnet drift samples; a magnet was suspended on a wire at approximately mid-depth as the survey vessel drifted across the drop zone areas for a distance of ~50 – 100 m. As above, the aim of the process is to check for the presence of any residual tracer that might be in suspension immediately following tracer introduction.

Table 4: Samples collected following tracer deployment on 13th June 2013 (*t*=0; Drift M = drift magnet sample M = Magnet; G = Sediment Grab).

Sample Location	Date &Time Sampled
Drift M01	13th June 2013: 13:10 – 13:18
Drift M01	13th June 2013: 16:09 – 16:15
Drift M01	13th June 2013: 17:32 – 17:38
G05	13th June 2013: 18:36
G06	13th June 2013: 18:48

The objective of the use of frozen block method for tracer introduction is to emplace the tracers onto the seabed quickly, in a localised area and with minimal dispersion of tracer as possible. These samples effectively form a useful quality assurance on the success of the tracer deployment.

4.4.2 Day 1 (+24 hours after tracer deployment)

Table 5 shows the order and timing of the magnet and grab samples collected on Day 1 (14th June 2013)

Table 5: Order and timing of sample collection on Day 1, 14th June 2013 (M = Magnet; G = Sediment Grab).

Sample Location	Date &Time Sampled
G11	14th June 2013: 09:39
G12	14th June 2013: 09:52
G01	14th June 2013: 10:01
G02	14th June 2013: 10:08
G03	14th June 2013: 10:15
G04	14th June 2013: 10:18
G05	14th June 2013: 10:22
G06	14th June 2013: 10:28
G07	14th June 2013: 10:32
G08	14th June 2013: 10:37
G09	14th June 2013: 10:40
G10	14th June 2013: 10:45
M01	14th June 2013: 10:54
M02	14th June 2013: 11:10

Sample Location	Date &Time Sampled
M03	14th June 2013: 11:27
M04	14th June 2013: 11:37
M05	14th June 2013: 11:52
M06	14th June 2013: 12:07
M07	14th June 2013: 12:24
M08	14th June 2013: 12:30
M09	14th June 2013: 12:38
M10	14th June 2013: 12:55
M11	14th June 2013: 09:39
M12	14th June 2013: 09:39

4.4.3 **Day 2 (+48 hours after tracer deployment)**

Table 6 shows the order and timing of the magnet and grab samples collected on Day 2 (15th June 2013).

Table 6: Order and timing of sample collection on Day 2, 15th June 2013 (M = Magnet; G = Sediment Grab).

Sample Location	Date &Time Sampled
M07	15th June 2013: 09:38
G10	15th June 2013: 09:51
M08	15th June 2013: 09:57
M09	15th June 2013: 10:11
M10	15th June 2013: 10:22
M12	15th June 2013: 10:37
M11	15th June 2013: 10:55
M01	15th June 2013: 11:07
M02	15th June 2013: 11:16
M03	15th June 2013: 11:38
M04	15th June 2013: 11:46
M05	15th June 2013: 12:04
M06	15th June 2013: 12:18
G08	15th June 2013: 12:29
G09	15th June 2013: 12:41
G07	15th June 2013: 12:49
G06	15th June 2013: 12:56
G05	15th June 2013: 13:02
G04	15th June 2013: 13:08
G03	15th June 2013: 13:11
G02	15th June 2013: 13:28
G01	15th June 2013: 13:36
G12	15th June 2013: 13:41
G11	15th June 2013: 13;47

4.4.1 Day 4 (+72 hours after tracer deployment)

Table 7 shows the order and timing of the magnet and grab samples collected on Day 4 (17th June 2013).

Table 7: Order and timing of sample collection on Day 4, 17th June 2013 (M = Magnet; G = Sediment Grab).

Sample Location	Date &Time Sampled
M06	17th June 2013: 09:38
G08	17th June 2013: 09:51
M07	17th June 2013: 09:57
G10	17th June 2013: 10:11
M08	17th June 2013: 10:22
M09	17th June 2013: 10:37
M10	17th June 2013: 10:55
M11	17th June 2013: 11:07
M12	17th June 2013: 11:16
M02	17th June 2013: 11:38
M03	17th June 2013: 11:46
M04	17th June 2013: 12:04
M05	17th June 2013: 12:18
G09	17th June 2013: 12:29
G07	17th June 2013: 12:41
G06	17th June 2013: 12:49
G05	17th June 2013: 12:56
G04	17th June 2013: 13:02
M01	17th June 2013: 13:08
G12	17th June 2013: 13:11
G03	17th June 2013: 13:28
G02	17th June 2013: 13:36
G01	17th June 2013: 13:41
G11	17th June 2013: 13;47

4.4.1 Day 6 (+120 hours after tracer deployment)

Table 8 shows the order and timing of the magnet and grab samples collected on Day 6 (19th June 2013).

Table 8: Order and timing of sample collection on Day 6, 19th June 2013 (M = Magnet; G = Sediment Grab)

Sample Location	Date &Time Sampled
M06	19th June 2013: 08:15
G08	19th June 2013: 08:21
M07	19th June 2013: 08:25
G10	19th June 2013: 08:35
G09	19th June 2013: 08:39
M08	19th June 2013: 08:45
M05	19th June 2013: 08:50
G07	19th June 2013: 09:01
M09	19th June 2013: 09:09
G06	19th June 2013: 09:18
M04	19th June 2013: 09:24
M03	19th June 2013: 09;32
M10	19th June 2013: 09:41
M11	19th June 2013: 09:47
G05	19th June 2013: 09:55
M02	19th June 2013: 09:57
G04	19th June 2013: 10:03
M12	19th June 2013: 10:07
G01	19th June 2013: 10:17
G02	19th June 2013: 10:22
G03	19th June 2013: 10:25
M01	19th June 2013: 10:29
G12	19th June 2013: 10:38
G11	19th June 2013: 10:38

5. TRACER ENUMERATION

5.1 Introduction

A method known as *spectrofluorimetry* was used to determine the dry mass of tracer (in grammes) within a sample. A fluorimeter is a device used to measure parameters of fluorescence: its intensity and wavelength distribution of emission spectrum after excitation by a certain spectrum of light. These parameters can be used to identify the presence and the amount of specific dye molecules in a fluid medium. Modern fluorimeters are capable of detecting fluorescent molecule concentrations as low as 1 part per trillion. This approach offers a means with which to obviate the additional mass due to the presence of magnetic but non-fluorescent particulates[2] simply and directly. It also provided a very high analytic resolution which would facilitate detection of very low (mg quantities) tracer mass. The fluorimeter signal output can be empirically related to tracer mass (kg or g) through a series of tracer (colour) specific, reference standards.

5.2 Unilux™ Fluorimeters

The analyses were carried out using two specially manufactured high performance, miniature Unilux™ fluorimeters from Chelsea Technologies Group (one for each tracer colour analysis). The sensors comprise a small (26.5 mm) diameter housing with a single window geometry (Figure 8). The front lens of the fluorimeter is designed to refract the output from the 6 LEDs so that it converges in the solution approximately 7 mm in front of the lens, forming an evenly illuminated spot approximately 5 mm in diameter. Any fluorescence generated is then collected by the same lens and directed down the central axis of the instrument to the detector. High quality filters are used to select the specific excitation and emission wavelengths required (see Table 1).

Figure 8: The CTG Unilux miniature laboratory fluorimeter (right) and the measurement cell (left); note the fluorimeter shines from beneath during acquisition of data.

The Unilux series are especially suited to the present task as they are small, highly stable, possess a high ambient light rejection capability and have low noise-high sensitivity attributes. The general technical specification of the Unilux instrument is provided in Appendix I.

2 Magnetic (but non-fluoresent) particles would be expected in relatively high abundance in an industrialised port environment.

5.3 Methodology

A detailed **Standard Operating Procedure** for the analysis is given in Appendix II. The method in general terms, for situations where two tracer colours may be found in the same sample, involves a series of steps:

1. drying and weighing of the sample (sieving if necessary);
2. dissolution of the fluorescent pigment into a special solvent for a period of 168 hours (7 days);
3. centrifugation if necessary (to remove all particulates);
4. dilution to a known level using analytical grade solvent;
5. analysis of the fluorescence intensity of the dye solution using both Unilux™ sensors (sampling frequency 1 Hz, duration 30-40 s); and then
6. derivation of tracer particle dry mass (*M*) using calibration functions (dose response curves) for each Unilux for each dye colour.

By testing each sample with both fluorimeters, and using data obtained from the dose response curves for each sensor in both dyes (Section 5.3.1), there are two simultaneous equations with two unknowns:

SignalF = SlopeFG x [Green] + SlopeFP x [Red] + OffsetF 1.

and

SignalR = SlopeRG x [Green] + SlopeRP x [Red] + OffsetR 2.

Where:

SignalF : is the sample signal from the Fluorescein UniLux (measured).
SlopeFG : is the slope of the Green Dye response on the Fluorescein UniLux (known).
SlopeFP : is the slope of the Red Dye response on the Fluorescein UniLux (known).
OffsetF : is the solvent blank signal (known).

and

SignalP : is the sample signal from the Rhodamine UniLux (measured).
SlopePG : is the slope of the Green Dye response on the Rhodamine UniLux (known).
SlopeRP : is the slope of the Red Dye response on the Rhodamine UniLux (known).
OffsetR : is the solvent blank signal (known).

These two simultaneous equations can be solved (using matrix algebra) to give the two unknown concentrations for both dyes. As the fluorimeter calibrations are established using solutions based on a known dry mass of tracer particle, the mass ratio for particles in the unknown sample solution is simply the ratio of the calculated concentrations.

5.3.1 Standard (Dose Response) Curves

Eluted dye solutions for both tracer colours were prepared by adding a known dry mass of tracer particles (10^{-1} g) to 40ml of acetone in an Eppendorf tube, mixing and then allowing the solution to equilibrate for 168 hours (7 days). This time period has been established as optimal for maximal extraction of the pigment into the acetone. 200µl of the eluted dye solution was then mixed with 2ml of analytical grade acetone (dilution of 1 in 10) to create a stock solution. Dose response curves were obtained by filling the calibration cell with 75 ml of analytical grade acetone, recording a baseline reading and then adding sequential 20 µl aliquots of the stock solution, mixing and recording further readings. Approximately 20 seconds worth of raw data was recorded for each measurement using a 1 second sampling rate. Average and standard deviation values were calculated for the 20 sequential readings from each of the data sets. Due to the (significant) non-fluorescent magnetic background material present at the site dose response curves were prepared with just tracer present and tracer and ~ 1g (the average of the dry mass of all samples) of non-fluorescent native magnetic material present to effectively measure the quenching effects of the native sediment. Dose response curves were prepared as follows:

1. 0.1g tracer; no background material, sequential readings through to 1g (both tracer colours); and
2. 0.1g tracer; ~ 1.0g background native material (average background material concentration) sequential readings through to 1g (both tracer colours).

Least-squares regression analysis (Fowler *et al*., 1998) was performed on the data to generate calibration functions.

5.3.2 Quality Assurance

An analytical quality control/assurance methodology was developed in tandem with development with the fluorimetric method. This involved inclusion of the following within the laboratory testing strategy:

1. Periodic testing of blanks (1 in every 7 tests);
2. Periodic testing of blind samples (i.e. tracer masses unknown to the technician);
    a. 4 samples tested.
3. Evaluation of Unilux sensor drift (temporal stability); and
4. Evaluation of Unilux sensor bias (accuracy and precision).

5.3.3 Visual Observations

Prior to fluorimetric analysis all samples were routinely visually inspected under UV illumination to assess tracer presence. Qualitative descriptions were developed as follows:

- Trace
- Low
- Intermediate
- High
- Very high

Note:- Due to quenching effects of the background non-fluorescent, magnetic material and the low wavelength of a standard UV-A inspection lamp (~ 400nm), and since not all the sample is examined in depth, the probability exists *of a negative visual inspection and a positive fluorimetric result*. Cross-comparison of qualitative descriptions with fluorimetric data should accordingly be undertaken with caution.

Quenching is any process that decreases the fluorescent intensity of a sample (Lakowicz, 2006).

6. RESULTS

6.1 Dose Response (Calibration) Functions

Standard (dose response) curves were developed to relate fluorimetric measurements (probe reading in volts) to tracer dye concentration over the range of dry masses (0 – 1 g, as follows: (0.0g; 0.1g; 0.2g; 0.3g; 0.4g; 0.5g; 0.6g; 0.7g; 0.8g; 0.9g and 1g) (Figure 9). Since there is a probability of both tracer colours occurring in a given sample, functions were generated for both sensors in both dyes (note the weak but linear responses of the probes in contrary dyes, which is expected). Since there is a non-fluorescent, magnetic background (non-tracer) fraction in most samples, this was repeated for the dose response curves prepared with tracer and 1 g of the non-fluorescent, magnetic background material (the average mass for this fraction across all samples collected). Least squares regression analysis on the data provides 4 transfer functions for use in data analysis (Table 9). Consistently high coefficients of determination (r^2) are found. The practical, minimum resolvable tracer mass (MRM) is 10^{-3} g (i.e 1 mg).

Table 9: Summary of standard (dose response) equations for the fluorescein and rhodamine sensors for both dyes with no background (magnetic, non-fluorescent) material present.

Probe	Dye	Slope	Intercept	r^2
Fluorescein	Green	0.0004	+0.0655	0.99
Rhodamine	Red	0.0006	+0.0506	0.99
Fluorescein	Red	0.0002	+0.0585	0.99
Rhodamine	Green	$1x10^{-7}$	+0.0618	0.00

Table 10: Summary of standard (dose response) equations for the fluorescein and rhodamine sensors for both dyes with1 g of background (magnetic, non-fluorescent) material present.

Probe	Dye	Slope	Intercept	r^2
Fluorescein	Green	0.0003	+0.0489	0.9916
Rhodamine	Red	-2E-05	+0.0607	0.7748
Fluorescein	Red	7E-05	+0.0538	0.9942
Rhodamine	Green	-1E-05	+0.06	0.7380

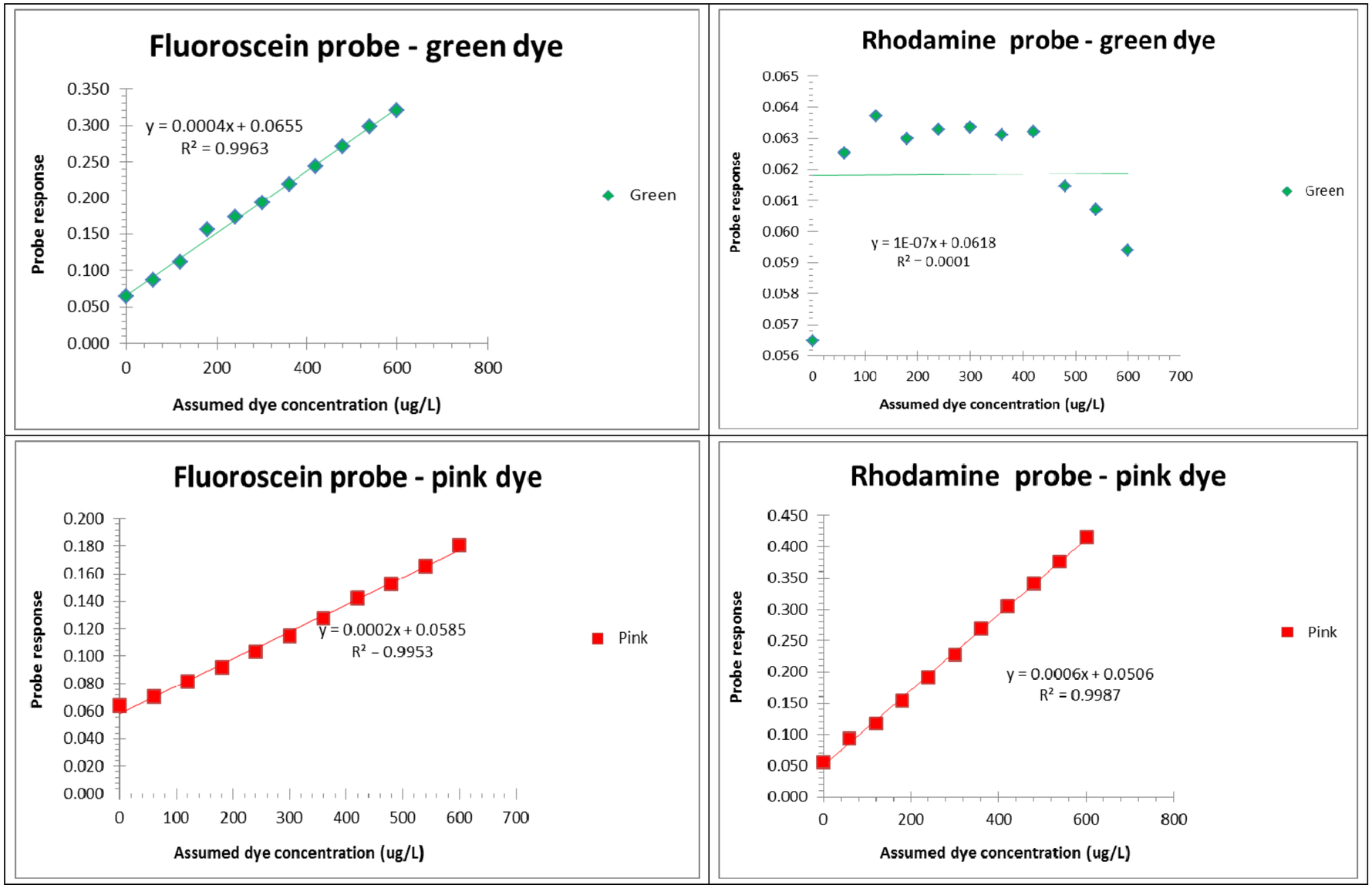

Figure 9: Dose response curves – neat tracer only (no background non-fluorescent, magnetic material). In practise the point concentration values on the x-axis are interchangeable with the tracer dry masses (0.0g; 0.1g; 0.2g; 0.3g; 0.4g; 0.5g; 0.6g; 0.7g; 0.8g; 0.9g and 1g).

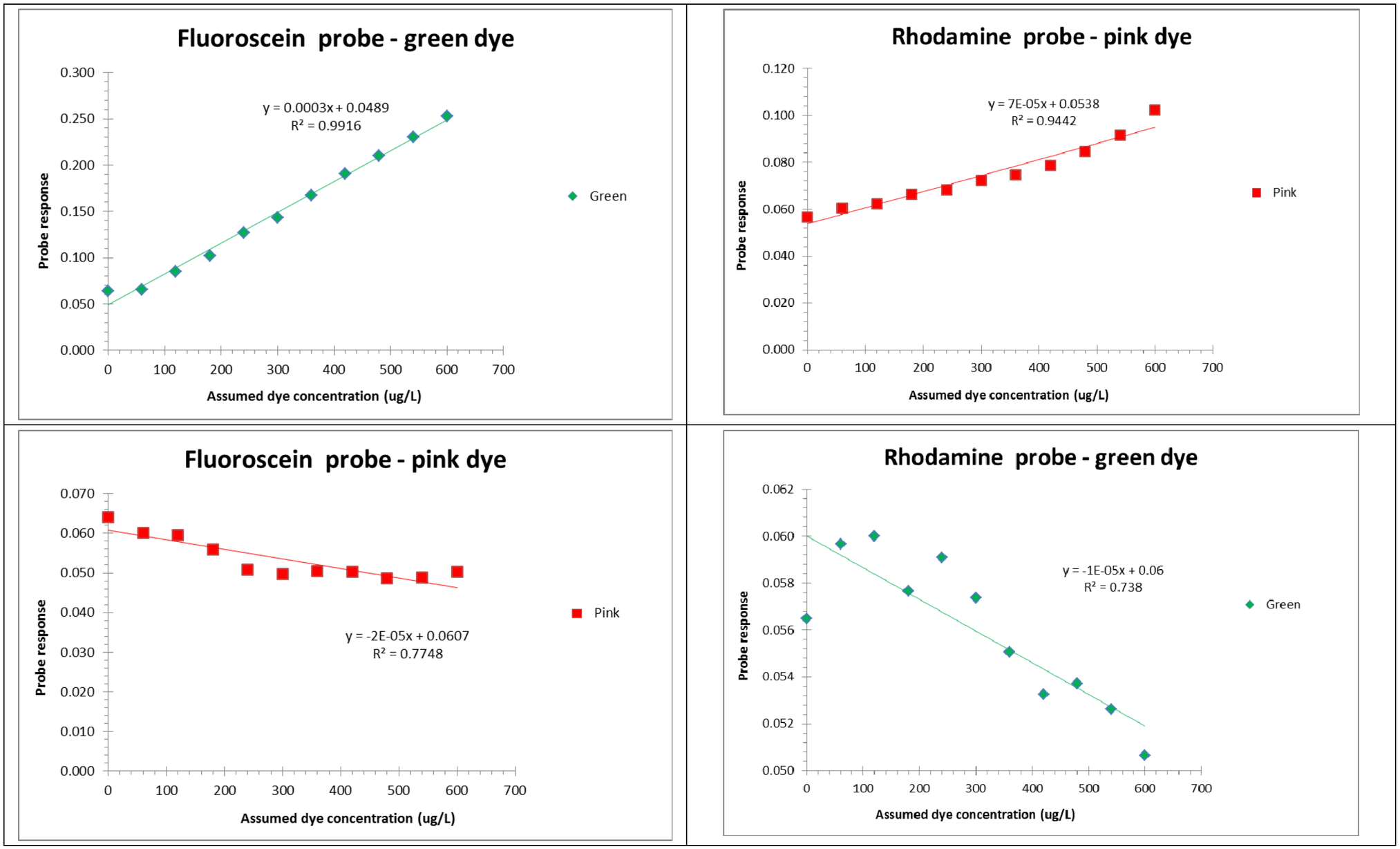

Figure 10: Dose response (calibration) functions for both Unilux fluorimeters for both dyes inclusive of 1 g of non-fluorescent, magnetic background material. In practise the point concentration values on the x-axis are interchangeable with the tracer dry masses (0.0g; 0.1g; 0.2g; 0.3g; 0.4g; 0.5g; 0.6g; 0.7g; 0.8g; 0.9g and 1g).

6.2 QC Data – Periodic Testing of Blanks

A check on the performance of the fluorimetric analytical procedure is made through periodic testing of blanks. Blanks are solutions made up in entirely the same manner as samples but without inclusion of a sediment/tracer sample. Note due to the use of a solvent (rather than water) zero values were not recorded (the fluorescein Unilux returns raw values ~0.064; the rhodamine Unilux 0.056; these are the y-axis intercepts in Figure 9 and 10). However, a value of zero for the *derived* tracer mass (Table 11) confirms proper functioning of the fluorimeters.

Table 11: Periodic testing of laboratory blanks for mono-colour dyes (i.e. green tracer, red tracer).

Sample #	Measured Blank Tracer Mass M_{blank} g
1	0.000
2	0.000
3	0.000
4	0.000
5	0.000
6	0.000
7	0.000
8	0.000
9	0.000
10	0.000

6.3 QC Data – Periodic Testing of Blind Samples (Methodological Accuracy)

In order to establish the fluorimetric analytical procedure together with operator efficiency function as desired, periodic blind samples were submitted for testing to the laboratory. These provide information on the methodological accuracy, which is the degree of closeness of measurements of a quantity to that quantity's actual (true) value. Blind samples are prefabricated mono-colour sediment samples within which the tracer dry mass is unknown to the analyst. Table 12 summarises results from testing of four samples. The results are good (within 16% of true value) in terms of analytical accuracy and reasonably consistent over the range of tracer masses tested.

Table 12: Periodic testing of blind samples (green tracer).

Sample #	Doped Tracer Mass M_{dop} (g)	Measured Tracer Mass M (g)	Mean Error (%)
1	0.151	0.165	9
2	1.250	1.111	12
3	0.165	0.146	12
4	0.016	0.019	16

6.4 QC Data – Unilux Sensor Precision

The precision of a measurement system, also called reproducibility or repeatability, is the degree to which repeated measurements under unchanged conditions show the same results. The precision of the Unilux fluorometer instrument was tested by carefully preparing a series of known tracer dry masses, eluting into the solvent and then collecting 10 consecutive (repeat) fluorescence intensity measurements from the solutions (Table 13). These data show relatively low standard deviation values, which indicates a relatively high precision for the methodology.

Table 13 Assessment of method precision.

Tracer Mass (g)	*Fluorimeter Response (Raw Data) ± standard deviation*
0.025	0.190 ± 5%
0.100	0.216 ± 6%
0.200	0.284 ± 5%
0.500	0.443 ± 6%
0.750	0.684 ± 9%
1.000	0.790 ± 12%

6.5 Tracer Dry Mass

Table 14 presents results for all samples tested. Background samples (i.e. collected before any tracer was deployed), and samples of the seabed immediately following tracer introduction, are found at the top of the table. Qualitative visual descriptions (inspection under black light) are given for every sample (note the general use of caution in Section 6.3.3 if cross-referencing these to fluorimetric data is undertaken). A reference number is also given for a digital photograph for each sample (photographs are not provided in this report).

N.B. All data has been reported however caution should be exercised with any reported tracer mass data that is at or below ~0.005g

Table 14 Summary of tracer dry mass (g) for all samples. Data omissions are where samples were either not collected or the results of the analyses were not considered to be sensible/reliable.

Day - Date - Sample Number Day 1 (13th June 2013)	Visual Description under Black Light	Photo Number	Mass of Red Tracer (g)	Mass of Green Tracer (g)
Background Magnet (M09)	no tracer present (prior to deployment)	5167	0.000	0.000
Post Deployment Grab (G05)	trace: green	5022	0.267	0.062
Post Deployment Grab (G06)	no tracer present	5171	0.031	0.122
Drift Magnet 01	no tracer present	-	0.000	0.000
Drift Magnet 02	no tracer present	-	0.000	0.000
Drift Magnet 03	no tracer present	-	0.000	0.000

Day 2 (14th June 2013) Sample Number	Visual Description under Black Light	Photo Number	Mass of Red Tracer (g)	Mass of Green Tracer (g)
M01A	no tracer present	5166	0.000	0.000
M01B	no tracer present	5157	0.000	0.000
M02A	no tracer present	5165	0.000	0.000
M02B	no tracer present	5164	0.000	0.000
M02C	no tracer present	5163	0.000	0.000
M03A	no tracer present	5162	0.000	0.000
M03B	No Sample recovered			
M03C	no tracer present	5160	0.000	0.000
M04A	no tracer present	5159	0.000	0.000
M04B	no tracer present	5158	0.000	0.000
M04C	no tracer present	5155	0.000	0.000

Day 2 (14th June 2013) Sample Number	Visual Description under Black Light	Photo Number	Mass of Red Tracer (g)	Mass of Green Tracer (g)
M05A	no tracer present	5154	0.000	0.000
M05B	no tracer present	5153	0.000	0.000
M05C	no tracer present	5152	0.000	0.000
M06A	no tracer present	5151	0.000	0.000
M06B	no tracer present	5150	0.000	0.000
M07A	no tracer present	5149	0.000	0.000
M07B	no tracer present	5148	0.005	0.000
M08A	no tracer present	5147	0.000	0.000
M08B	no tracer present	5146	0.000	0.000
M09A	no tracer present	5145	0.000	0.000
M09B	no tracer present	5143	0.000	0.019
M10A	no tracer present	5142	0.000	0.000
M10B	no tracer present	5141	0.000	0.094
M11A	no tracer present	5139	0.000	0.132
M11B	no tracer present	5138	0.000	0.087
M12A	no tracer present	5137	0.000	0.144
M12B	no tracer present	5140	0.000	0.036
G01	no tracer present	5201	0.012	0.052
G02	no tracer present	5202	0.000	0.000
G03	no tracer present	5200	0.211	0.075
G04	no tracer present	5205	0.000	0.000
G05	no tracer present	5203	0.026	0.027
G06	no tracer present	5207	0.000	0.068
G07	no tracer present	5209	0.038	0.057
G08	no tracer present	5206	0.246	0.102

Day 2 (14th June 2013) Sample Number	Visual Description under Black Light	Photo Number	Mass of Red Tracer (g)	Mass of Green Tracer (g)
G09	no tracer present	5204	0.060	0.000
G10	no tracer present	5208	0.174	0.000
G11	no tracer present	5199	0.020	0.000
G12	no tracer present	5198	0.035	0.363

Day 3 (15th June 2013) Sample Number	Visual Description under Black Light	Photo Number	Mass of Red Tracer (g)	Mass of Green Tracer (g)
M01A	no tracer present	5136	0.000	0.134
M01B	no tracer present	5135	0.000	0.076
M02A	no tracer present	5134	0.000	0.063
M02B	no tracer present	5133	0.000	0.015
M02C	no tracer present	5132	0.000	0.155
M03A	no tracer present	5131	0.000	0.116
M03B	no tracer present	5130	0.000	0.066
M03C	no tracer present	5129	0.000	0.243
M04A	no tracer present	5128	0.000	0.000
M04B	no tracer present	5127	0.017	0.345
M04C	no tracer present	5126	0.000	0.031
M05A	no tracer present	5125	0.000	0.476
M05B	no tracer present	5124	0.121	0.205
M05C	no tracer present	5123	0.000	0.027
M06A	no tracer present	5122	0.196	0.047
M06B	no tracer present	5121	0.000	0.065
M07A	no tracer present	5120	0.000	0.088
M07B	no tracer present	5119	0.035	0.147

Day 3 (15th June 2013) Sample Number	Visual Description under Black Light	Photo Number	Mass of Red Tracer (g)	Mass of Green Tracer (g)
M08A	no tracer present	5118	0.000	0.216
M08B	no tracer present	5117	0.018	0.197
M09A	no tracer present	5116	0.159	0.015
M09B	Unreliable Analysis Result			
M10A	no tracer present	5114	0.102	0.170
M10B	Unreliable Analysis Result			
M11A	no tracer present	5112	0.000	0.250
M11B	no tracer present	5110	0.000	0.145
M12A	no tracer present	5109	0.000	0.403
M12B	no tracer present	5111	0.081	0.223
G01	no tracer present	5174	0.050	0.000
G02	no tracer present	5175	0.000	0.000
G03	no tracer present	5176	0.010	0.050
G04	no tracer present	5177	0.002	0.000
G05	no tracer present	5178	0.010	0.000
G06	low: green	5182	0.000	0.140
G07	no tracer present	5181	0.360	0.237
G08	no tracer present	5184	0.017	0.080
G09	no tracer present	5185	0.000	0.063
G10	no tracer present	5179	0.192	0.049
G11	no tracer present	5180	0.023	0.000
G12	no tracer present	5183	0.000	0.101

Day 4 (17th June 2013) Sample Number	Visual Description under Black Light	Photo Number	Mass of Red Tracer (g)	Mass of Green Tracer (g)
M01A	no tracer present	5108	0.000	0.056
M01B	no tracer present	5107	0.000	0.000
M02A	No Sample Recovered			
M02B	no tracer present	5106	0.000	0.053
M02C	no tracer present	5105	0.000	0.000
M03A	no tracer present	5104	0.000	0.000
M03B	no tracer present	5103	0.004	0.012
M03C	no tracer present	5102	0.000	0.066
M04A	no tracer present	5101	0.000	0.014
M04B	no tracer present	5100	0.001	0.048
M04C	no tracer present	5099	0.000	0.000
M05A	no tracer present	5098	0.055	0.000
M05B	no tracer present	5097	0.000	0.018
M05C	no tracer present	5096	0.000	0.065
M06A	no tracer present	5095	0.011	0.190
M06B	no tracer present	5094	0.000	0.000
M07A	no tracer present	5093	0.000	0.000
M07B	no tracer present	5092	0.000	0.000
M08A	no tracer present	5091	0.000	0.000
M08B	Unreliable Analysis Result			
M09A	no tracer present	5089	0.000	0.000
M09B	no tracer present	5088	0.000	0.000
M10A	no tracer present	5087	0.000	0.000
M10B	no tracer present	5086	0.000	0.000
M11A	no tracer present	5085	0.000	0.000

Day 4 (17th June 2013) Sample Number	Visual Description under Black Light	Photo Number	Mass of Red Tracer (g)	Mass of Green Tracer (g)
M11B	no tracer present	5084	0.906	0.000
M12A	no tracer present	5083	0.000	0.000
M12B	no tracer present	5082	0.000	0.000
G01	no tracer present	5217	0.035	0.081
G02	no tracer present	5212	0.028	0.000
G03	no tracer present	5221	0.035	0.037
G04	no tracer present	5220	0.008	0.108
G05	Unreliable Analysis Result			
G06	no tracer present	5211	0.231	0.190
G07	no tracer present	5210	0.000	0.087
G08	no tracer present	5216	0.361	0.061
G09	no tracer present	5213	0.177	0.171
G10	no tracer present	5214	0.098	0.109
G11	no tracer present	5219	0.000	0.022
G12	no tracer present	5215	0.000	0.066

Day 6 (19th June 2013) Sample Number	Visual Description under Black Light	Photo Number	Mass of Red Tracer (g)	Mass of Green Tracer (g)
M01A	no tracer present	5081	0.000	0.000
M01B	no tracer present	5079	0.000	0.000
M02A	no tracer present	5078	0.000	0.000
M02B	no tracer present	5077	0.000	0.000
M02C	no tracer present	5076	0.000	0.000
M03A	no tracer present	5075	0.002	0.000
M03B	no tracer present	5074	0.000	0.000

Day 6 (19th June 2013) Sample Number	Visual Description under Black Light	Photo Number	Mass of Red Tracer (g)	Mass of Green Tracer (g)
M03C	no tracer present	5073	0.000	0.000
M04A	no tracer present	5072	0.000	0.142
M04B	no tracer present	5071	0.000	0.000
M04C	no tracer present	5070	0.000	0.000
M05A	no tracer present	5069	0.000	0.000
M05B	no tracer present	5068	0.000	0.000
M05C	no tracer present	5067	0.000	0.000
M06A	no tracer present	5066	0.000	0.000
M06B	no tracer present	5065	0.000	0.000
M07A	no tracer present	5064	0.000	0.000
M07B	no tracer present	5063	0.000	0.000
M08A	no tracer present	5062	0.000	0.000
M08B	no tracer present	5059	0.000	0.000
M09A	no tracer present	5061	0.000	0.000
M09B	no tracer present	5058	0.000	0.000
M10A	no tracer present	5057	0.000	0.000
M10B	no tracer present	5169	0.000	0.000
M11A	no tracer present	5170	0.000	0.000
M11B	no tracer present	5168	0.000	0.000
M12A	no tracer present	5055	0.000	0.000
M12B	no tracer present	5054	0.000	0.000
G01	no tracer present	5224	0.030	0.157
G02	no tracer present	5226	0.014	0.258
G03	no tracer present	5223	0.019	0.051
G04	no tracer present	5225	0.000	0.162

Day 6 (19th June 2013) Sample Number	Visual Description under Black Light	Photo Number	Mass of Red Tracer (g)	Mass of Green Tracer (g)
G05	no tracer present	5229	0.005	0.047
G06	trace: green	5227	0.000	0.255
G07	no tracer present	5222	0.021	0.083
G08	no tracer present	5233	0.000	0.000
G09	Unreliable Analysis Result			
G10	no tracer present	5230	0.000	0.000
G11	no tracer present	5231	0.000	0.065
G12	no tracer present	5232	0.000	0.000

Day 14 (27th June 2013) Sample Number	Visual Description under Black Light	Photo Number	Mass of Red Tracer (g)	Mass of Green Tracer (g)
M01A	no tracer present	5053	0.000	0.000
M01B	no tracer present	5052	0.000	0.000
M02A	no tracer present	5051	0.000	0.000
M02B	no tracer present	5050	0.000	0.000
M02C	no tracer present	5049	0.000	0.000
M03A	No Sample Recovered			
M03B	no tracer present	5048	0.000	0.000
M03C	no tracer present	5047	0.000	0.011
M04A	no tracer present	5046	0.000	0.000
M04B	no tracer present	5045	0.000	0.000
M04C	no tracer present	5044	0.000	0.056
M05A	no tracer present	5041	0.000	0.046
M05B	no tracer present	5042	0.000	0.000
M05C	no tracer present	5040	0.010	0.105

Day 14 (27th June 2013) Sample Number	Visual Description under Black Light	Photo Number	Mass of Red Tracer (g)	Mass of Green Tracer (g)
M06A	no tracer present	5039	0.000	0.155
M06B	no tracer present	5038	0.000	0.076
M07A	no tracer present	5037	0.094	0.124
M07B	no tracer present	5036	0.000	0.000
M08A	no tracer present	5035	0.000	0.002
M08B	no tracer present	5034	0.000	0.028
M09A	trace: green	5033	0.082	0.150
M09B	no tracer present	5032	0.000	0.047
M10A	no tracer present	5031	0.054	0.170
M10B	no tracer present	5030	0.000	0.000
M11A	No Sample Recovered			
M11B	no tracer present	5029	0.055	0.133
M12A	no tracer present	5027	0.000	0.173
M12B	no tracer present	5024	0.000	0.083
G01	no tracer present	5187	0.018	0.203
G02	no tracer present	5188	0.000	0.154
G03	no tracer present	5192	0.446	0.220
G04	no tracer present	5193	0.187	0.226
G05	no tracer present	5190	0.000	0.114
G06	no tracer present	5189	0.004	0.119
G07	low: green	5194	0.033	0.151
G08	no tracer present	5196	0.123	0.215
G09	no tracer present	5195	0.091	0.331
G10	no tracer present	5197	0.118	0.369
G11	no tracer present	5186	0.047	0.080

Day 14 (27th June 2013) Sample Number	Visual Description under Black Light	Photo Number	Mass of Red Tracer (g)	Mass of Green Tracer (g)
G12	no tracer present	5191	0.000	0.058
Eastdrop 1	no tracer present	5172	0.000	0.000
Eastdrop2	no tracer present	5173	0.080	0.000

7. REFERENCES

Black, K.S., Wilson, P., Athey, S., Black, I., and Evans, D., (2007). The use of particle tracking in marine sediment transport studies: a review. Measuring Sediment Transport in Coastal and Shelf Environments. Coastal and Shelf Sediment Transport, J. Geological Society of London (Special Issue), 274, 73-91pp.

Cochran, S.A., Roberts, L.M., and Evans, K.R., 2002. Moloka'i Fieldtrip Guidebook: Selected Aspects of the Geology, Geography, and Coral Reefs of Moloka'i. U.S. Geological Survey Open-File Report 02-158.

Fabricius, K.E., 2005. Effects of terrestrial runoff on the ecology of corals and coral reefs; review and synthesis: Marine Pollution Bulletin, v. 50, p. 125–146.

Foster, I. D. L. 2000. Tracers in Geomorphology, Chichester, Wiley.

Fowler, J., Cohen, L., and Jarvis, P., (1998) Practical Statistics for Field Biology Wiley, 259pp.

Field, M.E., Cochran, S.A., Logan, J.B., and Storlazzi, C.D. (Eds.), (2008). The Coral Reef of South Moloka‘i, Hawai‘i—Portrait of a Sediment-Threatened Fringing Reef. U.S. Geological Survey Scientific Investigations Report 2007-5101.

Lakowicz, J. R. 2006. Principles of Fluorescence spectroscopy, Springer Science and Business Media.

Martin Solan, Benjamin D. Wigham, Ian R. Hudson, Robert Kennedy, Christopher H. Coulon, Karl Norling, Hans C. Nilsson and Rutger Rosenberg 2004 *In situ* quantification of bioturbation using time-lapse fluorescent sediment profile imaging (f-SPI), luminophore tracers and model simulation. MEPS Vol. 271: 1–12, 2004.

Takesue, R.K., 2010, Terrigenous sediment provenance from geochemical tracers, south Molokai reef flat, Hawaii. U.S. Geological Survey Open-File Report 2010-1155.

White, T.E., (1998). Status of measurement techniques for coastal sediment transport. Coastal Engineering 35, 17-45 pp.

8. APPENDIX I GENERAL TECHNICAL SPECIFICATION OF THE UNILUX

SPECIFICATION

The UniLux is calibrated over the following ranges:

Performance

Wavelength Option Dynamic Range* Limit of Detection
Chlorophyll a 0 to 100 µg/L <0.01 µg/L
Fluorescein 0 to 100 µg/L <0.005 µg/L
Rhodamine WT 0 to 100 µg/L <0.02 µg/L
Phycoerythrin Cyanobacteria 0 to 100 µg/L <0.02 µg/L
Phycocyanin Cyanobacteria 0 to 100 µg/L <0.01 µg/L
Turbidity 0 to 100 FTU <0.02 FTU
* User configurable up to 500 µg/L

Mechanical

Size: 26.5mm dia. x 105mm (140mm including connector)
Weight in air: 100g
Pressure housing: Acetal C
Depth rating: 600 metres
Connector: MCBH-6-MP-SS
Electrical
Input voltage: 11 to 25Vdc
Data output: Digital RS232 and analogue 0 to 5Vdc (RS422 and SDI-12 options)
Power requirements: <1Watt @ 12 volt

9. APPENDIX II SPECTROFLUORIMETRIC ANALYSIS OF SEDIMENT SAMPLES (STANDARD OPERATING PROCEDURE)

Objectives: Determination of the weight of tracer particles within a sample that contains naturally magnetic but non-fluorescent particles, using a miniature, low cost multi-wavelength fluorimeter (Unilux).

Scientific Background: Partrac Ltd has developed a series of fluorescent-magnetic particulate tracers which are used on a commercial basis for tracking the movement of particulates in aquatic environments. The tracer possesses two signatures which are used to unequivocally identify tracer in samples within studies: fluorescent colour and para-magnetic character. The inclusion of para-magnetism in each particle means that permanent magnetism can be used to separate the tracer from the environment whilst in the environment. The fluorescence colour is used as a second signature to unequivocally identify tracer in samples. An inherent drawback of the magnetic particle methodology is that there are a variety of naturally magnetic (i.e. ferrous rich), but non-fluorescent particles in nature. In the methodology used these particles are included within samples, and this effectively constitutes 'noise' in data. The overall objective for samples is to derive the dry mass of tracer within samples, and the presence of magnetic but non-fluorescent particles constitutes additional mass.

Sample Analysis Methodology (SoP):

1. Record the dry weight of the sample and place in a labelled vial that is able to withstand exposure to acetone.
2. Formulate a blank sample (i.e. use an ashed sand or silt, independently tested to be pigment free).
3. Visually inspect dry sample using a handheld fluorescent lamp to establish tracer presence.
4. Add a known volume of analytical grade acetone (90%) to the vial containing the sediment. The volume of acetone is dependent on the amount of sediment, but should adequately cover the sample. The volume chosen *must* remain the same through a given sample batch run.
5. Place the samples in a fridge for 24 hours.
6. Remove the extractant for flourimetric analysis. Samples should be filtered if particles are in suspension.
7. Each sample should be analysed using the appropriate CTG Unilux probe for the tracer dye, or using both probes for mixed colour studies.
8. Most samples will require dilution (e.g. 1 in 100 or 1 in 1000) before being analysed. Each sample should be diluted in analytical grade acetone, using a pipette and volumetric flask for accuracy.
9. Measure the blank (i.e. volume of acetone).
10. Place approximately 100ml of diluted sample into a glass measuring beaker and place under the Unilux probe. Allow the probe to measure the sample for approximately 20 seconds.
11. Remove the sample and wash the probe with distilled water before placing the next sample underneath.
12. A continuing calibration blank should be run at the beginning, after every 10 samples, and at the end of each run.
13. Wash and rinse all glassware with acetone and distilled water between samples.
14. Routinely run blanks and spiked samples as part of methodology QA.
15. Routinely assess sensor drift and reproducibility (bias).

Calibration Methodology: Calibration experiments should be performed for each batch of samples run, and these standards should be processed regularly to check the performance of the Unilux. Calibration must be completed individually for each tracer pigment that will be determined, and jointly where there are or might be two tracers in the same sample. Decide on the calibration range needed, which is typically determined based on the typical concentrations observed in the sample extracts and the desire to establish that the calibration is linear throughout the working range. The lowest concentration standard is at or less than the practical quantification limit. Ideally, in order for a calibration to be acceptable, the correlation coefficient for the linear regression should be greater than 0.990. However, this will depend on a number of factors such as degree of coating, particle size distribution, solvent and dye properties. Have 3-5 replicate samples per calibration weight and analyse as described above.

Calibration samples are made up by adding a known dry mass of tracer particles to 5ml of acetone in an Eppendorf tube, mixing and then allowing the solution to equilibrate for 24h hours. 100µl of the eluted dye solution is then mixed with 1ml of analytical grade acetone (dilution of 1 in 10) to create a stock solution. Dose response curves are obtained by filling the calibration cell with 75 ml of analytical grade acetone, recording a baseline reading and then adding sequential 50 µl aliquots of the stock solution, mixing and recording further readings. Approximately 20 seconds worth of raw data is recorded for each measurement using a 1 second sampling rate. An average and standard deviation was calculated for 20 sequential readings from each of the data sets. This procedure is continued for another 3 times or for as many points required on the calibration curve.

10. APPENDIX III: NAVIGATION FIX DATA FOR TRACER MATERIAL SAMPLING DEPLOYMENT AND LOCATIONS

Location	Latitude (Digital Degrees)	Longitude (Digital Degrees)
Centre of GREEN Tracer deployment area	37.922741	-122.367279
Centre of RED Tracer deployment area	37.922229	-122.366994
M01	37.92058817	-122.3685177
M02	37.92160255	-122.3676715
M03	37.92262179	-122.3674927
M04	37.92296956	-122.3673701
M05	37.92374312	-122.3671938
M06	37.92430278	-122.3668711
M07	37.92425325	-122.3665549
M08	37.92383306	-122.3665889
M09	37.92301071	-122.3666834
M10	37.92239548	-122.3667615
M11	37.92185367	-122.3667468
M12	37.91997169	-122.3670779
G01	37.9202833	-122.36725
G02	37.92055	-122.36755
G03	37.9207167	-122.3677833
G04	37.9213167	-122.3673167
G05	37.9216833	-122.3672167
G06	37.9228167	-122.367
G07	37.9236667	-122.3668833
G08	37.9243833	-122.3668167
G09	37.9244	-122.3667167
G10	37.9242667	-122.36655
G11	37.9191833	-122.36755
G12	37.92035	-122.3687333

Appendix C. Sedflume Analysis

United Heckathorn Sedflume Analysis
Richmond Harbor, CA
August 2013

Prepared for:

CH2M HILL

Prepared by:
Sea Engineering, Inc.
200 Washington Street, Suite 101
Santa Cruz, CA 95060
Tel: (831) 421-0871
Fax: (831) 421-0875

Executive Summary

Morphological bed changes in any aquatic system are dictated by complex and dynamically linked relationships between biological activity, hydrodynamic forcing, and sediment characteristics. When analyzing the sediment transport occurring within a system, numerous variables must be considered; one key aspect is the erosion properties and stability of a site's sediments. Sea Engineering, Inc. (SEI) conducted a Sediment Erosion at Depth Flume (Sedflume) analysis on 10 sediment cores obtained from Richmond Harbor, CA in the Lauritzen Channel. The Lauritzen channel is part of the United Heckathorn Superfund Site. The cores were collected in water depths ranging between 5.8 m to 7.9 m. The primary goal of this work was to characterize the erosion properties and physical characteristics of the sites sediments. The Sedflume analysis determined sediment erosion rates, critical shear stresses, particle sizes and bulk densities at specific down-core depth intervals.

Critical shear stress is a difficult parameter to quantify; for Sedflume analysis it is typically defined as the shear stress required to erode sediment at a rate of 10^{-4}centimeter per second (cm/s) (Roberts et al. 1998). To reduce uncertainty, critical shear stresses were estimated by combining a power law regression analysis with critical shear stress thresholds based on direct erosion rate measurements. Calculated critical shear stresses ranged from 0.1 Pa to 1.28 Pa.

The presence of detritus, pebbles and shells had a noticeable effect on erosion. The Sedflume analysis provided a quantification of the overall effect of each of these constituents on sediment erosion. Although erosion rates fluctuated between intervals, core sediments generally stiffened with depth. This trend is common for sites with cohesive sediments. Cohesive sediments will often compact due to the weight of the overlying material. Compaction reduces the potential for sediment mobility. However, Sedflume results must be analyzed in conjunction with other system characteristics, such as hydrodynamic forcing, to assess overall site stability and sediment transport trends.

CONTENTS

EXECUTIVE SUMMARY ..... **I**

SECTION 1: INTRODUCTION **1**

1.1 INTRODUCTION 1
1.2 CORE COLLECTION 1
1.3 EXPERIMENTAL PROCEDURES 4
1.3.1 Description of Sedflume Setup *4*
1.3.2 Measurements of Sediment Erosion Rate *6*
1.3.3 Determination of Critical Shear Stress *7*
1.3.4 Measurement of Sediment Bulk Properties *8*
1.3.5 Intra-core and Inter-core Comparisons *10*

SECTION 2: RESULTS **12**

2.1 SF01 12
2.2 SF02 15
2.3 SF03 18
2.4 SF04 21
2.5 SF05 24
2.6 SF06 27
2.7 SF07 30
2.8 SF08 33
2.9 SF09 36
2.10 SF10 39

SECTION 3: SUMMARY **42**

SECTION 4: REFERENCES **44**

APPENDIX A – PARTICLE SIZE DISTRIBUTIONS **45**

Section 1
Introduction to Sedflume

1.1 Introduction

Morphological bed changes in any aquatic system are dictated by complex and dynamically linked relationships between biological activity, hydrodynamic forcing, and sediment characteristics. When analyzing the sediment transport occurring within a system, numerous variables must be considered; one key aspect is the erosion properties and stability of a site's sediments. Sea Engineering, Inc. (SEI) conducted a Sediment Erosion at Depth Flume (Sedflume) analysis on 10 sediment cores obtained from Richmond Harbor, CA in the Lauritzen Channel. The Lauritzen channel is part of the United Heckathorn Superfund Site. The cores were collected in water depths ranging between 5.8 m to 7.9 m. The primary goal of this work was to characterize the erosion rates and physical properties of the sediments within the study area. The cores were eroded during the Sedflume analysis to determine erosion rates as a function of shear stress and depth. In addition, each core was sub-sampled to determine sediment bulk density and particle size distribution at specific depths within the core. Critical shear stresses were also deduced for five vertical intervals in each core (unless otherwise stated).The following report outlines the procedures used in the Sedflume analysis, presents the measured data, and provides a description and analysis of the results.

1.2 Core Collection

Ten sediment cores were collected by SEI personnel on July10 and 11, 2013. At each coring location, a differential global positioning system (DGPS) was used to position a vessel at pre-determined fixed sampling stations in the Lauritzen Channel. The 10 coring locations are shown in Figure 1, where the white squares represent the coring locations. A pole was attached with clamps to the 10 cm by 15 cm rectangular core. The core tube was lowered into the water and positioned perpendicular to the sediment bed. Pressure was applied by hand until at least 30 cm (approximately) and no more than 60 cm of the core tube penetrated into the sediment bed. A valve affixed to the top of the core tube was temporally closed to provide suction when the core was pulled out of the sediment bed. The sediment bed near the mouth of the channel (SF08, SF04, SF05, SF03 and SF09) was stiff and required additional force from a fence-post hammer to achieve core penetration; smaller than 30 cm cores were kept if several core attempts were made at a location and each lead to recoveries less than 30 cm.

After cores reached the water surface, they were visually inspected for length and quality. Undisturbed cores were capped and secured to minimize sediment disturbance from sloshing water and vessel/vehicle motion. Cores were then transferred from the vessel to land, and packed in secure Sedflume core shipping boxes. The cores were then driven by SEI personnel to SEI's Sedflume laboratory in Santa Cruz, California. Upon arrival, the cores were again visually inspected to ensure sediment structure and surface had been

preserved. The cores were then placed in an ambient water bath for preservation until processing.

Table 1. Sedflume core extraction coordinates, time and date, and water depth.

Core ID	Lat (°N)	Long (°W)	Coring Date	Time (PST)	Depth (m)*
SF01	37.92442	-122.36678	7/10/2013	12:45	5.8
SF02	37.92442	-122.36668	7/10/2013	13:45	5.8
SF03	37.92237	-122.36730	7/10/2013	17:15	7.6
SF04	37.92167	-122.36747	7/11/2013	10:20	6.1
SF05	37.92187	-122.36742	7/11/2013	12:35	7.3
SF06	37.92395	-122.36668	7/10/2013	14:40	7.3
SF07	37.92353	-122.36690	7/10/2013	15:15	7.3
SF08	37.92127	-122.36750	7/11/2013	09:30	6.4
SF09	37.92267	-122.36712	7/11/2013	07:50	7.9
SF10	37.92308	-122.36677	7/11/2013	11:45	6.4

* Water depths are as recorded during core extractions and are not referenced to any datum.

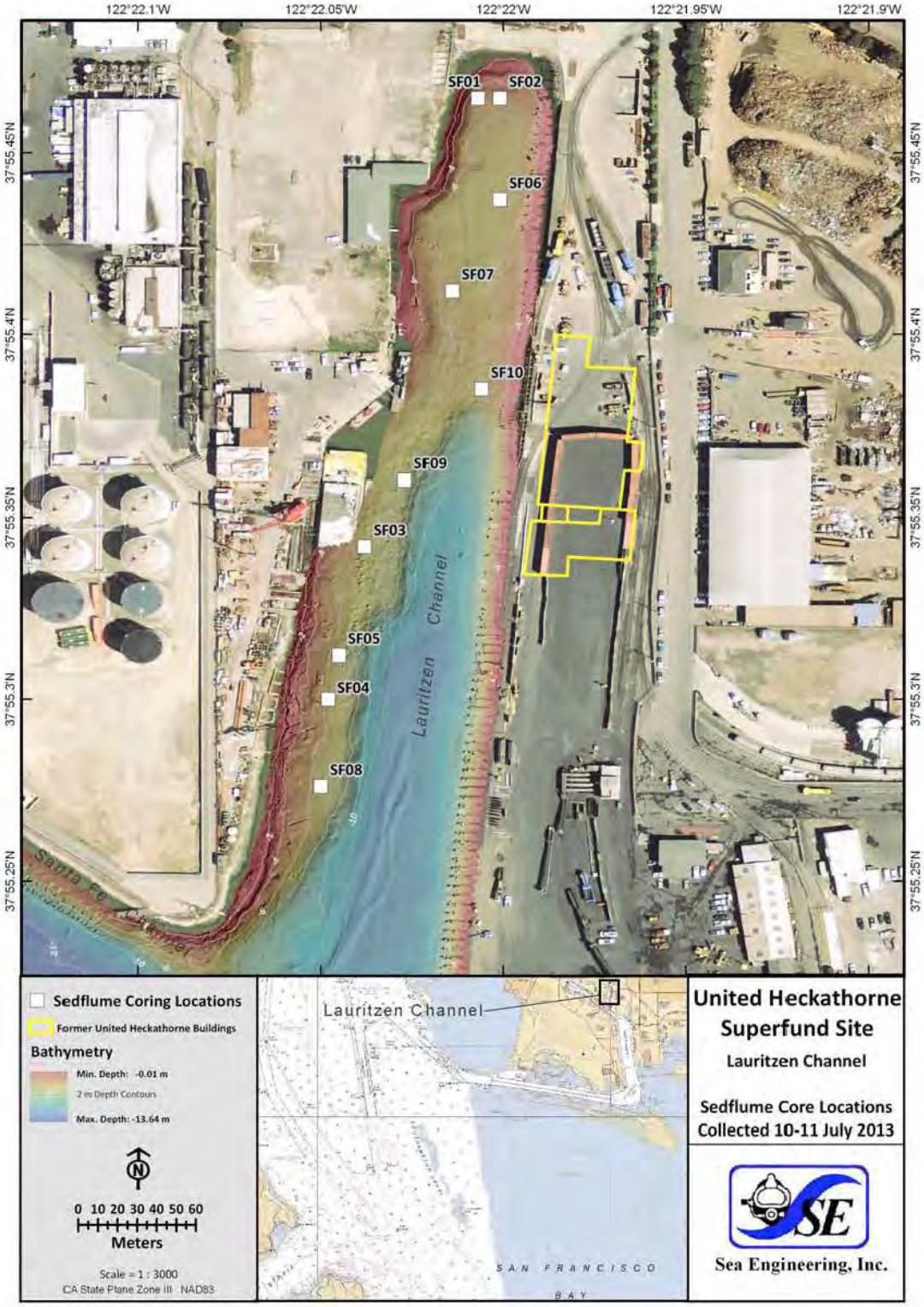

Figure 1. Map of coring locations in Lauritzen Channel.

1.3 Experimental Procedures

A detailed description of Sedflume analysis and its application are given in McNeil et al. (1996) and Roberts et al. (1998). The following sections supplement those reports with a general description of the Sedflume analysis procedures conducted in this study.

1.3.1 Description of Sedflume Setup

A Sedflume is essentially a straight flume with an open bottom section through which a rectangular cross-section core barrel containing sediment can be inserted (schematic shown in Figure 2). The main components of the flume are the water tank, pump, inlet flow converter (which establishes uniform, fully-developed, turbulent flow), the main duct, test section, hydraulic jack and the core barrel containing sediment (Figure 3). The core barrel, test section, flow inlet section, and flow exit section are made of transparent acrylic so the sediment-water interactions can be observed visually. The core barrel has a rectangular cross-section, 10 cm by 15 cm, and a length of 60 cm.

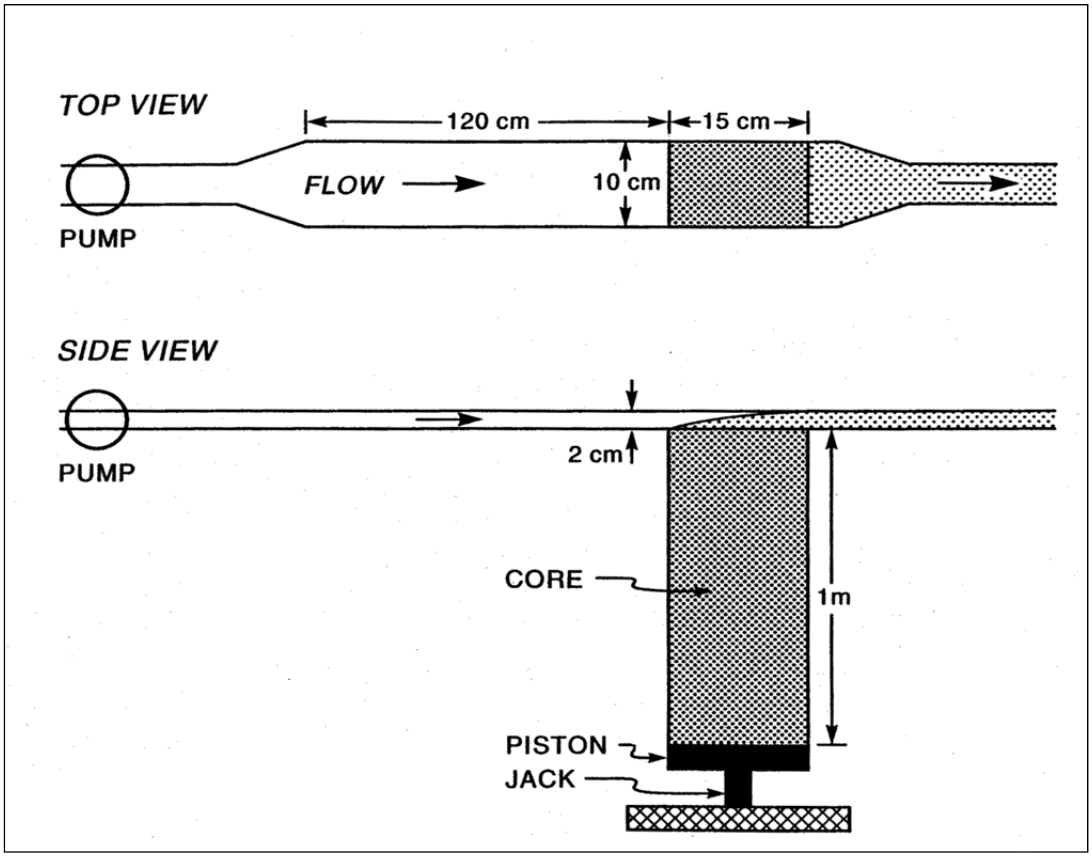

Figure 2. Schematic of the Sedflume setup showing top and side views.

Water is pumped through the system from a 300-gallon storage tank, through a 5 cm diameter pipe, and then through the flow converter into the main duct. This duct is

rectangular, 2 cm in height, 10 cm in width, and 120 cm in length; it connects to the test section, which has the same cross-sectional area (2 cm by 10 cm) and is 15 cm long. The flow converter changes the shape of the cross-section from circular to rectangular while maintaining a constant cross-sectional area. A ball valve regulates the amount of water entering the flume so that the flow rates can be carefully controlled. The flume also has a small valve immediately downstream from the test section that is opened to prevent a pressure vacuum from forming and enhancing erosion.

At the start of each test, a core barrel and the sediment it contains are inserted into the bottom of the test section. The sediment surface is aligned with the bottom of the Sedflume channel. When fully enclosed, water is forced through the duct and test section over the surface of the sediment. The shear stress produced by the flow, and imparted on the particles, causes the sediment to erode. As the sediment on the surface of the core erode, the remaining sediments in the core barrel are slowly moved upward so that the sediment-water interface remains level with the bottom of the flume.

An operator moves the sediment upward using a piston that is inside the core barrel and is controlled by a hydraulic jack with a 1m drive stroke. The jack is driven by the release of pressure that is regulated with a switch and valve system. In this manner, the sediments can be raised and made level with the bottom of the test section. The movement of the hydraulic jack can be controlled for measurable increments as small as 0.5 mm.

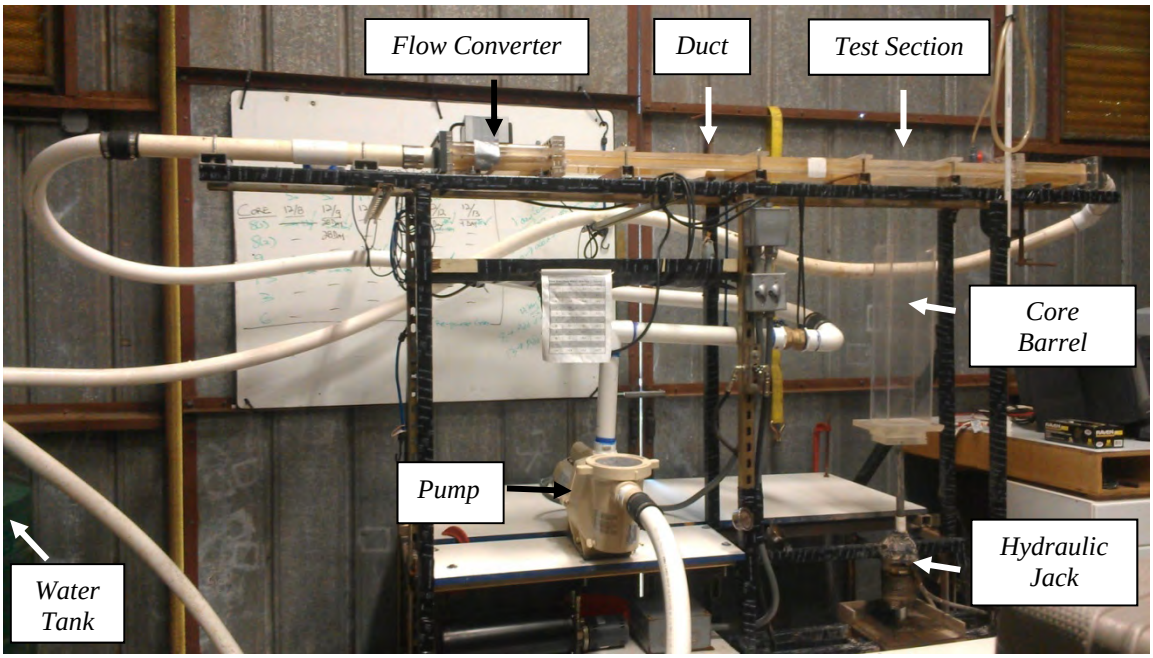

Figure 3. Sedflume in the Santa Cruz, CA, SEI laboratory.

1.3.2 Measurements of Sediment Erosion Rate

At the start of each core analysis an initial reference measurement was made of the starting core length. The flume was then operated at a specific flow rate corresponding to a particular shear stress, and sediment was eroded (McNeil et al., 1996). As erosion proceeded, the core was raised if needed to keep the core's surface level with the bottom of the flume. This continued until 10 minutes had passed, or the core had been raised roughly 2 cm. The erosion rate for the applied shear stress was then calculated as:

$$E = \frac{\Delta z}{T} \qquad [1]$$

E = Erosion rate
Δz = Amount that the sediment was raised during a particular measurement period
T = Measurement time interval

Because material is eroded and the core structure is broken down, repetitive erosion measurements at a given depth are not possible. To best determine the erosion rate at several different shear stresses and depths using only one core, the following procedures were performed for all cores:

1) The core was inserted into the bottom of the Sedflume test section.
2) The total length of sediment in the core barrel was measured and recorded.
3) Two 5-gram (approximately) subsamples of sediment from the core's surface were collected using a clean spoon. Sediment sampling was constrained to the "downstream" (relative to the Sedflume flow direction) end of surface.
4) Various shear stresses where applied to the cores surface from low to high, and sediment erosion was measured if it occurred (0.5 mm of erosion in 10 minutes was considered quantifiable). Applied shear stresses started at 0.1 Pa, and sequentially doubled until a given shear stress caused roughly 2 cm of erosion in 20 seconds. Each shear stress cycle was applied for a minimum of 20 seconds and a maximum of 10 minutes. To the extent possible, no more than 2 cm of sediment was allowed to erode at a single shear stress.
5) Once the threshold of 2 cm of erosion in 20 seconds was met, a new depth interval was started. Steps 3 and 4 were repeated[1]. Also, if the sediment composition changed noticeably in appearance or erosion properties, the depth interval was stopped, sediment sub-samples were collected, and a new depth interval was started (step 4).
6) Up to five depth intervals were tested per core.

[1] If a particular shear stress did not cause any observable erosion over a 10 minute period for consecutive depth intervals (e.g. less than 0.5 mm eroded in 10 minutes), that shear stress was removed from subsequent testing cycles; higher shear stresses were added, as appropriate, to attempt to measure at least 3 erosion rates.

1.3.3 Determination of Critical Shear Stress

The critical shear stress of a sediment bed, τ_{cr}, is the applied shear stress at which sediment motion is initiated. In this study it is operationally defined as the shear stress required to produce 0.001 mm of erosion in 1 second. This represents an erosion rate of 10^{-4} cm/s, or roughly 1 mm of erosion in 15 minutes[2].

Since it is difficult to measure τ_{cr} exactly at the 10^{-4} cm/s threshold, erosion was instead measured over a range of shear stresses designed to bracket the initiation of erosion threshold. The highest applied shear stress where erosion *did not occur* is defined by τ_0; and τ_1 is the lowest applied shear stress where erosion *did occur*.

Using the measured erosion rate data in each depth interval, a power law regression (described below) analysis was employed to determine the shear stress (τ_{power}) required to cause 10^{-4} cm/s of erosion. Assimilating the bracketed shear stress values (τ_0 and τ_1) and τ_{power}, the critical shear stress of each interval was then chosen according to the set of criteria described below:

- If $\tau_0 \leq \tau_{power} \leq \tau_1$, then $\tau_{power}$was the selected critical shear stress, τ_{cr}, for the interval
- If $\tau_0 \geq \tau_{power}$, then τ_0 was the selected critical shear stress for the interval
- If $\tau_{power} \geq \tau_1$, then τ_1 was the selected critical shear stress for the interval

where τ_0 and τ_1 are determined directly from the Sedflume measurements. The τ_{cr} criteria allowed for selection of critical shear stresses using the power law results where the regression analysis was in agreement with measured erosion rate data.

Power Law Regression

Following the methods of Roberts et al. (1998), the erosion rate for sediments can be approximated by the power law regression:

$$E = A\tau^n \rho^m \qquad [2]$$

E = erosion rate (cm/s)
τ = bed shear stress (Pa)
ρ = sediment bulk density (g/cm^3)
A, n and m = constants that depend on the sediment characteristics

The equation used in the present analysis is an abbreviated variation of Equation 2:

$$E = A\tau^n \qquad [3]$$

[2] Though other definitions of critical shear stress erosion rate thresholds can be argued (and considered valid), the value of 10^{-4} cm/s threshold is used here for consistency with previous Sedflume efforts and in order to keep testing times to a practical duration.

where the constant, *A*, is a function of the sediment bulk density and other difficult properties to measure such as sediment geochemistry and biological influences. The variation of erosion rate with density typically cannot be determined for field sediments due to natural variation in other sediment properties (e.g. mineralogy, particle size and electrochemical forces). Therefore, the density term from the equation above, for a particular interval of approximately constant density, is incorporated into the constant *A*.

For each depth interval, the measured erosion rates (*E*) and applied shear stresses (τ) were used to determine the *A* and *n* constants that provide a best fit power law curve to the data for that interval. Good regression fits of these parameters, where they existed, were then used to estimate the critical shear stress for the respective intervals. A coefficient of determination, r^2, of 0.80 was used as a criteria threshold for acceptance[3].

1.3.4 Measurement of Sediment Bulk Properties

In addition to measuring erosion rates during the analysis, sediment sub-samples were periodically collected at depth to determine the water content (for wet bulk density), particle size distribution, and loss on ignition of the sediments in each core. Sub-samples were collected from the undisturbed core surface (prior to analysis) as well as the sediment surface at the beginning of each subsequent depth interval.

Wet bulk density was determined by water content analysis using methods outlined in Hakanson and Jansson (2002). This was accomplished, first, by measuring the wet and dry weight of the collected sample to determine the water content (*W)* as described in the ASTM standard 2216-05:

$$W = \frac{M_w - M_d}{M_w} \qquad [4]$$

W = water content
M_w = wet weight of sample
M_d = dry weight of sample

Once the water content was calculated, the wet bulk density, ρ_b, was determined from Equation 5:

$$\rho_b = \frac{\rho_w \rho_s}{\rho_w + (\rho_s - \rho_w)W} \qquad [5]$$

ρ_w = density of water (assumed 1 g/cm^3)

[3]The coefficient of determination, r^2, is a function of the *Pearson's r,* which is a measure of the linear dependence (correlation) between two variables. *Pearson's r* can be positive or negative, and is a value between -1 and +1. The more common usage of the correlation coefficient is to square the *Pearson's r*, r^2, and report that value, the coefficient of determination.

ρ_s = density of sediment particle (assumed 2.65 g/cm^3)

Particle size distributions were determined using laser diffraction analysis in the SEI laboratory in Santa Cruz, CA. Sediment samples were screened with a 2000 µm sieve to remove large pieces of organic material, then they were dispersed in water and inserted into a Beckman Coulter LS 13 320 laser diffraction analyzer. Each sample was analyzed in three 1-minute intervals and the results of the three analyses were averaged.

Loss on ignition *(LOI)*was determined following ASTM D2974 Version C. Samples were first dried in the SEI Laboratory oven to remove moisture (following ASTM 2216-05 recommendations). Then, the samples were placed in a furnace and ignited at 440° C until the mass remained constant (typically 24 hours). The change in mass before and after indicates the fraction of combustible substances within each sub-sample, and can be used qualitatively to evaluate the organic versus inorganic fraction within each:

$$LOI = \frac{M_d - M_{d,combustion}}{M_d} \qquad [6]$$

M_d = dry weight of sample
$M_{d,\ combustion}$ = dry weight of sample after combustion

The relationships used to determine sediment bulk properties are summarized in Table 2.

Table 2. Parameters measured and computed during the Sedflume analysis.

Measurement	Definition	Units	Detection Limit	Internal Consistency
Water Content	$W = \frac{M_w - M_d}{M_w}$	unit-less	0.001 g in sample weight ranging from 1 to 50 g	0 < W < 1
Wet Bulk Density	$\rho_b = \frac{\rho_w \rho_s}{\rho_w + (\rho_s - \rho_w)W}$	g/cm^3	Same as water content	$\rho_w < \rho_b < 2.6\rho_w$
Particle Size Distribution Below 2000 µm	Distribution of particle sizes by volume percentage using laser diffraction	µm	Method Specific	1µm<Grain Size<2000µm
Loss on Ignition	$LOI = \frac{M_d - M_{d,combustion}}{M_d}$	unit-less	Same as water content	Wet and dry mass of sample

W_d = dry weight of sample
Mw = wet weight of sample
Md, combustion = dry weight of sample after combustion

ρ_w = *density of water (assumed 1 g/cm^3)*
ρ_s = *density of sediment particle (assumed 2.65 g/cm^3)*

1.3.5 Intra-core and Inter-core Comparisons

A potentially useful method of comparing sediment characteristics at a specific site is to compute *intra*-core and *inter*-core erosion rates. This method provides a means to quantify the erosion rates within each core (intra-core) as well as the general erosion rates of the cores at the site (inter-core).

Intra-core Erosion Rate Ratios

Once the power law regression *A* and *n* coefficients for each depth interval within an individual core were known, the *interval-average* erosion rate for the core was determined using Equation 3 and the logarithmic average of the range of shear stresses tested in the Sedflume analysis[4]. C*ore-average* erosion rates were then computed by:

1) Log-averaging the *A* coefficient values from each depth interval within a core to arrive at an average *A* coefficient for the entire core.
2) Arithmetically averaging the *n* coefficient values from each depth interval within a core to arrive at an average *n* coefficient for the entire core.
3) Solving for the *core-average* erosion rate following Equation 3 and using the log-average of the range of shear stresses applied to the depth interval (1.13 Pa).

An <u>intra-core</u> erosion rate *ratio* was then defined by dividing the *interval-average* erosion rate by the *core-average* erosion rate, providing a quantitative estimation of the relative erosion susceptibility of each depth interval. This method highlights the core intervals that are more or less susceptible to erosion within a particular core, and may indicate layering within a core. Intervals for which the coefficient of determination of the power law regression fit, r^2, was less than 0.80 were omitted from the comparison and the corresponding bar plots and tables.

Inter-core Erosion Rate Ratios

Two additional ratios were computed to evaluate large-scale spatial erosion susceptibility. An <u>inter-core</u> erosion rate ratio was computed by comparing the individual *core-average* erosion rate with a *site-wideaverage* erosion rate. The *site-wide average* erosion rate was computed by:

1) Log-averaging the *core-averageA* coefficient values from each core to arrive at an average *A* coefficient for the entire site.
2) Arithmetically averaging the *core-averagen* coefficient values in each core to arrive at an average *n* coefficient for the entire site.

[4]The shear stress values averaged were: 0.1, 0.2, 0.4, 0.8, 1.6, 3.2, 6.4 and 12.8 Pa. The logarithmic average of these, used to compute erosion rate ratios, was 1.13 Pa.

3) Solving for the *site-wide average* erosion rate following Equation 3 and using the log-average of the range of shear stresses (1.13 Pa).

The *inter-core* erosion rate ratio computed in this manner provided a qualitative estimate of the erosion susceptibility of each core (as a whole) relative to other cores in the site, potentially indicating spatial locations that are more or less susceptible to erosion than other locations.

Section 2
Results

This section of the report contains both qualitative and quantitative findings from the Sedflume analysis. Results will be presented on a core-by-core basis. Although median particle size data are presented here, Appendix A contains additional grain size statistics and distribution plots.

2.1 SF01

Core SF01 was collected in 5.8 m of water. Stringy organic material was present in the first 5 cm of the core. A layer of gray and tan sand 0.5 to 2.0 cm thick was present at the core's surface. The remainder of the core was a homogenous, dark gray sediment uniform in color and texture.

A photograph of core SF01 aligned vertically with the corresponding erosion rate is presented in Figure 4. An erosion rate of 10^{-5} cm/s is considered incapable of mobilizing sediment (this hold in all erosion rate plots). The sediment surface (depth= 0) is plotted at the top of all graphs with depth into the sediments increasing down the Y-axis. Shear stresses ranging between 0.1 Pa and 6.4 Pa were applied to the core. Vertical profiles of bulk density and median particle size (d_{50}) are presented in Figure 5. An average critical shear stress of 0.38 Pa was determined for the entire core.

Erosion rates decreased slightly within the core to a depth of 13.3 cm, and then increased for the final interval. Intra-core erosion rate ratios of tested intervals in SF01 are shown in Figure 6. The numbers plotted on the y-axis of all erosion rate plots represent interval (shear stress cycles) starting depths. The vertical dashed line denotes an erosion rate ratio of 1.0. Ratios to the right of the dashed line indicate intervals that were more susceptible to erosion than ratios to the left, relative to the vertically averaged erosion rate of the entire core. No Intra-Core erosion rate ratio is presented for the third interval because the interval had an r^2 value less than 0.8, as shown in Table 3. Bulk densities, medium particle sizes, organic fractions, and relevant shear stress values (τ_{power}, τ_{no}, τ_{first}, and τ_{crit},) are presented in Table 4, and power law fit parameters are presented in Table 3.

The average median particle size in SF01 was 9.41 µm. The Wentworth Size Classification (Wentworth Size Classification was used in all grain size determination) classifies this sediment as fine silt. Bulk densities ranged from 1.22 g/cm^3 at the surface to 1.31 g/cm^3 at the bottom of the core. The average bulk density was 1.28 g/cm^3. Core SF01 had an average *LOI* of 0.1. Loss on Ignition represents the amount of organic material within the core.

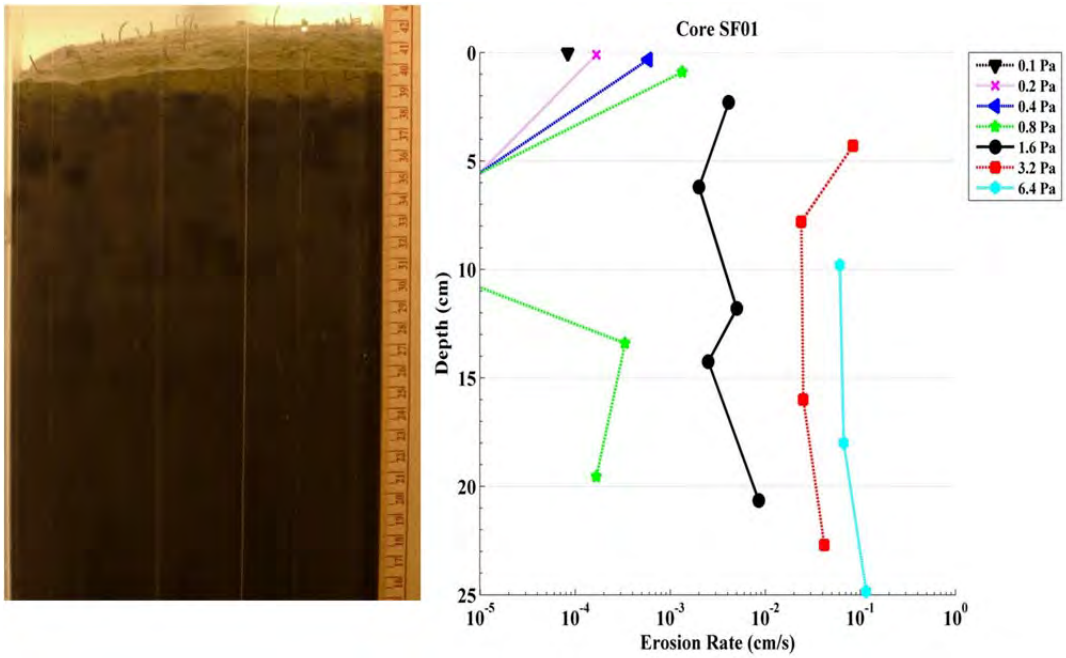

Figure 4. Photo of core SF01 aligned vertically with the corresponding erosion rates.

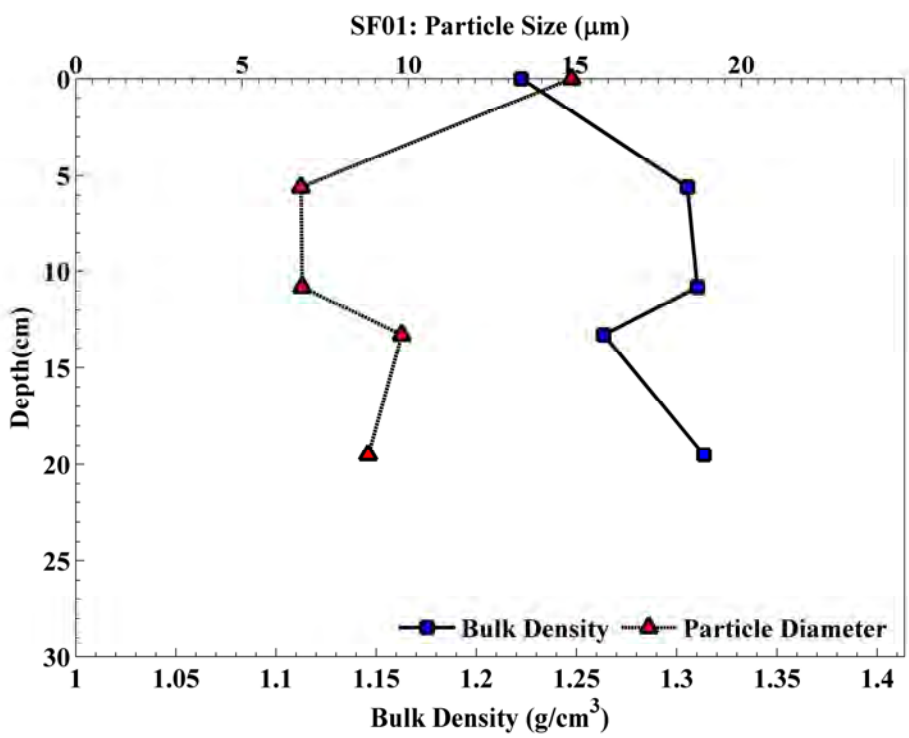

Figure 5. Bulk density and median particle size (d_{50}) with depth for core SF01.

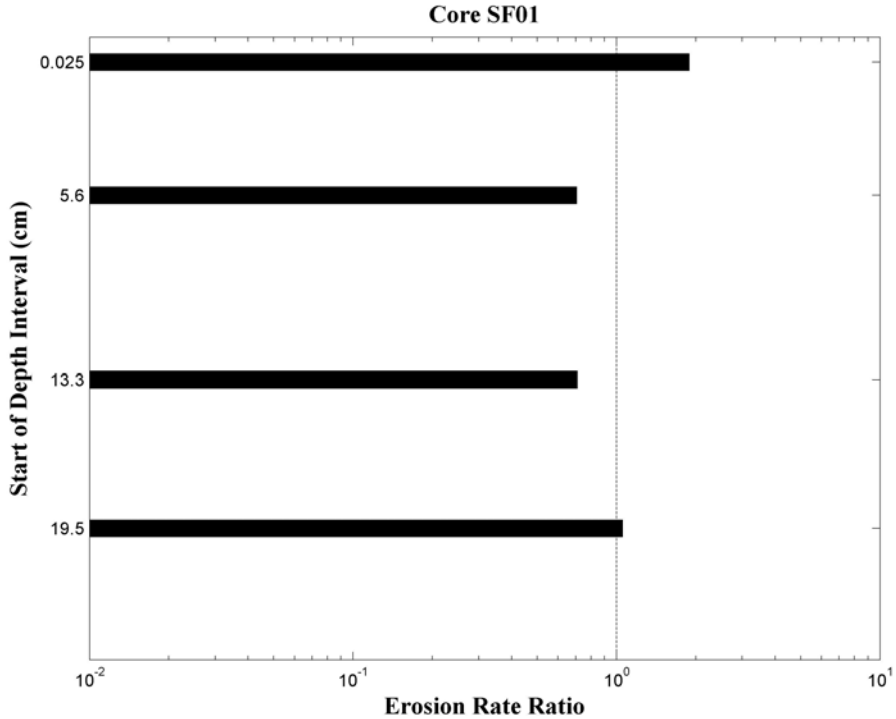

Figure 6. Intra-core erosion rate ratios for core SF01. The dashed line indicts conditions for the core's average erosion rate (i.e., erosion rate ratio equals 1).

Table 3.Power law best-fit variables for specified depth intervals in core SF01.

Interval	Depth Start (cm)	Depth Finish (cm)	A	N	r^2
1	0.00	4.30	0.00358	1.90	0.93
2	5.60	9.80	0.00081	2.50	0.94
3	10.8	11.8	NA	NA	0.50
4	13.3	18.0	0.00072	2.60	0.98
5	19.5	24.9	0.00075	3.10	0.91

Table 4. Median particle size, bulk density, loss on ignition, and critical shear stress with depth for core SF01.

Depth (cm)	d_{50} (µm)	ρ_b(g/cm^3)	*LOI*	Power Law τ_{cr} (Pa)	τ_{no} (Pa)	τ_{first} (Pa)	τ_{crit} (Pa)
0.00	14.9	1.22	0.11	0.15	NA	0.10	0.10
5.60	6.77	1.31	0.09	0.43	0.80	1.60	0.80
10.8	6.80	1.31	0.10	NA	0.80	1.60	0.80
13.3	9.80	1.26	0.09	0.47	0.40	0.80	0.47
19.5	8.79	1.31	0.10	0.52	0.40	0.80	0.52
Mean	**9.41**	**1.28**	**0.1**	**0.39**	**0.60**	**0.98**	**0.38**

2.2 SF02

Core SF02 was collected in 5.8 m of water. The surface of the core was covered by approximately 10% organic and detritus material. A 1 cm very fine gray, brown sediment layer extended from the surface. A 0.5 cm layer of fine gray material was found below the surface layer, extending to depth of roughly 1.0 to 1.5 cm. The remaining 30 cm was comprised of a homogenous black or dark grey material. Worm tubes were present over roughly the first 10 cm of the core.

A photograph of core SF02 aligned vertically with the corresponding erosion rate data is presented in Figure 7. A total of five intervals were tested, where shear stresses from 0.1 Pa to 3.2 Pa were applied. Erosion rates decreased over the top to the middle of the core, and then increased from the middle to the bottom of the core. Values of Intra-core erosion rates were not plotted in Figure 9 for intervals 2 and 4 because they both had an r^2 value less than 0.8. An average critical shear stress of 0.38 Pa was determined for Core SF02.

Median grain sizes were in the medium silt range, averaging to 21 µm. Bulk densities ranged from 1.22 g/cm^3 near the surface to 1.32 g/cm^3 towards the bottom of the core (Figure 8and Table 6). The average bulk density was 1.27 g/cm^3, and the average *LOI* was 0.13.

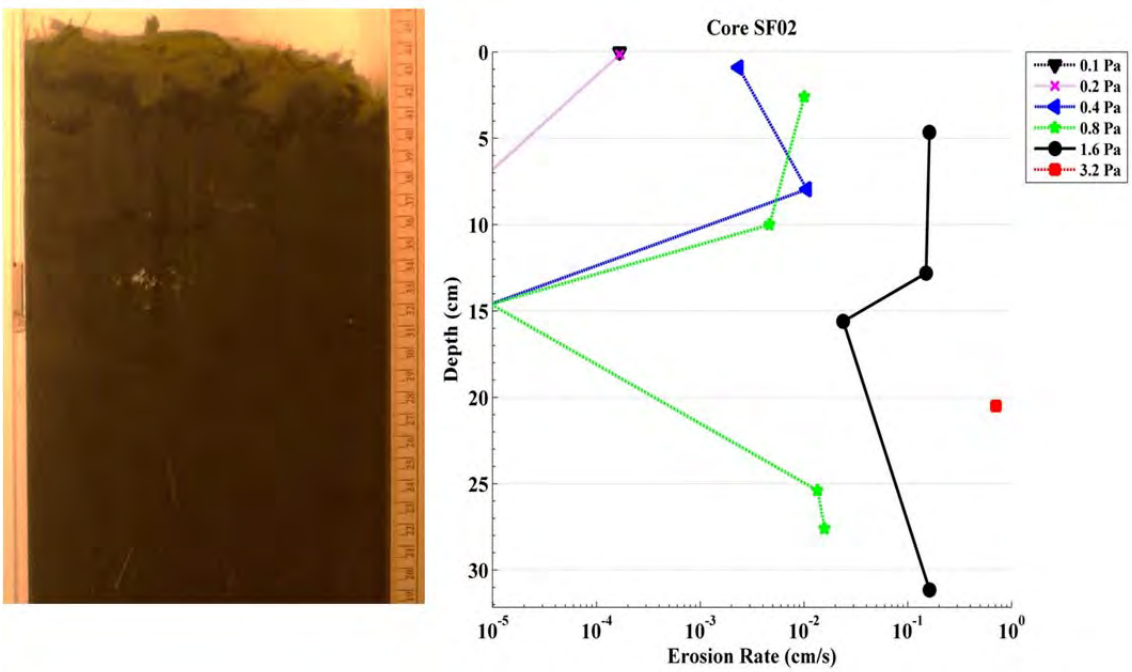

Figure 7.Photo of core SF02 aligned vertically with the corresponding erosion rates.

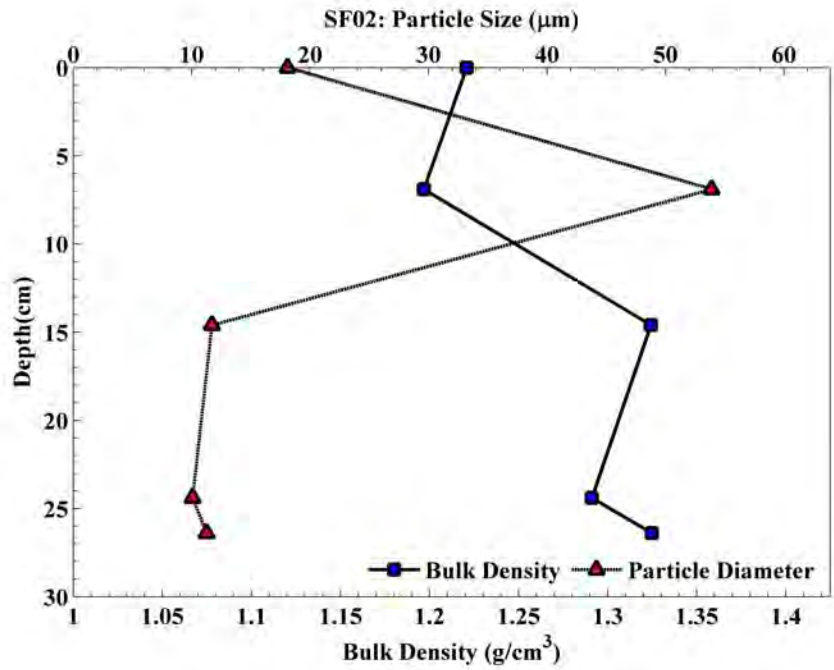

Figure 8. **Bulk density and median particle size (d_{50}) with depth for core SF02.**

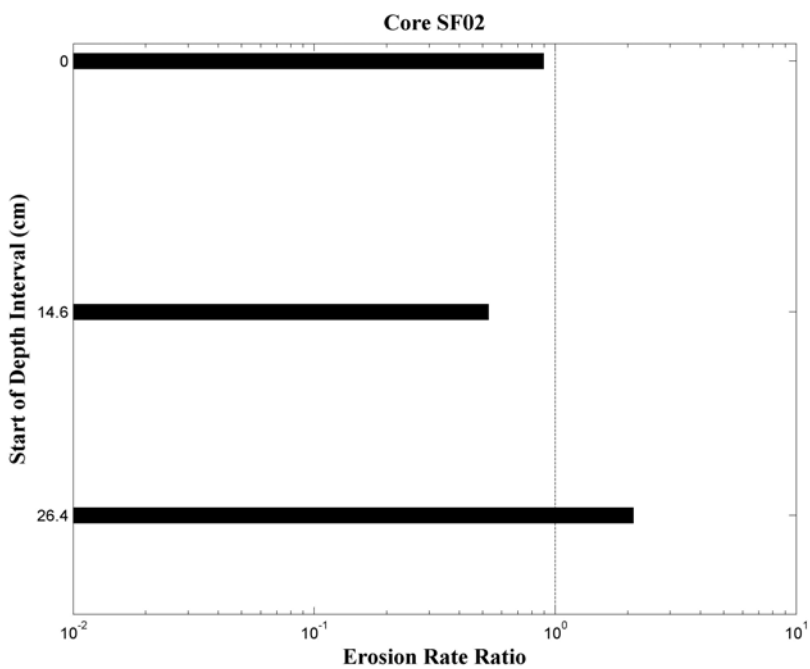

Figure 9. **Intra-core erosion rate ratios for core SF02. The dashed line indicates conditions for the core's average erosion rate (i.e., erosion rate ratio equals 1).**

Table 5. Power law best-fit variables for specified depth intervals in core SF02.

Interval	Depth Start (cm)	Depth Finish (cm)	A	n	r^2
1	0.00	4.60	0.02688	2.60	0.94
2	6.90	12.8	NA	NA	0.53
3	14.6	20.5	0.00238	4.90	1.00
4	24.4	25.4	NA	NA	0.50
5	26.4	31.2	0.03342	3.40	1.00

Table 6. Median particle size, bulk density, loss on ignition, and critical shear stress with depth for core SF02.

Depth (cm)	d_{50} (µm)	ρ_b(g/cm^3)	*LOI*	Power Law τ_{cr} (Pa)	τ_{no} (Pa)	τ_{first} (Pa)	τ_{crit} (Pa)
0.00	18.1	1.22	0.15	0.11	NA	0.01	0.10
6.90	53.9	1.20	0.18	NA	0.20	0.40	0.20
14.6	11.7	1.32	0.12	0.52	0.80	1.60	0.80
24.4	10.1	1.29	0.15	NA	0.40	0.80	0.40
26.4	11.3	1.32	0.1	0.18	0.40	0.80	0.40
Mean	**21.0**	**1.27**	**0.13**	**0.27**	**0.45**	**0.74**	**0.38**

2.3 SF03

Core SF03 was collected in 7.62 m of water. The top 5 cm of the core was mottled with gray and tan colored sediment containing bioturbation tunnels. Several faunal and algal growths were found at the surface, including 10 to 15 vertical stalks that were 1 to 2 cm in height. Detritus and black clumpy sediment extended from the surface to a depth of 1 cm. At 2 cm was black and gray mottled sediment with evidence of bioturbation, including detritus and small aggregations undulating from the horizon to the base. The remainder of the core was dark gray with several black striations.

A photograph of core SF03 aligned vertically with the corresponding erosion rate data is presented in Figure 10. Shear stresses ranging between 0.1 Pa and 10.0 Pa were applied to the core. Erosion rates fluctuated with depth; no apparent depth trends can be deduced from the erosion rate data (Figure 12). Sediment frequently mobilized in chunks while processing core SF03. The core's average critical shear stress was 0.57 Pa.

The median grain size generally consisted of fine silt, averaging to 6.56 µm. Bulk densities increased from 1.29 g/cm^3 at the surface to 1.53 g/cm^3 at a depth of 14.0 cm, and then decreased to 1.34 g/cm^3 at a depth of 28.5 cm (Figure 11 and Table 8). The average bulk density was 1.39 g/cm^3. The average Loss on Ignition (*LOI)* was 0.1.

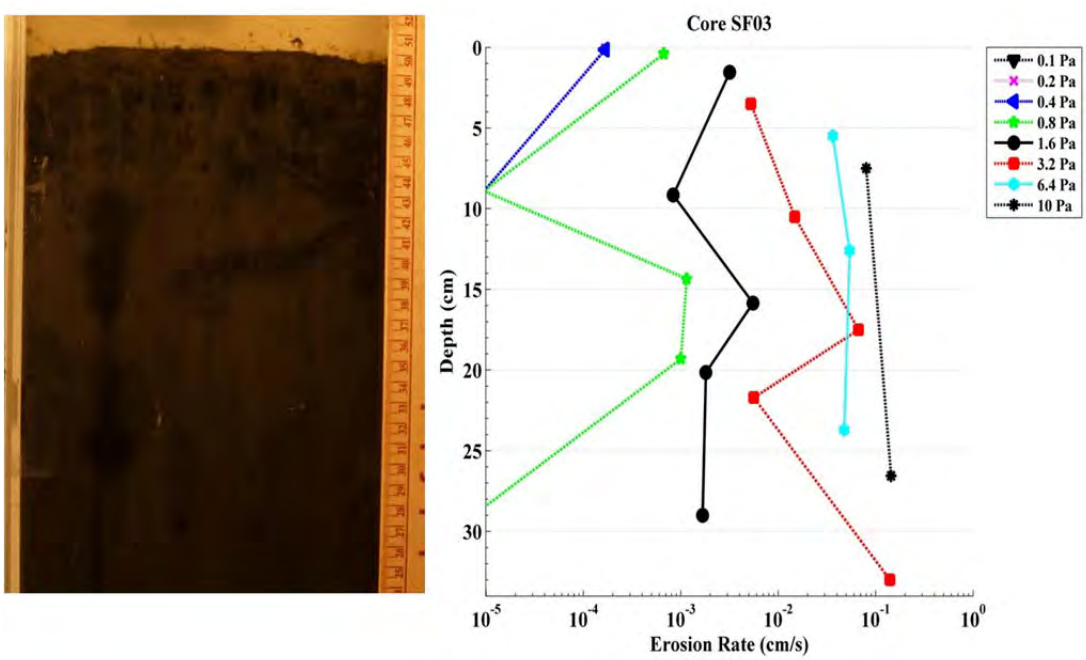

Figure 10. Photo of core SF03 aligned vertically with the corresponding erosion rates.

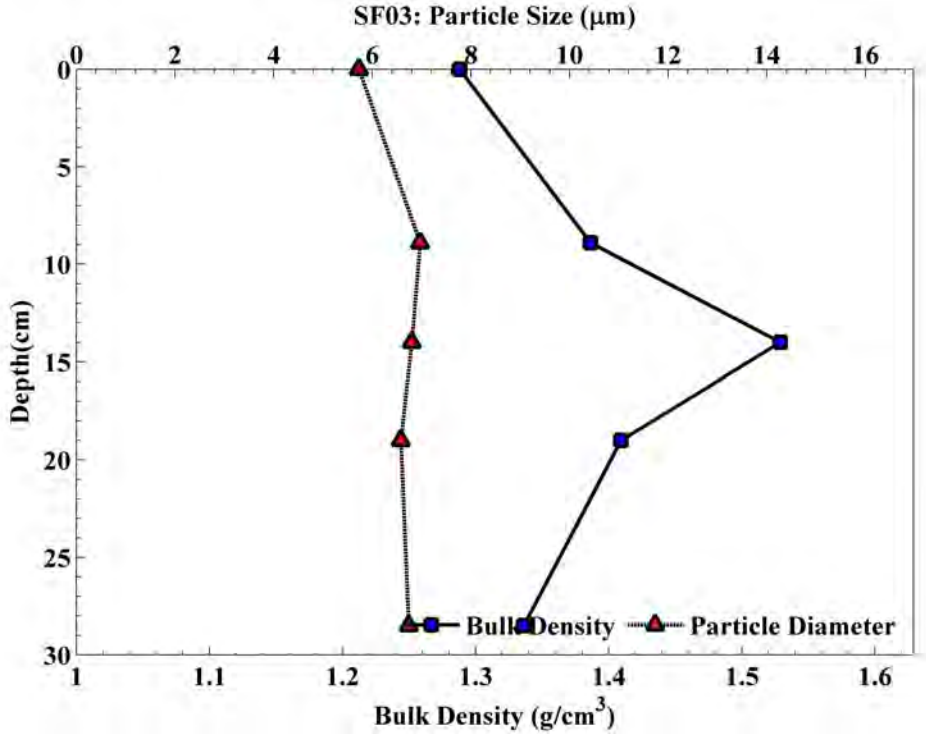

Figure 11. **Bulk density and median particle size (d_{50}) with depth for core SF03.**

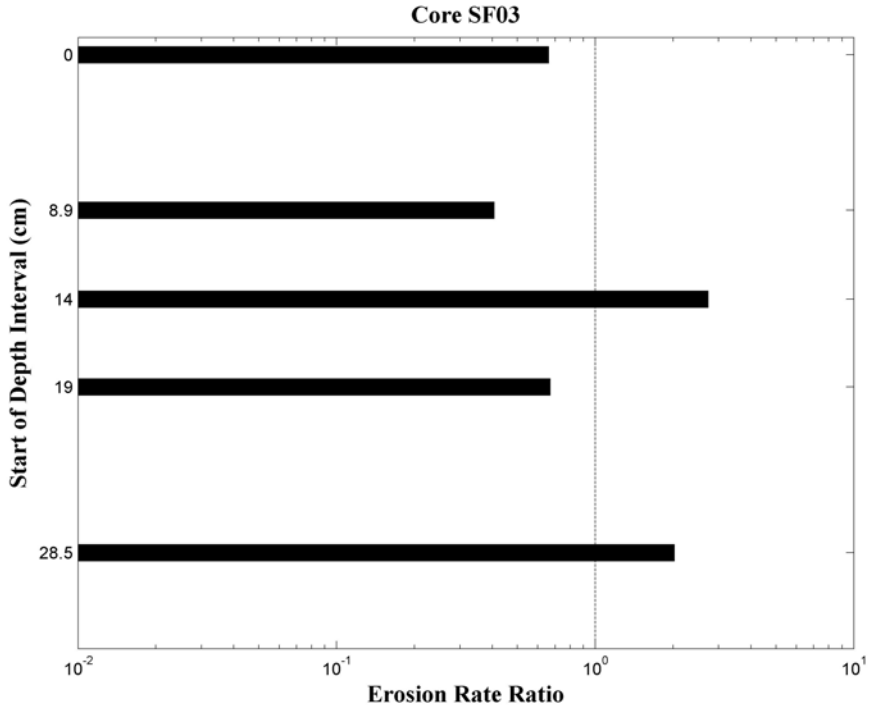

Figure 12. **Intra-core erosion rate ratios for core SF03. The dashed line indicates conditions for the core's average erosion rate (i.e., erosion rate ratio equals 1).**

Table 7. Power law best-fit variables for specified depth intervals in core SF03.

Interval	Depth Start (cm)	Depth Finish (cm)	A	n	r^2
1	0.00	7.50	0.00127	1.7	0.97
2	8.90	12.6	0.00026	3.0	0.95
3	14.0	17.5	0.00189	2.9	0.98
4	19.0	26.6	0.00096	2.0	0.95
5	28.5	33.0	0.00008	6.4	1.00

Table 8. Median particle size, bulk density, loss on ignition, and critical shear stress with depth for core SF03.

Depth (cm)	d_{50} (µm)	ρ_b(g/cm^3)	*LOI*	Power Law τ_{cr} (Pa)	τ_{no} (Pa)	τ_{first} (Pa)	τ_{crit} (Pa)
0.00	5.73	1.29	0.24	0.22	0.10	0.20	0.20
8.9	6.97	1.39	0.07	0.72	0.80	1.60	0.80
14.0	6.80	1.53	0.05	0.37	0.40	0.80	0.40
19.0	6.58	1.41	0.07	0.33	0.40	0.80	0.40
28.5	6.74	1.34	0.08	1.03	0.80	1.60	1.03
Mean	**6.56**	**1.39**	**0.1**	**0.53**	**0.50**	**1.00**	**0.57**

2.4 SF04

Core SF04 was collected in 6.1 m of water. The top 0.5 to 5 cm of the core was gray and tan in color. The top 1 cm of the core contained a light brown colored layer of very fine and somewhat clay-like material with vertically oriented detrital vegetation. The next 5 to 8 cm of the core was mottled gray and black sediment with a void at a depth of roughly 8 cm. Below this layer was a 5 to 10 cm horizon of thoroughly mixed gray and black sediment grains. The remanding 20 to 30 cm of the core was dark gray and uniform in color. At depths between 10 to 25 cm, pebbles and mussels were found mixed with core sediment. A six interval was run in Core SF04 to determine where the shells stopped; no shells were present below roughly 28 cm.

A photograph of core SF04 aligned vertically with the corresponding erosion rate data is presented in Figure 13. Shear stresses ranging between 0.1 Pa and 6.4 Pa were applied to the core. Erosion was dominated by the mobilization of large clumps of sediment. When shells and pebbles were present, they held sediment in place until the applied shear stress exceeded roughly 1 Pa. At this point, the pebbles and shells would mobilize and take sediment along with them. The core's average critical shear stress was 0.82 Pa. The power law regression analysis lead to r^2 values less than 0.8 for the last intervals, therefore no erosion rate ratios are presented for them (Figure 15).

Median particle sizes consisted of fine to medium silt, with a core average of 8.44 µm. Bulk densities increased from 1.24 g/cm^3 at the surface to 1.55 g/cm^3 at a depth of 10.8 cm, and then decreased to 1.43 g/cm^3 at a depth of 28.0 cm (Figure 14and Table 10). The average bulk density was 1.40 g/cm^3, and the core average *LOI* was 0.07.

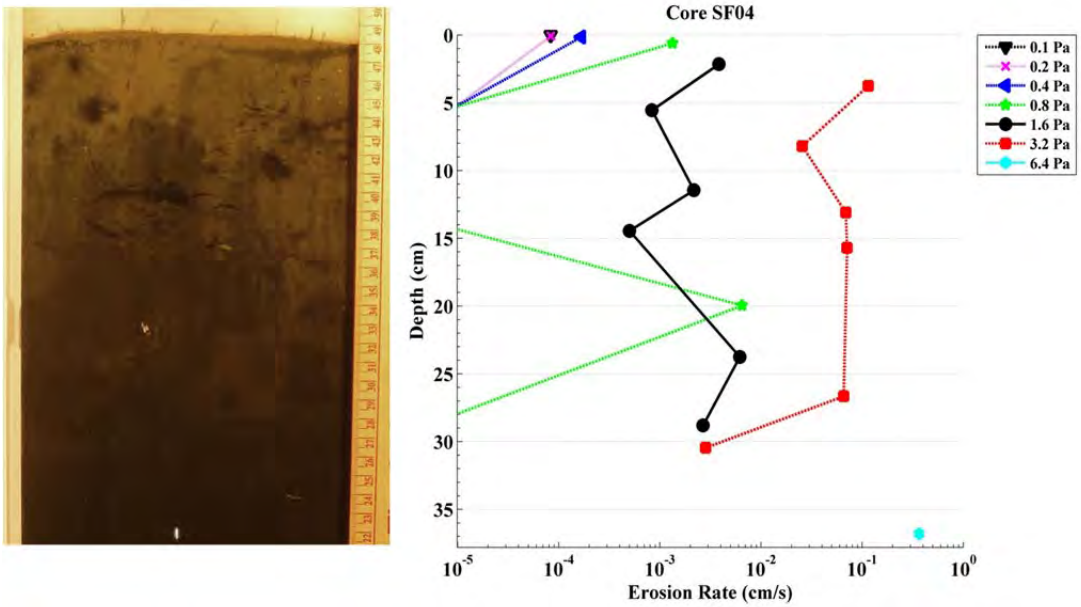

Figure 13. Photo of core SF04 aligned vertically with the corresponding erosion rates.

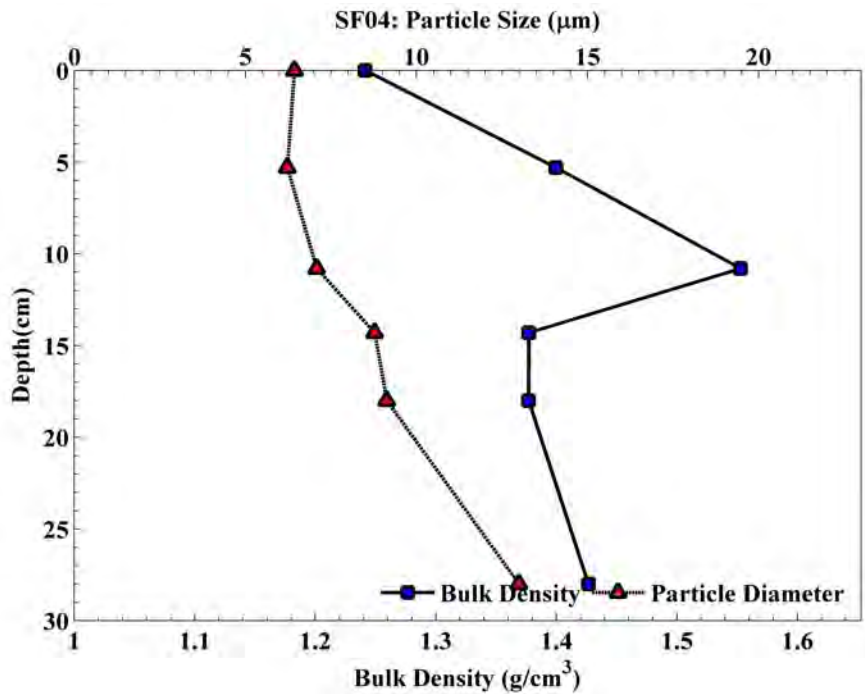

Figure 14. **Bulk density and median particle size (d_{50}) with depth for core SF04.**

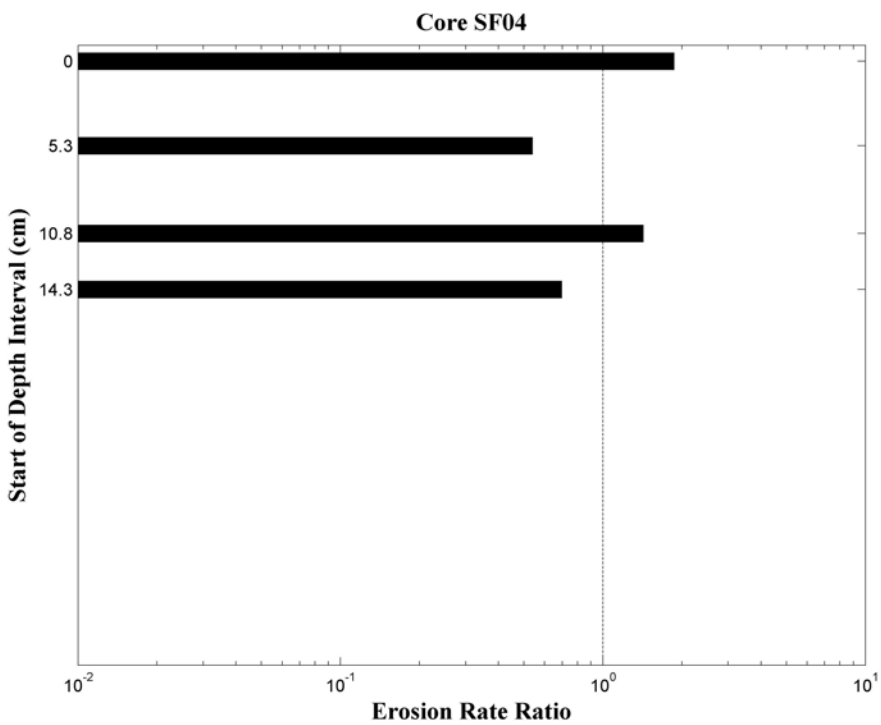

Figure 15. **Intra-core erosion rate ratios for core SF04. The dashed line indicates conditions for the core's average erosion rate (i.e., erosion rate ratio equals 1).**

Table 9. Power law best-fit variables for specified depth intervals in core SF04.

Interval	Depth Start (cm)	Depth Finish (cm)	A	n	r^2
1	0.00	3.80	0.00301	2.00	0.88
2	5.30	8.20	0.00008	4.90	1.00
3	10.8	13.1	0.00021	5.00	1.00
4	14.3	15.7	0.00002	7.10	1.00
5	18.0	26.7	NA	NA	0.73
6	28.0	36.8	NA	NA	0.76

Table 10. Median particle size, bulk density, loss on ignition, and critical shear stress with depth for core SF04.

Depth (cm)	d_{50} (µm)	ρ_b(g/cm^3)	*LOI*	Power Law τ_{cr} (Pa)	τ_{no} (Pa)	τ_{first} (Pa)	τ_{crit} (Pa)
0.00	6.43	1.24	0.08	0.19	NA	0.10	0.10
5.30	6.23	1.40	0.06	1.04	0.80	1.60	1.04
10.8	7.09	1.55	0.04	0.86	0.80	1.60	0.86
14.3	8.78	1.38	0.06	1.28	0.80	1.60	1.28
18.0	9.13	1.38	0.1	NA	0.40	0.80	0.40
28.0	13.0	1.43	0.6	NA	0.80	1.60	0.80
Mean	**8.44**	**1.40**	**0.07**	**0.84**	**0.72**	**1.22**	**0.74**

2.5 SF05

Core SF05 was collected in 7.32 m of water. The surface of the core was gray, tan, and buff mottled with black patches. Worm tubes were observed protruding from the core's surface, and a barnacle was encountered at a depth of 2 cm. The next 1 to 4 cm of the core was comprised of gray stiff sediment undulated unevenly with black spots. The remainder of the core was streaky black and gray with large 1 to 3 cm black spots. A 4x8 cm piece of steel was removed from interval two, and a large rock (4x6x8 cm) was also removed. Intervals 3 and 4 (depths between 15 and 25 cm) were found to contain rocks, gravel, and concrete.

A photograph of core SF05 is presented in Figure 16 along with its corresponding erosion rate data. Shear stresses ranging from 0.1 Pa to 6.4 Pa were applied to the core. Erosion rates generally increased with depth into the core (Figure 18 and Table 11). When applying shear stress above 0.8 Pa, sediment mobilized in large chunks. The core's average critical shear stress was 0.37 Pa.

Median particle sizes ranged from fine to nearly medium silt, with a core average of 9.58 µm. Bulk densities increased from 1.30 g/cm^3 at the surface to 1.88 g/cm^3 at a depth of 27.2 cm (Figure 17 and Table 12). The average bulk density was 1.63 g/cm^3. Core SF05 also had a core average *LOI* of 0.05.

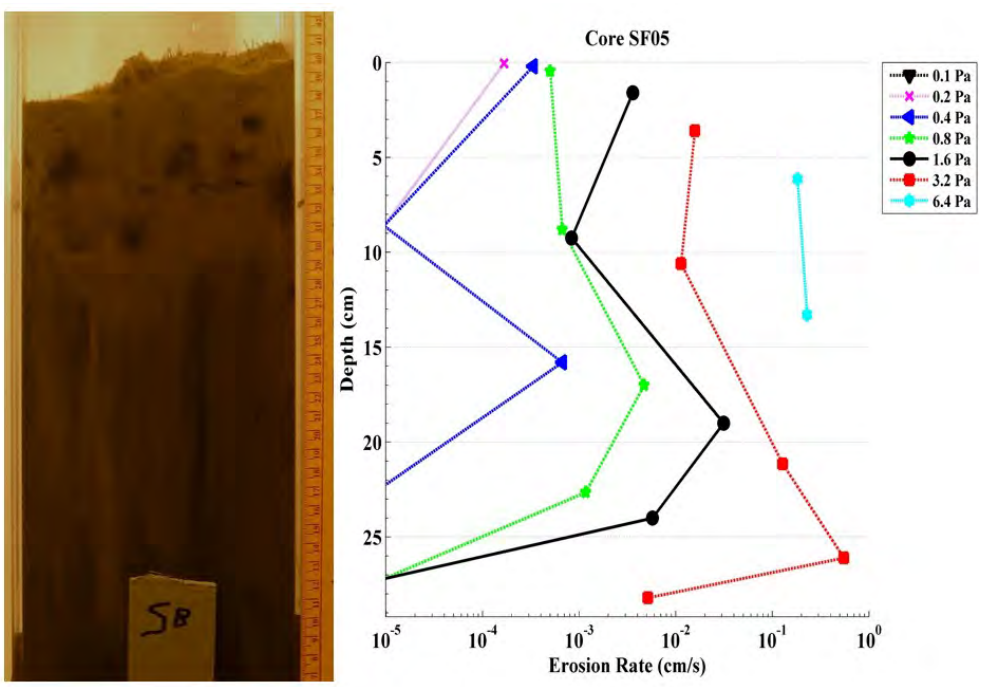

Figure 16 Photo of core SF05 aligned vertically with the corresponding erosion rates.

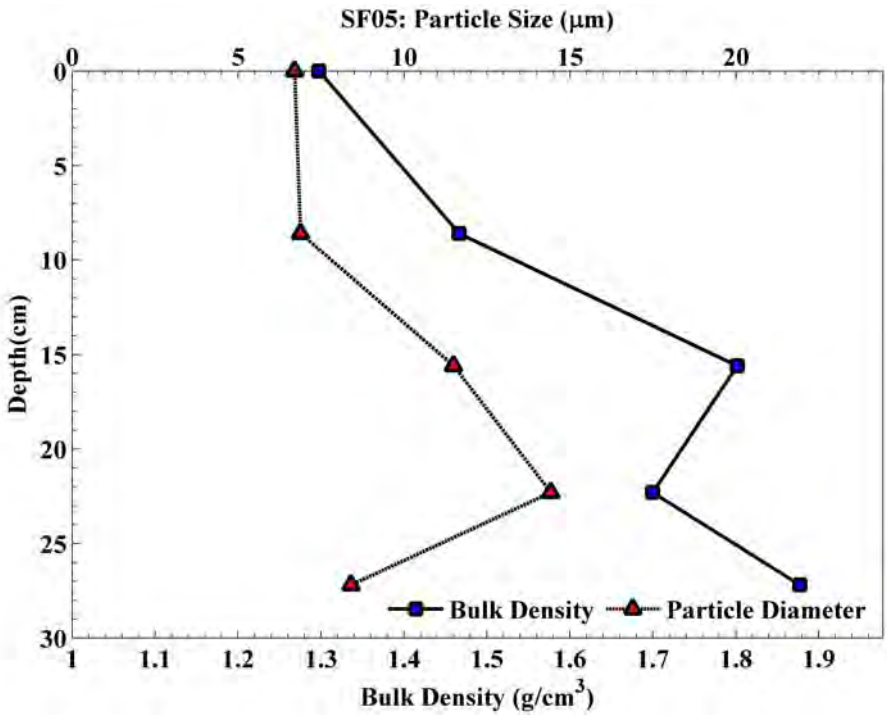

Figure 17. **Bulk density and median particle size (d_{50}) with depth for core SF05.**

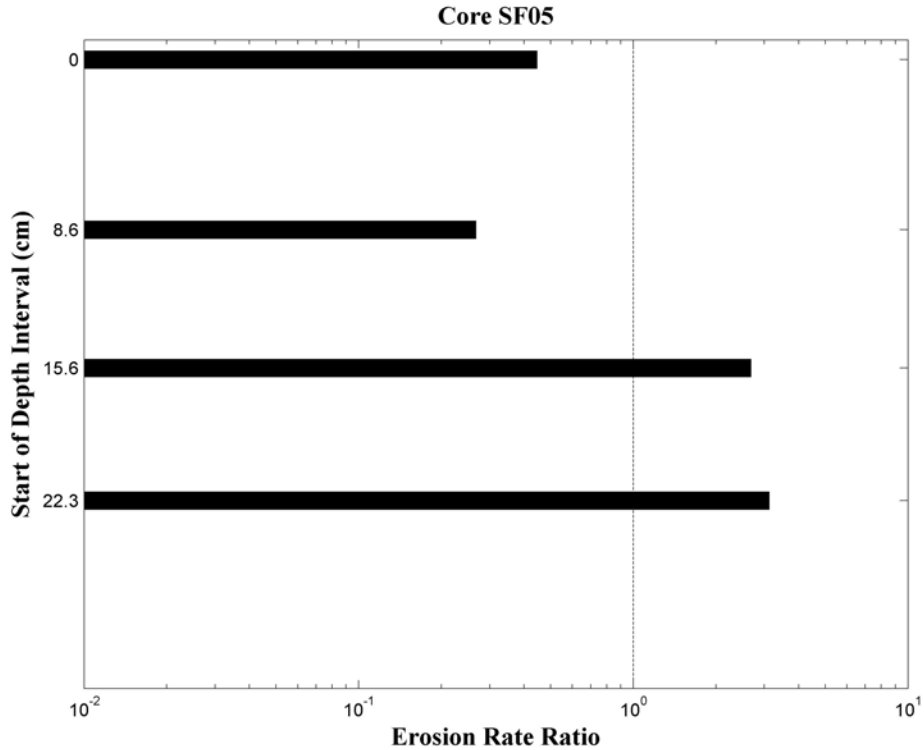

Figure 18. **Intra-core erosion rate ratios for core SF05. The dashed line indicates conditions for the core's average erosion rate (i.e., erosion rate ratio equals 1).**

Table 11. Power law best-fit variables for specified depth intervals in core SF05.

Interval	Depth Start (cm)	Depth Finish (cm)	A	n	r^2
1	0.00	6.10	0.00201	2.0	0.94
2	8.60	13.3	0.00058	2.9	0.90
3	15.6	21.2	0.00772	2.5	0.99
4	22.3	26.1	0.00191	4.4	0.93
5	27.2	30.8	NA	NA	0.00

Table 12. Median particle size, bulk density, loss on ignition, and critical shear stress with depth for core SF05.

Depth (cm)	d_{50} (µm)	ρ_b(g/cm^3)	*LOI*	Power Law τ_{cr} (Pa)	τ_{no} (Pa)	τ_{first} (Pa)	τ_{crit} (Pa)
0.00	6.70	1.30	0.07	0.22	0.10	0.20	0.20
8.60	6.88	1.47	0.05	0.55	0.40	0.80	0.55
15.6	11.5	1.80	0.02	0.18	0.20	0.40	0.20
22.3	14.4	1.70	0.04	0.51	0.40	0.80	0.51
27.2	8.40	1.88	0.04	NA	1.60	3.20	NA
Mean	**9.58**	**1.63**	**.05**	**0.37**	**0.54**	**1.08**	**0.37**

2.6 SF06

Core SF06 was collected in 7.32 m of water. The cores surface was convexed, with the sides roughly 1 cm below the center section. The core had a 3 cm surface layer that consisted of light gray, tan, and buff fine particles and sparse vertical sticks 0.5 cm to 1.5 cm in diameter. The remainder of the core was black and dark gray mottled sediment that appeared homogeneous and uniform. When begging to process the 5th interval, core sediment sucked into the flume. The analysis was stopped.

A photograph of core SF06 is presented in Figure 19 along with its corresponding erosion rate data. Shear stresses ranging from 0.1 Pa to 6.4 Pa were applied to the core. Though erosion rates fluctuated with depth, the sediment generally stiffened down core. This is apparent by the increase in critical shear stress with depth (Table 14). The core's average critical shear stress was 0.51 Pa. The power law regression analysis lead toan r^2 value less than 0.8 for the 4th and 5th interval. As a result, the erosion rate ratios for the last two intervals are not plotted in Figure 21.

Median particle sizes were generally fine silt, with a core average of 6.138 µm. Bulk densities increased from 1.19 g/cm^3 at the surface to 1.32 g/cm^3 at a depth of 21.2 cm (Figure 20 and Table 14). The average bulk density was 1.27 g/cm^3, and the core average *LOI* was 0.09.

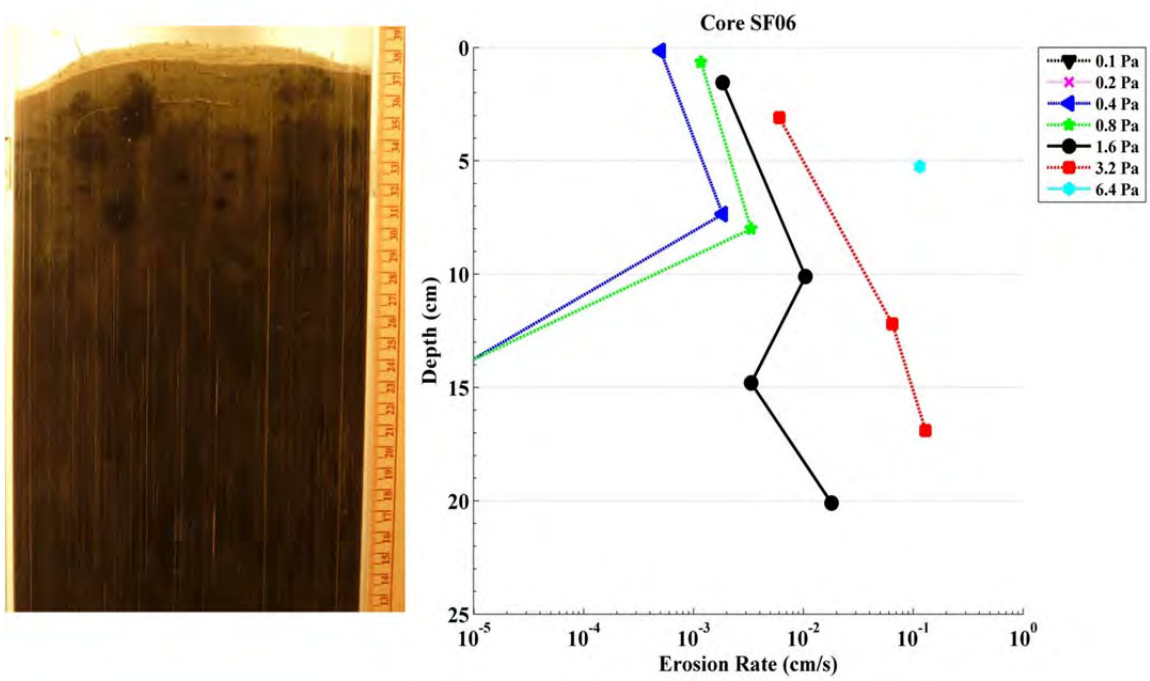

Figure 19. Photo of core SF06 aligned vertically with the corresponding erosion rates.

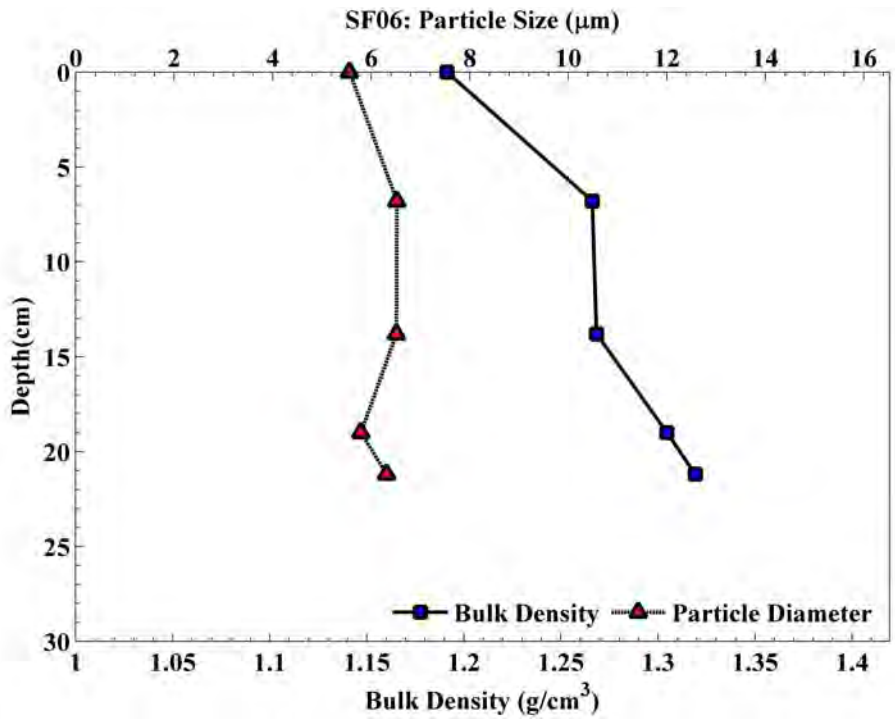

Figure 20. **Bulk density and median particle size (d_{50}) with depth for core SF06.**

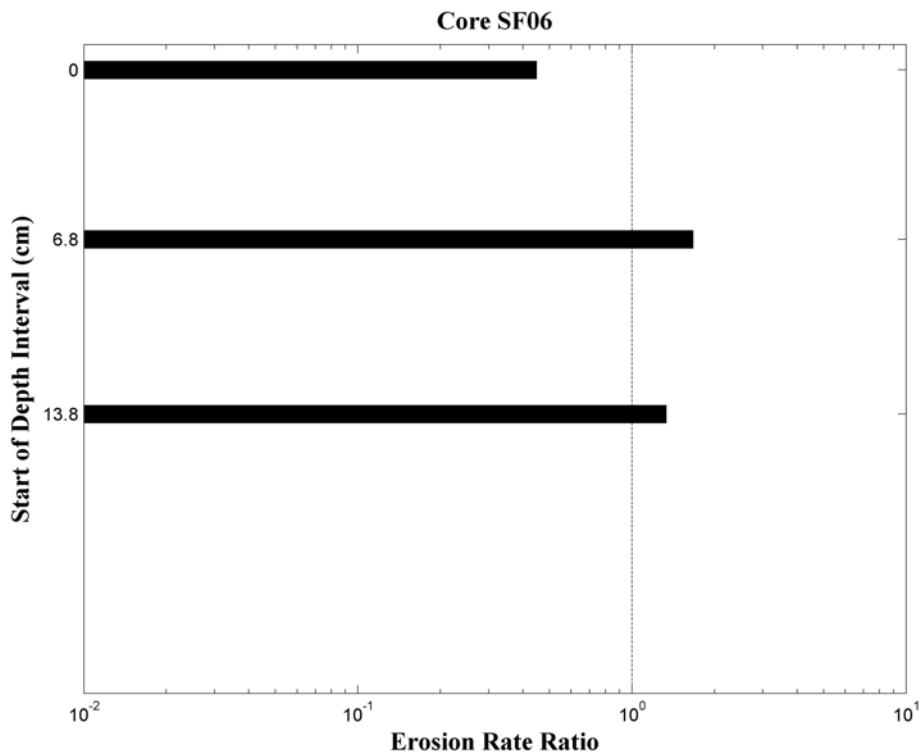

Figure 21. **Intra-core erosion rate ratios for core SF06. The dashed line indicates conditions for the core's average erosion rate (i.e., erosion rate ratio equals 1).**

Table 13. Power law best-fit variables for specified depth intervals in core SF06.

Interval	Depth Start (cm)	Depth Finish (cm)	A	n	r^2
1	0.00	5.30	0.00161	1.80	0.88
2	6.80	12.2	0.00649	1.70	0.95
3	13.8	16.9	0.00028	5.30	1.00
4	19.0	20.1	NA	NA	0.50

Table 14. Median particle size, bulk density, loss on ignition, and critical shear stress with depth for coreSF06.

Depth (cm)	d_{50} (µm)	ρ_b(g/cm^3)	*LOI*	Power Law τ_{cr} (Pa)	τ_{no} (Pa)	τ_{first} (Pa)	τ_{crit} (Pa)
0.00	5.56	1.19	NA	0.22	0.20	0.4	0.22
6.80	6.52	1.27	0.08	0.09	0.20	0.4	0.20
13.8	6.51	1.27	0.1	0.82	0.80	1.6	0.82
19.0	5.79	1.30	0.1	NA	0.80	1.6	0.80
21.2	6.31	1.32	0.1	NA	NA	NA	NA
Mean	**6.138**	**1.27**	**0.09**	**0.38**	**0.50**	**1.0**	**0.51**

2.7 SF07

Core SF07 was collected in 7.3 m of water. The top 2 to 4 cm of the core was a mix of black and gray sediment interspersed with organic detritus. Beneath the surface layer was a mottled layer of undulating black sediment that extended to a depth of 5 cm. The reminder of the core was gray to medium gray with black spots decreasing in frequency to the base of the core. Possible worm tubes were observed over the first 10 cm of the core (holes in sediment roughly 2 mm in diameter).

A photograph of core SF07 is presented in Figure 22 along with its corresponding erosion rate data. Shear stresses ranging from 0.1 Pa to 6.4 Pa were applied to the core. Generally, erosion rates remained constant until a depth of 10 cm, and then fluctuated with depth. Erosion was dominated by the mobilization of large chunks of sediment when applying shear stresses greater than 1.6 Pa. At the end of the fourth interval, air began to percolate though the bottom of the core. A Fifth interval was attempted, but the core sucked into the flume.The core's average critical shear stress was 0.23 Pa.

Median particle sizes ranged from fine to almost medium silt, with a core average of 6.83 µm. Bulk densities generally increased with depth, averaging to 1.29 g/cm^3 (Figure 23 and Table 16). Core SF07 had a core average *LOI* of 0.09.

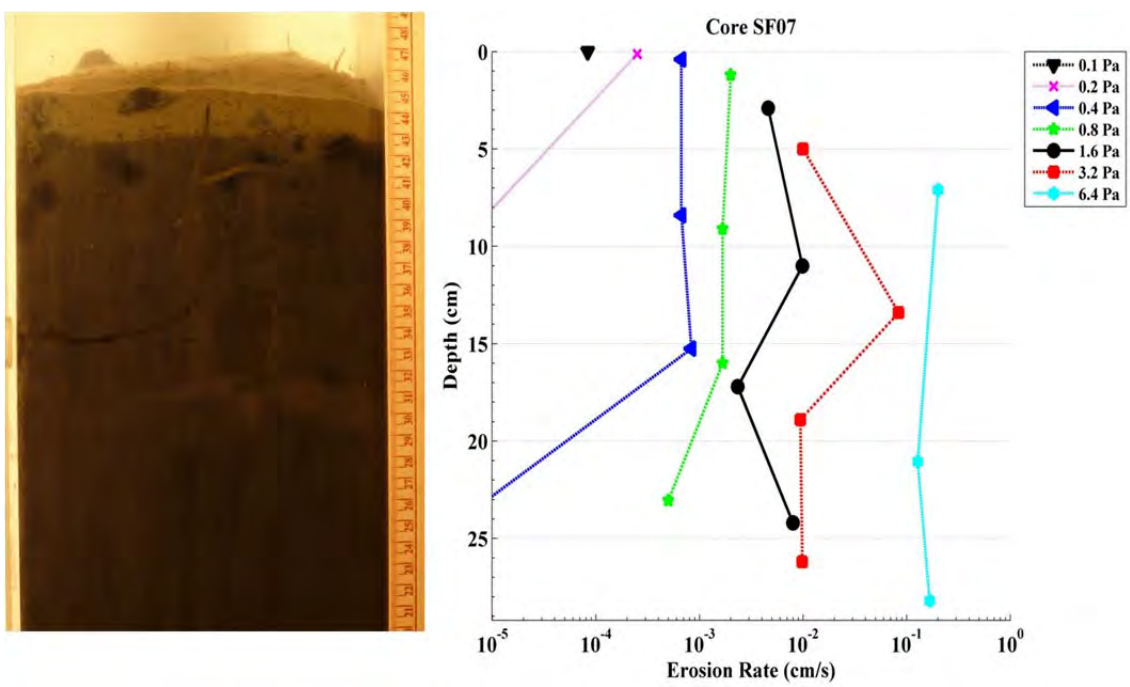

Figure 22. Photo of core SF07 aligned vertically with the corresponding erosion rates.

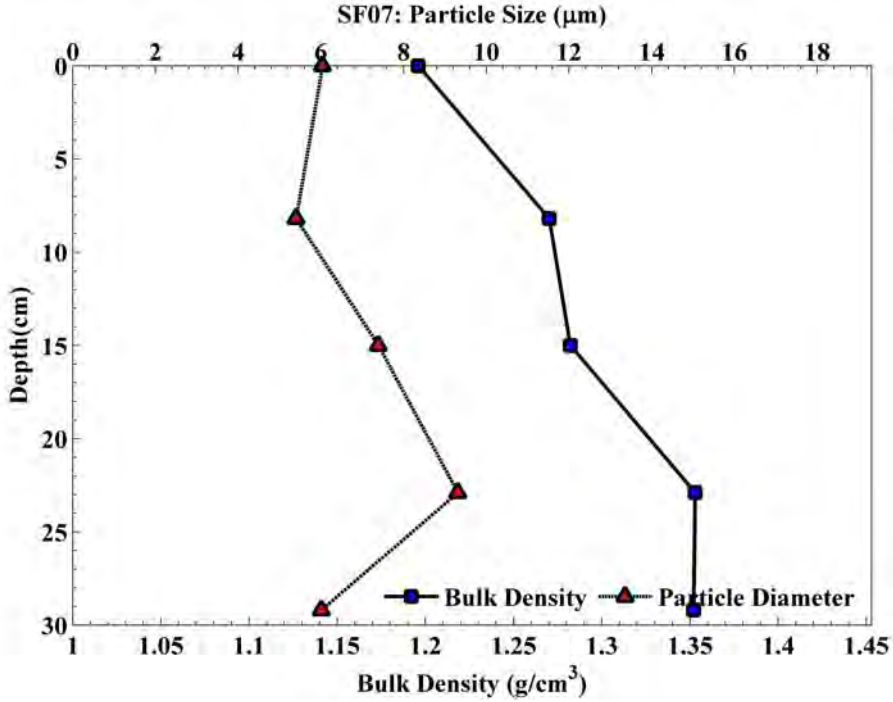

Figure 23. **Bulk density and median particle size (d_{50}) with depth for core SF07.**

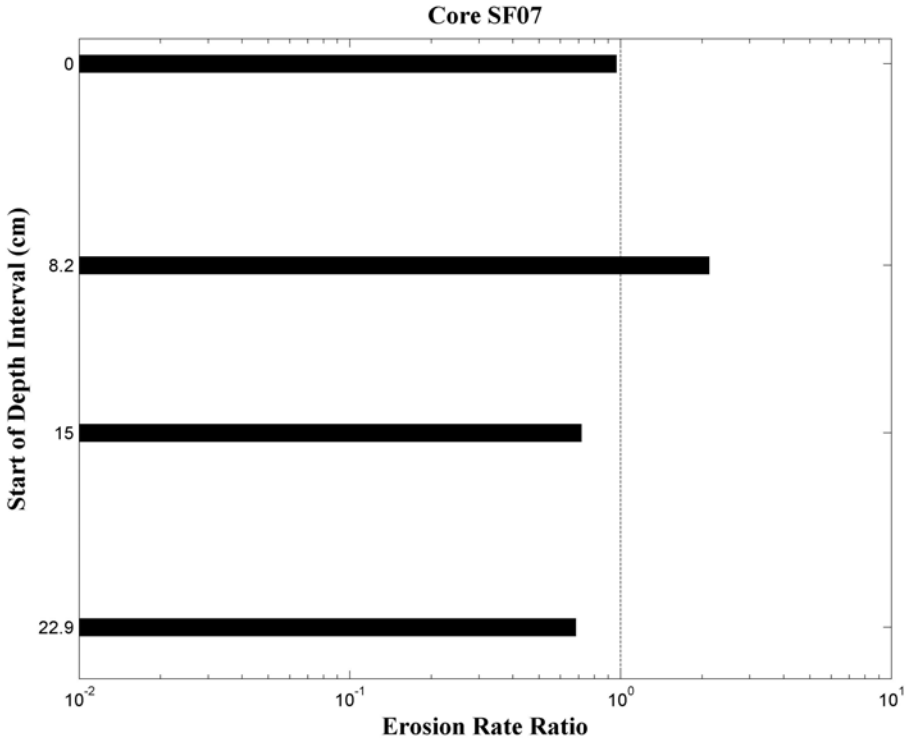

Figure 24. **Intra-core erosion rate ratios for core SF07. The dashed line indicates conditions for the core's average erosion rate (i.e., erosion rate ratio equals 1).**

Table 15. Power law best-fit variables for specified depth intervals in coreSF07.

Interval	Depth Start (cm)	Depth Finish (cm)	A	n	r^2
1	0.00	7.10	0.00321	1.70	0.95
2	8.20	13.4	0.00411	2.30	0.97
3	15.0	21.1	0.00235	1.70	0.88
4	22.9	28.2	0.00112	2.50	0.92

Table 16. Median particle size, bulk density, loss on ignition, and critical shear stress with depth for core SF07.

Depth (cm)	d_{50} (µm)	ρ_b(g/cm^3)	*LOI*	Power Law τ_{cr} (Pa)	τ_{no} (Pa)	τ_{first} (Pa)	τ_{crit} (Pa)
0.00	6.04	1.20	0.1	0.13	NA	0.10	0.10
8.20	5.40	1.27	0.09	0.21	0.20	0.40	0.21
15.0	7.39	1.28	0.08	0.16	0.20	0.40	0.20
22.9	9.31	1.35	0.08	0.39	0.40	0.80	0.40
29.2	6.01	1.35	0.08	NA	NA	NA	NA
Mean	**6.83**	**1.29**	**0.09**	**0.22**	**0.27**	**0.43**	**0.23**

2.8 SF08

Core SF08 was collected in 6.4 m of water. The core had roughly a 5 cm surface layer of light gray and tan sediment, undulating with scattered organic detritus. Sticks 1 cm in length protruded vertically from the cores surface. The top layer streaked vertically into darker sediment. Below roughly 12 cm the core sediment was black and dark gray with several void spaces seen on the cores edge, which may have been gas pockets. Large chuck erosion was prominent in later runs for each interval. A large (8x2 cm) rock was found at a depth of 8 cm. The rock was removed before processing proceeded. Because of the small size of the core, only three intervals were processed in Core SF08; water started to leak from the bottom of the core at the end of interval 3.

A photograph of core SF08 is presented in Figure 25 along with its corresponding erosion rate data. Shear stresses ranging from 0.1 Pa to 10.0 Pa were applied to the core. Erosion rates generally decreased with depth into the core. The core's average critical shear stress was 0.52 Pa.

Median particle remained in the fine silt range, with a core average of 6.92 µm. Bulk densities increased with depth from 1.28 g/cm^3 at the surface to 1.55 g/cm^3 at a depth of 12.9 cm (Figure 26 and Table 18). The average bulk density was 1.44 g/cm^3. Core SF08 had a core average *LOI* of 0.04.

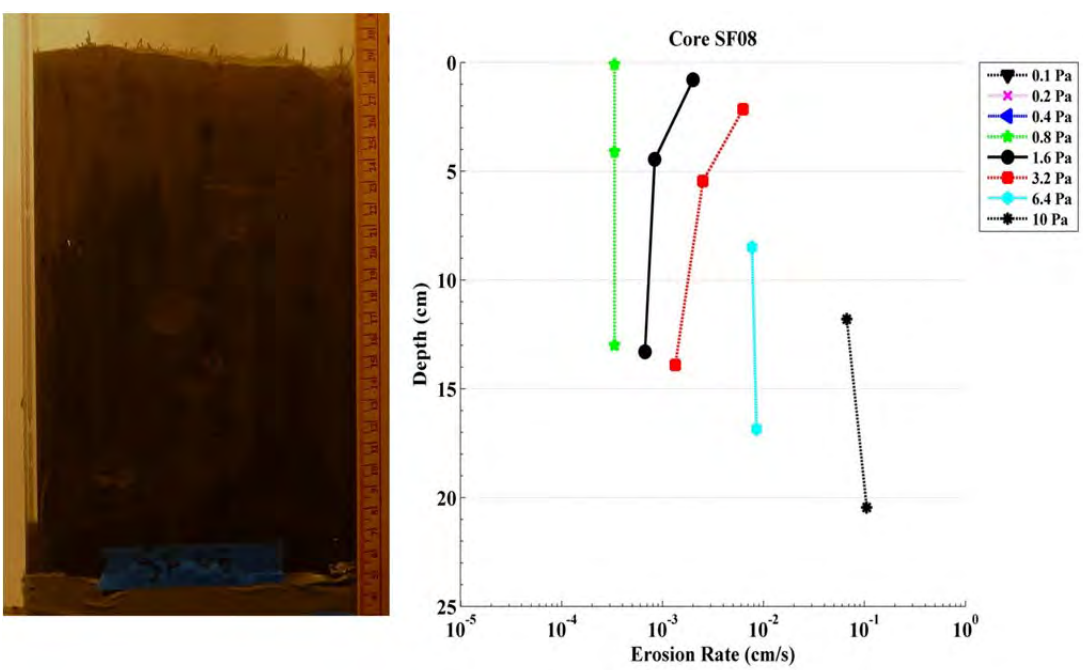

Figure 25. Photo of core SF08 aligned vertically with the corresponding erosion rates.

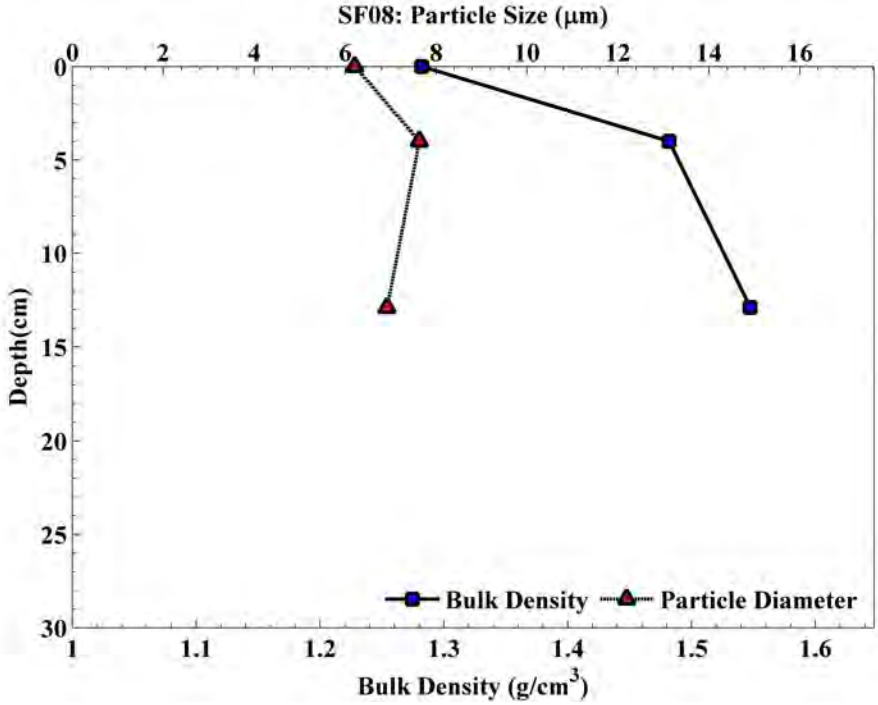

Figure 26. **Bulk density and median particle size (d_{50}) with depth for core SF08.**

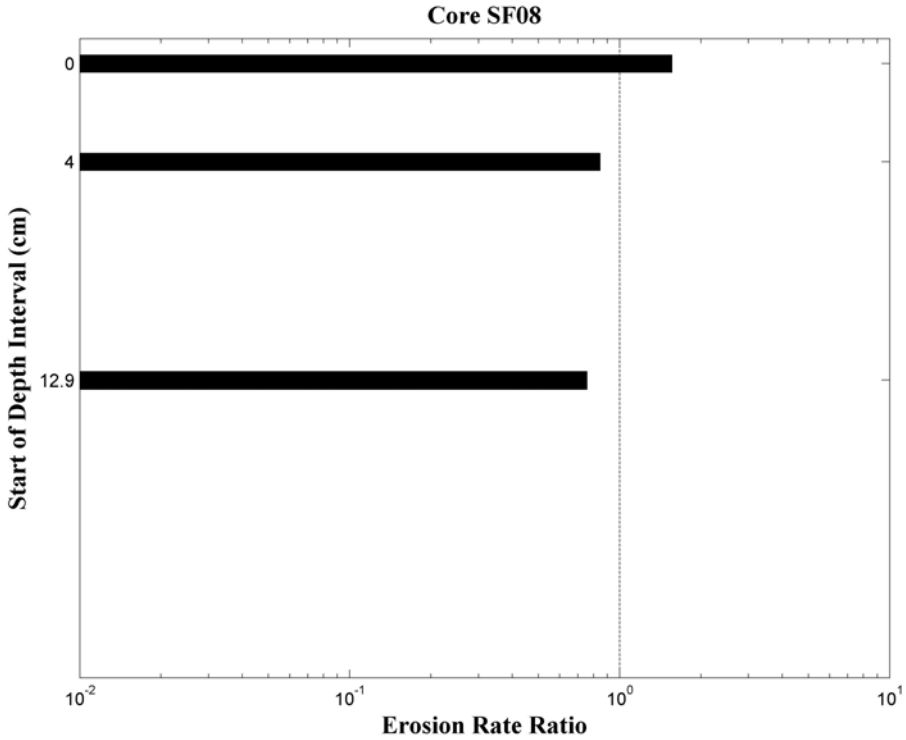

Figure 27. **Intra-core erosion rate ratios for core SF08. The dashed line indicates conditions for the core's average erosion rate (i.e., erosion rate ratio equals 1).**

Table 17. Power law best-fit variables for specified depth intervals in core SF08.

Interval	Depth Start (cm)	Depth Finish (cm)	A	n	r^2
1	0.00	2.10	0.00060	2.1	0.98
2	4.00	11.8	0.00037	2.0	0.94
3	12.9	20.5	0.00029	2.1	0.88

Table 18. Median particle size, bulk density, loss on ignition, and critical shear stress with depth for coreSF08.

Depth (cm)	d_{50} (µm)	ρ_b(g/cm^3)	*LOI*	Power Law τ_{cr} (Pa)	τ_{no} (Pa)	τ_{first} (Pa)	τ_{crit} (Pa)
0.00	6.21	1.28	0.07	0.43	0.40	0.80	0.43
4.00	7.63	1.48	0.05	0.51	0.40	0.80	0.51
12.9	6.92	1.55	0.05	0.61	0.40	0.80	0.61
Mean	**6.92**	**1.44**	**0.04**	**0.52**	**0.40**	**0.80**	**0.52**

2.9 SF09

Core SF09 was collected in 7.3 m of water. Six coring attempts were made at the site before extracting any sediment. The bottom was extremely hard-packed and could not be penetrated even with the additional force of a fence post hammer. Once a core was obtained, it was kept even though it had a slanted surface (makes processing difficult) and was short in length. The core's surface was sparsely populated by plant stalks and small bivalve shells. Uniform tan sediment extended from the surface to a depth of 4 cm. A medium to light gray sediment extended from 4 to 12 cm from the surface. Small black patches were interspersed throughout this section, reducing in frequency further from the surface. The remaining sediment was a heterogeneous mixture of brown sand in a clay matrix with black patches. The sandy clay mixture was extremely firm. Due to the small size of the core, only two intervals were run.

A photograph of core SF09 is presented in Figure 28 along with the corresponding erosion rate data. Shear stresses ranging from 0.1 Pa to 1.6 Pa were applied to the core. Erosion rates, for the portion of the core analyzed, decreased with depth as shown Figure 30. An average critical shear stress of 0.16 Pa was determined for the top 6 cm of the core, but the sandy clay layer likely had a much higher critical shear stress; the layer was hard packed. When processing the core, water started to leak from its bottom, so the clay layer was not tested.

The median grain size was in the very fine to fine silt range, having an average median particle size of 8.58 µm. Bulk densities increased from 1.3 g/cm^3 at the surface to 2.65 g/cm^3 at a depth of 3.9 cm (Figure 29 and Table 20). The average bulk density was 1.98 g/cm^3. The average Loss on Ignition (*LOI)* was 0.3.

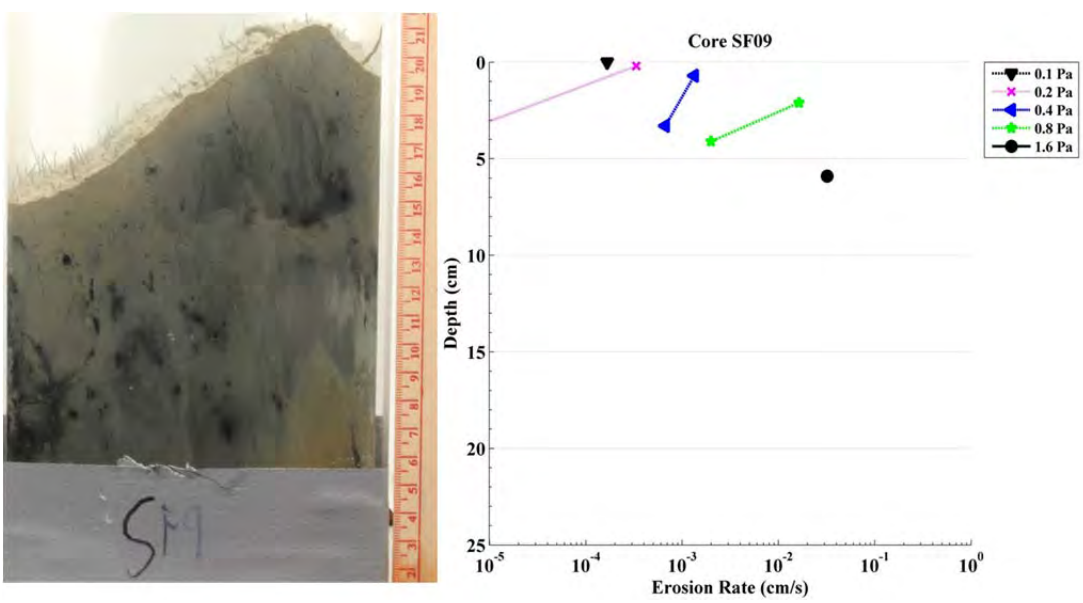

Figure 28. Photo of core SF09 aligned vertically with the corresponding erosion rates.

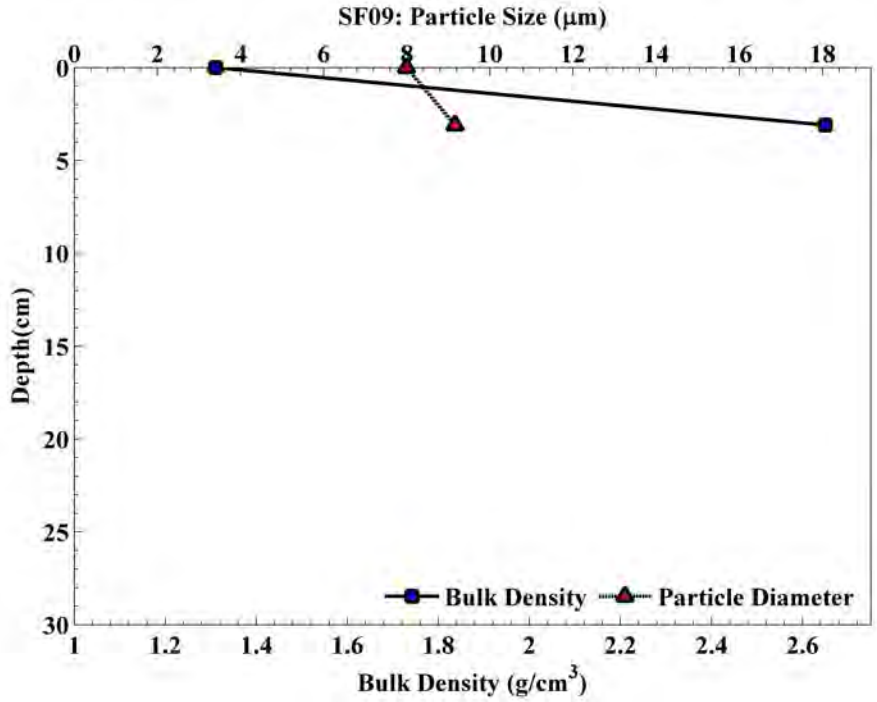

Figure 29. **Bulk density and median particle size (d_{50}) with depth for core SF09.**

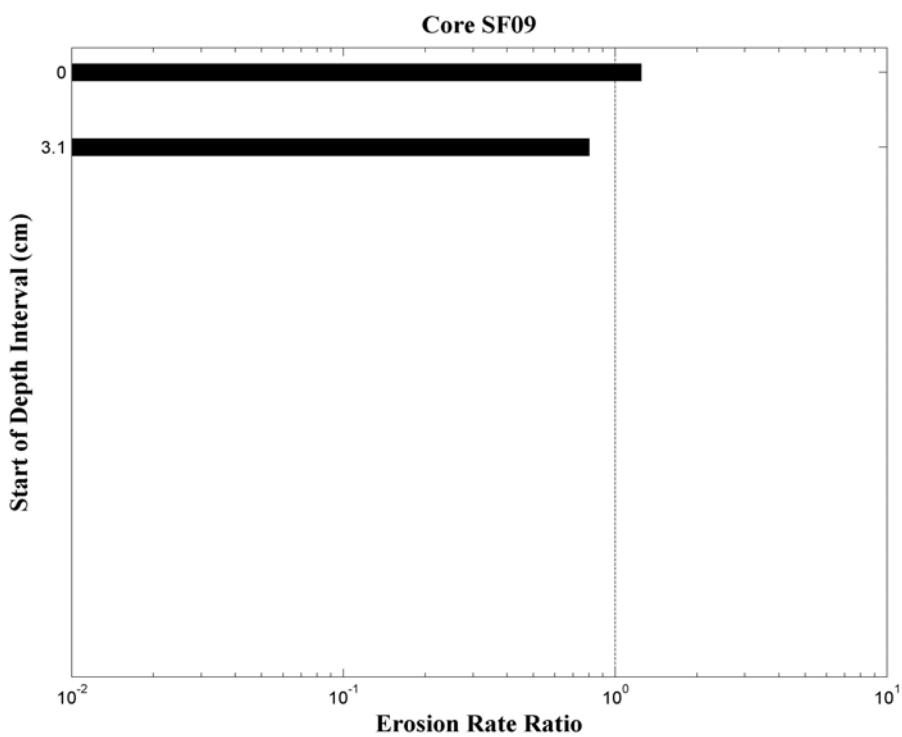

Figure 30. **Intra-core erosion rate ratios for core SF09. The dashed line indicates conditions for the core's average erosion rate (i.e., erosion rate ratio equals 1).**

Table 19. Power law best-fit variables for specified depth intervals in core SF09.

Interval	Depth Start (cm)	Depth Finish (cm)	A	n	r^2
1	0	2.1	0.01660	2.2	0.93
2	3.1	5.9	0.00652	2.8	0.94

Table 20. Median particle size, bulk density, loss on ignition, and critical shear stress with depth for core SF09.

Depth (cm)	d_{50} (µm)	ρ_b(g/cm^3)	*LOI*	Power Law τ_{cr} (Pa)	τ_{no} (Pa)	τ_{first} (Pa)	τ_{crit} (Pa)
0.00	7.99	1.31	0.06	0.10	NA	0.10	0.10
3.10	9.16	2.65	0.55	0.22	0.20	0.40	0.22
Mean	**8.58**	**1.98**	**0.3**	**0.16**	**0.20**	**0.25**	**0.16**

2.10 SF10

Core SF10 was collected in 6.1 m of water. The core had a 1 to 2 mm low density, flocculation layer. Below the surface layer was medium to dark gray fine sediment that extended roughly 1 cm into the core. Intermittent organic material and small bioturbation tracks were found in the top layer. The following 2 to 4 cm of the core was vertically streaked with medium to dark gray fine material. Black sediment patches 1 to 2 cm in diameter were interspersed within this layer. Dark gray fine material with sporadic vertical streaks of lighter gray material was found from 4 to 12 cm in depth. The remainder of the core was uniform and black in color.

A photograph of core SF10 is presented in Figure 31 along with the corresponding erosion rate data. Shear Stresses from 0.1 Pa to 6.4 Pa were applied to the core. Erosion rates were fairly constant at each applied stress greater than 0.2 Pa and less than 6.4 Pa. When applying a shear stress of 6.4 Pa, erosion rates fluctuated with depth. An average critical shear stress of 0.47 Pa was determined for the entire core.

The median particle size was in the fine silt range, with an average median particle size of 8.32 µm. Bulk densities generally increased with depth from 1.28 g/cm^3 at the surface to 1.39 g/cm^3 at a depth of 30.6 cm (Figure 32 and Table 22). The average bulk density was 1.31 g/cm^3. Core SF10 had an average *LOI* of 0.08.

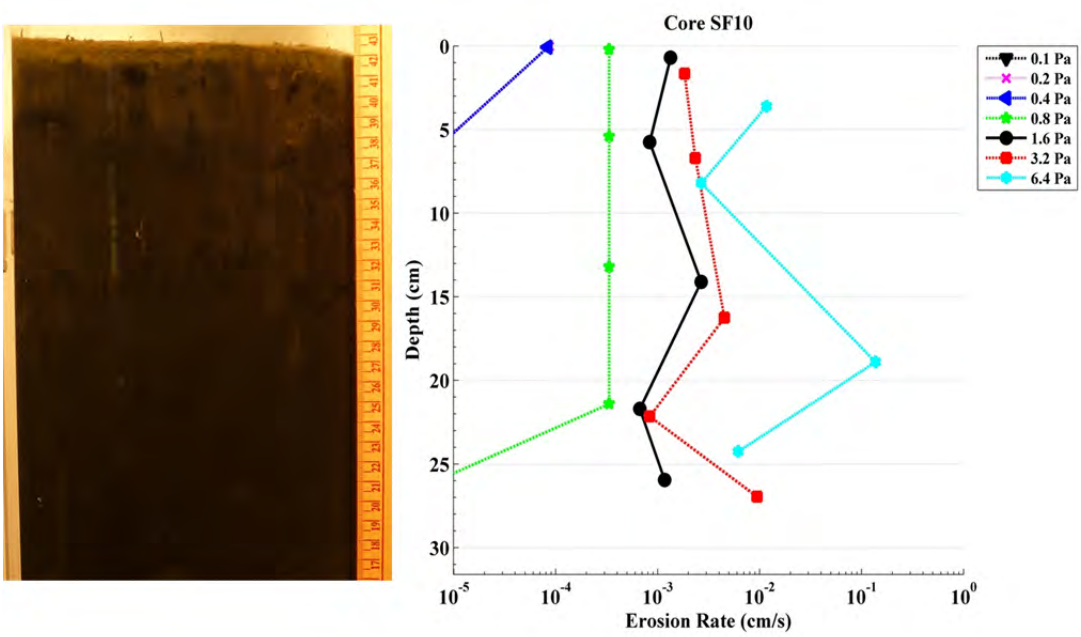

Figure 31. Photo of core SF10 aligned vertically with the corresponding erosion rates.

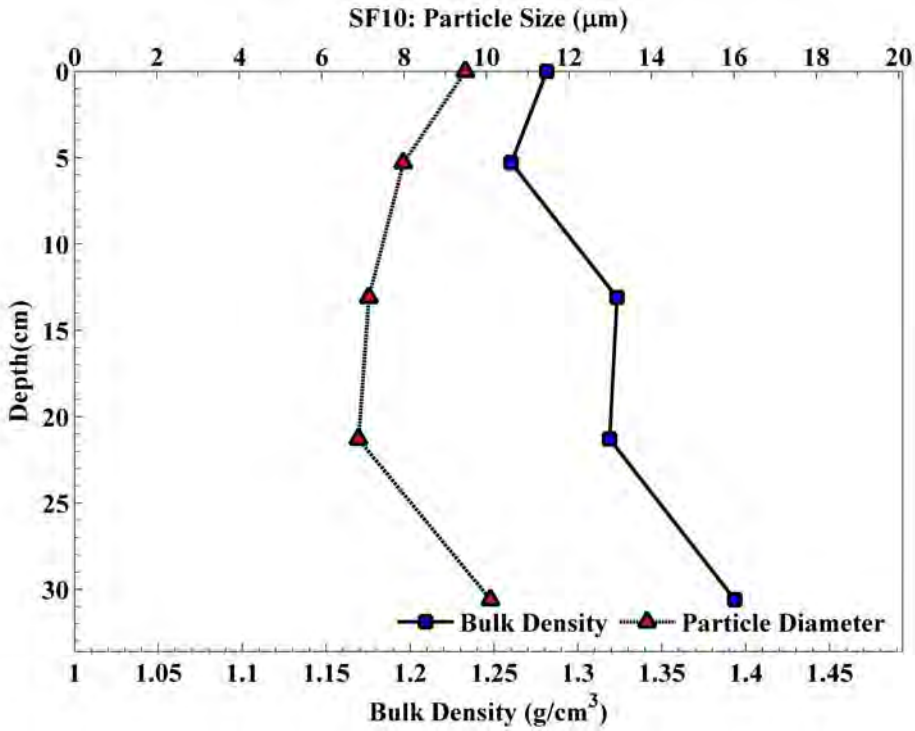

Figure 32. **Bulk density and median particle size (d_{50}) with depth for core SF10.**

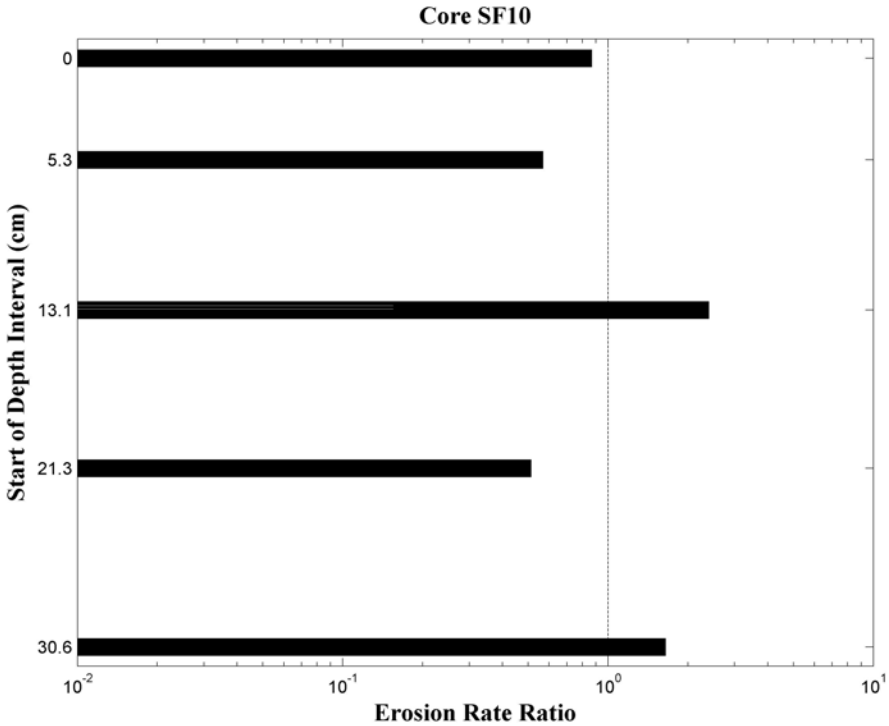

Figure 33. **Intra-core erosion rate ratios for core SF10. The dashed line indicates conditions for the core's average erosion rate (i.e., erosion rate ratio equals 1).**

Table 21. Power law best-fit variables for specified depth intervals in core SF10.

Interval	Depth Start (cm)	Depth Finish (cm)	A	n	r^2
1	0.00	3.60	0.00054	1.4	0.95
2	5.30	8.20	0.00049	1.0	0.93
3	13.1	18.9	0.00054	2.7	0.92
4	21.3	24.3	0.00036	1.3	0.86
5	30.6	27.0	0.00028	3.0	1.00

Table 22. Median particle size, bulk density, loss on ignition, and critical shear stress with depth for core SF10.

Depth (cm)	d_{50} (µm)	ρ_b(g/cm^3)	*LOI*	Power Law τ_{cr} (Pa)	τ_{no} (Pa)	τ_{first} (Pa)	τ_{crit} (Pa)
0.00	9.48	1.28	0.08	0.31	0.10	0.20	0.20
5.30	7.98	1.26	0.09	0.22	0.40	0.80	0.40
13.1	7.14	1.32	0.09	0.53	0.40	0.80	0.53
21.3	6.89	1.32	0.08	0.37	0.40	0.80	0.40
30.6	10.1	1.39	0.07	0.71	0.80	1.60	0.80
Mean	**8.32**	**1.31**	**0.08**	**0.43**	**0.42**	**0.84**	**0.47**

Section 3
Summary

Sea Engineering, Inc. (SEI) conducted a Sediment Erosion at Depth Flume (Sedflume) analysis on 10 sediment cores obtained from Richmond Harbor, CA in the Lauritzen Channel. The Lauritzen channel is part of the United Heckathorn Superfund Site. The cores were collected in water depths ranging between 5.8 m to 7.9 m. The primary goal of this work was to characterize the erosion rates and physical properties of the sediments within the Lauritzen channel. The cores were eroded to determine erosion rates as a function of shear stress and depth into core. In addition, cores were sub-sampled during the analysis to determine sediment bulk density, loss on ignition fraction and particle size distributions at specific depths within the core. Critical shear stresses were calculated from the erosion rate data for five intervals in each core, ranging from 0.1 Pa to 1.28 Pa.

The presence of detritus, pebbles and shells had a noticeable effect on erosion. The Sedflume analysis provided a quantification of the overall effect of each of these constituents on sediment erosion characteristics. When high concentrations of organic material were present in a core, erosion was often dominated by the mobilization of large chunks of material as organic pieces lifted from the test section taking sediment along with them. Pebbles and shells often acted to armor the bed until the applied shear stress was large enough to mobilize them.

Although erosion rates fluctuated between intervals, core sediments generally stiffened with depth. This trend is common for sites with cohesive sediments. Cohesive sediments will often self-compact due to the weight of the overlying material. Compaction reduces the potential for sediment mobility. However, Sedflume results must be analyzed in conjunction with other system characteristics, such as hydrodynamic forcing, to assess overall site stability and sediment transport trends.

To better visualize the relative erodibility of the sediment at the locations where cores were recovered, the ratio of the mean erosion rate of each core (core vertically averaged erosion rate) to the average mean erosion rate of all cores at the site was calculated and plotted (Figure 34). The dashed line in Figure 34 denotes a site-wide average erosion rate ratio of 1.0. A ratio above this line generally means the core is more susceptible to erosion than those below. It is important to note that this analysis does not take into account the hydrodynamic forces or sediment coarsening processes that are responsible for net in-situ transport. The cores where plotted in Figure 34 such that the cores closest to the mouth of the Lauritzen Channel are plotted on the left-hand side of the figure. Generally, sediment near the mouth of the channel was stiffer than sediment at the end of the channel.

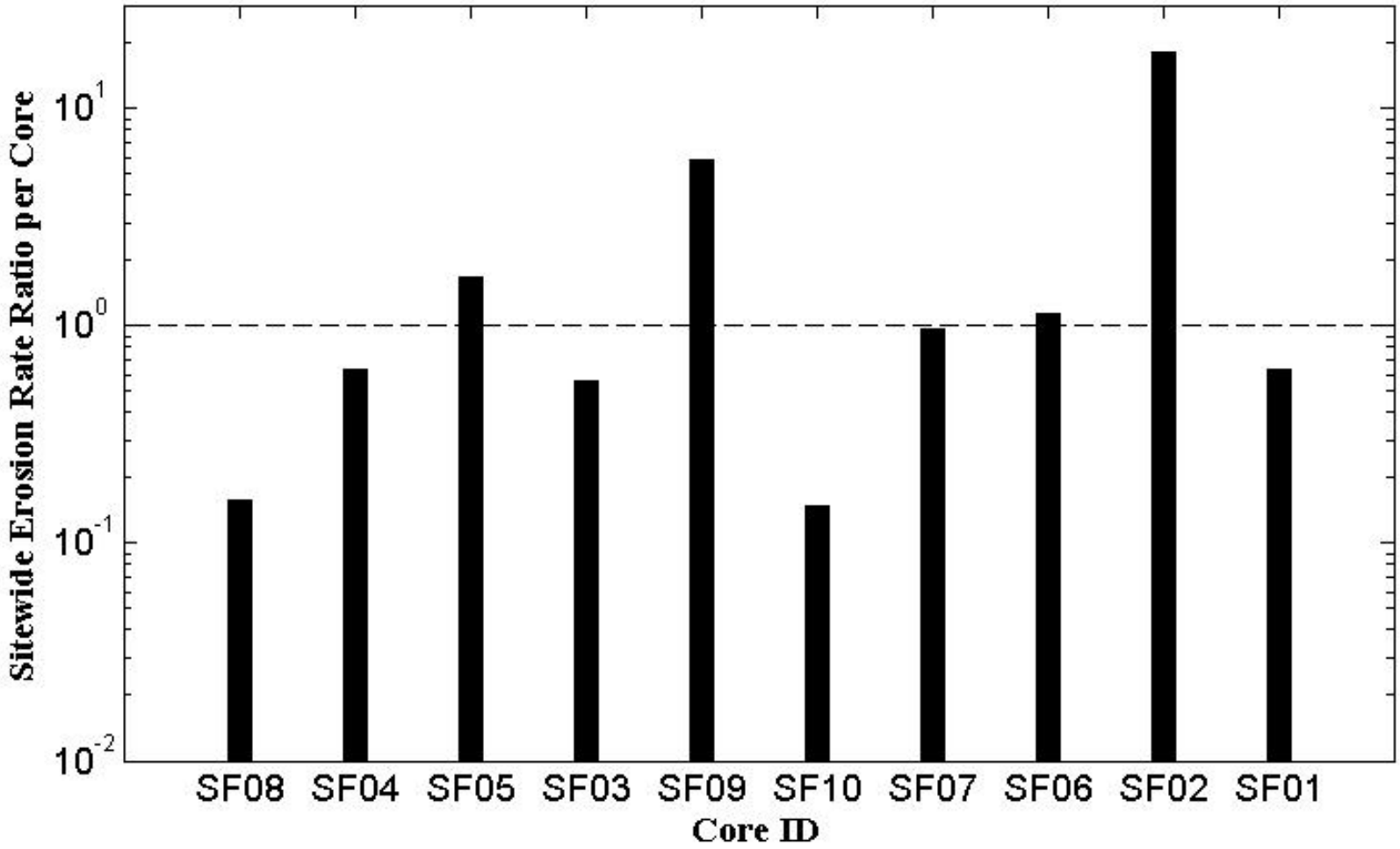

Figure 34. Inter-core erosion rate ratios. Depth-averaged core erosion rates compared to the site-wide average erosion rates.

Section 4
References

ASTM Standard, 2007, Annual Book of ASTM Standards. ASTM International, West Conshohocken, Pennsylvania, USA. Vol. 04.08 Soil and Rock (I): D 420 - D5611: 314-315.

Hakanson, L., and M. Jansson, 2002, Principles of Lake Sedimentology. Blackburn Press, Caldwell, New Jersey, USA.

Jepsen, R., J. Roberts, and W. Lick, 1997, Effects of bulk density on sediment erosion rates, Water, Air and Soil Pollution, 99:21-31.

McNeil, J., C. Taylor, and W. Lick, 1996, Measurements of erosion of undisturbed bottom sediments with depth, J. Hydr. Engr., 122(6):316-324.

Roberts, J., R. Jepsen, D. Gotthard, and W. Lick, 1998, Effects of particle size and bulk density on erosion of quartz particles, J. Hydr. Engr., 124(12):1261 1267.

Appendix – Particle Size Distributions

Beckman Coulter LS Particle Size Analyzer

6 Aug 2013

Heckathorn

File name:	C:\Users\Sam McWilliams\Desktop\sea_engineering\Sedflume\Heckathorne\Psd\1-1__195.$av
	1-1__195.$av
File ID:	1-1
Operator:	Szesciorka
Comment 1:	Heckathorne
Comment 2:	mixed, blended
Optical model:	garnet.rf780z
LS 13 320 SW	Aqueous Liquid Module
	Run length: 60 seconds
Pump speed:	66
Fluid:	water

Average of 3 files:
C:\LS13320\Projects\Heckathorne\1-1__193.$ls
C:\LS13320\Projects\Heckathorne\1-1__194.$ls
C:\LS13320\Projects\Heckathorne\1-1__195.$ls

Volume Statistics (Arithmetic) 1-1__195.$av

Calculations from 0.375 µm to 2000 µm

Volume:	100%		
Mean:	60.74 µm	S.D.:	108.9 µm
Median:	14.90 µm	Variance:	11869 μm^2
Mean/Median ratio:	4.076	C.V.:	179%
Mode:	6.453 µm	Skewness:	3.034 Right skewed
		Kurtosis:	9.688 Leptokurtic

<10%	<25%	<50%	<75%	<90%
2.406 µm	5.160 µm	14.90 µm	64.01 µm	163.4 µm

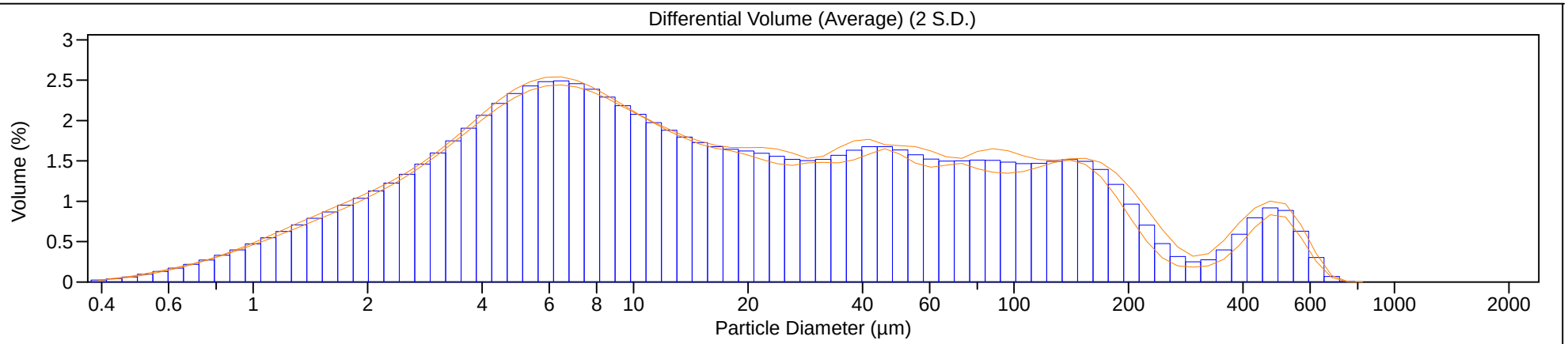

Beckman Coulter LS Particle Size Analyzer

6 Aug 2013

Heckathorn

File name:	C:\Users\Sam McWilliams\Desktop\sea_engineering\Sedflume\Heckathorne\Psd\1-2__252.$av
	1-2__252.$av
File ID:	1-2
Operator:	Reyes
Comment 1:	Heckathorne
Comment 2:	mixed, blended
Optical model:	garnet.rf780z
LS 13 320 SW	Aqueous Liquid Module
Pump speed:	66
Fluid:	water

Average of 3 files:
C:\LS13320\Projects\Heckathorne\1-2__250.$ls
C:\LS13320\Projects\Heckathorne\1-2__251.$ls
C:\LS13320\Projects\Heckathorne\1-2__252.$ls

Volume Statistics (Arithmetic) 1-2__252.$av

Calculations from 0.375 µm to 2000 µm

Volume:	100%		
Mean:	15.40 µm	S.D.:	23.70 µm
Median:	6.771 µm	Variance:	561.7 µm^2
Mean/Median ratio:	2.275	C.V.:	154%
Mode:	5.878 µm	Skewness:	3.285 Right skewed
		Kurtosis:	12.35 Leptokurtic

<10%	<25%	<50%	<75%	<90%
1.683 µm	3.271 µm	6.771 µm	16.00 µm	38.41 µm

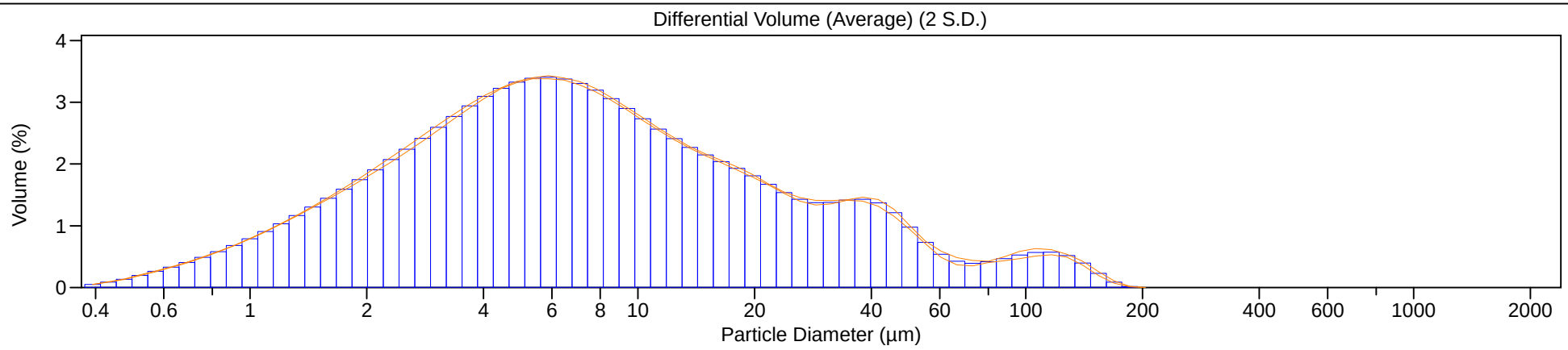

Beckman Coulter LS Particle Size Analyzer

6 Aug 2013

Heckathorn

File name:	C:\Users\Sam McWilliams\Desktop\sea_engineering\Sedflume\Heckathorne\Psd\1-3__204.$av
	1-3__204.$av
File ID:	1-3
Operator:	Szesciorka
Comment 1:	Heckathorne
Comment 2:	mixed, blended
Optical model:	garnet.rf780z
LS 13 320 SW	Aqueous Liquid Module
	Run length: 60 seconds
Pump speed:	66
Fluid:	water
Average of 3 files:	
C:\LS13320\Projects\Heckathorne\1-3__202.$ls	
C:\LS13320\Projects\Heckathorne\1-3__203.$ls	
C:\LS13320\Projects\Heckathorne\1-3__204.$ls	

Volume Statistics (Arithmetic) 1-3__204.$av

Calculations from 0.375 µm to 2000 µm

Volume:	100%		
Mean:	15.90 µm	S.D.:	22.61 µm
Median:	6.838 µm	Variance:	511.2 μm^2
Mean/Median ratio:	2.325	C.V.:	142%
Mode:	5.878 µm	Skewness:	2.591 Right skewed
		Kurtosis:	6.902 Leptokurtic

<10%	<25%	<50%	<75%	<90%
1.580 µm	3.138 µm	6.838 µm	17.75 µm	41.79 µm

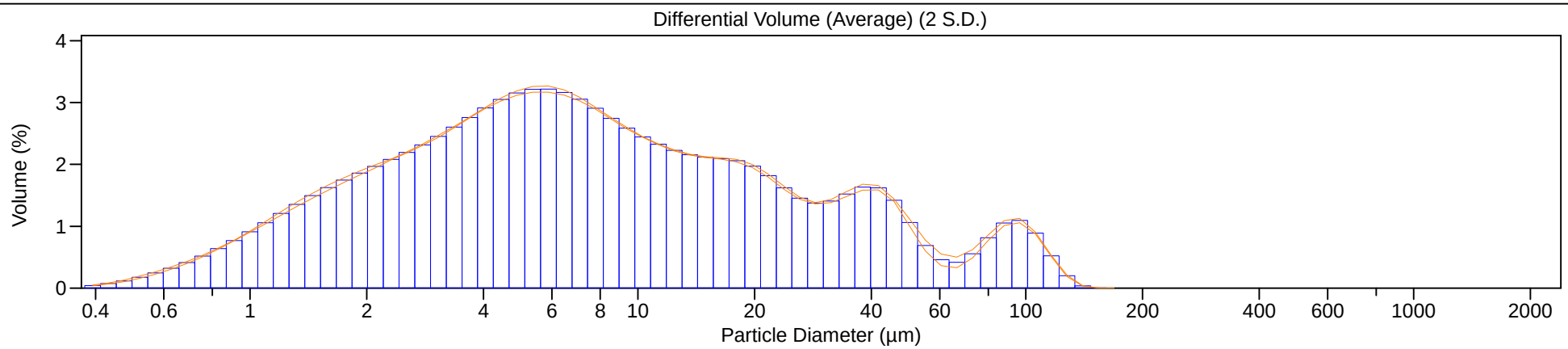

Beckman Coulter LS Particle Size Analyzer

6 Aug 2013

Heckathorn

File name:	C:\Users\Sam McWilliams\Desktop\sea_engineering\Sedflume\Heckathorne\Psd\1-4__207.$av
	1-4__207.$av
File ID:	1-4
Operator:	Szesciorka
Comment 1:	Heckathorne
Comment 2:	mixed, blended
Optical model:	garnet.rf780z
LS 13 320 SW	Aqueous Liquid Module
	Run length: 60 seconds
Pump speed:	66
Fluid:	water
Average of 3 files:	
C:\LS13320\Projects\Heckathorne\1-4__205.$ls	
C:\LS13320\Projects\Heckathorne\1-4__206.$ls	
C:\LS13320\Projects\Heckathorne\1-4__207.$ls	

Volume Statistics (Arithmetic) 1-4__207.$av

Calculations from 0.375 µm to 2000 µm

Volume:	100%		
Mean:	31.34 µm	S.D.:	53.35 µm
Median:	9.816 µm	Variance:	2847 μm^2
Mean/Median ratio:	3.193	C.V.:	170%
Mode:	7.084 µm	Skewness:	3.127 Right skewed
		Kurtosis:	11.33 Leptokurtic

<10%	<25%	<50%	<75%	<90%
2.046 µm	4.257 µm	9.816 µm	31.99 µm	90.57 µm

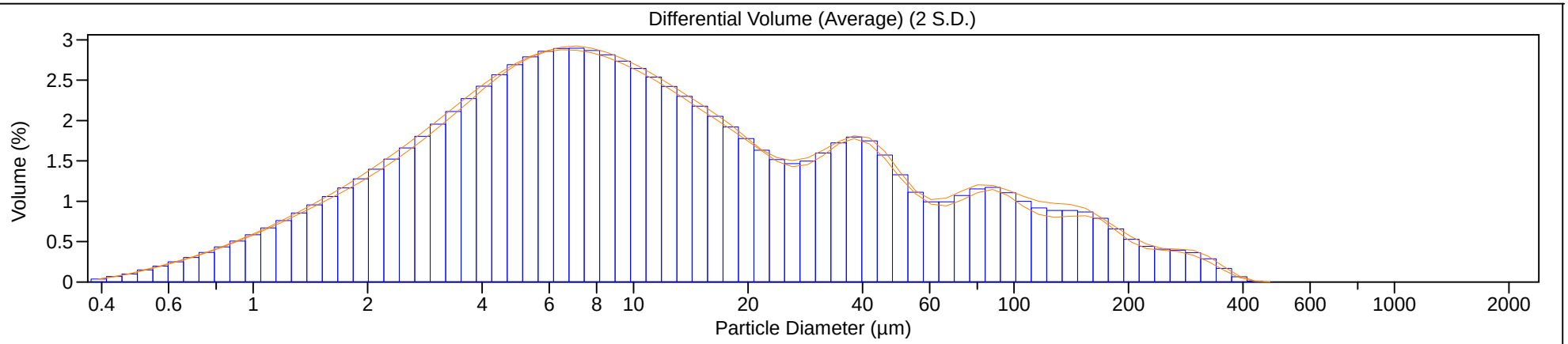

Beckman Coulter LS Particle Size Analyzer

6 Aug 2013

Heckathorn

File name:	C:\Users\Sam McWilliams\Desktop\sea_engineering\Sedflume\Heckathorne\Psd\1-5__222.$av
	1-5__222.$av
File ID:	1-5
Operator:	Reyes
Comment 1:	Heckathorne
Comment 2:	mixed, blended
Optical model:	garnet.rf780z
LS 13 320 SW	Aqueous Liquid Module
	Run length: 60 seconds
Pump speed:	66
Fluid:	water
Average of 3 files:	
C:\LS13320\Projects\Heckathorne\1-5__220.$ls	
C:\LS13320\Projects\Heckathorne\1-5__221.$ls	
C:\LS13320\Projects\Heckathorne\1-5__222.$ls	

Volume Statistics (Arithmetic) 1-5__222.$av

Calculations from 0.375 µm to 2000 µm

Volume:	100%		
Mean:	28.34 µm	S.D.:	48.39 µm
Median:	8.794 µm	Variance:	2342 μm^2
Mean/Median ratio:	3.223	C.V.:	171%
Mode:	6.453 µm	Skewness:	3.018 Right skewed
		Kurtosis:	10.18 Leptokurtic

<10%	<25%	<50%	<75%	<90%
2.019 µm	3.992 µm	8.794 µm	27.01 µm	86.35 µm

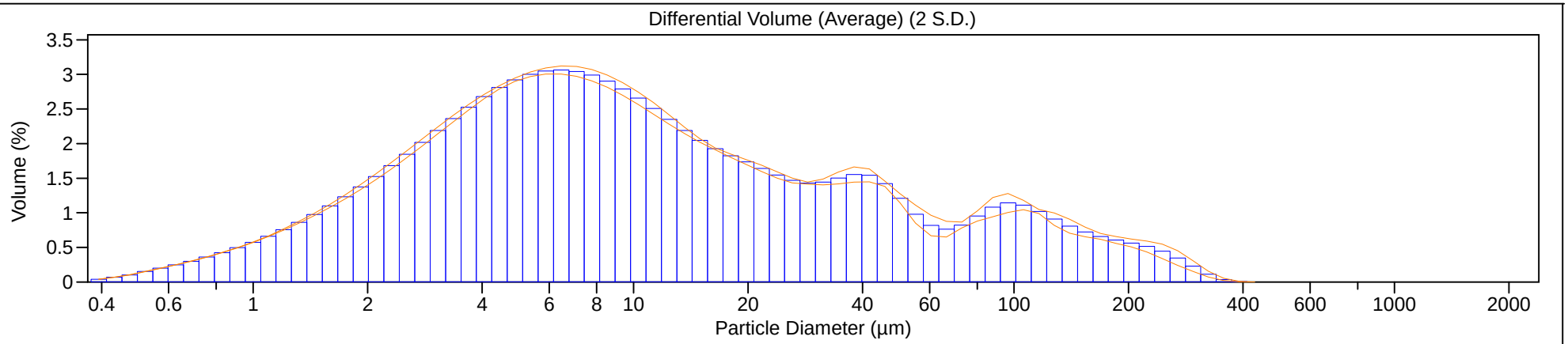

Beckman Coulter LS Particle Size Analyzer

6 Aug 2013

Heckathorn

File name:	C:\Users\Sam McWilliams\Desktop\sea_engineering\Sedflume\Heckathorne\Psd\2-1__180.$av
	2-1__180.$av
File ID:	2-1
Operator:	Szesciorka
Comment 1:	Heckathorne
Comment 2:	mixed, blended
Optical model:	garnet.rf780z
LS 13 320 SW	Aqueous Liquid Module
	Run length: 60 seconds
Pump speed:	66
Fluid:	water
Average of 3 files:	
C:\LS13320\Projects\Heckathorne\2-1__178.$ls	
C:\LS13320\Projects\Heckathorne\2-1__179.$ls	
C:\LS13320\Projects\Heckathorne\2-1__180.$ls	

Volume Statistics (Arithmetic) 2-1__180.$av

Calculations from 0.375 µm to 2000 µm

Volume:	100%		
Mean:	102.5 µm	S.D.:	182.6 µm
Median:	18.14 µm	Variance:	33332 μm^2
Mean/Median ratio:	5.651	C.V.:	178%
Mode:	5.878 µm	Skewness:	2.407 Right skewed
		Kurtosis:	5.348 Leptokurtic

<10%	<25%	<50%	<75%	<90%
2.109 µm	4.887 µm	18.14 µm	106.5 µm	369.3 µm

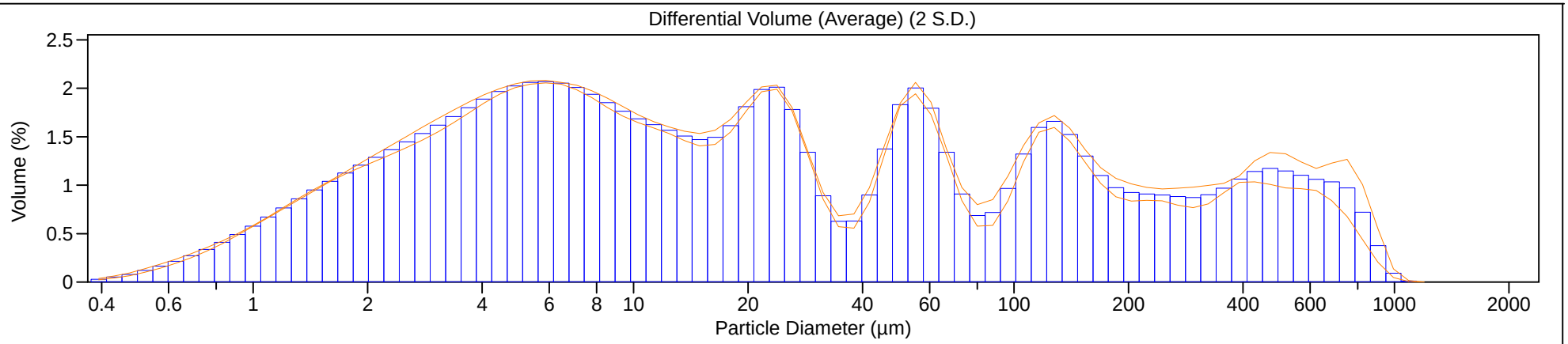

Beckman Coulter LS Particle Size Analyzer

6 Aug 2013

Heckathorn

File name:	C:\Users\Sam McWilliams\Desktop\sea_engineering\Sedflume\Heckathorne\Psd\2-2__288.$av
	2-2__288.$av
File ID:	2-2
Operator:	Reyes
Comment 1:	Heckathorne
Comment 2:	mixed, blended
Optical model:	garnet.rf780z
LS 13 320 SW	Aqueous Liquid Module
	Run length: 60 seconds
Pump speed:	66
Fluid:	water
Average of 3 files:	
C:\LS13320\Projects\Heckathorne\2-2__286.$ls	
C:\LS13320\Projects\Heckathorne\2-2__287.$ls	
C:\LS13320\Projects\Heckathorne\2-2__288.$ls	

Volume Statistics (Arithmetic) 2-2__288.$av

Calculations from 0.375 µm to 2000 µm

Volume:	100%		
Mean:	174.7 µm	S.D.:	236.3 µm
Median:	53.89 µm	Variance:	55822 μm^2
Mean/Median ratio:	3.241	C.V.:	135%
Mode:	471.1 µm	Skewness:	1.695 Right skewed
		Kurtosis:	2.464 Leptokurtic

<10%	<25%	<50%	<75%	<90%
2.970 µm	8.417 µm	53.89 µm	262.6 µm	530.6 µm

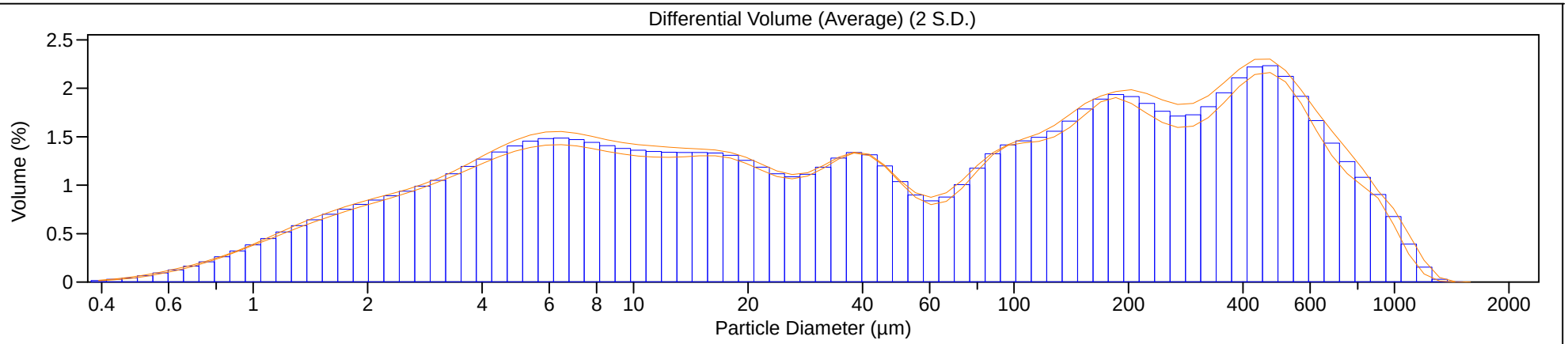

Beckman Coulter LS Particle Size Analyzer

6 Aug 2013

Heckathorn

File name:	C:\Users\Sam McWilliams\Desktop\sea_engineering\Sedflume\Heckathorne\Psd\2-3__192.$av
	2-3__192.$av
File ID:	2-3
Operator:	Szesciorka
Comment 1:	Heckathorne
Comment 2:	mixed, blended
Optical model:	garnet.rf780z
LS 13 320 SW	Aqueous Liquid Module
	Run length: 60 seconds
Pump speed:	66
Fluid:	water
Average of 3 files:	
C:\LS13320\Projects\Heckathorne\2-3__190.$ls	
C:\LS13320\Projects\Heckathorne\2-3__191.$ls	
C:\LS13320\Projects\Heckathorne\2-3__192.$ls	

Volume Statistics (Arithmetic) 2-3__192.$av

Calculations from 0.375 µm to 2000 µm

Volume:	100%		
Mean:	71.92 µm	S.D.:	136.7 µm
Median:	11.77 µm	Variance:	18698 μm^2
Mean/Median ratio:	6.110	C.V.:	190%
Mode:	6.453 µm	Skewness:	2.543 Right skewed
		Kurtosis:	5.713 Leptokurtic

<10%	<25%	<50%	<75%	<90%
2.130 µm	4.532 µm	11.77 µm	54.50 µm	239.3 µm

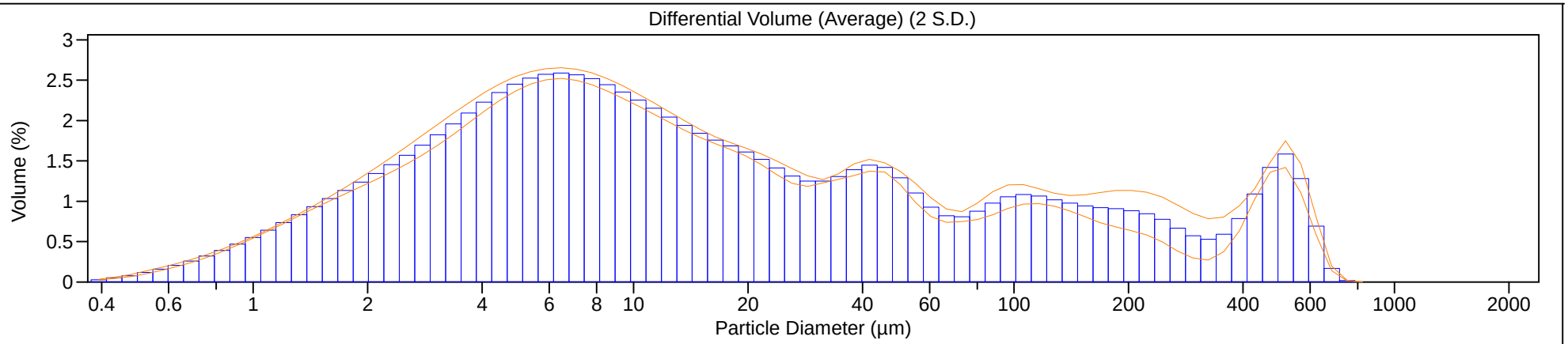

Beckman Coulter LS Particle Size Analyzer

6 Aug 2013

Heckathorn

File name:	C:\Users\Sam McWilliams\Desktop\sea_engineering\Sedflume\Heckathorne\Psd\2-4__234.$av
	2-4__234.$av
File ID:	2-4
Operator:	Reyes
Comment 1:	Heckathorne
Comment 2:	mixed, blended
Optical model:	garnet.rf780z
LS 13 320 SW	Aqueous Liquid Module
	Run length: 60 seconds
Pump speed:	66
Fluid:	water
Average of 3 files:	
C:\LS13320\Projects\Heckathorne\2-4__232.$ls	
C:\LS13320\Projects\Heckathorne\2-4__233.$ls	
C:\LS13320\Projects\Heckathorne\2-4__234.$ls	

Volume Statistics (Arithmetic) 2-4__234.$av

Calculations from 0.375 µm to 2000 µm

Volume:	100%		
Mean:	40.97 µm	S.D.:	70.34 µm
Median:	10.07 µm	Variance:	4948 μm^2
Mean/Median ratio:	4.067	C.V.:	172%
Mode:	5.878 µm	Skewness:	2.614 Right skewed
		Kurtosis:	6.752 Leptokurtic

<10%	<25%	<50%	<75%	<90%
2.126 µm	4.312 µm	10.07 µm	39.23 µm	130.7 µm

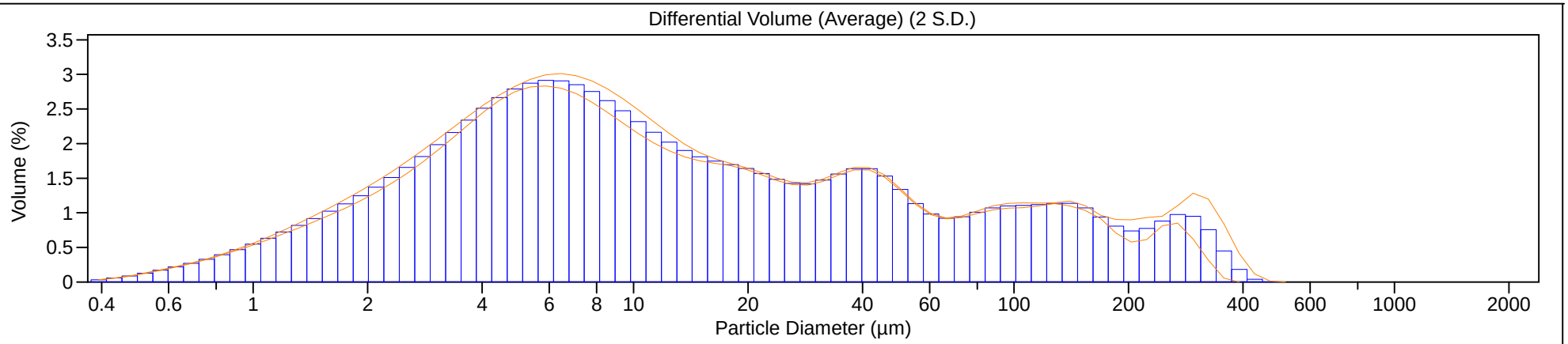

Beckman Coulter LS Particle Size Analyzer

6 Aug 2013

Heckathorn

File name:	C:\Users\Sam McWilliams\Desktop\sea_engineering\Sedflume\Heckathorne\Psd\2-5__237.$av
	2-5__237.$av
File ID:	2-5
Operator:	Reyes
Comment 1:	Heckathorne
Comment 2:	mixed, blended
Optical model:	garnet.rf780z
LS 13 320 SW	Aqueous Liquid Module
	Run length: 60 seconds
Pump speed:	66
Fluid:	water
Average of 3 files:	
C:\LS13320\Projects\Heckathorne\2-5__235.$ls	
C:\LS13320\Projects\Heckathorne\2-5__236.$ls	
C:\LS13320\Projects\Heckathorne\2-5__237.$ls	

Volume Statistics (Arithmetic) 2-5__237.$av

Calculations from 0.375 µm to 2000 µm

Volume:	100%		
Mean:	41.60 µm	S.D.:	67.31 µm
Median:	11.26 µm	Variance:	4531 μm^2
Mean/Median ratio:	3.696	C.V.:	162%
Mode:	5.878 µm	Skewness:	2.581 Right skewed
		Kurtosis:	7.093 Leptokurtic

<10%	<25%	<50%	<75%	<90%
2.121 µm	4.456 µm	11.26 µm	44.49 µm	130.2 µm

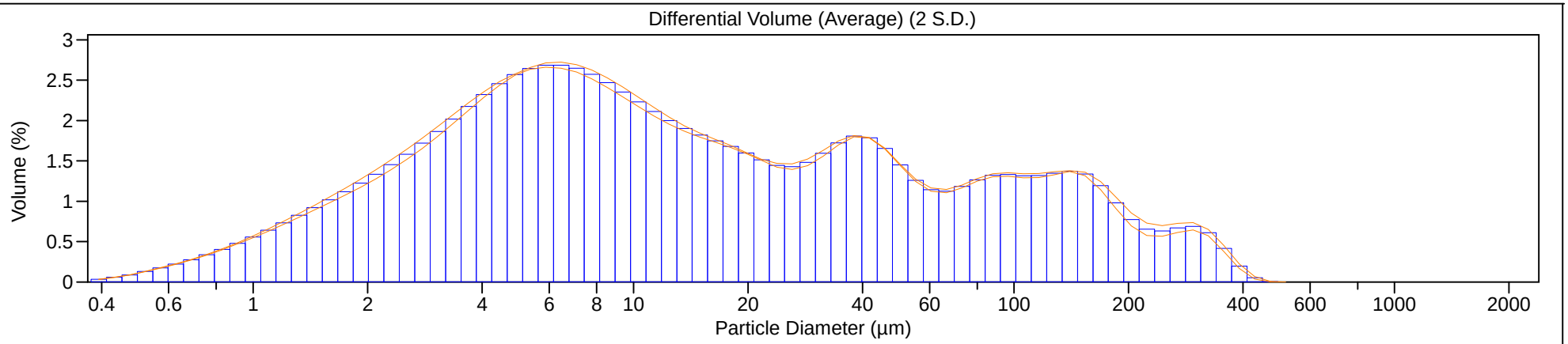

Beckman Coulter LS Particle Size Analyzer

6 Aug 2013

Heckathorn

File name:	C:\Users\Sam McWilliams\Desktop\sea_engineering\Sedflume\Heckathorne\Psd\3-1__276.$av
	3-1__276.$av
File ID:	3-1
Operator:	Reyes
Comment 1:	Heckathorne
Comment 2:	mixed, blended
Optical model:	garnet.rf780z
LS 13 320 SW	Aqueous Liquid Module
	Run length: 60 seconds
Pump speed:	66
Fluid:	water
Average of 3 files:	
C:\LS13320\Projects\Heckathorne\3-1__274.$ls	
C:\LS13320\Projects\Heckathorne\3-1__275.$ls	
C:\LS13320\Projects\Heckathorne\3-1__276.$ls	

Volume Statistics (Arithmetic) 3-1__276.$av

Calculations from 0.375 µm to 2000 µm

Volume:	100%		
Mean:	10.16 µm	S.D.:	11.21 µm
Median:	5.731 µm	Variance:	125.7 µm^2
Mean/Median ratio:	1.773	C.V.:	110%
Mode:	5.355 µm	Skewness:	1.869 Right skewed
		Kurtosis:	3.047 Leptokurtic

<10%	<25%	<50%	<75%	<90%
1.497 µm	2.798 µm	5.731 µm	12.77 µm	26.97 µm

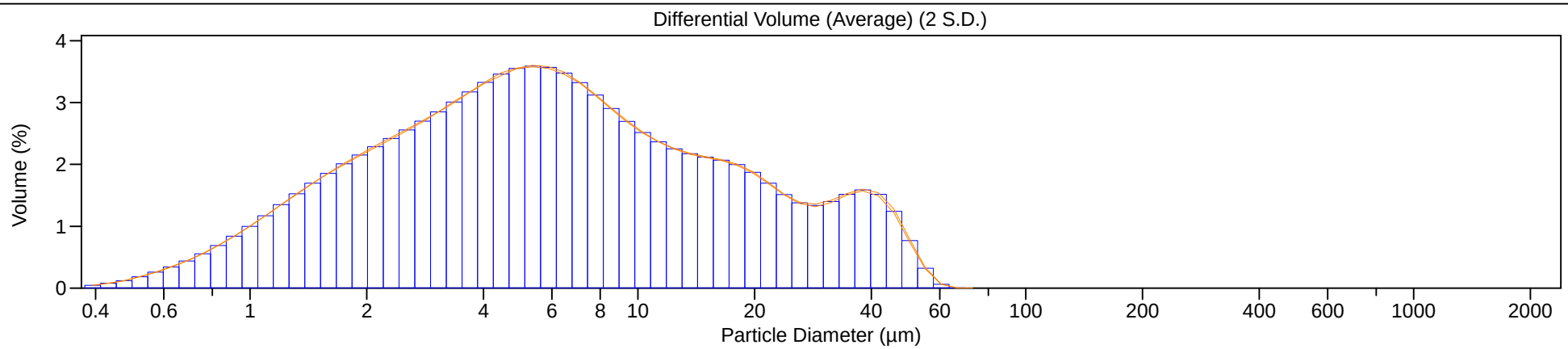

Beckman Coulter LS Particle Size Analyzer

6 Aug 2013

Heckathorn

File name:	C:\Users\Sam McWilliams\Desktop\sea_engineering\Sedflume\Heckathorne\Psd\3-2__264.$av
	3-2__264.$av
File ID:	3-2
Operator:	Reyes
Comment 1:	Heckathorne
Comment 2:	mixed, blended
Optical model:	garnet.rf780z
LS 13 320 SW	Aqueous Liquid Module
	Run length: 60 seconds
Pump speed:	66
Fluid:	water
Average of 3 files:	
C:\LS13320\Projects\Heckathorne\3-2__262.$ls	
C:\LS13320\Projects\Heckathorne\3-2__263.$ls	
C:\LS13320\Projects\Heckathorne\3-2__264.$ls	

Volume Statistics (Arithmetic) 3-2__264.$av

Calculations from 0.375 µm to 2000 µm

Volume:	100%		
Mean:	17.62 µm	S.D.:	28.98 µm
Median:	6.974 µm	Variance:	839.8 µm^2
Mean/Median ratio:	2.527	C.V.:	164%
Mode:	5.878 µm	Skewness:	3.835 Right skewed
		Kurtosis:	21.37 Leptokurtic

<10%	<25%	<50%	<75%	<90%
1.655 µm	3.263 µm	6.974 µm	17.75 µm	43.93 µm

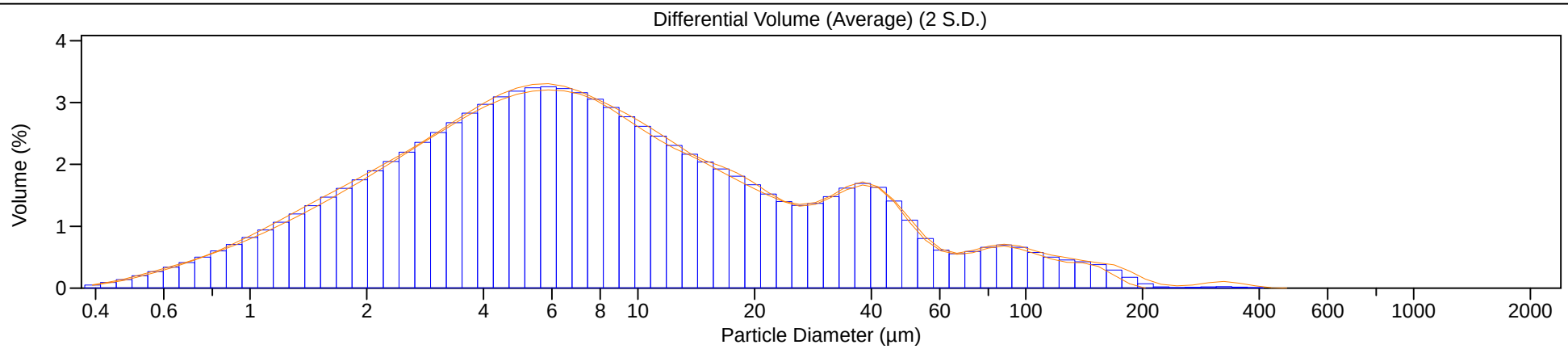

Beckman Coulter LS Particle Size Analyzer

6 Aug 2013

Heckathorn

File name:	C:\Users\Sam McWilliams\Desktop\sea_engineering\Sedflume\Heckathorne\Psd\3-3__270.$av
	3-3__270.$av
File ID:	3-3
Operator:	Reyes
Comment 1:	Heckathorne
Comment 2:	mixed, blended
Optical model:	garnet.rf780z
LS 13 320 SW	Aqueous Liquid Module
	Run length: 60 seconds
Pump speed:	66
Fluid:	water
Average of 3 files:	
C:\LS13320\Projects\Heckathorne\3-3__268.$ls	
C:\LS13320\Projects\Heckathorne\3-3__269.$ls	
C:\LS13320\Projects\Heckathorne\3-3__270.$ls	

Volume Statistics (Arithmetic) 3-3__270.$av

Calculations from 0.375 µm to 2000 µm

Volume:	100%		
Mean:	24.85 µm	S.D.:	56.81 µm
Median:	6.820 µm	Variance:	3228 μm^2
Mean/Median ratio:	3.644	C.V.:	229%
Mode:	5.878 µm	Skewness:	3.972 Right skewed
		Kurtosis:	16.13 Leptokurtic

<10%	<25%	<50%	<75%	<90%
1.610 µm	3.146 µm	6.820 µm	17.12 µm	44.12 µm

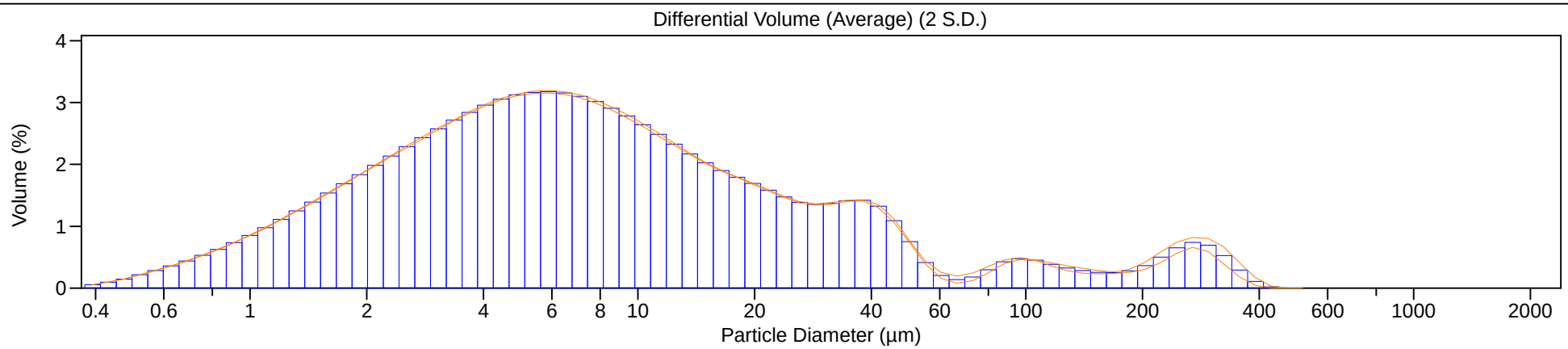

Beckman Coulter LS Particle Size Analyzer

6 Aug 2013

Heckathorn

File name:	C:\Users\Sam McWilliams\Desktop\sea_engineering\Sedflume\Heckathorne\Psd\3-4__291.$av
	3-4__291.$av
File ID:	3-4
Operator:	Reyes
Comment 1:	Heckathorne
Comment 2:	mixed, blended
Optical model:	garnet.rf780z
LS 13 320 SW	Aqueous Liquid Module
	Run length: 60 seconds
Pump speed:	66
Fluid:	water
Average of 3 files:	
C:\LS13320\Projects\Heckathorne\3-4__289.$ls	
C:\LS13320\Projects\Heckathorne\3-4__290.$ls	
C:\LS13320\Projects\Heckathorne\3-4__291.$ls	

Volume Statistics (Arithmetic) 3-4__291.$av

Calculations from 0.375 µm to 2000 µm

Volume:	100%		
Mean:	12.79 µm	S.D.:	19.23 µm
Median:	6.588 µm	Variance:	369.9 µm^2
Mean/Median ratio:	1.941	C.V.:	150%
Mode:	6.453 µm	Skewness:	4.262 Right skewed
		Kurtosis:	23.67 Leptokurtic

<10%	<25%	<50%	<75%	<90%
1.658 µm	3.231 µm	6.588 µm	14.01 µm	30.08 µm

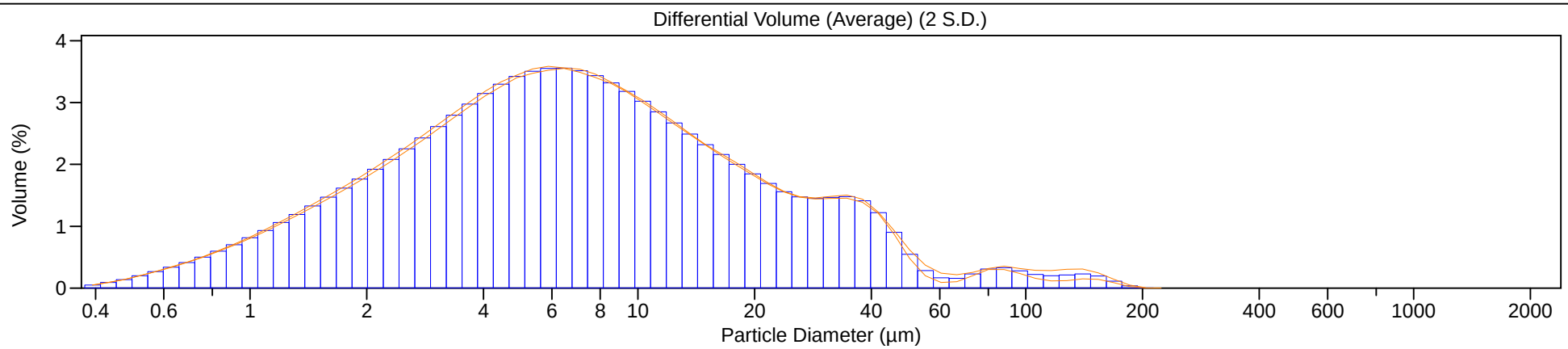

Beckman Coulter LS Particle Size Analyzer

6 Aug 2013

Heckathorn

File name:	C:\Users\Sam McWilliams\Desktop\sea_engineering\Sedflume\Heckathorne\Psd\3-5__294.$av
	3-5__294.$av
File ID:	3-5
Operator:	Reyes
Comment 1:	Heckathorne
Comment 2:	mixed, blended
Optical model:	garnet.rf780z
LS 13 320 SW	Aqueous Liquid Module
	Run length: 60 seconds
Pump speed:	66
Fluid:	water
Average of 3 files:	
C:\LS13320\Projects\Heckathorne\3-5__292.$ls	
C:\LS13320\Projects\Heckathorne\3-5__293.$ls	
C:\LS13320\Projects\Heckathorne\3-5__294.$ls	

Volume Statistics (Arithmetic) 3-5__294.$av

Calculations from 0.375 µm to 2000 µm

Volume:	100%		
Mean:	23.88 µm	S.D.:	50.75 µm
Median:	6.748 µm	Variance:	2576 μm^2
Mean/Median ratio:	3.539	C.V.:	213%
Mode:	5.878 µm	Skewness:	3.843 Right skewed
		Kurtosis:	16.11 Leptokurtic

<10%	<25%	<50%	<75%	<90%
1.658 µm	3.270 µm	6.748 µm	16.25 µm	53.07 µm

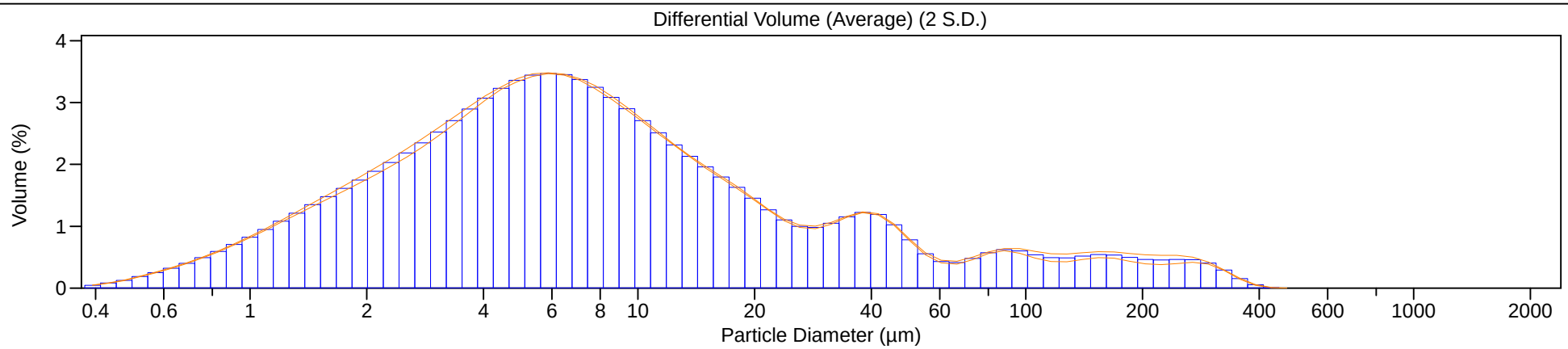

Beckman Coulter LS Particle Size Analyzer

6 Aug 2013

Heckathorn

File name:	C:\Users\Sam McWilliams\Desktop\sea_engineering\Sedflume\Heckathorne\Psd\4B-1__255.$av
	4B-1__255.$av
File ID:	4B-1
Operator:	Reyes
Comment 1:	Heckathorne
Comment 2:	mixed, blended
Optical model:	garnet.rf780z
LS 13 320 SW	Aqueous Liquid Module
	Run length: 60 seconds
Pump speed:	66
Fluid:	water
Average of 3 files:	
C:\LS13320\Projects\Heckathorne\4B-1__253.$ls	
C:\LS13320\Projects\Heckathorne\4B-1__254.$ls	
C:\LS13320\Projects\Heckathorne\4B-1__255.$ls	

Volume Statistics (Arithmetic) 4B-1__255.$av

Calculations from 0.375 µm to 2000 µm

Volume:	100%		
Mean:	14.64 µm	S.D.:	21.30 µm
Median:	6.431 µm	Variance:	453.5 μm^2
Mean/Median ratio:	2.276	C.V.:	145%
Mode:	5.355 µm	Skewness:	2.885 Right skewed
		Kurtosis:	9.149 Leptokurtic

<10%	<25%	<50%	<75%	<90%
1.585 µm	3.061 µm	6.431 µm	16.03 µm	38.48 µm

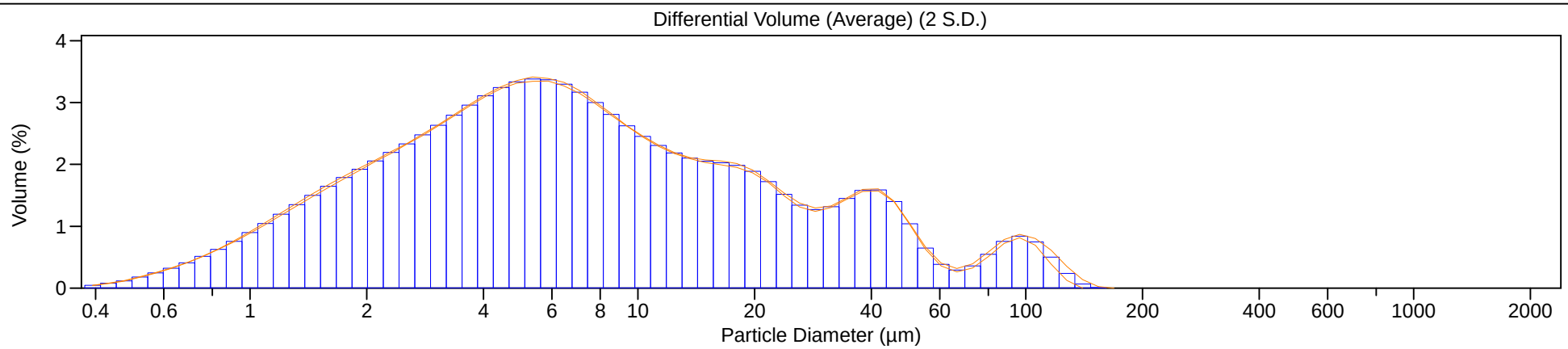

Beckman Coulter LS Particle Size Analyzer

6 Aug 2013

Heckathorn

File name:	C:\Users\Sam McWilliams\Desktop\sea_engineering\Sedflume\Heckathorne\Psd\4B-2__216.$av
	4B-2__216.$av
File ID:	4B-2
Operator:	Szesciorka
Comment 1:	Heckathorne
Comment 2:	mixed, blended
Optical model:	garnet.rf780z
LS 13 320 SW	Aqueous Liquid Module
	Run length: 60 seconds
Pump speed:	66
Fluid:	water
Average of 3 files:	
C:\LS13320\Projects\Heckathorne\4B-2__214.$ls	
C:\LS13320\Projects\Heckathorne\4B-2__215.$ls	
C:\LS13320\Projects\Heckathorne\4B-2__216.$ls	

Volume Statistics (Arithmetic) 4B-2__216.$av

Calculations from 0.375 µm to 2000 µm

Volume:	100%		
Mean:	13.28 µm	S.D.:	18.87 µm
Median:	6.225 µm	Variance:	356.2 μm^2
Mean/Median ratio:	2.133	C.V.:	142%
Mode:	5.878 µm	Skewness:	2.935 Right skewed
		Kurtosis:	9.652 Leptokurtic

<10%	<25%	<50%	<75%	<90%
1.554 µm	2.993 µm	6.225 µm	14.53 µm	34.35 µm

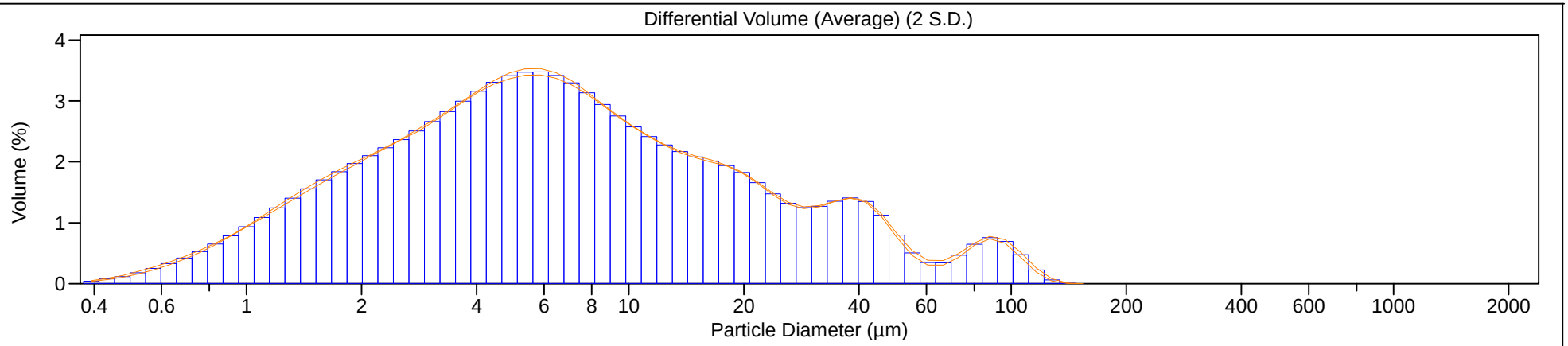

Beckman Coulter LS Particle Size Analyzer

6 Aug 2013

Heckathorn

File name:	C:\Users\Sam McWilliams\Desktop\sea_engineering\Sedflume\Heckathorne\Psd\4B-3__219.$av
	4B-3__219.$av
File ID:	4B-3
Operator:	Reyes
Comment 1:	Heckathorne
Comment 2:	mixed, blended
Optical model:	garnet.rf780z
LS 13 320 SW	Aqueous Liquid Module
	Run length: 60 seconds
Pump speed:	66
Fluid:	water
Average of 3 files:	
C:\LS13320\Projects\Heckathorne\4B-3__217.$ls	
C:\LS13320\Projects\Heckathorne\4B-3__218.$ls	
C:\LS13320\Projects\Heckathorne\4B-3__219.$ls	

Volume Statistics (Arithmetic) 4B-3__219.$av

Calculations from 0.375 µm to 2000 µm

Volume:	100%		
Mean:	25.50 µm	S.D.:	53.01 µm
Median:	7.088 µm	Variance:	2810 μm^2
Mean/Median ratio:	3.598	C.V.:	208%
Mode:	5.355 µm	Skewness:	3.863 Right skewed
		Kurtosis:	16.46 Leptokurtic

<10%	<25%	<50%	<75%	<90%
1.629 µm	3.199 µm	7.088 µm	19.57 µm	59.70 µm

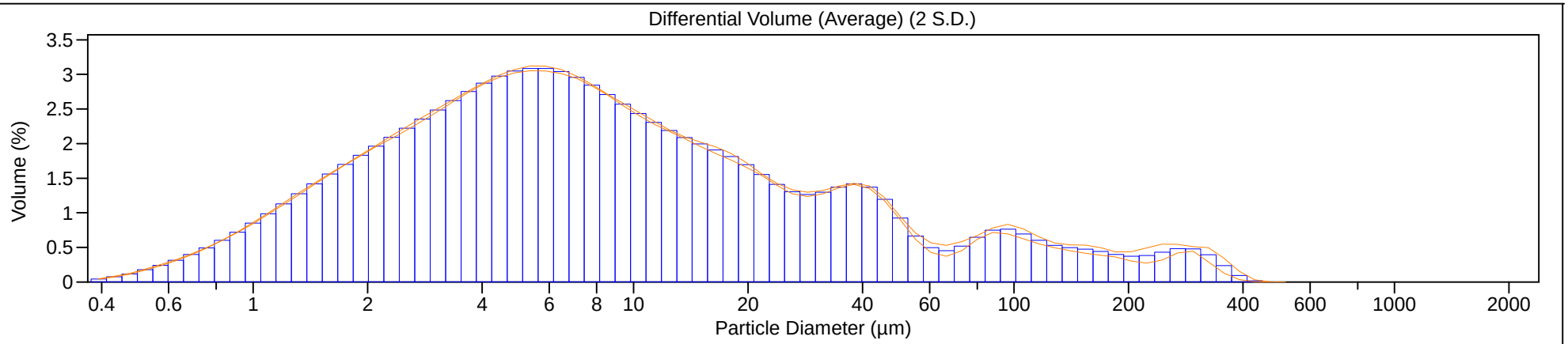

Beckman Coulter LS Particle Size Analyzer

6 Aug 2013

Heckathorn

File name:	C:\Users\Sam McWilliams\Desktop\sea_engineering\Sedflume\Heckathorne\Psd\4B-4__231.$av
	4B-4__231.$av
File ID:	4B-4
Operator:	Reyes
Comment 1:	Heckathorne
Comment 2:	mixed, blended
Optical model:	garnet.rf780z
LS 13 320 SW	Aqueous Liquid Module
	Run length: 60 seconds
Pump speed:	66
Fluid:	water
Average of 3 files:	
C:\LS13320\Projects\Heckathorne\4B-4__229.$ls	
C:\LS13320\Projects\Heckathorne\4B-4__230.$ls	
C:\LS13320\Projects\Heckathorne\4B-4__231.$ls	

Volume Statistics (Arithmetic) 4B-4__231.$av

Calculations from 0.375 µm to 2000 µm

Volume:	100%		
Mean:	24.05 µm	S.D.:	36.59 µm
Median:	8.778 µm	Variance:	1339 μm^2
Mean/Median ratio:	2.740	C.V.:	152%
Mode:	5.878 µm	Skewness:	2.608 Right skewed
		Kurtosis:	6.946 Leptokurtic

<10%	<25%	<50%	<75%	<90%
1.853 µm	3.787 µm	8.778 µm	26.73 µm	65.90 µm

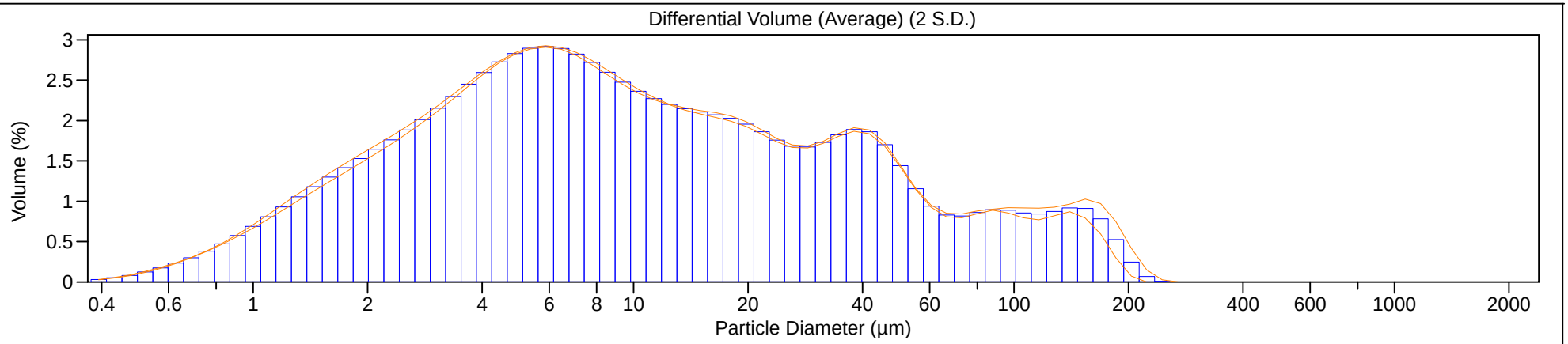

Beckman Coulter LS Particle Size Analyzer

6 Aug 2013

Heckathorn

File name:	C:\Users\Sam McWilliams\Desktop\sea_engineering\Sedflume\Heckathorne\Psd\4B-5__258.$av
	4B-5__258.$av
File ID:	4B-5
Operator:	Reyes
Comment 1:	Heckathorne
Comment 2:	mixed, blended
Optical model:	garnet.rf780z
LS 13 320 SW	Aqueous Liquid Module
	Run length: 60 seconds
Pump speed:	66
Fluid:	water
Average of 3 files:	
C:\LS13320\Projects\Heckathorne\4B-5__256.$ls	
C:\LS13320\Projects\Heckathorne\4B-5__257.$ls	
C:\LS13320\Projects\Heckathorne\4B-5__258.$ls	

Volume Statistics (Arithmetic) 4B-5__258.$av

Calculations from 0.375 µm to 2000 µm

Volume:	100%		
Mean:	24.09 µm	S.D.:	40.34 µm
Median:	9.132 µm	Variance:	1627 μm^2
Mean/Median ratio:	2.638	C.V.:	167%
Mode:	5.878 µm	Skewness:	3.856 Right skewed
		Kurtosis:	20.08 Leptokurtic

<10%	<25%	<50%	<75%	<90%
1.889 µm	3.863 µm	9.132 µm	25.86 µm	59.50 µm

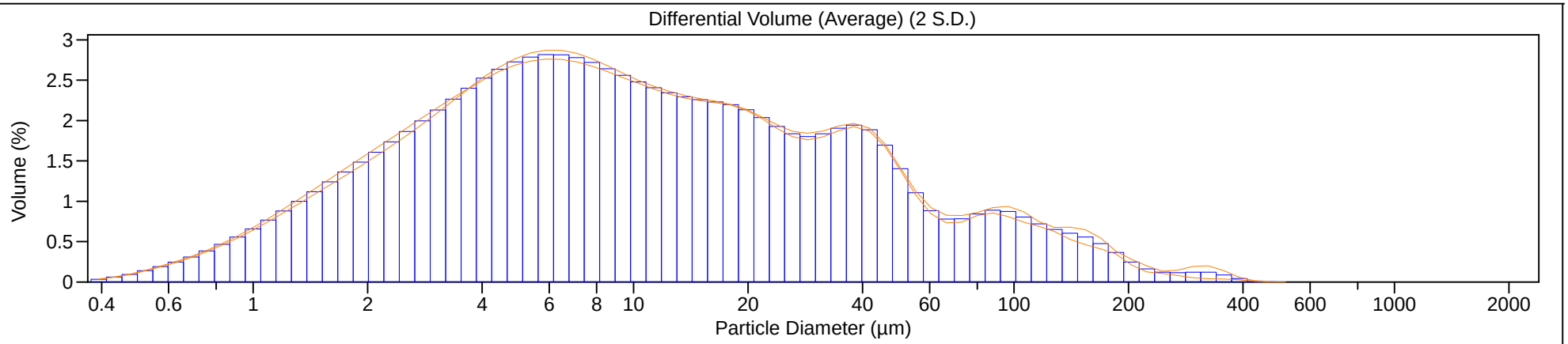

Beckman Coulter LS Particle Size Analyzer

6 Aug 2013

Heckathorn

File name:	C:\Users\Sam McWilliams\Desktop\sea_engineering\Sedflume\Heckathorne\Psd\4B-6__225.$av
	4B-6__225.$av
File ID:	4B-6
Operator:	Reyes
Comment 1:	Heckathorne
Comment 2:	mixed, blended
Optical model:	garnet.rf780z
LS 13 320 SW	Aqueous Liquid Module
	Run length: 60 seconds
Pump speed:	66
Fluid:	water
Average of 3 files:	
C:\LS13320\Projects\Heckathorne\4B-6__223.$ls	
C:\LS13320\Projects\Heckathorne\4B-6__224.$ls	
C:\LS13320\Projects\Heckathorne\4B-6__225.$ls	

Volume Statistics (Arithmetic) 4B-6__225.$av

Calculations from 0.375 µm to 2000 µm

Volume:	100%		
Mean:	43.63 µm	S.D.:	71.77 µm
Median:	13.05 µm	Variance:	5151 μm^2
Mean/Median ratio:	3.344	C.V.:	164%
Mode:	5.878 µm	Skewness:	3.654 Right skewed
		Kurtosis:	18.06 Leptokurtic

<10%	<25%	<50%	<75%	<90%
2.075 µm	4.459 µm	13.05 µm	56.38 µm	120.6 µm

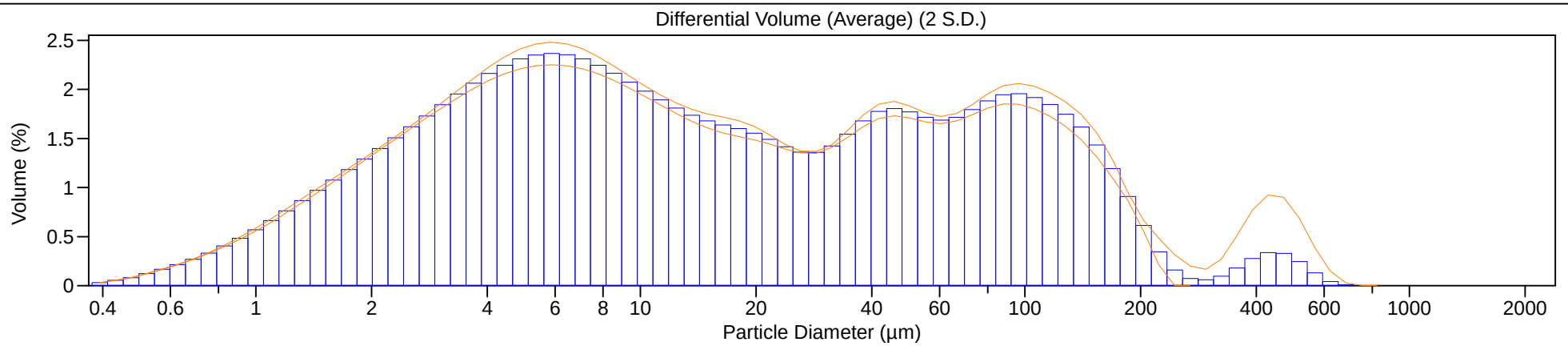

Beckman Coulter LS Particle Size Analyzer

6 Aug 2013

Heckathorn

File name:	C:\Users\Sam McWilliams\Desktop\sea_engineering\Sedflume\Heckathorne\Psd\4B-6__228.$av
	4B-6__228.$av
File ID:	4B-6
Operator:	Reyes
Comment 1:	Heckathorne
Comment 2:	mixed, blended
Optical model:	garnet.rf780z
LS 13 320 SW	Aqueous Liquid Module
	Run length: 60 seconds
Pump speed:	66
Fluid:	water
Average of 3 files:	
C:\LS13320\Projects\Heckathorne\4B-6__226.$ls	
C:\LS13320\Projects\Heckathorne\4B-6__227.$ls	
C:\LS13320\Projects\Heckathorne\4B-6__228.$ls	

Volume Statistics (Arithmetic) 4B-6__228.$av

Calculations from 0.375 µm to 2000 µm

Volume:	100%		
Mean:	44.58 µm	S.D.:	74.14 µm
Median:	12.99 µm	Variance:	5496 μm^2
Mean/Median ratio:	3.431	C.V.:	166%
Mode:	5.878 µm	Skewness:	3.477 Right skewed
		Kurtosis:	15.50 Leptokurtic

<10%	<25%	<50%	<75%	<90%
2.057 µm	4.407 µm	12.99 µm	56.21 µm	121.6 µm

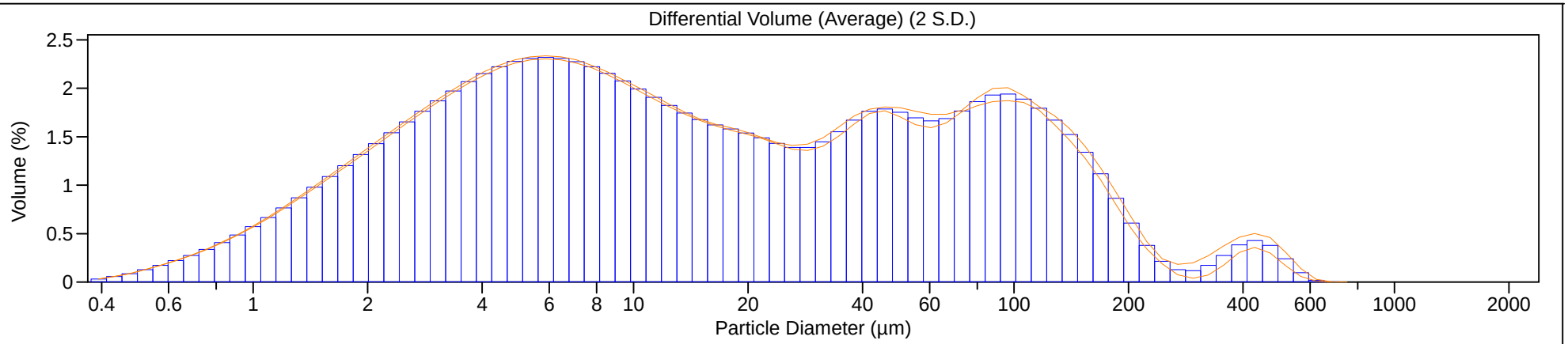

Beckman Coulter LS Particle Size Analyzer

6 Aug 2013

Heckathorn

File name:	C:\Users\Sam McWilliams\Desktop\sea_engineering\Sedflume\Heckathorne\Psd\5B-14__334.$av
	5B-14__334.$av
File ID:	5B-14
Operator:	Reyes/Szesciorka
Comment 1:	Heckathorne
Comment 2:	mixed, blended
Optical model:	garnet.rf780z
LS 13 320 SW	Aqueous Liquid Module
	Run length: 60 seconds
Pump speed:	66
Fluid:	water
Average of 3 files:	
C:\LS13320\Projects\Heckathorne\5B-14__332.$ls	
C:\LS13320\Projects\Heckathorne\5B-14__333.$ls	
C:\LS13320\Projects\Heckathorne\5B-14__334.$ls	

Volume Statistics (Arithmetic) 5B-14__334.$av

Calculations from 0.375 µm to 2000 µm

Volume:	100%		
Mean:	28.13 µm	S.D.:	63.46 µm
Median:	6.751 µm	Variance:	4027 μm^2
Mean/Median ratio:	4.167	C.V.:	226%
Mode:	5.355 µm	Skewness:	3.762 Right skewed
		Kurtosis:	14.50 Leptokurtic

<10%	<25%	<50%	<75%	<90%
1.616 µm	3.114 µm	6.751 µm	18.73 µm	57.84 µm

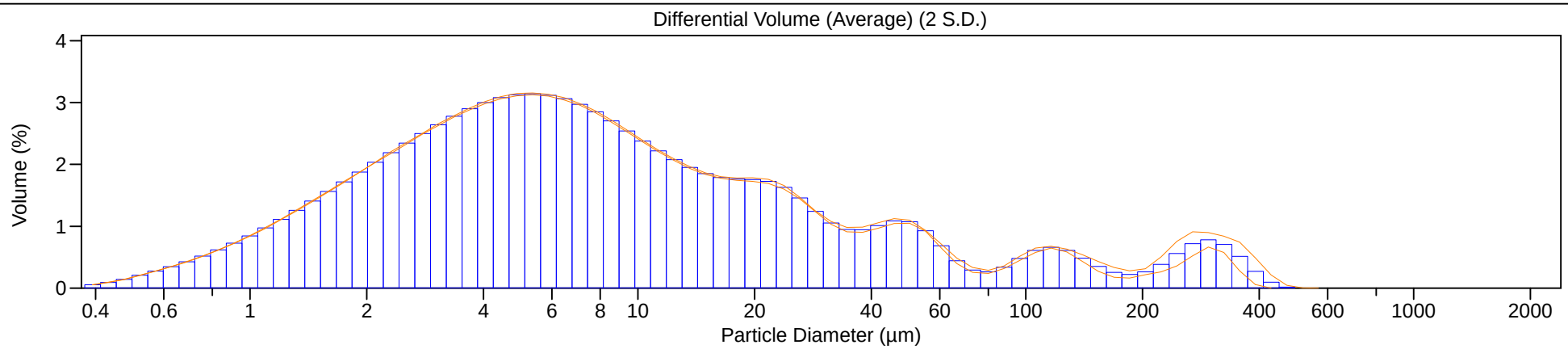

Beckman Coulter LS Particle Size Analyzer

6 Aug 2013

Heckathorn

File name:	C:\Users\Sam McWilliams\Desktop\sea_engineering\Sedflume\Heckathorne\Psd\5B-2__349.$av
	5B-2__349.$av
File ID:	5B-2
Operator:	Reyes/Szesciorka
Comment 1:	Heckathorne
Comment 2:	mixed, blended
Optical model:	garnet.rf780z
LS 13 320 SW	Aqueous Liquid Module
	Run length: 60 seconds
Pump speed:	66
Fluid:	water
Average of 3 files:	
C:\LS13320\Projects\Heckathorne\5B-2__347.$ls	
C:\LS13320\Projects\Heckathorne\5B-2__348.$ls	
C:\LS13320\Projects\Heckathorne\5B-2__349.$ls	

Volume Statistics (Arithmetic) 5B-2__349.$av

Calculations from 0.375 µm to 2000 µm

Volume:	100%		
Mean:	20.47 µm	S.D.:	34.79 µm
Median:	6.885 µm	Variance:	1211 μm^2
Mean/Median ratio:	2.973	C.V.:	170%
Mode:	5.878 µm	Skewness:	2.954 Right skewed
		Kurtosis:	9.110 Leptokurtic

<10%	<25%	<50%	<75%	<90%
1.646 µm	3.254 µm	6.885 µm	18.05 µm	56.71 µm

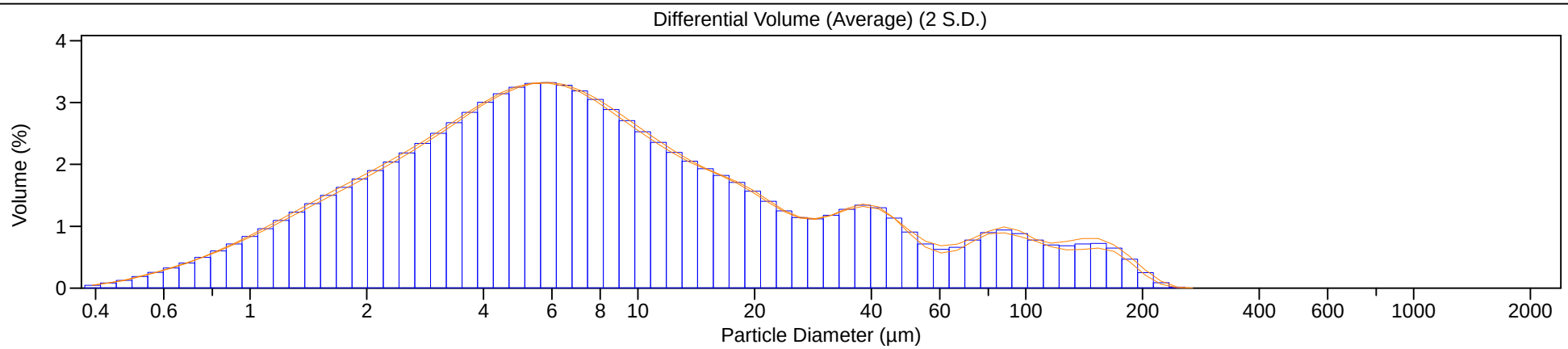

Beckman Coulter LS Particle Size Analyzer

6 Aug 2013

Heckathorn

File name:	C:\Users\Sam McWilliams\Desktop\sea_engineering\Sedflume\Heckathorne\Psd\5B-3__313.$av
	5B-3__313.$av
File ID:	5B-3
Operator:	Reyes/Szesciorka
Comment 1:	Heckathorne
Comment 2:	mixed, blended
Optical model:	garnet.rf780z
LS 13 320 SW	Aqueous Liquid Module
	Run length: 60 seconds
Pump speed:	66
Fluid:	water

Average of 3 files:
C:\LS13320\Projects\Heckathorne\5B-3__311.$ls
C:\LS13320\Projects\Heckathorne\5B-3__312.$ls
C:\LS13320\Projects\Heckathorne\5B-3__313.$ls

Volume Statistics (Arithmetic) 5B-3__313.$av

Calculations from 0.375 µm to 2000 µm

Volume:	100%		
Mean:	39.74 µm	S.D.:	66.31 µm
Median:	11.49 µm	Variance:	4396 μm^2
Mean/Median ratio:	3.458	C.V.:	167%
Mode:	21.70 µm	Skewness:	2.682 Right skewed
		Kurtosis:	7.506 Leptokurtic

<10%	<25%	<50%	<75%	<90%
1.870 µm	4.137 µm	11.49 µm	46.03 µm	124.4 µm

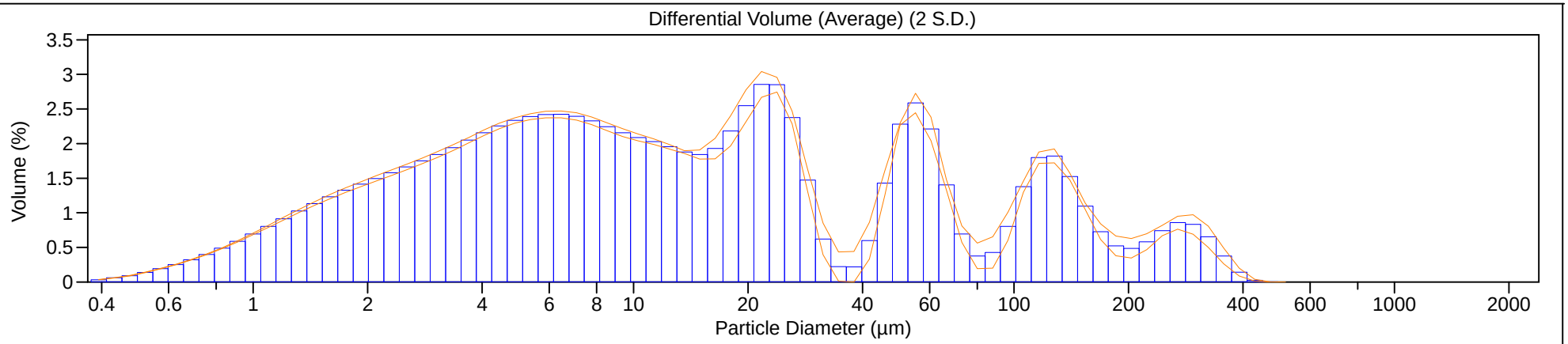

Beckman Coulter LS Particle Size Analyzer

6 Aug 2013

Heckathorn

File name:	C:\Users\Sam McWilliams\Desktop\sea_engineering\Sedflume\Heckathorne\Psd\5B-4__325.$av
	5B-4__325.$av
File ID:	5B-4
Operator:	Reyes/Szesciorka
Comment 1:	Heckathorne
Comment 2:	mixed, blended
Optical model:	garnet.rf780z
LS 13 320 SW	Aqueous Liquid Module
	Run length: 60 seconds
Pump speed:	66
Fluid:	water
Average of 3 files:	
C:\LS13320\Projects\Heckathorne\5B-4__323.$ls	
C:\LS13320\Projects\Heckathorne\5B-4__324.$ls	
C:\LS13320\Projects\Heckathorne\5B-4__325.$ls	

Volume Statistics (Arithmetic) 5B-4__325.$av

Calculations from 0.375 µm to 2000 µm

Volume:	100%		
Mean:	14.42 µm	S.D.:	21.40 µm
Median:	6.120 µm	Variance:	458.0 µm^2
Mean/Median ratio:	2.356	C.V.:	148%
Mode:	5.355 µm	Skewness:	3.084 Right skewed
		Kurtosis:	11.35 Leptokurtic

<10%	<25%	<50%	<75%	<90%
1.426 µm	2.741 µm	6.120 µm	16.24 µm	38.31 µm

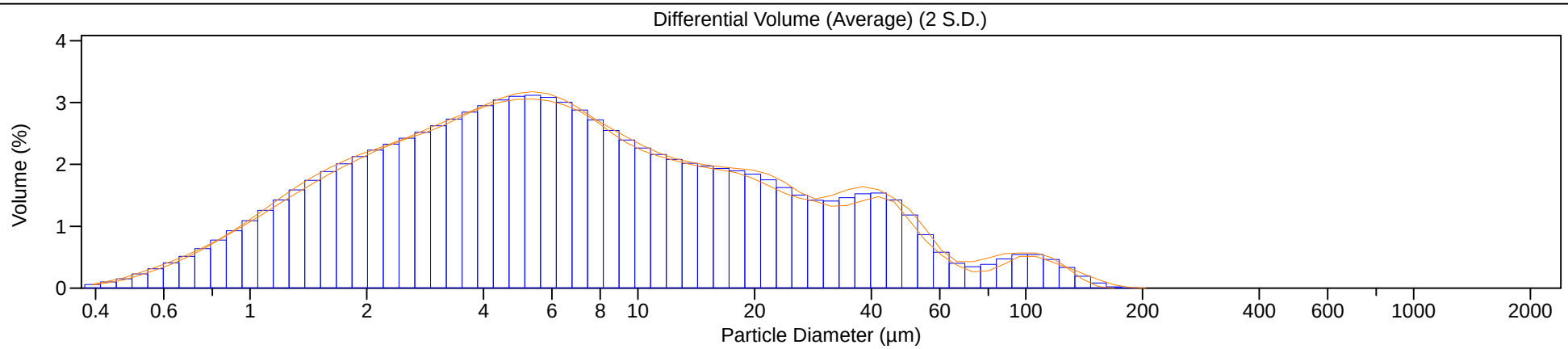

Beckman Coulter LS Particle Size Analyzer

6 Aug 2013

Heckathorn

File name:	C:\Users\Sam McWilliams\Desktop\sea_engineering\Sedflume\Heckathorne\Psd\5B-5__340.$av
	5B-5__340.$av
File ID:	5B-5
Operator:	Reyes/Szesciorka
Comment 1:	Heckathorne
Comment 2:	mixed, blended
Optical model:	garnet.rf780z
LS 13 320 SW	Aqueous Liquid Module
	Run length: 60 seconds
Pump speed:	66
Fluid:	water
Average of 3 files:	
C:\LS13320\Projects\Heckathorne\5B-5__338.$ls	
C:\LS13320\Projects\Heckathorne\5B-5__339.$ls	
C:\LS13320\Projects\Heckathorne\5B-5__340.$ls	

Volume Statistics (Arithmetic) 5B-5__340.$av

Calculations from 0.375 µm to 2000 µm

Volume:	100%		
Mean:	52.87 µm	S.D.:	104.3 µm
Median:	8.400 µm	Variance:	10880 μm^2
Mean/Median ratio:	6.294	C.V.:	197%
Mode:	5.355 µm	Skewness:	2.762 Right skewed
		Kurtosis:	7.635 Leptokurtic

<10%	<25%	<50%	<75%	<90%
1.650 µm	3.448 µm	8.400 µm	37.13 µm	197.2 µm

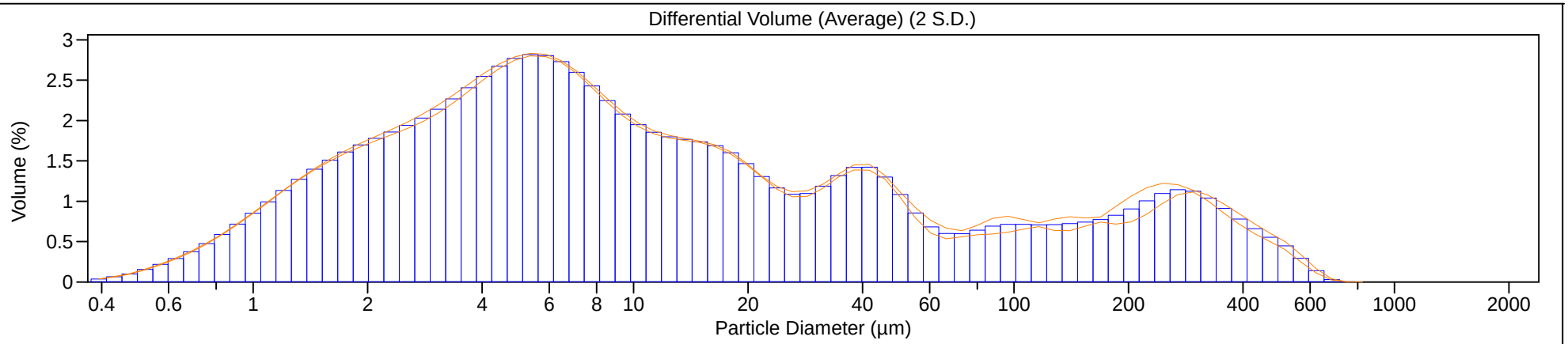

Beckman Coulter LS Particle Size Analyzer

6 Aug 2013

Heckathorn

File name:	C:\Users\Sam McWilliams\Desktop\sea_engineering\Sedflume\Heckathorne\Psd\6-1__279.$av
	6-1__279.$av
File ID:	6-1
Operator:	Reyes
Comment 1:	Heckathorne
Comment 2:	mixed, blended
Optical model:	garnet.rf780z
LS 13 320 SW	Aqueous Liquid Module
	Run length: 60 seconds
Pump speed:	66
Fluid:	water
Average of 3 files:	
C:\LS13320\Projects\Heckathorne\6-1__277.$ls	
C:\LS13320\Projects\Heckathorne\6-1__278.$ls	
C:\LS13320\Projects\Heckathorne\6-1__279.$ls	

Volume Statistics (Arithmetic) 6-1__279.$av

Calculations from 0.375 µm to 2000 µm

Volume:	100%		
Mean:	9.207 µm	S.D.:	9.924 µm
Median:	5.563 µm	Variance:	98.48 μm^2
Mean/Median ratio:	1.655	C.V.:	108%
Mode:	5.355 µm	Skewness:	2.037 Right skewed
		Kurtosis:	4.109 Leptokurtic

<10%	<25%	<50%	<75%	<90%
1.512 µm	2.813 µm	5.563 µm	11.25 µm	22.94 µm

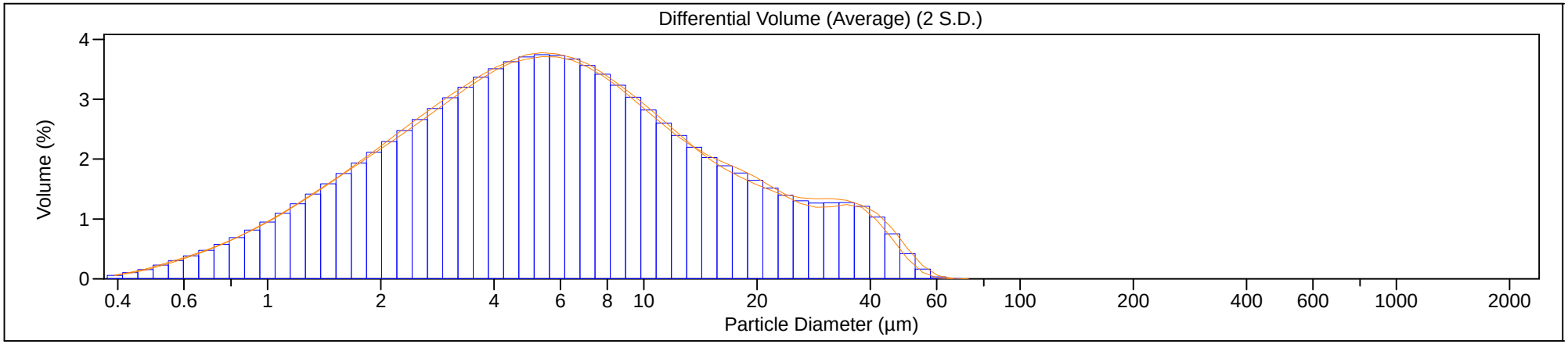

Beckman Coulter LS Particle Size Analyzer

6 Aug 2013

Heckathorn

File name:	C:\Users\Sam McWilliams\Desktop\sea_engineering\Sedflume\Heckathorne\Psd\6-2__213.$av
	6-2__213.$av
File ID:	6-2
Operator:	Szesciorka
Comment 1:	Heckathorne
Comment 2:	mixed, blended
Optical model:	garnet.rf780z
LS 13 320 SW	Aqueous Liquid Module
	Run length: 60 seconds
Pump speed:	66
Fluid:	water
Average of 3 files:	
C:\LS13320\Projects\Heckathorne\6-2__211.$ls	
C:\LS13320\Projects\Heckathorne\6-2__212.$ls	
C:\LS13320\Projects\Heckathorne\6-2__213.$ls	

Volume Statistics (Arithmetic) 6-2__213.$av

Calculations from 0.375 µm to 2000 µm

Volume:	100%		
Mean:	10.28 µm	S.D.:	13.24 µm
Median:	5.498 µm	Variance:	175.4 µm^2
Mean/Median ratio:	1.869	C.V.:	129%
Mode:	5.355 µm	Skewness:	3.028 Right skewed
		Kurtosis:	12.32 Leptokurtic

<10%	<25%	<50%	<75%	<90%
1.461 µm	2.729 µm	5.498 µm	11.63 µm	25.92 µm

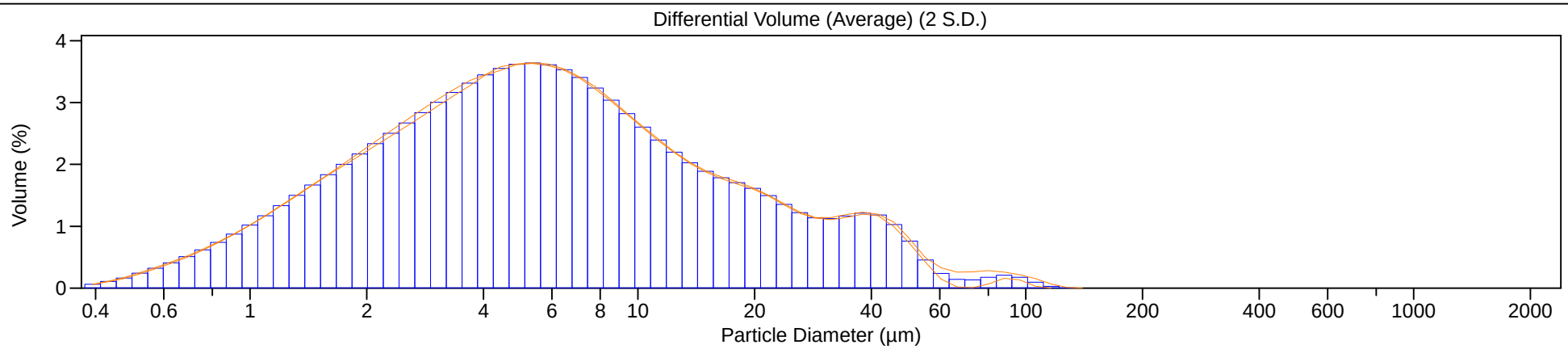

Beckman Coulter LS Particle Size Analyzer

6 Aug 2013

Heckathorn

File name:	C:\Users\Sam McWilliams\Desktop\sea_engineering\Sedflume\Heckathorne\Psd\6-3__240.$av
	6-3__240.$av
File ID:	6-3
Operator:	Reyes
Comment 1:	Heckathorne
Comment 2:	mixed, blended
Optical model:	garnet.rf780z
LS 13 320 SW	Aqueous Liquid Module
	Run length: 60 seconds
Pump speed:	66
Fluid:	water
Average of 3 files:	
C:\LS13320\Projects\Heckathorne\6-3__238.$ls	
C:\LS13320\Projects\Heckathorne\6-3__239.$ls	
C:\LS13320\Projects\Heckathorne\6-3__240.$ls	

Volume Statistics (Arithmetic) 6-3__240.$av

Calculations from 0.375 µm to 2000 µm

Volume:	100%		
Mean:	14.67 µm	S.D.:	23.60 µm
Median:	6.515 µm	Variance:	556.9 μm^2
Mean/Median ratio:	2.251	C.V.:	161%
Mode:	5.878 µm	Skewness:	3.506 Right skewed
		Kurtosis:	14.08 Leptokurtic

<10%	<25%	<50%	<75%	<90%
1.742 µm	3.317 µm	6.515 µm	13.91 µm	36.30 µm

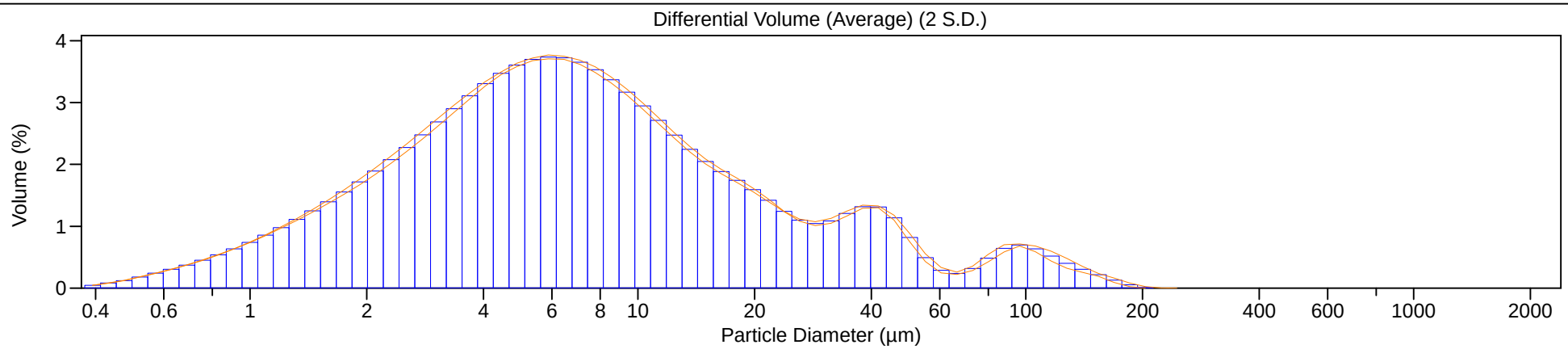

Beckman Coulter LS Particle Size Analyzer

6 Aug 2013

Heckathorn

File name:	C:\Users\Sam McWilliams\Desktop\sea_engineering\Sedflume\Heckathorne\Psd\6-4__243.$av
	6-4__243.$av
File ID:	6-4
Operator:	Reyes
Comment 1:	Heckathorne
Comment 2:	mixed, blended
Optical model:	garnet.rf780z
LS 13 320 SW	Aqueous Liquid Module
	Run length: 60 seconds
Pump speed:	66
Fluid:	water
Average of 3 files:	
C:\LS13320\Projects\Heckathorne\6-4__241.$ls	
C:\LS13320\Projects\Heckathorne\6-4__242.$ls	
C:\LS13320\Projects\Heckathorne\6-4__243.$ls	

Volume Statistics (Arithmetic) 6-4__243.$av

Calculations from 0.375 µm to 2000 µm

Volume:	100%		
Mean:	12.87 µm	S.D.:	19.57 µm
Median:	5.795 µm	Variance:	383.0 μm^2
Mean/Median ratio:	2.221	C.V.:	152%
Mode:	5.355 µm	Skewness:	3.272 Right skewed
		Kurtosis:	12.47 Leptokurtic

<10%	<25%	<50%	<75%	<90%
1.573 µm	2.929 µm	5.795 µm	12.73 µm	34.27 µm

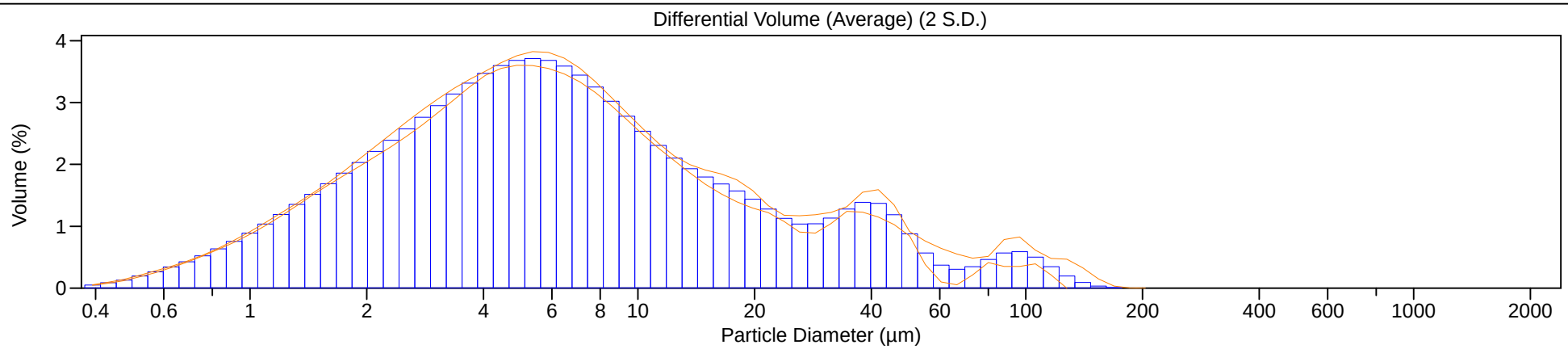

Beckman Coulter LS Particle Size Analyzer

6 Aug 2013

Heckathorn

File name:	C:\Users\Sam McWilliams\Desktop\sea_engineering\Sedflume\Heckathorne\Psd\6-5__198.$av
	6-5__198.$av
File ID:	6-5
Operator:	Szesciorka
Comment 1:	Heckathorne
Comment 2:	mixed, blended
Optical model:	garnet.rf780z
LS 13 320 SW	Aqueous Liquid Module
	Run length: 60 seconds
Pump speed:	66
Fluid:	water
Average of 3 files:	
C:\LS13320\Projects\Heckathorne\6-5__196.$ls	
C:\LS13320\Projects\Heckathorne\6-5__197.$ls	
C:\LS13320\Projects\Heckathorne\6-5__198.$ls	

Volume Statistics (Arithmetic) 6-5__198.$av

Calculations from 0.375 µm to 2000 µm

Volume:	100%		
Mean:	14.95 µm	S.D.:	23.50 µm
Median:	6.361 µm	Variance:	552.0 µm^2
Mean/Median ratio:	2.351	C.V.:	157%
Mode:	5.355 µm	Skewness:	3.256 Right skewed
		Kurtosis:	11.99 Leptokurtic

<10%	<25%	<50%	<75%	<90%
1.625 µm	3.112 µm	6.361 µm	14.93 µm	38.44 µm

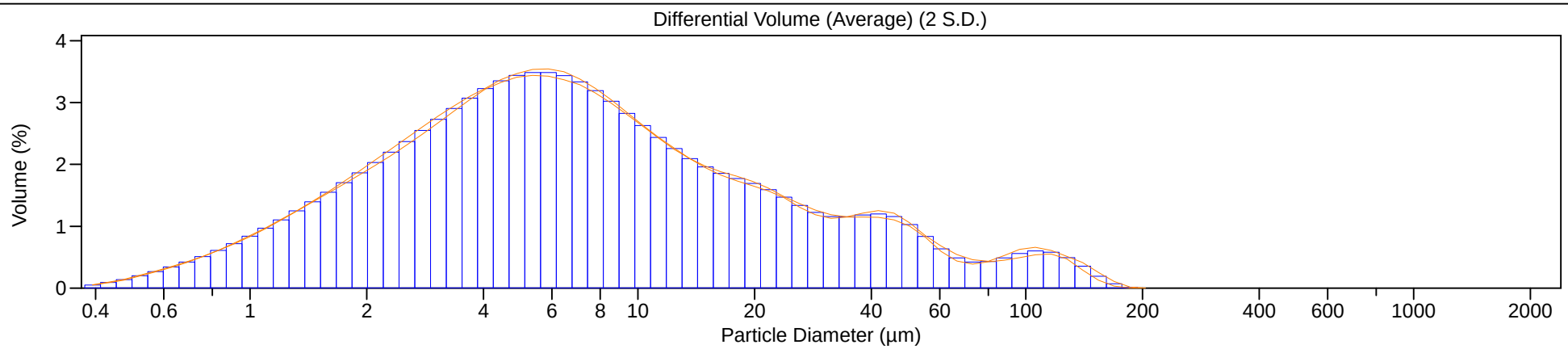

Beckman Coulter LS Particle Size Analyzer

6 Aug 2013

Heckathorn

File name:	C:\Users\Sam McWilliams\Desktop\sea_engineering\Sedflume\Heckathorne\Psd\7-1__316.$av
	7-1__316.$av
File ID:	7-1
Operator:	Reyes/Szesciorka
Comment 1:	Heckathorne
Comment 2:	mixed, blended
Optical model:	garnet.rf780z
LS 13 320 SW	Aqueous Liquid Module
	Run length: 60 seconds
Pump speed:	66
Fluid:	water
Average of 3 files:	
C:\LS13320\Projects\Heckathorne\7-1__314.$ls	
C:\LS13320\Projects\Heckathorne\7-1__315.$ls	
C:\LS13320\Projects\Heckathorne\7-1__316.$ls	

Volume Statistics (Arithmetic) 7-1__316.$av

Calculations from 0.375 µm to 2000 µm

Volume:	100%		
Mean:	12.83 µm	S.D.:	18.07 µm
Median:	6.142 µm	Variance:	326.5 µm^2
Mean/Median ratio:	2.088	C.V.:	141%
Mode:	5.878 µm	Skewness:	3.213 Right skewed
		Kurtosis:	13.93 Leptokurtic

<10%	<25%	<50%	<75%	<90%
1.570 µm	3.030 µm	6.142 µm	14.98 µm	27.02 µm

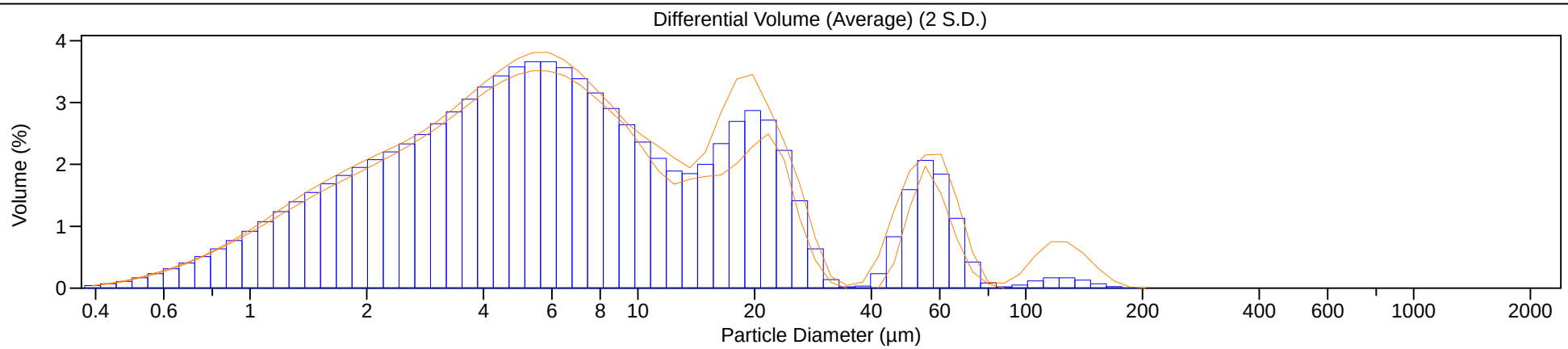

Beckman Coulter LS Particle Size Analyzer

6 Aug 2013

Heckathorn

File name:	C:\Users\Sam McWilliams\Desktop\sea_engineering\Sedflume\Heckathorne\Psd\7-2__310.$av
	7-2__310.$av
File ID:	7-2
Operator:	Reyes/Szesciorka
Comment 1:	Heckathorne
Comment 2:	mixed, blended
Optical model:	garnet.rf780z
LS 13 320 SW	Aqueous Liquid Module
	Run length: 60 seconds
Pump speed:	66
Fluid:	water
Average of 3 files:	
C:\LS13320\Projects\Heckathorne\7-2__308.$ls	
C:\LS13320\Projects\Heckathorne\7-2__309.$ls	
C:\LS13320\Projects\Heckathorne\7-2__310.$ls	

Volume Statistics (Arithmetic) 7-2__310.$av

Calculations from 0.375 µm to 2000 µm

Volume:	100%		
Mean:	10.19 µm	S.D.:	12.77 µm
Median:	5.401 µm	Variance:	163.1 μm^2
Mean/Median ratio:	1.887	C.V.:	125%
Mode:	5.355 µm	Skewness:	2.440 Right skewed
		Kurtosis:	5.992 Leptokurtic

<10%	<25%	<50%	<75%	<90%
1.431 µm	2.654 µm	5.401 µm	11.74 µm	24.18 µm

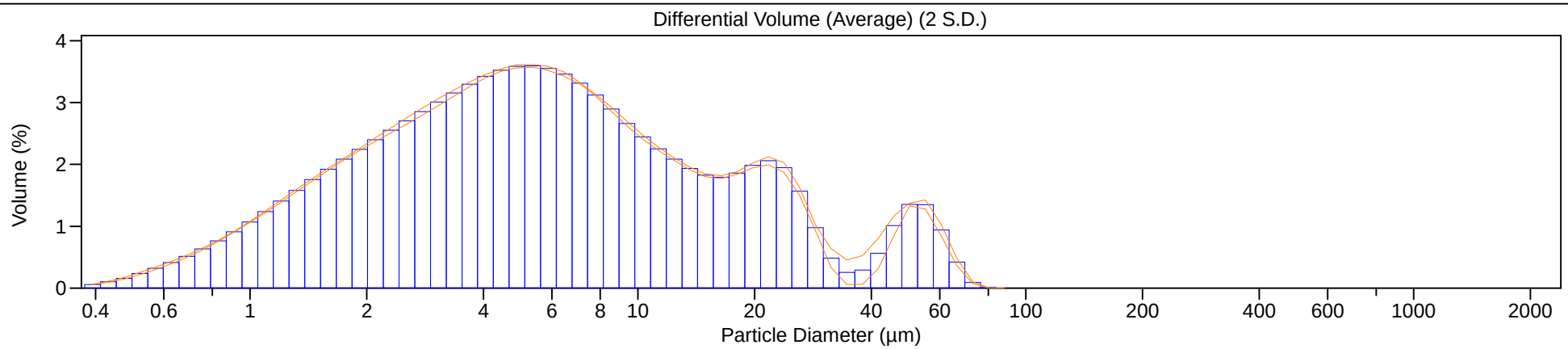

Beckman Coulter LS Particle Size Analyzer

6 Aug 2013

Heckathorn

File name:	C:\Users\Sam McWilliams\Desktop\sea_engineering\Sedflume\Heckathorne\Psd\7-3__337.$av
	7-3__337.$av
File ID:	7-3
Operator:	Reyes/Szesciorka
Comment 1:	Heckathorne
Comment 2:	mixed, blended
Optical model:	garnet.rf780z
LS 13 320 SW	Aqueous Liquid Module
	Run length: 60 seconds
Pump speed:	66
Fluid:	water
Average of 3 files:	
C:\LS13320\Projects\Heckathorne\7-3__335.$ls	
C:\LS13320\Projects\Heckathorne\7-3__336.$ls	
C:\LS13320\Projects\Heckathorne\7-3__337.$ls	

Volume Statistics (Arithmetic) 7-3__337.$av

Calculations from 0.375 µm to 2000 µm

Volume:	100%		
Mean:	27.40 µm	S.D.:	54.29 µm
Median:	7.394 µm	Variance:	2947 μm^2
Mean/Median ratio:	3.705	C.V.:	198%
Mode:	5.878 µm	Skewness:	3.530 Right skewed
		Kurtosis:	13.61 Leptokurtic

<10%	<25%	<50%	<75%	<90%
1.753 µm	3.475 µm	7.394 µm	21.19 µm	72.69 µm

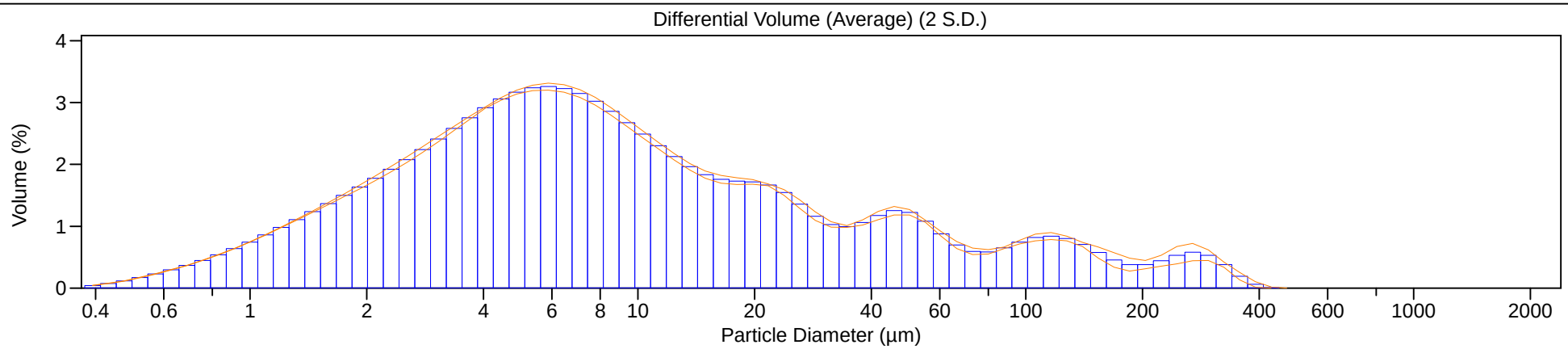

Beckman Coulter LS Particle Size Analyzer

6 Aug 2013

Heckathorn

File name:	C:\Users\Sam McWilliams\Desktop\sea_engineering\Sedflume\Heckathorne\Psd\7-4__03.$av
	7-4__03.$av
File ID:	7-4
Operator:	Szesciorka
Comment 1:	Heckathorne
Comment 2:	mixed, sonicated
Optical model:	garnet.rf780z
LS 13 320 SW	Aqueous Liquid Module
	Run length: 60 seconds
Pump speed:	66
Fluid:	water
Average of 3 files:	
C:\LS13320\Projects\Heckathorne\7-4__01.$ls	
C:\LS13320\Projects\Heckathorne\7-4__02.$ls	
C:\LS13320\Projects\Heckathorne\7-4__03.$ls	

Volume Statistics (Arithmetic) 7-4__03.$av

Calculations from 0.375 µm to 2000 µm

Volume:	100%		
Mean:	30.53 µm	S.D.:	53.33 µm
Median:	9.310 µm	Variance:	2844 μm^2
Mean/Median ratio:	3.279	C.V.:	175%
Mode:	6.453 µm	Skewness:	3.046 Right skewed
		Kurtosis:	10.02 Leptokurtic

<10%	<25%	<50%	<75%	<90%
1.976 µm	4.039 µm	9.310 µm	27.24 µm	90.46 µm

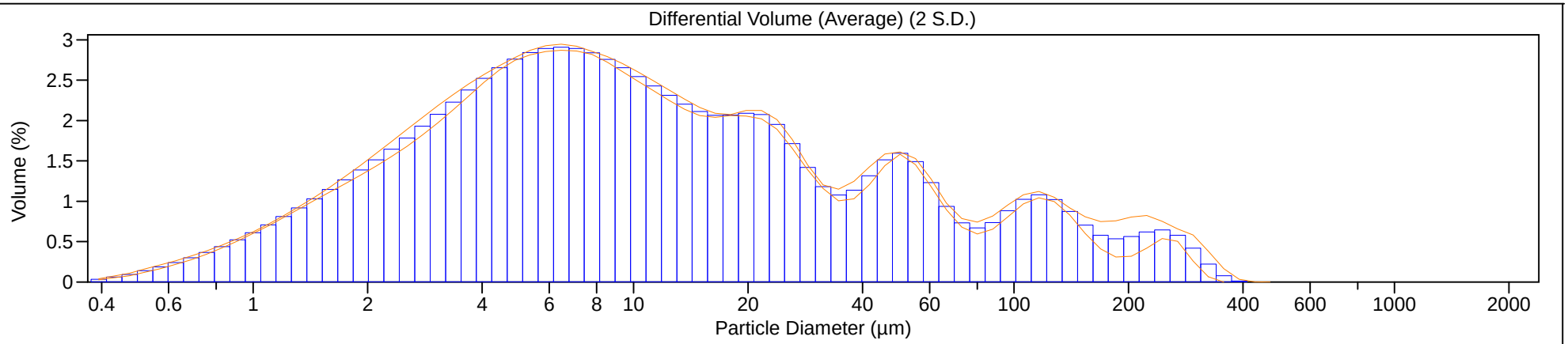

Beckman Coulter LS Particle Size Analyzer

6 Aug 2013

Heckathorn

File name:	C:\Users\Sam McWilliams\Desktop\sea_engineering\Sedflume\Heckathorne\Psd\7-5__343.$av
	7-5__343.$av
File ID:	7-5
Operator:	Reyes/Szesciorka
Comment 1:	Heckathorne
Comment 2:	mixed, blended
Optical model:	garnet.rf780z
LS 13 320 SW	Aqueous Liquid Module
	Run length: 60 seconds
Pump speed:	66
Fluid:	water
Average of 3 files:	
C:\LS13320\Projects\Heckathorne\7-5__341.$ls	
C:\LS13320\Projects\Heckathorne\7-5__342.$ls	
C:\LS13320\Projects\Heckathorne\7-5__343.$ls	

Volume Statistics (Arithmetic) 7-5__343.$av

Calculations from 0.375 µm to 2000 µm

Volume:	100%		
Mean:	13.13 µm	S.D.:	19.72 µm
Median:	6.009 µm	Variance:	389.0 μm^2
Mean/Median ratio:	2.185	C.V.:	150%
Mode:	5.355 µm	Skewness:	3.182 Right skewed
		Kurtosis:	11.34 Leptokurtic

<10%	<25%	<50%	<75%	<90%
1.541 µm	2.958 µm	6.009 µm	13.52 µm	33.82 µm

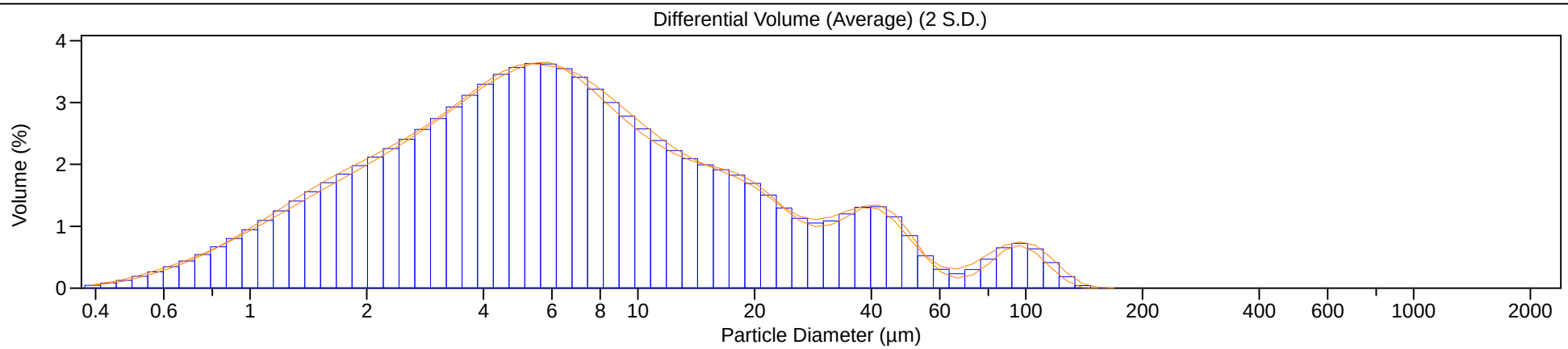

Beckman Coulter LS Particle Size Analyzer

6 Aug 2013

Heckathorn

File name:	C:\Users\Sam McWilliams\Desktop\sea_engineering\Sedflume\Heckathorne\Psd\8-1__246.$av
	8-1__246.$av
File ID:	8-1
Operator:	Reyes
Comment 1:	Heckathorne
Comment 2:	mixed, blended
Optical model:	garnet.rf780z
LS 13 320 SW	Aqueous Liquid Module
	Run length: 60 seconds
Pump speed:	66
Fluid:	water
Average of 3 files:	
C:\LS13320\Projects\Heckathorne\8-1__244.$ls	
C:\LS13320\Projects\Heckathorne\8-1__245.$ls	
C:\LS13320\Projects\Heckathorne\8-1__246.$ls	

Volume Statistics (Arithmetic) 8-1__246.$av

Calculations from 0.375 µm to 2000 µm

Volume:	100%		
Mean:	13.46 µm	S.D.:	19.70 µm
Median:	6.214 µm	Variance:	387.9 μm^2
Mean/Median ratio:	2.166	C.V.:	146%
Mode:	5.355 µm	Skewness:	3.110 Right skewed
		Kurtosis:	10.88 Leptokurtic

<10%	<25%	<50%	<75%	<90%
1.576 µm	3.015 µm	6.214 µm	14.54 µm	34.20 µm

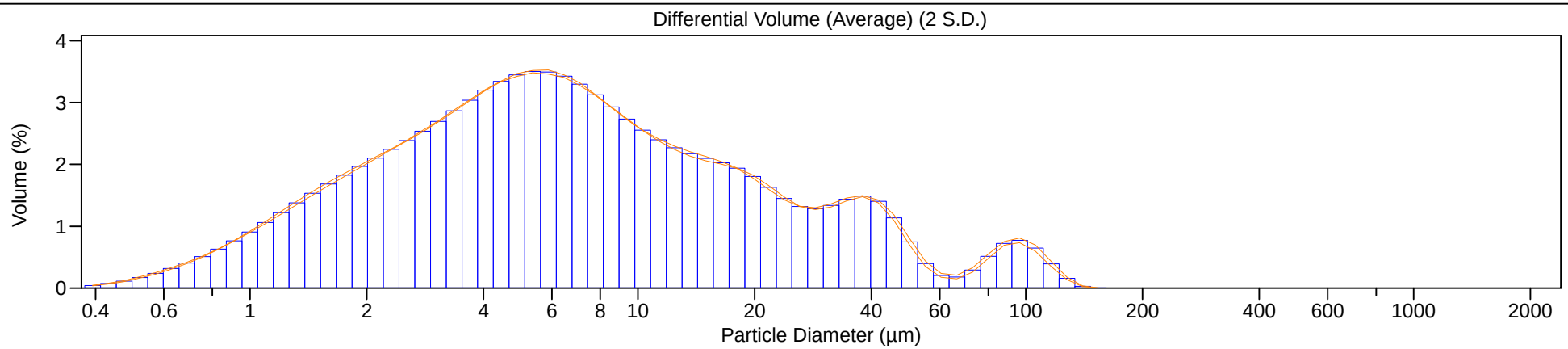

Beckman Coulter LS Particle Size Analyzer

6 Aug 2013

Heckathorn

File name:	C:\Users\Sam McWilliams\Desktop\sea_engineering\Sedflume\Heckathorne\Psd\8-2__249.$av
	8-2__249.$av
File ID:	8-2
Operator:	Reyes
Comment 1:	Heckathorne
Comment 2:	mixed, blended
Optical model:	garnet.rf780z
LS 13 320 SW	Aqueous Liquid Module
	Run length: 60 seconds
Pump speed:	66
Fluid:	water
Average of 3 files:	
C:\LS13320\Projects\Heckathorne\8-2__247.$ls	
C:\LS13320\Projects\Heckathorne\8-2__248.$ls	
C:\LS13320\Projects\Heckathorne\8-2__249.$ls	

Volume Statistics (Arithmetic) 8-2__249.$av

Calculations from 0.375 µm to 2000 µm

Volume:	100%		
Mean:	38.26 µm	S.D.:	76.01 µm
Median:	7.623 µm	Variance:	5777 μm^2
Mean/Median ratio:	5.018	C.V.:	199%
Mode:	5.355 µm	Skewness:	2.702 Right skewed
		Kurtosis:	6.484 Leptokurtic

<10%	<25%	<50%	<75%	<90%
1.651 µm	3.314 µm	7.623 µm	24.41 µm	128.9 µm

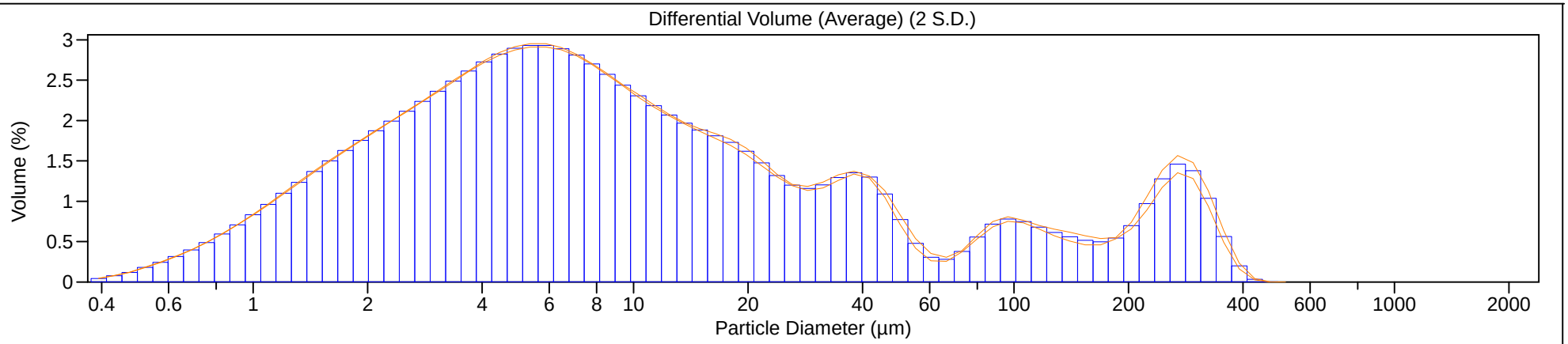

Beckman Coulter LS Particle Size Analyzer

6 Aug 2013

Heckathorn

File name:	C:\Users\Sam McWilliams\Desktop\sea_engineering\Sedflume\Heckathorne\Psd\8-3__261.$av
	8-3__261.$av
File ID:	8-3
Operator:	Reyes
Comment 1:	Heckathorne
Comment 2:	mixed, blended
Optical model:	garnet.rf780z
LS 13 320 SW	Aqueous Liquid Module
	Run length: 60 seconds
Pump speed:	66
Fluid:	water
Average of 3 files:	
C:\LS13320\Projects\Heckathorne\8-3__259.$ls	
C:\LS13320\Projects\Heckathorne\8-3__260.$ls	
C:\LS13320\Projects\Heckathorne\8-3__261.$ls	

Volume Statistics (Arithmetic) 8-3__261.$av

Calculations from 0.375 µm to 2000 µm

Volume:	100%		
Mean:	30.08 µm	S.D.:	60.36 µm
Median:	6.962 µm	Variance:	3643 μm^2
Mean/Median ratio:	4.320	C.V.:	201%
Mode:	5.355 µm	Skewness:	3.090 Right skewed
		Kurtosis:	9.340 Leptokurtic

<10%	<25%	<50%	<75%	<90%
1.555 µm	3.085 µm	6.962 µm	21.61 µm	86.70 µm

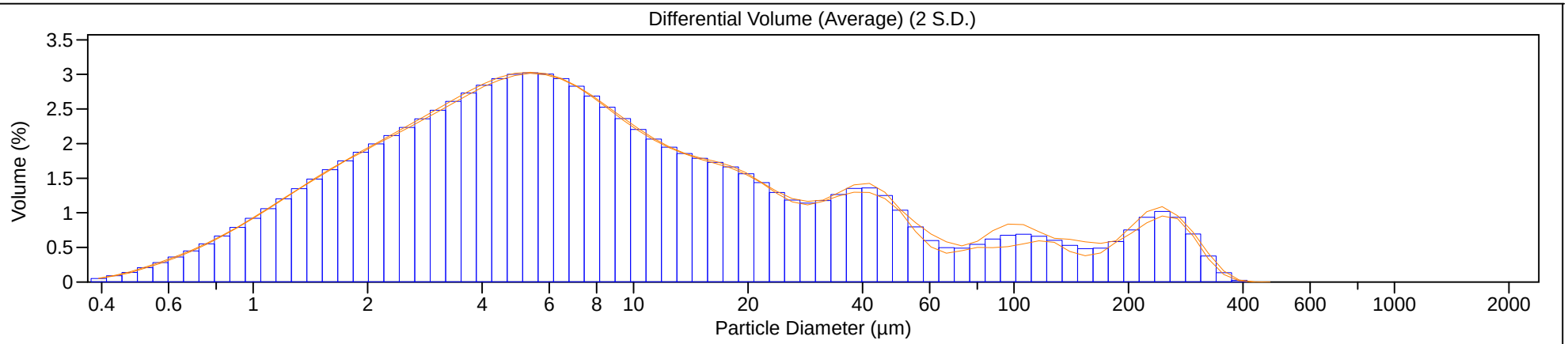

Beckman Coulter LS Particle Size Analyzer

6 Aug 2013

Heckathorn

File name:	C:\Users\Sam McWilliams\Desktop\sea_engineering\Sedflume\Heckathorne\Psd\9-1__328.$av
	9-1__328.$av
File ID:	9-1
Operator:	Reyes/Szesciorka
Comment 1:	Heckathorne
Comment 2:	mixed, blended
Optical model:	garnet.rf780z
LS 13 320 SW	Aqueous Liquid Module
	Run length: 60 seconds
Pump speed:	66
Fluid:	water
Average of 3 files:	
C:\LS13320\Projects\Heckathorne\9-1__326.$ls	
C:\LS13320\Projects\Heckathorne\9-1__327.$ls	
C:\LS13320\Projects\Heckathorne\9-1__328.$ls	

Volume Statistics (Arithmetic) 9-1__328.$av

Calculations from 0.375 µm to 2000 µm

Volume:	100%		
Mean:	22.67 µm	S.D.:	39.95 µm
Median:	7.991 µm	Variance:	1596 μm^2
Mean/Median ratio:	2.837	C.V.:	176%
Mode:	5.878 µm	Skewness:	3.835 Right skewed
		Kurtosis:	19.15 Leptokurtic

<10%	<25%	<50%	<75%	<90%
1.674 µm	3.407 µm	7.991 µm	22.26 µm	56.91 µm

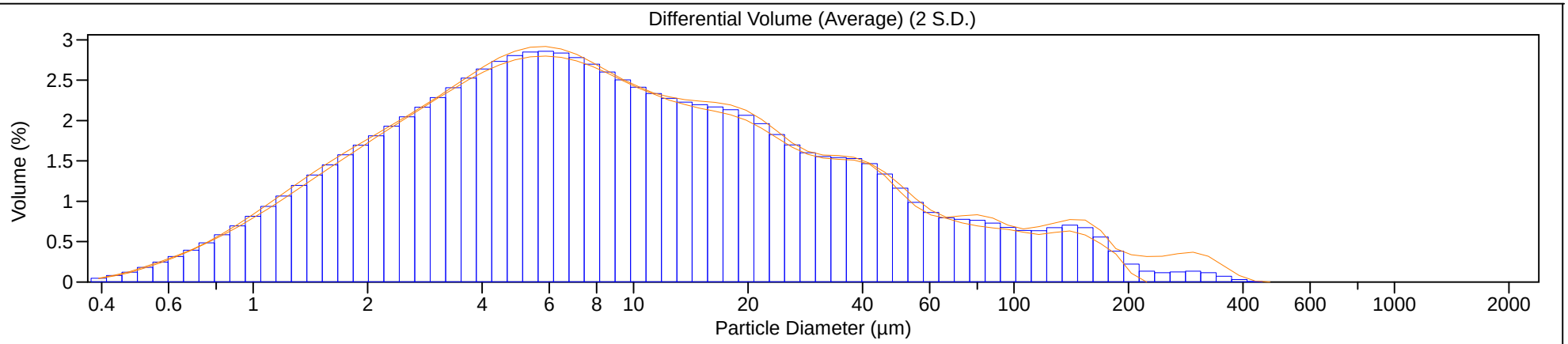

Beckman Coulter LS Particle Size Analyzer

6 Aug 2013

Heckathorn

File name:	C:\Users\Sam McWilliams\Desktop\sea_engineering\Sedflume\Heckathorne\Psd\9-2__352.$av
	9-2__352.$av
File ID:	9-2
Operator:	Reyes/Szesciorka
Comment 1:	Heckathorne
Comment 2:	mixed, blended
Optical model:	garnet.rf780z
LS 13 320 SW	Aqueous Liquid Module
	Run length: 60 seconds
Pump speed:	66
Fluid:	water
Average of 3 files:	
C:\LS13320\Projects\Heckathorne\9-2__350.$ls	
C:\LS13320\Projects\Heckathorne\9-2__351.$ls	
C:\LS13320\Projects\Heckathorne\9-2__352.$ls	

Volume Statistics (Arithmetic) 9-2__352.$av

Calculations from 0.375 µm to 2000 µm

Volume:	100%		
Mean:	20.89 µm	S.D.:	28.41 µm
Median:	9.167 µm	Variance:	807.1 µm^2
Mean/Median ratio:	2.279	C.V.:	136%
Mode:	6.453 µm	Skewness:	2.321 Right skewed
		Kurtosis:	5.495 Leptokurtic

<10%	<25%	<50%	<75%	<90%
1.685 µm	3.584 µm	9.167 µm	25.32 µm	55.85 µm

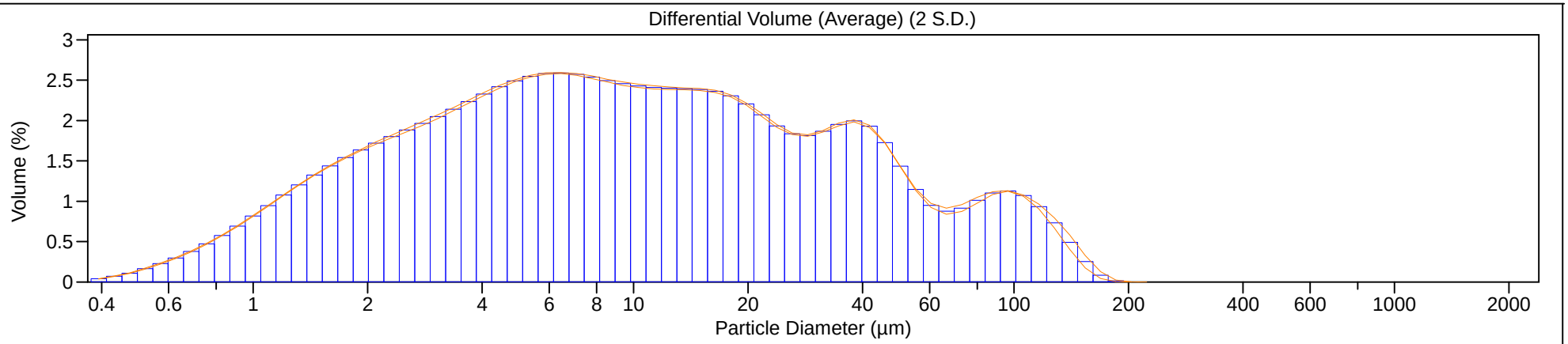

Beckman Coulter LS Particle Size Analyzer

6 Aug 2013

Heckathorn

File name:	C:\Users\Sam McWilliams\Desktop\sea_engineering\Sedflume\Heckathorne\Psd\10-1__162.$av
	10-1__162.$av
File ID:	10-1
Operator:	Szesciorka
Comment 1:	Maurice River
Comment 2:	mixed, blended
Optical model:	garnet.rf780z
LS 13 320 SW	Aqueous Liquid Module
	Run length: 60 seconds
Pump speed:	66
Fluid:	water
Average of 3 files:	
C:\LS13320\Projects\Heckathorne\10-1__160.$ls	
C:\LS13320\Projects\Heckathorne\10-1__161.$ls	
C:\LS13320\Projects\Heckathorne\10-1__162.$ls	

Volume Statistics (Arithmetic) 10-1__162.$av

Calculations from 0.375 µm to 2000 µm

Volume:	100%		
Mean:	34.89 µm	S.D.:	58.11 µm
Median:	9.483 µm	Variance:	3377 μm^2
Mean/Median ratio:	3.680	C.V.:	167%
Mode:	5.878 µm	Skewness:	2.679 Right skewed
		Kurtosis:	7.697 Leptokurtic

<10%	<25%	<50%	<75%	<90%
1.953 µm	4.073 µm	9.483 µm	35.82 µm	110.9 µm

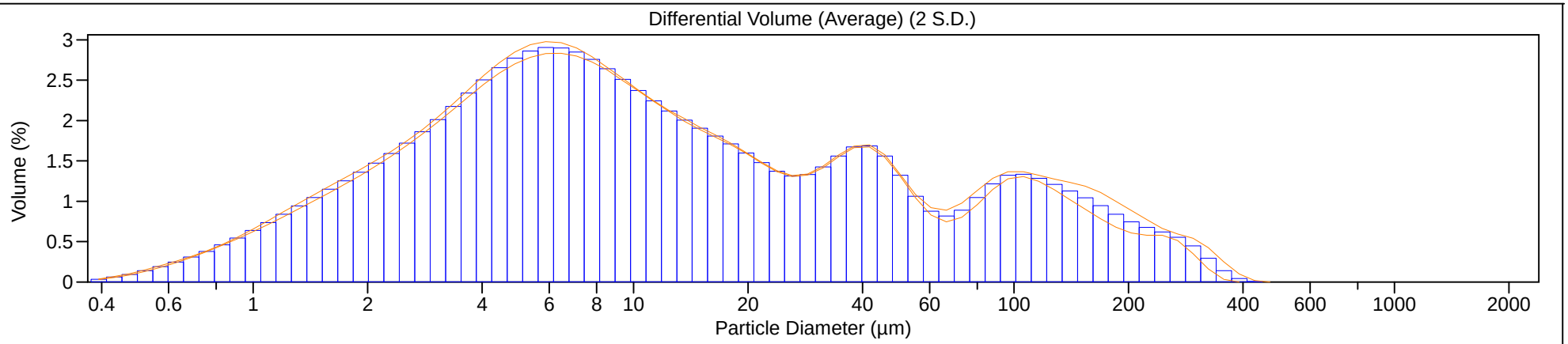

Beckman Coulter LS Particle Size Analyzer

6 Aug 2013

Heckathorn

File name:	C:\Users\Sam McWilliams\Desktop\sea_engineering\Sedflume\Heckathorne\Psd\10-2__159.$av
	10-2__159.$av
File ID:	10-2
Operator:	Szesciorka
Comment 1:	Maurice River
Comment 2:	mixed, blended
Optical model:	garnet.rf780z
LS 13 320 SW	Aqueous Liquid Module
	Run length: 60 seconds
Pump speed:	66
Fluid:	water

Average of 3 files:
C:\LS13320\Projects\Heckathorne\10-2__157.$ls
C:\LS13320\Projects\Heckathorne\10-2__158.$ls
C:\LS13320\Projects\Heckathorne\10-2__159.$ls

Volume Statistics (Arithmetic) 10-2__159.$av

Calculations from 0.375 µm to 2000 µm

Volume:	100%		
Mean:	24.83 µm	S.D.:	43.22 µm
Median:	7.980 µm	Variance:	1868 μm^2
Mean/Median ratio:	3.111	C.V.:	174%
Mode:	5.878 µm	Skewness:	3.652 Right skewed
		Kurtosis:	17.31 Leptokurtic

<10%	<25%	<50%	<75%	<90%
1.864 µm	3.674 µm	7.980 µm	25.25 µm	67.87 µm

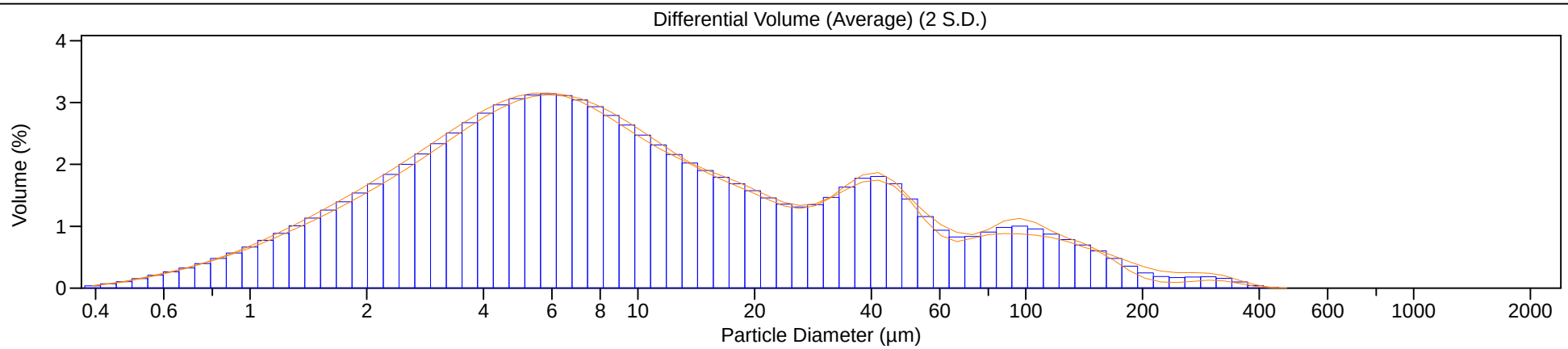

Beckman Coulter LS Particle Size Analyzer

6 Aug 2013

Heckathorn

File name:	C:\Users\Sam McWilliams\Desktop\sea_engineering\Sedflume\Heckathorne\Psd\10-3__156.$av
	10-3__156.$av
File ID:	10-3
Operator:	Szesciorka
Comment 1:	Maurice River
Comment 2:	mixed, blended
Optical model:	garnet.rf780z
LS 13 320 SW	Aqueous Liquid Module
	Run length: 60 seconds
Pump speed:	66
Fluid:	water
Average of 3 files:	
C:\LS13320\Projects\Heckathorne\10-3__154.$ls	
C:\LS13320\Projects\Heckathorne\10-3__155.$ls	
C:\LS13320\Projects\Heckathorne\10-3__156.$ls	

Volume Statistics (Arithmetic) 10-3__156.$av

Calculations from 0.375 µm to 2000 µm

Volume:	100%		
Mean:	23.99 µm	S.D.:	43.60 µm
Median:	7.143 µm	Variance:	1901 μm^2
Mean/Median ratio:	3.359	C.V.:	182%
Mode:	4.878 µm	Skewness:	3.782 Right skewed
		Kurtosis:	18.16 Leptokurtic

<10%	<25%	<50%	<75%	<90%
1.605 µm	3.094 µm	7.143 µm	24.56 µm	62.41 µm

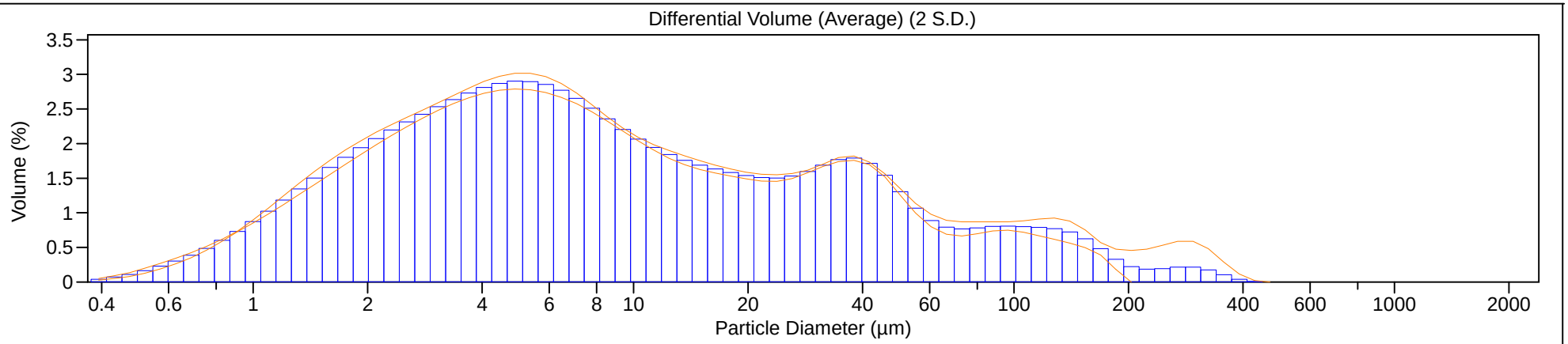

Beckman Coulter LS Particle Size Analyzer

6 Aug 2013

Heckathorn

File name:	C:\Users\Sam McWilliams\Desktop\sea_engineering\Sedflume\Heckathorne\Psd\10-4__165.$av
	10-4__165.$av
File ID:	10-4
Operator:	Szesciorka
Comment 1:	Maurice River
Comment 2:	mixed, blended
Optical model:	garnet.rf780z
LS 13 320 SW	Aqueous Liquid Module
	Run length: 60 seconds
Pump speed:	66
Fluid:	water

Average of 3 files:
C:\LS13320\Projects\Heckathorne\10-4__163.$ls
C:\LS13320\Projects\Heckathorne\10-4__164.$ls
C:\LS13320\Projects\Heckathorne\10-4__165.$ls

Volume Statistics (Arithmetic) 10-4__165.$av

Calculations from 0.375 µm to 2000 µm

Volume:	100%		
Mean:	15.17 µm	S.D.:	22.28 µm
Median:	6.896 µm	Variance:	496.4 µm^2
Mean/Median ratio:	2.200	C.V.:	147%
Mode:	5.878 µm	Skewness:	3.087 Right skewed
		Kurtosis:	11.01 Leptokurtic

<10%	<25%	<50%	<75%	<90%
1.708 µm	3.343 µm	6.896 µm	16.12 µm	38.34 µm

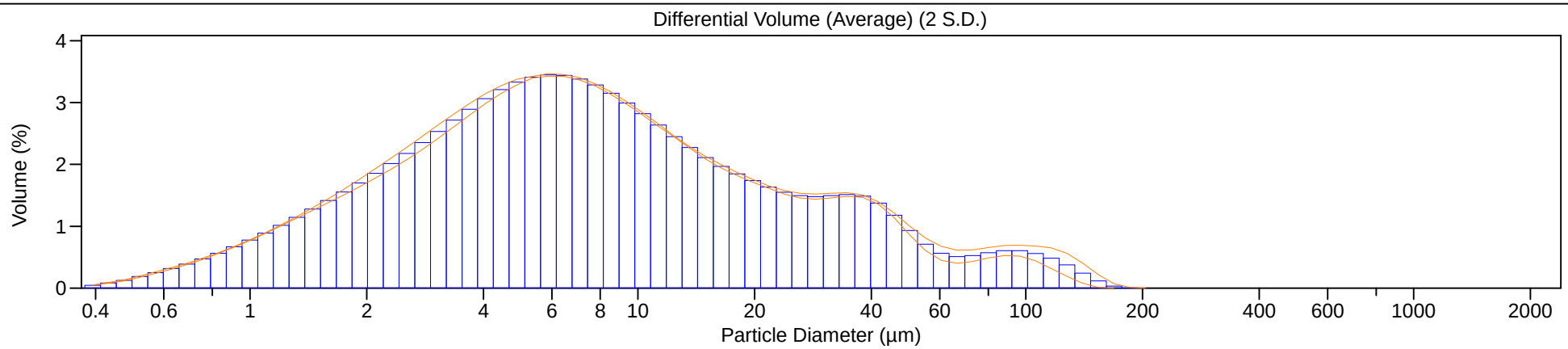

Beckman Coulter LS Particle Size Analyzer

6 Aug 2013

Heckathorn

File name:	C:\Users\Sam McWilliams\Desktop\sea_engineering\Sedflume\Heckathorne\Psd\10-5__168.$av
	10-5__168.$av
File ID:	10-5
Operator:	Szesciorka
Comment 1:	Maurice River
Comment 2:	mixed, blended
Optical model:	garnet.rf780z
LS 13 320 SW	Aqueous Liquid Module
	Run length: 60 seconds
Pump speed:	66
Fluid:	water

Average of 3 files:
C:\LS13320\Projects\Heckathorne\10-5__166.$ls
C:\LS13320\Projects\Heckathorne\10-5__167.$ls
C:\LS13320\Projects\Heckathorne\10-5__168.$ls

Volume Statistics (Arithmetic) 10-5__168.$av

Calculations from 0.375 µm to 2000 µm

Volume:	100%		
Mean:	35.38 µm	S.D.:	58.03 µm
Median:	10.09 µm	Variance:	3367 μm^2
Mean/Median ratio:	3.505	C.V.:	164%
Mode:	6.453 µm	Skewness:	2.547 Right skewed
		Kurtosis:	6.516 Leptokurtic
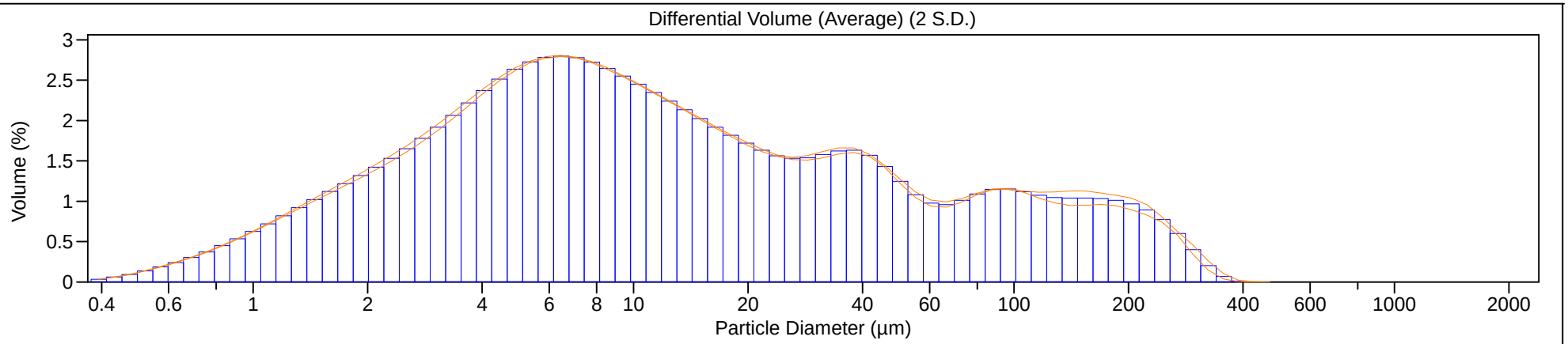
<10%	<25%	<50%	<75%	<90%
1.985 µm	4.217 µm	10.09 µm	35.42 µm	112.7 µm